NASA Contractor Report 3695

Mean Velocities and Reynolds Stresses Upstream of a Simulated Wing-Fuselage Juncture

H. McMahon, J. Hubbartt,
and L. R. Kubendran

GRANT NAG1-40
JUNE 1983

25th Anniversary
1958-1983

NASA

NASA Contractor Report 3695

Mean Velocities and Reynolds Stresses Upstream of a Simulated Wing-Fuselage Juncture

H. McMahon, J. Hubbartt,
and L. R. Kubendran
Georgia Institute of Technology
Atlanta, Georgia

Prepared for
Langley Research Center
under Grant NAG1-40

National Aeronautics
and Space Administration

**Scientific and Technical
Information Branch**

1983

Use of trade names or names of manufacturers in this report does not constitute an official endorsement of such products or manufacturers, either expressed or implied, by the National Aeronautics and Space Administration.

SUMMARY

Values of three mean velocity components and six turbulence stresses measured in a turbulent shear layer upstream of a simulated wing-fuselage juncture and immediately downstream of the start of the juncture are presented and discussed.

The wing and fuselage are simulated by using a body of constant thickness mounted perpendicular to a large flat plate. The body has an elliptical leading edge, and a two-dimensional turbulent boundary layer is developing on the plate far upstream of the body nose. The measurements were conducted at three streamwise stations upstream of the body and at one station in the juncture just downstream of the body leading edge. Two single-sensor hot-wire probes were used in the measurements.

The separated region just upstream of the nose of the body contains an area of reversed flow near the plate surface where the turbulence level is high. Outside of this area the flow skews as it passes around the body. This skewing has begun by 1.75 body widths upstream of the nose. In this skewed region, the magnitude and distribution of the turbulent normal and shear stresses within the shear layer are modified slightly by the skewing and deceleration of the flow.

At a streamwise distance in the juncture 1.3 body widths downstream of the body nose the secondary flow vortex is tightly rolled up and re-distributes both mean flow and turbulence in the juncture.

The data acquisition technique employed here allows a hot wire to be used in reversed flow to indicate flow direction.

INTRODUCTION

The flow in a wing-fuselage juncture or corner is an example of a three-dimensional shear flow where there is a significant secondary flow present, which is to say that there are significant velocity components normal to the main flow direction. Similar types of flows occur in the juncture of wing-pylons and wing-winglets and in the corners formed by a two-dimensional airfoil model and the walls of a wind tunnel.

The presence of a strong secondary flow in these flow situations is due to two effects. When a body such as a wing projects from a fuselage surface, the oncoming boundary layer (here considered as a turbulent boundary layer) skews as it passes around the obstruction. This skewing stretches and rotates the vortex lines within the

approaching boundary layer, producing a streamwise vorticity in the juncture. Secondly, the blockage associated with the presence of the body causes the oncoming boundary layer to experience steep adverse pressure gradients in the vicinity of the body leading edge. As a result, the boundary layer generally separates and a strong vortex sheet rolls up and trails downstream in the juncture. Commonly, this trailing vortex dominates the juncture flow. These two mechanisms for depositing streamwise vorticity in the juncture are shown schematically in figure 1.

The secondary flow in streamwise junctures described above has been investigated both experimentally and numerically because it may have an important effect on the drag of the juncture as well as on the flow on a surface downstream of the juncture. In addition to the effect on aircraft performance, juncture flows can have a significant effect on airfoil drag measurements in two-dimensional wind tunnel tests. This provides another motivation for the study and understanding of such flows.

Numerical analyses of turbulent juncture flows (e.g., refs. 1, 2) have concentrated on the flow in a juncture formed by two bodies with coincident leading edges. Such analyses would be applicable to the juncture flow considered here when applied downstream of the separation region using assumed or measured initial conditions at one station in the juncture to predict the flow behavior at a station further downstream in the juncture. In support of analyses such as these, detailed measurements of mean flow components and turbulence quantities have been carried out in a juncture by Shabaka and Bradshaw (refs. 3, 4) and by the authors (ref. 5).

Experiments such as those noted above have defined the character of the juncture flow downstream of the body leading edge. The initial development of this juncture flow, that is, the behavior of the oncoming turbulent boundary layer as it experiences and reacts to the presence of a body protruding from a surface, is not well documented. Detailed experimental measurements in the shear layer upstream of and around the leading edge of such a body are the subject of this report.

The three-dimensional turbulent boundary layer near the leading edge of a body mounted perpendicular to the surface of a flat plate has been studied by several investigators, but the studies have been confined to the use of pressure probes or surface flow visualization. Hornung and Joubert (ref. 6) considered a circular cylinder standing on a flat plate and took data using a total-head probe fitted with yaw tubes on the sides in order to calculate velocity profiles. No measurements of the reversed flow in the separated flow region upstream of the body leading edge are presented. East and

Hoxey (ref. 7) measured mean velocity profiles, yaw angle profiles, skin friction, and static pressure distributions in the vicinity of the leading edge of a blunt body mounted on a flat plate. Again, the primary objective of this work was to gather experimental data for the three-dimensional turbulent boundary layer. Accordingly, their measurement stations were at or outside the separation line and a three-tube yaw probe was used to measure mean-flow quantities. Peake, Rainbird, and Atraghji (ref. 8) discuss the extent of the separated region ahead of various blunt bodies protruding from a flat plate as deduced from surface flow visualization studies. Briley and McDonald (ref. 9), in discussing numerical solutions for a horseshoe vortex resulting from the interaction of a laminar boundary layer developing along a flat plate with an elliptical strut, point out that numerous flow visualization studies are available but that little is available in the way of detailed flow measurements, particularily downstream of reattachment. The same comment may be made regarding the turbulent flow problem, which has prompted the work reported herein.

The juncture flow problem investigated here was generated by a constant-thickness body ("wing"), having an elliptical leading edge, which was mounted perpendicular to a large flat plate ("fuselage") along which a turbulent boundary layer was developing (fig. 2). Three mean velocity components and six turbulence stresses were measured in the unseparated turbulent boundary layer at four streamwise stations located upstream and just downstream of the leading edge of the body (fig. 3). In addition, some hot-wire measurements were made within the separated region upstream of the body leading edge so as to bring out the features of the roll-up of the separation vortex. These measurements near the leading edge of the body, when combined with the existing detailed measurements of reference 5 in the juncture itself, provide a comprehensive set of data for the entire juncture flow field which should be of value in numerical analyses of the problem.

The equipment and instrumentation used in these experiments, as well as the data analysis and most of the data acquistion procedures, are the same as reported earlier in reference 5. A summary of each of these items will be given here for completeness, and further details may be found in reference 5. A detailed discussion of the model and actuator is found in reference 10.

SYMBOLS

a Coefficients of polynominal approximation (eq. 20)

A-F	Constants used in data reduction, defined in equations 10-15
e_ℓ	AC component of E_ℓ, volts
E	Nonlinear output voltage of constant-temperature anemometer, volts
E_ℓ	Linearized output voltage of hot-wire anemometer, volts
E_o	Output voltage of hot-wire anemometer at zero velocity, volts
h	Binormal velocity coefficient (eq. 2)
ℓ_{ij}	Cosine of angle between x'_i and x_j coordinates axes
s, y, n	Hot-wire coordinate system (figs. 7 and 10)
S	Constant of proportionality (eq. 4), volts/m/s
T_{pq}, T'_{ij}	Second order tensor components (velocity correlations) used in coordinate transformations (eqs. 25 and 26)
u	Instantaneous fluctuating velocity, m/s
u'	Root-mean-square fluctuating velocity, i.e., $u' = \sqrt{\overline{u^2}}$, m/s
U	Local mean or time-averaged velocity, m/s
U_{BN}	Binormal velocity component, normal both to U_N and U_T (eq. 2), m/s
U_{eff}	Effective cooling velocity (eq. 1), m/s
U_N	Velocity component normal to hot wire in plane of wire-support needles (eq. 2), m/s
U_T	Velocity component tangent to the hot wire (eq. 2), m/s
V_i, V'_i	Velocity components used in coordinate transformations (eqs. 22 and 23), m/s
V_∞	Undisturbed freestream velocity, m/s
x, y, z	Laboratory coordinate system (figs. 7 and 10), m
x_i, x'_i	Cartesian coordinate axes used in coordinate transformation, m
α, θ, λ, ψ	Angles expressing hot-wire orientation (fig. 7)

Subscripts:

i, j, p, q	Indices for coordinate, velocity, and tensor components (1, 2, 3)
ℓ	Linearized output
n	Component in n direction
s	Component in s direction
x	Component in x direction
y	Component in y direction
z	Component in z direction
α, ψ	Indicates that quantity is evaluated with wire angles α and ψ (fig. 7)

EQUIPMENT

Wind Tunnel

The experiments were carried out in the Georgia Tech Low Speed Wind Tunnel, which is an open return type with a velocity continuously variable to a maximum of 22.9 m/s (75 ft/s). The test section is 1.07 x 1.09 x 6.10 m (42 x 43 x 240 in.) and the freestream turbulent intensity, u'_∞/V_∞, near the exit of the test section was measured to be 0.5%.

Body and Flat Plate

The body, which was mounted perpendicular to the flat plate and aligned with the wind tunnel axis, consisted of a leading edge which was a 1.5:1 ellipse attached to an afterbody of constant thickness 57.9 mm (2.28 in.) and length 1.22 m (48 in.). The leading edge had a strip of distributed glass-bead roughness, (average bead diameter 0.25 mm (0.01 in)), which was 6.35 mm (0.25 in.) wide beginning 25.4 mm (1.0 in.) downstream of the nose.

The body and flat plate were mounted in the free jet at the exit of the open return wind tunnel (fig. 2) in order to allow a simple way to move the measurement probes over a considerable distance in the transverse and streamwise directions. The flat plate was mounted above the floor of the wind tunnel and an extension of the plate, which served as a boundary layer development section, protruded 572 mm (22.5 in.) upstream into the wind tunnel. The flat plate was fitted with a trip wire 0.97mm (0.038 in.) in diameter located 102 mm (4.0 in.) downstream of the leading edge.

The plate was designed with interchangeable segments (fig. 2) so that the particular segment containing the probe and actuator (fig. 4) could be located at arbitrary streamwise stations. The step at any joint between segments was at most $\pm$ 0.13 mm (0.005 in) compared to a nominal boundary layer thickness of 25.4 mm (1.0 in.).

Hot Wires

Two hot-wire probes were used in this investigation (fig. 5). These probes were

used with the probe axis perpendicular to the plate surface. The hot-wire sensor was supported on needles which protruded through the surface of the flat plate.

The probe with the wire held parallel to the plate surface (i.e., support needles of equal length) is shown in fig. 5(a)) and is called the "horizontal wire". The needles were 3.18 mm (0.125 in.) apart and supported a platinum-coated tungsten wire 0.0051 mm (0.0002 in.) in diameter with an etched center portion 1.27 mm (0.050 in.) long. The probe needles could be extended to a maximum height above the plate surface of approximately 35.6 mm (1.40 in.) and rotated a full 360° about the probe axis.

Since the data analysis required the use of a hot wire oriented at an angle to the surface of the flat plate, a second hot-wire probe was constructed with needles of unequal length (fig. 5(b)) and is called the "slant wire". In order that the wire not be in the wake of the longer needle at certain angular orientations as the probe rotated about its axis, the longer needle was offset by a distance of 5.1 mm (0.20 in.) as shown. The wire was the same type and diameter as the horizontal wire and was 4.5 mm (0.177 in.) long. Because of the needle geometry, the sensor portion of the slant wire was limited to an excursion in y, the distance above the plate surface, of $27.9 \text{ mm} > y > 2.3 \text{ mm}$ ($1.10 \text{ in.} > y > 0.090 \text{ in.}$). The wire orientation angle, α , was approximately 45°, with the precise angle being measured to within $\pm 0.05^{\circ}$ by using an optical comparator.

Both probes were calibrated by extending the needles upward until the sensor portion of the wire was at the outer edge of the boundary layer and normal to the velocity vector. Then the output voltage was measured in this flow of known (measured) velocity.

Actuator Linear Motion

The segment of the flat plate which contained the hot-wire probe consisted of a slide and slide bed (fig. 4). The probe was held in an actuator which hung below the slide and moved with the slide.

The streamwise (x) location of the survey station was changed by manually interchanging suitable segments of the flat plate (fig. 2). Linear movements of the hot-wire sensor in directions perpendicular to the plate (y) and normal to the body surface (z) were accomplished by using lead screws driven by stepper motors. Since two probes (horizontal and slant wire) had to be used sequentially in order to determine all of the required mean flow and turbulence quantities at any measurement station, it was

important that the sensor portion of each wire be located at the identical point when the probes were interchanged. This was accomplished to an accuracy of $\pm$ 0.025 mm (0.001 in.) using special optics and techniques (ref. 5) developed for this purpose. Including this uncertainty, it is estimated that the y location of the probes was accurate to within $\pm$ 0.05 mm (0.002 in.) while the z location was accurate to within $\pm$ 0.10 mm (0.004 in.).

Actuator Angular Motion

In addition to linear motion, the hot-wire probes had to be rotated about their own axes in order to generate the necessary data. The local flow yaw angle, θ, was found with the horizontal wire and formed the basis for the coordinate system used in taking data with the slant wire. The determination of this angle involved a measurement of both the reference main flow direction (i.e., the x axis) and the local flow direction. The uncertainty in the magnitude of the local skew angle, θ, when obtained in this manner was estimated to be $\pm$ 1.0°. Using the special optics mentioned above, the slant wire was oriented with respect to the data coordinate system to within less than 0.5°.

INSTRUMENTATION AND PROCEDURES

Freestream Velocity

The velocity of the wind tunnel flow was measured with a pitot-static probe mounted just outside the boundary layer. The dynamic pressure was read with a Barocel electronic manometer and digital voltmeter. The wind tunnel velocity was held constant to within $\pm$ 0.5% and was in error by less than $\pm$ 0.5%.

During hot-wire velocity calibration the pitot-static probe and hot-wire sensor were located near each other and at z = 152 mm (6.0 in.) where the flow is effectively two-dimensional.

Hot-Wire Anemometer

The hot-wire probes were connected to a TSI Model 1050 anemometer, with the output of the anemometer going to a TSI Model 1052 polynominal linearizer.

Local Mean Velocity

The linearized output of the anemometer was read with an HP 2401C integrating digital voltmeter. This voltmeter was set for maximum integrating time (1.0s). Mean D.C. voltages were taken by arithmetically averaging 30 voltmeter samples (i.e., a total of 30 seconds of integration) for U_y and 20-25 voltmeter samples for U_s . A discussion of the choice of averaging times is found in Appendix A of reference 5.

Turbulence Measurements

The A. C. component of the linearized hot-wire output was measured with an HP Model 3400 A true RMS meter and read with the HP 2401C digital voltmeter set to integrate over 1.0s. By using repeated samples, an averaging time of 20-25 seconds was used for u'_s, u'_n, and $\overline{u_s u_n}$ and 30 seconds for u'_y, $\overline{u_s u_y}$, and $\overline{u_y u_n}$. The averaging time for some of these quantities is longer than that used in reference 5 in order to improve confidence in the arithmetically averaged values and to further decrease the scatter in the data.

Data Handling

Movement of the actuator stepper motors and data acquisition were controlled in real time by an on-site computer. Both the DC and RMS average signals were output on paper tape and later read into storage to be processed on a central computer.

Operating Conditions

All of the tests were run at a nominal freestream velocity of 15.24 m/s (50 ft./s) giving a Reynolds number of 994,000/m (300,000/ft.). The turbulent boundary layer thickness on the flat plate at the streamwise location corresponding to the nose of the body was approximately 22.9 mm (0.9 in.), corresponding to a ratio of body thickness to boundary layer thickness of 2.53.

Coordinate Systems

Two Cartesian coordinate systems were used in presenting and taking the data

(fig. 6). The first coordinate system was the x-y-z coordinate system used in data presentation. These are laboratory coordinates, with x in the freestream direction, y perpendicular to the surface of the flat plate, and z normal to the body surface. The laboratory coordinates are defined such that $x = 0$ at the nose of the body, $y = 0$ at the plate surface, and $z = 0$ on the body surface. Thus, $x < 0$ implies a location upstream of the body while $-29.0 \text{ mm} < z < 0$ denotes a transverse location upstream of the body and between the vertical plane of symmetry and the vertical plane containing the body surface (fig. 3). Since the body has a constant thickness of 57.9 mm (2.28 in.), a value of $z = -29.0$ mm corresponds to the plane of symmetry.

The second coordinate system was the working coordinate system s-y-n used in the taking of data. The local yaw angle, θ, was found for each value of x, y, and z using the horizontal hot wire. This value of θ defined a local s-y-n coordinate system which rotated about the vertical y axis as the value of y changed (fig. 7). When all of the required measurements with the horizontal wire had been taken, the probe was removed and replaced with the slant-wire probe. The slant wire was then oriented at an appropriate angle ψ with respect to the local s-axis (s-y-n) previously determined (fig. 7).

General Method

The four streamwise measurement stations used in these experiments were located ahead of and around the body leading edge (fig. 3) at $x = -102$ mm (- 4.0 in.), $x = -38$ mm (- 1.5 in.), $x = -11$ mm (- 0.44 in.) and $x = 76$ mm (+ 3.0 in.). At each of these streamwise stations, mean flow and turbulence data were taken from near the plate surface to the maximum allowable value of y at several transverse locations, z. Specific values of y and z where measurements were made are found in Tables 1 - 4.

There was no flow reversal or local skew angle in excess of 90° at any of the streamwise stations except for the station at $x = -11$ mm (- 0.44 in.). At this station, which is just ahead of the nose of the body, there was flow reversal inside the separated region (i.e., for some negative values of z). As will be described in the next section, the local yaw angle, θ, was determined at each value of y by rotating the horizontal wire and taking data on both sides of a flow direction which had been established in the measurement at the previous step in y. A new, correct, direction then was established and the process was repeated. Measurements were begun at the largest value of y,

where the flow direction was known approximately, and then the horizontal wire was "marched" toward the plate surface from the outer edge of the shear layer. This was the technique employed in reference 5 and in the measurements made here outside of the separated region.

When this same technique was tried within the separated region, starting from the outer edge and using suitably small steps in y, it was found that the local flow angle could be tracked without ambiguity through 90° (i.e., reversed flow) and beyond. Previously, the hot-wire has not been considered an attractive device in such a flow region because it gives the same output signal (same cooling) whether the flow is from a given direction or 180° from that given direction. The "marching" technique employed here, when carefully done, eliminated this directional ambiguity.

In making hot-wire measurements within the separated region it was found that, as well as starting at a suitable distance above the plate surface and "marching" inward, the probe could be "marched" in the z direction at constant y by starting at a suitably large value of z where the local yaw angle was small. A "marching" technique in both the y and z directions was used in taking the data within the separated region which is presented here. It should be noted that, although this technique eliminates directional ambiguity, there are still uncertainties in the data within some segments of the separated flow region because of a combination of high turbulence level and low mean flow velocity in these areas. The linear analysis used here is not suitable for such situations.

Data Quality Control

The hot-wire calibrations and the polynomial coefficients for the linearizer were updated periodically as required. Close attention was paid to drift in the electronic instruments, and compensation was made for variations in the temperature of the wind tunnel air as described in Appendix B of reference 5. The output of both probes was monitored for vibration and, in the case of the slant wire, operated so as to minimize wake effects due to the needles.

Except in certain areas of high turbulence in the separated region, the repeatability of the data was considered to be excellent and consistent with the repeatability shown in reference 5. An error analysis is included as Appendix A in this report.

DATA ACQUISITION AND ANALYSIS

Equations for Evaluating Velocities and Velocity Correlations

The hot wire is shown schematically in figure 7 with an arbitrary orientation in both the laboratory (x,y,z) and hot-wire (s,y,n) Cartesian coordinate systems. The y ordinate is measured normal to the flat plate whereas x, z, s, and n are in the plane of the plate. The hot-wire coordinates were used for data acquisition and the data results then were transformed into the laboratory coordinates for all data presentations.

The orientation of the hot wire in the wire coordinate system is specified by the two angles α and ψ shown in figure 7. The angle α is the angle between the axis of wire rotation and a normal to the wire defined to be in the plane containing the hot wire and the axis of wire rotation. The angle ψ is the angle between the s axis and the projection of the hot wire on the s-n plane (i.e., the plane of the flat plate).

The voltage output of the constant-temperature anemometer is related to α, ψ, and the three instantaneous velocity components. That is,

$$E = E(U_s + u_s, U_y + u_y, u_n, \alpha, \psi)$$

Introduce an effective cooling velocity, U_{eff}, such that

$$E = E(U_{eff}) \tag{1}$$

where

$$U_{eff} = f(U_s + u_s, U_y + u_y, u_n, \alpha, \psi) .$$

The expression for E will be linearized. For the present investigation, the relationship for U_{eff} first suggested and studied by Jorgensen (ref. 11) was used. This expression is

$$U_{eff} = \left(U_N^2 + k^2 U_T^2 + h^2 U_{BN}^2 \right)^{1/2} \tag{2}$$

where U_N is the velocity component normal to the wire in the plane of the wire-support needles, U_T is the velocity component tangent to the wire, and U_{BN} is the binormal

velocity component which is normal to both U_N and U_T. The coefficients k and h must be determined by calibration. In terms of α, ψ, and the three instantaneous velocity components equation (2) becomes

$$U_{eff} = \left\{ \left\{ \left[\left(U_s + u_s \right) \cos \psi + u_n \sin \psi \right] \sin \alpha - \left(U_y + u_y \right) \cos \alpha \right\}^2 \right.$$
$$+ k^2 \left\{ \left[\left(U_s + u_s \right) \cos \psi + u_n \sin \psi \right] \cos \alpha + \left(U_y + u_y \right) \sin \alpha \right\}^2$$
$$\left. + h^2 \left\{ - \left(U_s + u_s \right) \sin \psi + u_n \cos \psi \right\}^2 \right\}^{1/2} \qquad (3)$$

The relation between U_{eff} and E, as expressed by equation (1), was determined by experiment for both wires used in this study. These data were then used along with the linearizer circuit of the constant-temperature anemometer to generate, for each wire, a linearized output voltage E_ℓ which is directly proportional to U_{eff}. Thus

$$E_\ell = SU_{eff} \qquad (4)$$

where S is the constant of proportionality.

E_ℓ can be decomposed into a mean or DC component, $\bar{E}_\ell$, and a fluctuating or AC component, e_ℓ, where the bar denotes taking the time average or mean and $\bar{e}_\ell = 0$. Thus, equation (4) becomes

$$\bar{E}_\ell + e_\ell = SU_{eff} \qquad (5)$$

$\bar{E}_\ell$ and the root-mean-square of e_ℓ (i.e., $\sqrt{\overline{e_\ell^2}}$) are the measureable quantities which are related to the velocities. Taking the mean of equation (5) gives

$$\frac{\bar{E}_\ell}{S} = \bar{U}_{eff} \qquad (6)$$

Squaring equation (5) and then taking the mean and using equation (6) gives

$$\frac{\overline{e_\ell^2}}{S^2} = \overline{U_{eff}^2} - \bar{U}_{eff}^2 \qquad (7)$$

Equations (3), (6), and (7) yield two equations relating $\bar{E}_\ell$ and $\overline{e_\ell^2}$ to mean values of the various velocity components and turbulence quantities for fixed values of α and ψ through equation (3).

To relate $\bar{E}_\ell$ and $\overline{e_\ell^2}$ to the unknowns velocity components and turbulence quantities using equations (6) and (7), it is necessary to evaluate $\overline{U_{eff}^2}$, $\bar{U}_{eff}$, and $\bar{U}^2_{eff}$ from equation (3). The evaluation of $\overline{U_{eff}^2}$ simply requires squaring and averaging, yielding terms in U_s, U_y, and averages in products of the fluctuating velocity components. However, the evaluation of the latter two mean quantities requires that equation (3) be expanded in a truncated Taylor's series. For the hot-wire axes of figure 7, U_s is the only zeroth order velocity component while U_y, u_s, u_y, and u_n are first order terms. Therefore, for this analysis equation (3) was expanded in a series using U_s as the zeroth order term and then averaged over time to obtain $\bar{U}_{eff}$ first. Both $\bar{U}_{eff}$ and $\bar{U}^2_{eff}$ were truncated by neglecting third and higher order terms. After squaring and collecting terms under the square root radical on the right-hand side, equation (3) may be rewritten in the form

$$U_{eff} = U_s \; A \; (1 + \epsilon)^{1/2} \tag{8}$$

where ϵ involves first and second order terms only and is given by

$$\epsilon = 2\frac{u_s}{U_s} + \left(\frac{u_s}{U_s}\right)^2 + B\left[\left(\frac{U_y}{U_s}\right)^2 + 2\frac{U_y u_y}{U_s U_s} + \left(\frac{u_y}{U_s}\right)\right]^2$$

$$+ C\left(\frac{u_n}{U_s}\right)^2 + D\left[\frac{U_y}{U_s} + \frac{u_y}{U_s} + \frac{u_s}{U_s}\frac{U_y}{U_s} + \frac{u_s}{U_s}\frac{u_y}{U_s}\right]$$

$$+ E\left(\frac{U_y u_n}{U_s U_s} + \frac{u_y u_n}{U_s U_s}\right) + F\left(\frac{u_n}{U_s} + \frac{u_s u_y}{U_s U_s}\right) \tag{9}$$

where

$$A = \cos^2\psi \sin^2\alpha + k^2 \cos^2\psi \cos^2\alpha + h^2 \sin^2\psi \tag{10}$$

$$B = (\cos^2\alpha + k^2 \sin^2\alpha)/A \tag{11}$$

$$C = (\sin^2\psi \sin^2\alpha + k^2 \sin^2\psi \cos^2\alpha + h^2 \cos^2\psi)/A \tag{12}$$

$$D = 2 \cos \psi \sin \alpha \cos \alpha \, (k^2 - 1)/A \tag{13}$$

$$E = 2(\sin \psi \sin \alpha \cos \alpha)\,(k^2 - 1)/A \tag{14}$$

$$F = 2 \cos \psi \sin \psi \, (\sin^2 \alpha + k^2 \cos^2 \alpha - 2h^2)/A \tag{15}$$

Expanding equation (8) in a Taylor's series, dropping terms of ε^3 and higher order, and introducing the results into equations (6) and (7) gives

$$\frac{\bar{E}_\ell}{S} = U_s \sqrt{A} \left(1 + \frac{1}{2}\bar{\varepsilon} - \frac{1}{8}\overline{\varepsilon^2}\right) \tag{16}$$

and

$$\frac{\overline{e_\ell^2}}{S^2} = \frac{U_s^2 A}{4}\left(\overline{\varepsilon^2} - \bar{\varepsilon}^2\right) \tag{17}$$

Finally, using equation (9) to evaluate $\bar{\varepsilon}$, $\bar{\varepsilon}^2$, and $\overline{\varepsilon^2}$ and dropping third and higher order terms, equations (16) and (17) become, after rearranging,

$$\frac{\bar{E}_\ell}{S} = U_s \sqrt{A} \left[1 + \left(\frac{B}{2} - \frac{D^2}{8}\right)\left(\frac{U_y^2}{U_s^2} + \frac{\overline{u_y^2}}{U_s^2}\right) + \frac{D}{2}\frac{U_y}{U_s}\right.$$

$$\left. + \left(\frac{C}{2} - \frac{F^2}{8}\right)\frac{\overline{u_n^2}}{U_s^2} + \left(\frac{E}{2} - \frac{DF}{4}\right)\frac{\overline{u_y u_n}}{U_s^2}\right] \tag{18}$$

and

$$\frac{\overline{e_\ell^2}}{S^2} = U_s^2 A \left[\frac{\overline{u_s^2}}{U_s^2} + \frac{D^2}{4}\frac{\overline{u_y^2}}{U_s^2} + \frac{F^2}{4}\frac{\overline{u_n^2}}{U_s^2} + D\frac{\overline{u_s u_y}}{U_s^2}\right.$$

$$\left. + \frac{DF}{2}\frac{\overline{u_y u_n}}{U_s^2} + F\frac{\overline{u_s u_n}}{U_s^2}\right] \tag{19}$$

Equations (18) and (19) are the general form of the hot-wire response equations used for evaluating the mean velocity components U_s and U_y and the six turbulence

quantities u'_s, u'_y, u'_n, $\overline{u_s u_y}$, $\overline{u_s u_n}$, and $\overline{u_y u_n}$. This was accomplished by using the horizontal wire ($\alpha = 0$) at the three orientations $\psi = 90^\circ$ and $\psi = \pm 45^\circ$ and by using the slant wire ($\alpha = 47.3^\circ$) at the four orientations $\psi = 0$, $\psi = 180^\circ$, and $\psi = \pm 25^\circ$. The specific equations for these wire orientations are given in reference 5.

Methods and Calibrations

The orientation of the hot-wire coordinates was determined experimentally at each point in the flow field by rotating the horizontal wire ($\alpha = 0$) around its axis of rotation. A typical variation in the nonlinearized mean voltage output with angle of rotation, λ, (see fig. 7) is shown in figure 8. This bell-shaped curve is symmetrical around $\lambda = \theta$, in which case the wire is normal to the local mean velocity vector and, thus, normal to the s axis. This symmetry was used to evaluate θ as described in detail in reference 5.

The variation in the nonlinearized output voltage E with the effective velocity U_{eff}, as expressed in functional form by equation (1), was determined experimentally using a pitot-static pressure probe to evaluate U_{eff}. These tests were conducted in the freestream (i.e., $U_{eff} = V_\infty$) where the effect of turbulence is negligible. The hot-wire was oriented normal to the freestream flow. Typical calibration results for the horizontal wire are shown in figure 9(a). The linear relation between velocity and voltage, as given by equation (4), was obtained by fitting the nonlinear calibration data (e.g., the calibration data of figure 9(a)) to the fourth-degree polynomial

$$U_{eff} = a_1(E - E_o) + a_2(E - E_o)^2 + a_3(E - E_o)^3 + a_4(E - E_o)^4 \qquad (20)$$

where E_o is the output voltage with $U_{eff} = 0$. The coefficients a_1, a_2, a_3, and a_4 were determined by a least-squares fit to the calibration data. The operations on the right-hand side of equation (20), for given values of the coefficients and E_o, were performed by the hot-wire linearizer. This electrical analog circuitry, with an input voltage E, outputs a voltage given by

$$E_\ell/S = a_1(E - E_o) + a_2(E - E_o)^2 + a_3(E - E_o)^3 + a_4(E - E_o)^4$$

in accordance with equation (4). The constant S was selected so as to yield a convenient

numerical relationship between E_ℓ and U_{eff} (ref. 5). Figure 9(b) shows the linearized form of the calibration data of figure 9(a). Typically, the velocities are within $\pm$ 0.5% of the straight line approximation for the range of velocities covered herein. Calibrations were made periodically during the tests to assure that accuracy was maintained (i.e., periodic corrections were made to account for drifts in the wire and electronics).

The binormal velocity coefficient, h, in equation (2) may differ from 1.0 because of wire asymmetries and the effects of the needles and needle support. The effect of the needles was calculated to be small. The needle support was outside the flow field in the present investigation and, therefore, could have no effect. Furthermore, several tests in the freestream were carried out with each wire where the flow was normal to the wire but at two angular orientations 180° apart (i.e., using opposite sides of the wire). Any differences were within data scatter. Therefore, for these investigations the coefficient h has been taken to be unity.

The tangential velocity coefficients, k, for the horizontal and slant wire were determined by testing the wires in the uniform freestream at several yaw angles λ. The magnitude of k was evaluated by least squares fitting the date to the equation

$$U_{eff}^2 = U_N^2 + k^2 U_T^2 + U_{BN}^2$$

From these tests it was determined that for the horizontal wire ($\alpha = 0$)

$$k^2 = 0.025$$

and for the slant wire ($\alpha = 47.3$)

$$k^2 = 0.055$$

Transformation to Laboratory Coordinates

The hot-wire coordinate system rotates with the mean flow velocity vector and, therefore, with respect to the fixed laboratory Cartesian coordinate system as shown in figure 7. For theoretical analysis, it is usually convenient to work in the fixed laboratory coordinates. Therefore, the results expressed in the hot-wire coordinates

have been transformed to the laboratory coordinates for all data presentations. This is accomplished by using the tensor transformations for Cartesian coordinate rotation.

For convenience, let the hot-wire coordinates be represented by x'_i where i = 1,2,3 and the laboratory coordinates be represented by x_j where j = 1,2,3 so that

$$x'_1 = s, \quad x'_2 = y, \quad x'_3 = n$$

and

$$x_1 = x, \quad x_2 = y, \quad x_3 = z.$$

The corresponding coordinate systems are shown in figure 10. Rotation is about the $x_2 = x'_2 = y$ axis. Using conventional index notation, the general form for the vector transformation is

$$V_p = \ell_{ip} V'_i \tag{21}$$

where the indices i and p take on values 1, 2, and 3, V'_i is the i component of the vector in the hot-wire coordinates (x'_i), V_p is the i component of the vector in the laboratory coordinates (x_i), and ℓ_{ip} is the direction cosine or the cosine of the angle between x'_i and x_p. The local velocity components V'_i are related to those used in the previous equations by the identities

$$V'_1 \equiv U_s, \quad V'_2 \equiv U_y, \quad V'_3 \equiv 0 \tag{22}$$

The local velocity components V_p are related to those used in the data presentations by the identities

$$V_1 \equiv U_x, \quad V_2 \equiv U_y, \quad V_3 \equiv U_z \tag{23}$$

These relationships are also indicated in figure 10.

The general form for the second order tensor transformation for the x'_i and x_j coordinates is

$$T_{pq} = \ell_{ip} \ell_{jq} T'_{ij} \tag{24}$$

where T'_{ij} is the ij component of the tensor in the hot-wire coordinates, and T_{pq} is the pq component of the tensor in the laboratory coordinates. The six components of each of these symmetric tensors are related to those used in the previous equations and those used in the data presentations by the identities

$$T'_{ij} \equiv \begin{bmatrix} \overline{u_s^2} & \overline{u_s u_y} & \overline{u_s u_n} \\ \overline{u_s u_y} & \overline{u_y^2} & \overline{u_y u_n} \\ \overline{u_s u_n} & \overline{u_y u_n} & \overline{u_n^2} \end{bmatrix} \tag{25}$$

and

$$T_{pq} \equiv \begin{bmatrix} \overline{u_x^2} & \overline{u_x u_y} & \overline{u_x u_z} \\ \overline{u_x u_y} & \overline{u_y^2} & \overline{u_y u_z} \\ \overline{u_x u_z} & \overline{u_y u_z} & \overline{u_z^2} \end{bmatrix} \tag{26}$$

respectively.

RESULTS AND DISCUSSION

The experimental results as presented in tabular form are discussed first, followed by a description of the general flow features taken from vector and velocity contour plots. Next, representative results at the various streamwise stations are presented in graphical form and discussed. This section concludes with a presentation of selected results at three streamwise stations which is in the form of composite plots. These plots are intended to be examined as an array so as to bring out the relative behavior of the various quantities.

Tabulated Results

The primary aim of this experimental investigation was to determine measured values of the mean velocity components U_x, U_y, and U_z and the turbulence quantities u'_x, u'_y, u'_z, $\overline{u_x u_y}$, $\overline{u_y u_z}$, and $\overline{u_x u_z}$ at selected locations ahead of and around the nose of the constant thickness body. These values are given in Tables 1-4. Although all of the measured values of the nine quantities are presented in these tables, the data taken in certain areas of the separated region must be considered to be qualitative only. This is because the turbulence level is high within these areas while at the same time the mean velocity is low. As detailed in the previous section, the data were analyzed and the desired quantities were extracted by simultaneously solving a system of equations which had been derived using the usual assumption that third and higher order terms are negligible (eqns. 18, 19). While such an assumption yields good accuracy for usual two-dimensional turbulent boundary layers and for the shear flow in the juncture itself (ref. 5), it can result in serious errors for higher turbulence intensities such as those encountered here in some areas of the separated region. Without further analysis, it is not possible to specify a criterion to denote those values in the tables which should be considered qualitative due to the limitations of the data analysis. In jet flows, Bradshaw (ref. 12) suggests that when the local turbulent intensity reaches 0.30 the correlations become uncertain.

General Flow Features

The thin boundary layer on the flat plate upstream of the bluff body is skewed into a three-dimensional flow due to lateral pressure gradients imposed on the boundary layer as the flow decelerates. Also, very close to the leading edge of the bluff body the steep adverse static pressure gradients cause the boundary layer to separate and create a strong concentrated three-dimensional viscous flow. The extent of the separated region for the present experiments was determined by flow visualization using a film of oil on the plate surface. The resulting photograph is shown in figure 11. Superimposed on the photograph are lines denoting the location of the vertical plane of symmetry $z = -29.0$ mm (- 1.14 in.), the plane of the body surface $z = 0$, and the location of two of the four streamwise measurement stations.

Vector plots of the mean velocity component in the $y - z$ plane at the four

streamwise stations (plus two more taken from ref. 5) are given in figure 12. This figure presents a view looking downstream. Mean velocity vectors in the x - y plane of symmetry are shown in figure 13.

Figures 12(a) and 12(b) indicate that the flow is symmetrical in that, in the plane of symmetry, z = - 29.0 mm (- 1.14 in.), the z component of mean velocity is very small and random in direction within the accuracy of measurement. At the furthest upstream measurement station, shown in figure 12(a), the oncoming boundary layer has already sensed the presence of the body and is beginning to skew. Surprisingly, there is a significant skewing of the two-dimensional boundary layer at least out to z = 152.4 mm (6.0 in.) or 2.6 body widths. This skewing at the outermost measurement station is greater at x = - 38 mm (fig. 12(b)). However, downstream of the body leading edge (fig. 12(d)) the juncture flow is very compact so that at z = 152.4 mm (6.0 in.) the boundary layer is essentially two-dimensional.

Between the plane of the body surface, z = 0, and the plane of symmetry, the character of the flow has changed dramatically by x = - 11 mm (- 0.44 in.), as illustrated in figure 12(c). In the plane of symmetry, the flow is directed downward until very near the plate where it reverses direction upward. This is also seen in figure 13, which shows flow reversal and, thus, separation. At larger values of z there is a significant downflow in the outer portion of the separated region and a small upflow near the plate surface. At z = 0 the boundary layer is skewed and essentially parallel with the surface of the flat plate.

Downstream of the leading edge of the body (fig. 12(d)), the vortex which has rolled up as a result of the separation has turned and is trailing downstream. The data coverage around the leading edge was not dense enough to allow the plotting of vectors in radial planes centered at the origin of the elliptical leading edge, so it is not possible to illustrate the details of this roll-up history.

The secondary flow vortex weakens and diffuses downstream in the juncture (figs. 12(d), (e), (f)). Also, the effective core of the vortex continually moves away from the surface of the body. Using these three vector plots it is estimated that the core is located above the plate at a value of y = 9.0 mm (0.35 in.) at the first two stations in the juncture and then trails upward to y = 17.8 mm (0.70 in.).

Vector plots of the velocity component in the vertical, x - y,plane of symmetry are shown in figure 13. At the furthest upstream station, the velocity profile is less full than for a normal two-dimensional flat-plate turbulent boundary layer, indicating that

the profile is being influenced by the adverse pressure gradient due to the blockage of the body. This behavior is more pronounced at x = - 38 mm (- 1.5 in.) but there is no evidence of flow reversal. Flow reversal has occurred at the measurement station closest to the leading edge of the body. In the region above the reversed flow, the velocity vectors are inclined downward. Apparently this is a manifestation of the impending reattachment and thinning of the shear layer as the boundary layer is swept laterally by the favorable pressure gradients which are created due to the flow around the nose of the body.

The flow features in the vector plots just discussed can be explored further by inspection of graphs of contours of constant mean streamwise velocity, U_x. These graphs were constructed at the four streamwise measurements stations and are shown in figure 14. Two additional station in the juncture, taken from reference 5, are included in the figure. The deceleration of the oncoming boundary layer at the most upstream station (fig. 14(a)), due to the blockage of the body, is evident. This behavior accentuates and broadens (fig. 14(b)) as the body is approached. Very near the body (fig. 14(c)) there is a large region of low streamwise momentum bounding the separation zone, and the shear layer does not exhibit velocity contours which are parallel to the plate surface until a distance in excess of the half-width of the body away from the vertical plane of symmetry. In the juncture itself (fig. 14(d)) the constant velocity contours exhibit the same behavior as noted previously in reference 5. Namely, the counterclockwise (looking downstream) secondary flow transports high velocity fluid toward the plate near the body surface and low velocity fluid upward and away from the plate surface further outboard (figs. 14(e), (f)).

Skewing in the Viscous Layer

The skewing of the oncoming two-dimensional turbulent boundary layer due to the pressure gradients induced by flow around the body can be seen in figure 15, which shows the variation of the local mean flow direction, θ , with distance above the flat plate as a function of z at the four x stations. A positive value of θ signifies a local flow direction away from the body, while a negative θ denotes flow directed toward the body.

As pointed out in discussing the vector plots, the flow displays symmetry about the centerline vertical plane, z = - 29.0 mm (- 1.14 in.), as seen in figures 15(a) and

15(c). At the most upstream station (x = - 102 mm), the maximum skew angle of 6° occurs near the plate surface at z = 50.8 mm (2.0 in.). Nearer to the body (figs. 15(b), (c)) the viscous layer near the plate surface skews to an angle of 30° at z = 0 and to a lesser angle for other values of z. Figures 15(d) and (e) show that at x = 11 mm (- 0.44 in.) the velocity outside the plane of the body surface (z = 0) exhibits large skewing near the plate surface. Inboard of this, z < 0, the local skew angles near the plate surface are in excess of 90°. This implies that the flow has reversed in the lower portions of the separated region ahead of the body. However, in this separated region there is substantial lateral flow as indicated by the fact that $\theta < 180^{\circ}$. Finally, in the juncture itself (fig. 15(f)) the skew angles are moderate, with the mean flow being directed toward the body at the outer edge of the viscous region and away from the body near the plate surface. This is the same behavior noted previously (ref. 5) at survey stations further downstream in the juncture.

Mean Velocities and Reynolds Stresses

Comparisons of the mean velocity components U_x, U_y, and U_z and of the six turbulence stresses with varying z are shown in figures 16 through 19 as a function of distance above the plate at the four streamwise measurement stations.

The deceleration of the oncoming boundary layer at the most upstream station x = - 102 mm (- 4.0 in.) near the vertical plane of symmetry (fig. 16(a)) has been pointed out previously, as has the skewing (figs. 16(b), (c)). The magnitude and distribution of the turbulent normal and shear stresses (figs. 16(d) through 16(i)) are very similar to those in a comparable two-dimensional turbulent boundary layer with the exception of $\overline{u_y u_z}$ (fig. 16(i)). For a two-dimensional turbulent boundary layer, $\overline{u_x u_z}$ and $\overline{u_y u_z}$ would be zero. Since the boundary layer at this upstream station is starting to skew and to become three-dimensional, these shear stresses would not be expected to have their two-dimensional (i.e., zero) values. However, because of symmetry one would expect the values of both $\overline{u_x u_z}$ and $\overline{u_y u_z}$ to be zero in the x - y symmetry plane z = - 29.0 mm (- 1.14 in.). This is true for $\overline{u_x u_z}$ at both x = - 102 mm and x = - 38 mm, but inspection of figure 16(i), and also of the tabulated data at x = - 38 mm, z = 29.0 mm, shows that this is not the case for $\overline{u_y u_z}$. There are two possible reasons for this. One is that the flow is not symmetrical, yet the mean flow quantities indicate symmetry as has been discussed. The second and more likely reason is inaccuracy in the

determination of $\overline{u_y u_z}$. As was noted in reference 5, this turbulent shear stress is the most difficult to measure, and care was taken (Appendix C, ref. 5) to choose suitable orientations of the hot wires so as to minimize the uncertainty in the determination of this shear stress. While the scatter in $\overline{u_y u_z}$ was worse than that in the other measured quantities in reference 5, the value of $\overline{u_y u_z}$ was very small at the greatest distance away from the body juncture (where the flow was effectively two-dimensional) and $\overline{u_y u_z}$ varied in the expected manner as the body surface was approached. The present results for $\overline{u_y u_z}$ at $x = -102$ mm (- 4.0 in.) in the plane of symmetry suggest that the uncertainties in the quantity are larger than those experienced in reference 5. While errors in $\overline{u_y u_z}$ at measuring stations near the body leading edge at or near the plane of symmetry can be attributed to high turbulent intensity, this would not explain the unexpectedly large values of $\overline{u_y u_z}$ in the plane of symmetry at the furthest upstream measurement station. The maximum allowable distance from the first measuring station to the body leading edge was constrained by interference between the actuator (which hung beneath the plate) and the tunnel outflow between the plate and the floor of the wind tunnel. Thus, it was not possible to make measurements in the undisturbed oncoming boundary layer.

As seen in figures 17(a) - (c), the mean flow measurements at $x = -38$ mm (- 1.5 in.) give no evidence of flow separation. The boundary layer is decelerated and thickened in the vicinity of the body, with relatively little skewing. The maximum skew angle occurs outboard of the vertical plane containing the body surface (i.e., $z = 12.7$ mm, fig. 17(c)). Inboard of this plane, the turbulent normal stresses have essentially the same magnitude and distribution as at the station further upstream with the exception of u'_x (fig. 17(d)), which has changed because of retardation near the wall and transport of turbulence away from the wall layer, giving rise to a peak in the observed u'_x distribution.

The results at the third streamwise measurement station $x = -11$ mm (- 0.44 in.), shown in figure 18, are all for positive values of z, that is, for transverse locations outboard of the plane of the body surface. The hot-wire measurements within the separated region are discussed in the next section. Outside of the plane of the body, the mean flow profiles show that, near the body, the boundary layer is thickened (fig. 18(a)) and there is a significant down-flow velocity component (fig. 18(b)) and the skewing component (fig. 18(c)) becomes very large. Regarding the turbulence stresses, the turbulent normal stresses outside of the separated region have changed slightly in

response to the retardation and transportation of fluid.

The measurements in the juncture downstream of the leading edge at x = 76 mm (3.0 in.) are presented in figure 19. The profiles of the x - component of mean velocity (fig. 19(a)) show that at small values of z (near the body surface) the profiles are fuller than those for the essentially undisturbed two-dimensional boundary layer, z = 152.4 mm (6.0 in.), indicating that high momentum fluid from near the outer edge of the shear layer is being transported to the vicinity of the plate surface by the action of the secondary flow vortex. Near the effective core of the vortex, the U_x profile is highly distorted. The counterclockwise sense of the secondary flow is evident by the sign change of U_y as z decreases in figure 19(b) and also by the sign change of U_z as y increases in figure 19(c). Plots of the turbulent normal stresses in the juncture (figs. 19(d), (e), (f)) again point up one of the conclusions in reference 5, namely that the secondary flow redistributes the turbulence as well as modifying the mean flow. Near the effective core of the secondary flow vortex, the profiles of turbulent normal stress are highly distorted. The profiles of turbulent shear stress shown in figures 19(g) - (i) also show the pronounced effect of the secondary flow vortex. These profiles are similar in character to those observed further downstream in the juncture (ref. 5), with the added feature that, very close to the body, the turbulent shear stress $\overline{u_x u_z}$ is significantly larger near the plate surface.

Flow in the Separated Region

As noted previously, there is a separated region upstream of the leading edge of the body; the extent of this region in the vicinity of the plate surface has been illustrated in figure 11.

There are two difficulties inherent in making hot-wire measurements in such a separated region. The first is the problem of encountering larger turbulent fluctuations in areas where the mean velocity is simultaneously small. An example of this is illustrated in figure 20, which shows the variation of u'_x and U_x versus y in the plane of symmetry at x = - 11 mm (- 0.44 in.). At approximately y = 2.5 mm (0.1 in.) the turbulent normal stress, u'_x, is significant while the streamwise mean flow velocity component is small and becomes zero as the flow reverses. In areas such as this within the separated flow region, the truncated series expansion method used here to derive the equations for data analysis becomes inaccurate and the results within these areas

become qualitative because u'_x/U_x is so large as $U_x \to 0$. This was pointed out earlier in the caution which was given regarding the accuracy of some of the values in Tables 1 - 4. In addition to the shortcomings of the data reduction method, there are also unanswered questions regarding the use of hot-wire steady-flow calibration curves (fig. 9) in an environment where the mean flow is slow or zero and the wire is responding primarily to large oscillating turbulent fluctuations.

The second major problem experienced in making hot-wire measurements in a separated, reversed-flow, region is the ambiguity of the results because of the inability of the hot-wire to distinguish between a flow from a given direction and one 180° from that direction. The introduction to this report describes the "marching" technique employed here which eliminated this ambiguity. As was noted, data may be taken by "marching" in y at constant z or in z at constant y.

An example of the results obtained by "marching" in y from the outer edge of the separated region toward the surface of the flat plate is shown in figures 21 and 22 at threes constant values of z. Referring to figure 21, the flow near the plate surface skews outward with an angle of about 60° at z = 0, which corresponds to the plane of the body surface. Inboard of this location, at z = - 15.2 mm (- 0.6 in.), the skew angle near the plate surface has reached 90°, that is, the flow has turned outward at right flow near the plate surface has reversed direction. This same behavior is indicated in the values of U_x/V_∞ (fig. 22(a)), where a negative value of the streamwise mean velocity component denotes a reversed flow. Indications of flow reversal also are evident in the variations of U_y (fig. 22(b)), which reverses direction in the free shear layer, and in the variations of U_z (fig. 22(c)) which, along with the U_x data, imply skewing of the boundary layer.

Figures 22(d) - (i) show the behavior of the turbulent normal and shear stresses within the separated flow region. Notice the large values on the ordinates of these six figures, and particularly on the last three. It is emphasized that the results presented for the turbulence stresses at $y < 5$ mm ($y < 0.20$ in.) must be considered to be questionable for reasons already discussed. These results are included in figure 22 (and also in the tables) for completeness and because no criteria were established for data rejection. However, the normal stresses in the separation region are large as they must be, and likewise the shear stresses. By the time y has reached a value of approximately 10 mm (0.39 in.), the turbulence stresses in figures 22(d) - (i) have magnitudes that are reasonable.

Results obtained by the alternative "marching" scheme, namely "marching" in z at constant y, are presented in Table 5 and are shown in figure 23, where the skew angle of the flow is plotted versus z for various fixed values of y. Figure 23(a) gives the results obtained at x = -38 mm (- 1.5 in.). It will be recalled that the data presented earlier showed no flow reversal at this streamwise measurement station. This is reinforced in figure 23(a). Note that, at all values of y from 0.5 mm (0.02 in.) above the plate surface to the outer edge of the region, the maximum skew angle is less than 30°, confirming the absence of flow reversal. The quality of the data and of the flow is evidenced by the magnitude of the measured mean flow angle (ideally zero) in the vertical plane of symmetry at z = - 29.0 mm (- 1.14 in.) and by the symmetry of the results with respect to this plane. Figure 23(b), which shows results for x = - 11 mm (- 0.44 in.), clearly indicates reversed flow near the plate surface within a transverse distance from approximately z = - 15.2 mm (- 0.60 in.) to the vertical plane of symmetry. The surveys at the three largest values of y shown that the maximum skew angle is about 50° as the flow turns around the body in the outer part of the viscous region. However, the surveys at the three smallest values of y, namely $y \leq 2$ mm ($\leq$ 0.08 in.), indicate a completely different behavior. At approximately z = - 15.2 mm (- 0.60 in.) the flow has turned through an angle of 90°, or at right angles to its original direction. In the plane of symmetry, z = - 29.0 mm (- 1.14 in.), the flow angle is 180°, meaning that the flow is completely reversed. For larger negative values of z, the angle is greater than 180°, implying symmetry about z = - 29.0 mm (- 1.14 in.). Again, note the quality of the data in that the results pass through either 0° or 180° in the vertical plane of symmetry.

Besides providing insight into the details of the separated flow within and near the area of reversed flow, figures 22 and 23 confirm that the "marching" technique can be used in a reversed flow to determine flow direction. It must be noted that this "marching" technique cannot be used in a two-dimensional reversed-flow region, as, for example, in a backward-facing step. When "marching" downward in y the instantaneous flow reversal cannot be detected. It was possible to get data for the present experiment in the plane of symmetry (z = - 29.0 mm) because of the three-dimensional character of the flow in the separated region away from the plane of symmetry, which allowed the flow behavior at z = - 29.0 mm to be deduced as the plane of symmetry was approached. Thus, the "marching" technique is applicable only in a three-dimensional reversed-flow situation.

Composite Graphs

A summary of the behavior of the flow ahead and just downstream of the leading edge of the blunt body is presented in figure 24, 25, and 26. These graphs are intended to illustrate trends and relative behavior among the various quantities. At x = - 102 mm (-.4.0 in.) the mean flow and turbulence quantities are nearly those of a two-dimensional boundary layer and show small variation with z. Accordingly, the results at this most upstream station are not presented in composite form. These composite graphs show that the measured quantities vary in a significant and consistent manner.

CONCLUDING REMARKS

Hot-wire measurements carried out upstream of and near the beginning of a juncture formed by a flat plate and a body of constant thickness having a 1.5:1 elliptical leading edge have led to results from which the following conclusions may be drawn.

1. At 1.75 body widths upstream of the nose of the body the oncoming turbulent boundary layer is affected by the presence of the body, with significant skewing out to at least 2.6 body widths away from the vertical plane of symmetry.
2. At 0.66 body widths upstream of the nose there is no flow reversal but the maximum skew angle near the plate surface has increased to about 30°.
3. At 0.19 body widths upstream of the nose the flow near the plate surface has turned through an angle of 90° or greater with respect to its undisturbed direction over a distance outward from the vertical plane of symmetry to about one-quarter the width of the body.
4. In the juncture 1.3 body widths downstream of the nose the secondary flow vortex is tightly rolled up with the effective core being located about 0.4 body widths away from the body surface. This distance from the surface increases slowly with increasing downstream travel in the juncture, while at the same time the vortex weakens and diffuses.
5. The magnitude and distribution of the turbulent normal and shear stresses in the boundary layer upstream of the body nose and outside of the separated region are much like those for a two-dimensional turbulent boundary layer. Near the body leading edge the indicated turbulence level is high.

6. The secondary flow vortex observed in the juncture just downstream of the body leading edge transports turbulence toward and away from the plate surface in the same manner as previously observed further downstream in the juncture.
7. The "marching" technique of data acquisition employed here can be used in a reversed flow to indicate flow direction.

APPENDIX A

ERROR ANALYSIS

An important aspect of the presentation of experimental results is the inclusion of an estimate of uncertainties in the measured quantities. In this appendix, a list of possible sources of error that were encountered during the course of the experiments is given. This is followed by a simple error analysis to calculate the uncertainties present in the various experimental results.

Error Sources

Freestream Velocity. The tunnel flow velocity was in error by less than $\pm$ 0.5%. This error influenced the results as an uncertainty in the mean voltage both during hot-wire calibration and during data acquisition.

Hot-Wire Probe. There was no interference error from the probe support since it was located outside the flow field. The blockage effect of the hot-wire needles was automatically taken care of when measurements were carried out with the orientation of the needles corresponding to that of the hot-wire calibration. It was not possible to calculate the blockage effect when the measurement orientations were different from that of the hot-wire calibration.

Hot-Wire Anemometer. The anemometer output drift due to changes in the temperature of the wind tunnel air was compensated for by the use of a correction procedure which introduced a maximum error of $\pm$ 0.5% in the mean voltage output and negligible error in the RMS voltage. The signal linearizer has an accuracy of $\pm$ 0.5% in curve-fitting the calibration curves. This leads to an error of the same magnitude in the mean voltage.

RMS Voltmeter. The true RMS voltmeter used in the present work has an AC-to-DC converter accuracy of $\pm$ 5% in the frequency range of 10 Hz to 50 Hz and $\pm$ 0.75% in the range of 50 Hz to 1 MHz. In an energy spectrum of the hot-wire signal corresponding to a typical hot-wire orientation, the contribution from the frequencies less than 50 Hz is about 25%. This results in an average error of about $\pm$ 1.8% in the RMS voltage output which in turn affects the accuracy of all of the turbulence stresses.

Integrating Digital Voltmeter. The voltmeter used here is a high precision instrument whose accuracy is in the microvolts range.

The Data Reduction Scheme. As explained in the main text, a linear analysis was used to interpret the hot-wire output voltages. In this procedure, terms involving products of various turbulence quantities as well as triple and higher order correlations were neglected. This truncation error enters the data reduction method as an uncertainty in the effective cooling velocity. This uncertainty can normally be neglected if the ratio of the mean velocity to the turbulence level is high. This was true for most of the flow field excluding a small region very close to the flat plate surface where the turbulence level was high, and the region of reversed flow immediately upstream of the body leading edge where the turbulence level was high and the flow velocity was small.

Estimation of Uncertainties

The inaccuracies involved in the measurements of the mean voltages (about 1%) and the RMS voltages (about 1.8%) were introduced into the equations used for data reduction in order to calculate the uncertainties in the reduced results. To keep this error analysis simple, the wire angles (α and ψ) and the hot-wire sentitivity coefficients (h and k) were not treated as variables. Using the general rules of error propagation the following estimates were obtained.

Uncertainty in U_s and U_y	-	about 1%
Uncertainty in u'_s	-	about 2%
Uncertainty in u'_y and u'_n	-	about 4%
Uncertainty in $\overline{u_s u_y}$ and $\overline{u_s u_n}$	-	about 2%
Uncertainty in $\overline{u_y u_n}$	-	about 3%

In regions where the turbulence level is high, there will be larger uncertainties in the results.

REFERENCES

1. Baker, A. J., Manhardt, P. D., and Orzechowski, J. A., "Numerical Prediction of Turbulent Three-Dimensional Juncture Region Flow Using a Parabolic Navier Stokes Equation", NASA CR-159024, March, 1979.

2. Baker, A. J., "The CMC:3DPNS Computer Program for Prediction of Three-Dimensional, Subsonic, Turbulent Aerodynamic Juncture Region Flow. Volume I-Theoretical", NASA CR-3645, 1982.

3. Shabaka, I. M. M. A., "Turbulent Flow in an Idealized Wing-Body Junction", Ph.D. Thesis, Imperial College, London, April, 1979.

4. Shabaka, I. M. M. A., and Bradshaw, P., "Turbulent Flow in an Idealized Wing-Body Junction", AIAA Journal, Vol. 19, No. 12, February, 1981.

5. McMahon, H., Hubbartt, J., and Kubendran, L., "Mean Velocities and Reynolds Stresses in a Juncture Flow", NASA CR-3605, 1982.

6. Hornung, H. G., and Joubert, P. N., "The Mean Velocity Profile in Three-Dimensional Turbulent Boundary Layers", JFM Vol. 15, 1963, pp. 368-384.

7. East, L. F., and Hoxey, R. P., "Low Speed Three-Dimensional Turbulent Boundary-Layer Data". Parts 1 and 2, R. & M. No. 3653, British A. R. C., 1971.

8. Peake, D. J., Rainbird, W. J., and Atraghji, E. G., "Three-Dimensional Flow Separation on Aircraft and Missiles", AIAA J., Vol. 10, No. 5, May 1972, pp. 567-581.

9. Briley, W. R., and McDonald, H., "Computation of Three-Dimensional Horseshoe Vortex Flow using the Navier Stokes Equations", 7th International Conference on Numerical Methods in Fluid Dynamics, June, 1980.

10. Oguz, E. A., "An Experimental Investigation of the Turbulent Flow in the Junction of a Flat Plate and a Body of Constant Thickness", Ph.D. Thesis, Georgia Institute of Technology, 1981.

11. Jorgensen, F. E., "Directional Sensitivity of Wire and Fiber-Film Probes", DISA Information Bulletin No. 11, 1971, pp. 31-37.

12. Bradshaw, P., An Introduction to Turbulence and its Measurement, Pergamon Press, 1971.

Table 1

Mean velocities and turbulence stresses upstream of the juncture (x = - 102 mm).

z (mm)	y (mm)	y (in.)	$\frac{U_x}{V_\infty}$	$\frac{U_y}{V_\infty}$	$\frac{U_z}{V_\infty}$	$\frac{u'_x}{V_\infty}$	$\frac{u'_y}{V_\infty}$	$\frac{u'_z}{V_\infty}$	$-\frac{\overline{u_x u_y}}{V_\infty^2}\times 10^4$	$-\frac{\overline{u_x u_z}}{V_\infty^2}\times 10^4$	$-\frac{\overline{u_y u_z}}{V_\infty^2}\times 10^4$
152.4	.5	.02	.49	-	.033	.089	-	.051	-	-2.2	-
	.8	.03	.54	-	.033	.084	-	.051	-	-1.2	-
	1.0	.04	.57	-	.039	.080	-	.050	-	-1.3	-
	1.3	.05	.60	-	.042	.076	-	.053	-	-.5	-
	1.5	.06	.61	-	.045	.075	-	.051	-	-.9	-
	1.8	.07	.63	-	.037	.073	-	.052	-	-.6	-
	2.0	.08	.64	-	.034	.073	-	.050	-	.2	-
	2.3	.09	.65	.007	.042	.072	.053	.050	15.2	-.6	3.9
	2.5	.10	.66	.001	.040	.071	.054	.050	15.7	-.0	6.0
	3.8	.15	.70	.004	.042	.067	.056	.050	15.0	-.4	6.5
	5.1	.20	.74	.001	.034	.066	.055	.047	15.5	.2	4.4
	6.4	.25	.78	.001	.033	.063	.052	.049	13.5	-.1	5.9
	7.6	.30	.80	.004	.030	.061	.051	.048	12.9	.6	7.1
	8.9	.35	.83	.003	.040	.059	.047	.046	11.8	.1	6.5
	10.2	.40	.85	.003	.027	.056	.047	.045	10.9	.6	5.8
	11.4	.45	.87	.006	.030	.053	.045	.044	10.1	.5	3.6
	12.7	.50	.89	.005	.037	.050	.044	.042	8.7	.4	5.6
	15.2	.60	.93	.010	.026	.044	.039	.036	6.6	.3	1.5
	17.8	.70	.95	.006	.022	.037	.034	.028	4.4	.2	3.9
	20.3	.80	.97	.010	.032	.026	.030	.021	2.2	.1	.6
	22.9	.90	.99	.008	.031	.018	.023	.015	1.1	.2	1.6
	25.4	1.00	1.00	.015	.028	.012	.015	.010	.2	.0	.3
	27.9	1.10	1.00	.010	.028	.010	.011	.006	-.2	.0	.3
	33.0	1.30	1.00	-	.026	.007	-	.005	-	-.0	-

Table 1. - Continued.

z (mm)	y (mm)	y (in.)	$\frac{U_x}{V_\infty}$	$\frac{U_y}{V_\infty}$	$\frac{U_z}{V_\infty}$	$\frac{u'_x}{V_\infty}$	$\frac{u'_y}{V_\infty}$	$\frac{u'_z}{V_\infty}$	$-\frac{\overline{u_x u_y}}{V_\infty^2}\times 10^4$	$-\frac{\overline{u_x u_z}}{V_\infty^2}\times 10^4$	$-\frac{\overline{u_y u_z}}{V_\infty^2}\times 10^4$
101.6	.5	.02	.47	-	.042	.088	-	.050	-	-3.3	-
	.8	.03	.52	-	.046	.083	-	.052	-	-2.0	-
	1.0	.04	.55	-	.049	.079	-	.051	-	-.8	-
	1.3	.05	.57	-	.049	.076	-	.051	-	-.1	-
	1.5	.06	.59	-	.049	.074	-	.051	-	-.5	-
	1.8	.07	.61	-	.055	.073	-	.051	-	-.4	-
	2.0	.08	.62	-	.049	.073	-	.049	-	.3	-
	2.3	.09	.62	.005	.046	.071	.051	.051	15.6	-.0	3.1
	2.5	.10	.64	.003	.054	.071	.049	.049	15.1	-.6	7.2
	3.8	.15	.68	-.001	.043	.068	.051	.049	14.6	.4	6.1
	5.1	.20	.71	.001	.035	.066	.052	.048	14.6	.4	4.8
	6.4	.25	.74	.003	.035	.064	.049	.049	13.3	.8	3.0
	7.6	.30	.77	.001	.039	.063	.047	.046	12.7	.4	5.4
	8.9	.35	.80	.004	.032	.059	.047	.048	12.1	.9	4.0
	10.2	.40	.82	.004	.042	.057	.045	.046	11.4	.8	6.3
	11.4	.45	.85	.002	.040	.055	.042	.044	10.0	.9	6.5
	12.7	.50	.87	.003	.039	.052	.041	.042	8.9	.8	5.1
	15.2	.60	.91	.006	.041	.045	.034	.037	6.3	.6	2.3
	17.8	.70	.94	.004	.028	.037	.029	.030	4.1	.6	4.6
	20.3	.80	.96	.002	.022	.026	.020	.024	1.3	.6	1.7
	22.9	.90	.98	.002	.031	.017	.015	.013	.3	-.0	.8
	25.4	1.00	.98	.004	.022	.012	.012	.009	-.2	.1	.3
	27.9	1.10	.99	.006	.036	.010	.009	.006	-.4	.0	.2
	33.0	1.30	.98	-	.027	.008	-	.006	-	.0	-

Table 1. - Continued.

z (mm)	y (mm)	y (in.)	$\frac{U_x}{V_\infty}$	$\frac{U_y}{V_\infty}$	$\frac{U_z}{V_\infty}$	$\frac{u'_x}{V_\infty}$	$\frac{u'_y}{V_\infty}$	$\frac{u'_z}{V_\infty}$	$-\frac{\overline{u_x u_y}}{V_\infty^2} \times 10^4$	$-\frac{\overline{u_x u_z}}{V_\infty^2} \times 10^4$	$-\frac{\overline{u_y u_z}}{V_\infty^2} \times 10^4$
50.8	.5	.02	.44	-	.042	.087	-	.049	-	-3.3	-
	.8	.03	.49	-	.051	.083	-	.052	-	-2.6	-
	1.0	.04	.52	-	.049	.079	-	.051	-	-1.8	-
	1.3	.05	.54	-	.046	.077	-	.052	-	-.7	-
	1.5	.06	.56	-	.045	.075	-	.052	-	-.2	-
	1.8	.07	.57	-	.046	.074	-	.050	-	.4	-
	2.0	.08	.58	-	.044	.073	-	.051	-	-.1	-
	2.3	.09	.59	.010	.052	.074	.048	.050	14.4	-.2	2.9
	2.5	.10	.60	.011	.045	.073	.048	.050	15.0	-.1	1.9
	3.8	.15	.65	.007	.048	.071	.048	.049	14.8	.4	3.5
	5.1	.20	.68	.011	.043	.068	.049	.049	14.5	.4	2.2
	6.4	.25	.72	.008	.044	.067	.046	.050	13.4	1.0	5.1
	7.6	.30	.75	.008	.034	.064	.047	.049	13.8	.4	1.9
	8.9	.35	.77	.010	.028	.063	.044	.048	12.5	1.0	4.8
	10.2	.40	.80	.011	.028	.060	.042	.048	11.3	.8	3.3
	11.4	.45	.82	.011	.026	.057	.041	.046	10.2	.6	4.1
	12.7	.50	.84	.014	.028	.055	.038	.044	9.1	.8	3.5
	15.2	.60	.87	.008	.030	.049	.034	.039	6.8	.7	3.8
	17.8	.70	.90	.008	.033	.042	.031	.033	4.2	.6	2.5
	20.3	.80	.93	.013	.024	.034	.027	.026	1.9	.3	3.1
	22.9	.90	.95	.007	.035	.024	.021	.018	-.1	.1	1.3
	25.4	1.00	.96	.008	.027	.016	.019	.012	-.5	.2	-.1
	27.9	1.10	.96	.010	.037	.013	.016	.007	-.8	-.0	-.0
▼	33.0	1.30	.97	-	.027	.011	-	.006	-	.0	-

Table 1. - Continued.

z (mm)	y (mm)	y (in.)	$\frac{U_x}{V_\infty}$	$\frac{U_y}{V_\infty}$	$\frac{U_z}{V_\infty}$	$\frac{u'_x}{V_\infty}$	$\frac{u'_y}{V_\infty}$	$\frac{u'_z}{V_\infty}$	$-\frac{\overline{u_x u_y}}{V_\infty^2} \times 10^4$	$-\frac{\overline{u_x u_z}}{V_\infty^2} \times 10^4$	$-\frac{\overline{u_y u_z}}{V_\infty^2} \times 10^4$
12.7	.5	.02	.42	-	.025	.088	-	.045	-	-2.2	-
	.8	.03	.46	-	.031	.083	-	.050	-	.0	-
	1.0	.04	.50	-	.026	.081	-	.049	-	-.7	-
	1.3	.05	.52	-	.026	.078	-	.052	-	.8	-
	1.5	.06	.53	-	.034	.076	-	.052	-	.2	-
	1.8	.07	.55	-	.026	.076	-	.051	-	.5	-
	2.0	.08	.56	-	.026	.075	-	.052	-	1.5	-
	2.3	.09	.57	.014	.029	.075	.048	.049	15.2	.7	4.2
	2.5	.10	.58	.007	.024	.074	.048	.050	14.9	.6	8.3
	3.8	.15	.63	.008	.029	.072	.048	.050	14.7	.4	3.7
	5.1	.20	.66	.010	.028	.071	.047	.048	14.0	.6	6.9
	6.4	.25	.70	.010	.016	.068	.048	.049	14.1	1.2	4.1
	7.6	.30	.72	.008	.023	.067	.043	.047	13.1	1.7	7.4
	8.9	.35	.75	.009	.026	.064	.044	.048	12.4	1.1	5.8
	10.2	.40	.78	.009	.023	.062	.041	.046	11.3	1.0	4.1
	11.4	.45	.80	.009	.018	.059	.040	.046	10.7	1.3	6.1
	12.7	.50	.82	.009	.026	.057	.037	.042	9.4	1.0	5.1
	15.2	.60	.85	.007	.013	.050	.037	.039	7.1	1.2	5.8
	17.8	.70	.88	.011	.015	.043	.032	.033	4.4	1.0	3.2
	20.3	.80	.91	.006	.017	.034	.032	.027	2.0	.4	3.4
	22.9	.90	.92	.007	.023	.024	.024	.019	.4	.2	1.0
	25.4	1.00	.93	.010	.010	.017	.021	.014	-.5	.0	.5
	27.9	1.10	.94	.008	.015	.013	.017	.008	-.8	.1	.6
	33.0	1.30	.94	-	.020	.010	-	.005	-	.0	-

Table 1. - Continued.

z (mm)	y (mm)	y (in.)	$\frac{U_x}{V_\infty}$	$\frac{U_y}{V_\infty}$	$\frac{U_z}{V_\infty}$	$\frac{u'_x}{V_\infty}$	$\frac{u'_y}{V_\infty}$	$\frac{u'_z}{V_\infty}$	$-\frac{\overline{u_x u_y}}{V_\infty^2} \times 10^4$	$-\frac{\overline{u_x u_z}}{V_\infty^2} \times 10^4$	$-\frac{\overline{u_y u_z}}{V_\infty^2} \times 10^4$
0.0	.5	.02	.41	-	.016	.088	-	.047	-	-1.8	-
	.8	.03	.46	-	.022	.084	-	.050	-	-.9	-
	1.0	.04	.49	-	.014	.080	-	.051	-	-.0	-
	1.3	.05	.51	-	.024	.079	-	.051	-	-.2	-
	1.5	.06	.53	-	.025	.078	-	.050	-	0.0	-
	1.8	.07	.54	-	.016	.076	-	.052	-	1.2	-
	2.0	.08	.56	-	.017	.077	-	.049	-	.5	-
	2.3	.09	.57	.011	.022	.076	.047	.050	15.1	.5	4.6
	2.5	.10	.58	.012	.023	.076	.044	.049	14.4	.5	3.9
	3.8	.15	.62	.009	.020	.074	.045	.047	15.0	-.1	4.1
	5.1	.20	.65	.009	.007	.072	.046	.048	14.5	-.2	1.6
	6.4	.25	.69	.009	.013	.069	.046	.049	13.8	.7	4.0
	7.6	.30	.72	.009	.006	.067	.045	.049	13.4	.6	5.1
	8.9	.35	.74	.009	.014	.065	.041	.048	12.3	.8	6.3
	10.2	.40	.76	.009	.020	.063	.039	.046	11.3	.0	3.8
	11.4	.45	.78	.009	.005	.060	.038	.045	10.8	.5	3.7
	12.7	.50	.80	.009	.015	.057	.038	.044	9.6	.4	3.8
	15.2	.60	.84	.010	.012	.051	.035	.041	7.5	.5	2.3
	17.8	.70	.88	.007	.009	.044	.032	.035	4.6	.4	3.5
	20.3	.80	.90	.008	.009	.037	.028	.029	2.4	.5	2.3
	22.9	.90	.92	.011	.008	.028	.022	.020	.6	.0	.7
	25.4	1.00	.93	.010	.010	.019	.020	.015	-.3	.4	1.5
	27.9	1.10	.94	.008	.010	.013	.017	.011	-.8	.0	.6
	33.0	1.30	.94	-	.010	.009	-	.006	-	.1	-

Table 1. - Continued.

z (mm)	y (mm)	y (in.)	$\frac{U_x}{V_\infty}$	$\frac{U_y}{V_\infty}$	$\frac{U_z}{V_\infty}$	$\frac{u'_x}{V_\infty}$	$\frac{u'_y}{V_\infty}$	$\frac{u'_z}{V_\infty}$	$-\frac{\overline{u_x u_y}}{V_\infty^2}\times 10^4$	$-\frac{\overline{u_x u_z}}{V_\infty^2}\times 10^4$	$-\frac{\overline{u_y u_z}}{V_\infty^2}\times 10^4$
-15.2	.5	.02	.41	-	.005	.088	-	.048	-	-.2	-
	.8	.03	.45	-	.010	.085	-	.049	-	-1.5	-
	1.0	.04	.48	-	.008	.081	-	.050	-	-.2	-
	1.3	.05	.50	-	.008	.079	-	.050	-	-.8	-
	1.5	.06	.52	-	.011	.077	-	.050	-	-.2	-
	1.8	.07	.53	-	.007	.077	-	.051	-	.2	-
	2.0	.08	.55	-	.006	.076	-	.050	-	.4	-
	2.3	.09	.56	.003	.006	.074	.049	.052	15.1	.3	2.6
	2.5	.10	.56	.001	.045	.075	.047	.050	15.0	-2.3	4.5
	3.8	.15	.61	.001	.004	.074	.045	.046	15.0	.0	1.5
	5.1	.20	.65	.002	.009	.071	.048	.049	14.8	.1	4.0
	6.4	.25	.68	0.000	.010	.070	.047	.048	14.2	.4	5.7
	7.6	.30	.71	.004	.002	.068	.044	.048	13.0	.6	5.5
	8.9	.35	.74	.001	.019	.065	.045	.048	12.7	.7	6.3
	10.2	.40	.76	.002	0.000	.063	.043	.047	12.1	.2	5.6
	11.4	.45	.78	.001	.007	.060	.043	.045	10.9	.2	4.4
	12.7	.50	.80	.007	0.000	.057	.041	.044	10.2	.5	4.1
	15.2	.60	.84	.008	.009	.051	.038	.039	8.3	.5	5.8
	17.8	.70	.87	0.000	.006	.044	.035	.034	5.6	.2	3.0
	20.3	.80	.90	.003	.002	.038	.031	.026	3.6	.3	3.6
	22.9	.90	.92	.006	.013	.027	.025	.019	1.6	.0	1.6
	25.4	1.00	.93	.006	-.006	.019	.019	.016	.6	.1	.2
	27.9	1.10	.93	.005	.018	.014	.014	.009	-.0	.0	.3
	33.0	1.30	.94	-	-.002	.011	-	.006	-	.1	-

Table 1. - Concluded.

z (mm)	y (mm)	y (in.)	$\frac{U_x}{V_\infty}$	$\frac{U_y}{V_\infty}$	$\frac{U_z}{V_\infty}$	$\frac{u'_x}{V_\infty}$	$\frac{u'_y}{V_\infty}$	$\frac{u'_z}{V_\infty}$	$-\frac{\overline{u_x u_y}}{V_\infty^2}\times 10^4$	$-\frac{\overline{u_x u_z}}{V_\infty^2}\times 10^4$	$-\frac{\overline{u_y u_z}}{V_\infty^2}\times 10^4$
-29.0	.5	.02	.40	-	-.005	.087	-	.049	-	.2	-
	.8	.03	.45	-	-.004	.083	-	.050	-	-.1	-
	1.0	.04	.48	-	-.003	.081	-	.051	-	-.0	-
	1.3	.05	.50	-	.003	.080	-	.049	-	-.5	-
	1.5	.06	.52	-	-.002	.078	-	.052	-	.1	-
	1.8	.07	.53	-	.001	.078	-	.050	-	.1	-
	2.0	.08	.55	-	-.003	.077	-	.050	-	.2	-
	2.3	.09	.55	.007	-.009	.076	.050	.050	15.6	.4	1.7
	2.5	.10	.56	.010	.005	.075	.052	.051	16.0	.2	4.8
	3.8	.15	.61	.006	0.000	.075	.048	.046	15.1	.2	5.2
	5.1	.20	.65	.009	-.003	.072	.050	.049	15.6	.2	2.7
	6.4	.25	.68	.009	-.006	.071	.048	.048	15.1	-.0	7.9
	7.6	.30	.71	.007	.002	.068	.049	.050	14.4	-.3	6.8
	8.9	.35	.73	.007	-.004	.066	.045	.048	13.6	.3	8.3
	10.2	.40	.76	.009	.004	.062	.044	.047	11.9	-.2	4.1
	11.4	.45	.78	.012	-.001	.060	.042	.044	11.0	-.1	5.6
	12.7	.50	.80	.010	.004	.057	.041	.044	9.9	.1	4.6
	15.2	.60	.84	.012	-.003	.052	.037	.039	7.5	.2	5.1
	17.8	.70	.87	.013	.003	.045	.037	.033	5.3	.3	4.4
	20.3	.80	.90	.011	.006	.038	.032	.029	3.2	-.0	2.3
	22.9	.90	.92	.010	-.002	.027	.028	.021	1.0	-.4	.1
	25.4	1.00	.92	.012	.005	.020	.022	.014	-.1	-.0	1.9
	27.9	1.10	.94	.015	-.003	.014	.018	.010	-.8	0.0	.4
	33.0	1.30	.94	-	-.011	.012	-	.004	-	.1	-

Table 2

Mean velocities and turbulence stresses upstream of the juncture (x = - 38 mm).

z (mm)	y (mm)	y (in.)	$\frac{U_x}{V_\infty}$	$\frac{U_y}{V_\infty}$	$\frac{U_z}{V_\infty}$	$\frac{u'_x}{V_\infty}$	$\frac{u'_y}{V_\infty}$	$\frac{u'_z}{V_\infty}$	$-\frac{\overline{u_x u_y}}{V_\infty^2}\times 10^4$	$-\frac{\overline{u_x u_z}}{V_\infty^2}\times 10^4$	$-\frac{\overline{u_y u_z}}{V_\infty^2}\times 10^4$
152.4	.5	.02	.50	-	.044	.088	-	.050	-	-3.6	-
	.8	.03	.55	-	.051	.082	-	.050	-	-3.2	-
	1.0	.04	.58	-	.060	.077	-	.052	-	-1.5	-
	1.3	.05	.60	-	.061	.074	-	.051	-	-.8	-
	1.5	.06	.62	-	.061	.072	-	.052	-	-.6	-
	1.8	.07	.63	-	.061	.071	-	.052	-	-.0	-
	2.0	.08	.64	-	.063	.070	-	.051	-	.0	-
	2.3	.09	.65	.006	.054	.070	.052	.049	15.9	.3	-4.6
	2.5	.10	.66	.004	.058	.069	.052	.049	15.4	.5	-4.1
	3.8	.15	.70	.001	.053	.065	.054	.049	15.4	.2	-4.7
	5.1	.20	.74	.001	.064	.063	.053	.048	14.4	.5	-2.4
	6.4	.25	.77	.004	.054	.062	.051	.048	13.6	1.2	-1.8
	7.6	.30	.80	.004	.060	.060	.050	.048	13.0	1.0	.8
	8.9	.35	.82	.004	.054	.057	.047	.047	11.9	1.2	.4
	10.2	.40	.84	.005	.062	.055	.046	.046	11.0	1.2	-.9
	11.4	.45	.86	.007	.059	.052	.043	.045	10.0	1.3	1.0
	12.7	.50	.89	.006	.062	.050	.041	.043	8.5	1.2	4.1
	15.2	.60	.92	.007	.050	.044	.035	.038	6.5	1.0	.3
	17.8	.70	.95	.007	.055	.037	.028	.031	4.2	.9	-.4
	20.3	.80	.98	.008	.053	.028	.019	.023	2.0	.2	.4
	22.9	.90	.99	.011	.052	.018	.013	.016	.6	.1	.6
	25.4	1.00	1.00	.012	.050	.013	.007	.009	.2	.0	.1
	27.9	1.10	1.00	.011	.053	.008	.007	.008	.0	.1	.0
	33.0	1.30	1.00	-	.051	.006	-	.005	-	-.0	-

Table 2. - Continued.

z (mm)	y (mm)	y (in.)	$\frac{U_x}{V_\infty}$	$\frac{U_y}{V_\infty}$	$\frac{U_z}{V_\infty}$	$\frac{u'_x}{V_\infty}$	$\frac{u'_y}{V_\infty}$	$\frac{u'_z}{V_\infty}$	$-\frac{\overline{u_x u_y}}{V_\infty^2}\times 10^4$	$-\frac{\overline{u_x u_z}}{V_\infty^2}\times 10^4$	$-\frac{\overline{u_y u_z}}{V_\infty^2}\times 10^4$
101.6	.5	.02	.50	-	.085	.086	-	.051	-	-6.1	-
	.8	.03	.54	-	.094	.081	-	.051	-	-3.4	-
	1.0	.04	.57	-	.097	.076	-	.052	-	-1.8	-
	1.3	.05	.59	-	.101	.073	-	.052	-	-.6	-
	1.5	.06	.60	-	.105	.072	-	.051	-	-.9	-
	1.8	.07	.62	-	.099	.070	-	.051	-	-.5	-
	2.0	.08	.63	-	.099	.069	-	.051	-	-.2	-
	2.3	.09	.64	.006	.097	.068	.053	.049	15.6	.1	-4.0
	2.5	.10	.65	.005	.099	.068	.054	.049	15.7	.7	-5.1
	3.8	.15	.69	.002	.095	.066	.054	.049	15.4	.3	-3.3
	5.1	.20	.73	.003	.098	.064	.053	.048	15.1	.6	-2.1
	6.4	.25	.76	.003	.094	.062	.052	.048	14.1	1.5	-1.7
	7.6	.30	.78	.004	.096	.060	.050	.048	13.0	1.3	1.3
	8.9	.35	.81	.004	.093	.059	.048	.048	12.6	1.2	-.4
	10.2	.40	.84	.005	.090	.056	.046	.046	11.3	1.4	-.4
	11.4	.45	.86	.004	.095	.053	.044	.045	10.0	1.3	.9
	12.7	.50	.88	.007	.086	.050	.040	.042	8.6	1.1	.4
	15.2	.60	.91	.005	.083	.043	.034	.037	5.8	1.0	1.9
	17.8	.70	.94	.006	.086	.035	.027	.030	3.7	.7	.7
	20.3	.80	.97	.007	.091	.026	.018	.022	1.7	.4	.7
	22.9	.90	.98	.010	.084	.018	.011	.015	.6	.1	-.4
	25.4	1.00	.99	.009	.094	.012	.008	.010	.2	.0	.2
	27.9	1.10	.99	.011	.106	.009	.003	.006	.0	-.0	-.0
	33.0	1.30	.99	-	.083	.006	-	.005	-	0.0	-

Table 2. - Continued.

z (mm)	y (mm)	y (in.)	$\frac{U_x}{V_\infty}$	$\frac{U_y}{V_\infty}$	$\frac{U_z}{V_\infty}$	$\frac{u'_x}{V_\infty}$	$\frac{u'_y}{V_\infty}$	$\frac{u'_z}{V_\infty}$	$-\frac{\overline{u_x u_y}}{V_\infty^2}\times 10^4$	$-\frac{\overline{u_x u_z}}{V_\infty^2}\times 10^4$	$-\frac{\overline{u_y u_z}}{V_\infty^2}\times 10^4$
50.8	.5	.02	.47	-	.123	.082	-	.051	-	-7.7	-
	.8	.03	.51	-	.145	.077	-	.052	-	-3.2	-
	1.0	.04	.53	-	.160	.074	-	.053	-	-.8	-
	1.3	.05	.55	-	.164	.073	-	.053	-	-1.1	-
	1.5	.06	.56	-	.159	.072	-	.052	-	.0	-
	1.8	.07	.57	-	.157	.070	-	.051	-	.6	-
	2.0	.08	.59	-	.153	.070	-	.051	-	.0	-
	2.3	.09	.60	.004	.149	.070	.054	.051	16.5	.8	-5.2
	2.5	.10	.61	.005	.143	.069	.054	.051	15.9	.6	-3.5
	3.8	.15	.65	.002	.142	.068	.055	.049	15.9	-.2	-3.1
	5.1	.20	.68	.001	.142	.067	.053	.048	15.5	.1	-3.2
	6.4	.25	.72	.002	.130	.064	.054	.049	14.6	1.4	-1.7
	7.6	.30	.75	.002	.119	.063	.051	.048	14.2	1.0	-1.8
	8.9	.35	.77	.002	.120	.061	.049	.048	13.0	1.5	-.9
	10.2	.40	.80	.002	.115	.057	.047	.046	11.8	1.2	-1.8
	11.4	.45	.82	.004	.117	.055	.044	.045	10.2	1.4	.1
	12.7	.50	.84	.005	.108	.051	.041	.042	9.0	1.5	.6
	15.2	.60	.88	.003	.106	.044	.035	.038	6.3	1.2	.8
	17.8	.70	.90	.008	.103	.037	.028	.031	3.9	.8	1.0
	20.3	.80	.93	.005	.118	.028	.018	.023	1.8	.5	.6
	22.9	.90	.95	.008	.095	.019	.012	.016	.7	.1	-.2
	25.4	1.00	.96	.007	.114	.013	.008	.010	.1	.0	-.0
	27.9	1.10	.96	.006	.111	.010	.005	.008	.1	.0	.2
	33.0	1.30	.96	-	.092	.007	-	.005	-	-.0	-

Table 2. - Continued.

z (mm)	y (mm)	y (in.)	$\frac{U_x}{V_\infty}$	$\frac{U_y}{V_\infty}$	$\frac{U_z}{V_\infty}$	$\frac{u'_x}{V_\infty}$	$\frac{u'_y}{V_\infty}$	$\frac{u'_z}{V_\infty}$	$-\frac{\overline{u_x u_y}}{V_\infty^2}\times 10^4$	$-\frac{\overline{u_x u_z}}{V_\infty^2}\times 10^4$	$-\frac{\overline{u_y u_z}}{V_\infty^2}\times 10^4$
25.4	.5	.02	.40	-	.171	.078	-	.053	-	-5.0	-
	.8	.03	.44	-	.173	.076	-	.050	-	-3.3	-
	1.0	.04	.46	-	.174	.074	-	.052	-	-.8	-
	1.3	.05	.49	-	.168	.074	-	.052	-	-.3	-
	1.5	.06	.50	-	.170	.073	-	.052	-	-.3	-
	1.8	.07	.52	-	.169	.073	-	.051	-	.2	-
	2.0	.08	.53	-	.161	.072	-	.050	-	-.8	-
	2.3	.09	.54	.001	.162	.073	.057	.051	18.5	.3	-8.4
	2.5	.10	.54	.003	.158	.073	.057	.052	17.7	-.3	-7.3
	3.8	.15	.59	0.000	.147	.072	.056	.050	17.1	-.3	-4.4
	5.1	.20	.62	.004	.145	.071	.058	.049	17.4	.6	-4.2
	6.4	.25	.66	.002	.135	.070	.054	.049	16.3	1.1	-2.6
	7.6	.30	.69	.003	.138	.067	.055	.050	15.6	2.2	-3.9
	8.9	.35	.72	.002	.129	.066	.051	.049	14.5	1.7	-3.8
	10.2	.40	.74	.004	.130	.063	.051	.049	12.9	2.5	2.1
	11.4	.45	.77	.003	.124	.059	.049	.047	11.4	2.5	4.4
	12.7	.50	.79	.004	.124	.057	.045	.044	10.4	2.0	1.2
	15.2	.60	.83	.002	.107	.050	.038	.039	7.6	2.4	1.6
	17.8	.70	.86	.006	.116	.043	.033	.034	4.8	1.8	2.2
	20.3	.80	.88	.006	.129	.034	.025	.027	2.7	1.0	1.1
	22.9	.90	.90	.006	.120	.025	.016	.020	1.0	.5	1.5
	25.4	1.00	.92	.006	.116	.016	.011	.013	.4	.1	.1
	27.9	1.10	.92	.004	.126	.011	.007	.008	.0	-.0	.0
↓	33.0	1.30	.92	-	.107	.008	-	.006	-	-.0	-

Table 2. - Continued.

z (mm)	y (mm)	y (in.)	$\frac{U_x}{V_\infty}$	$\frac{U_y}{V_\infty}$	$\frac{U_z}{V_\infty}$	$\frac{u'_x}{V_\infty}$	$\frac{u'_y}{V_\infty}$	$\frac{u'_z}{V_\infty}$	$-\frac{\overline{u_x u_y}}{V_\infty^2}\times 10^4$	$-\frac{\overline{u_x u_z}}{V_\infty^2}\times 10^4$	$-\frac{\overline{u_y u_z}}{V_\infty^2}\times 10^4$
12.7	.5	.02	.35	-	.177	.077	-	.051	-	-5.8	-
	.8	.03	.39	-	.180	.077	-	.050	-	-5.1	-
	1.0	.04	.42	-	.179	.076	-	.052	-	-2.0	-
	1.3	.05	.44	-	.177	.076	-	.051	-	-.7	-
	1.5	.06	.45	-	.168	.076	-	.051	-	-1.0	-
	1.8	.07	.46	-	.167	.075	-	.052	-	-.2	-
	2.0	.08	.48	-	.165	.076	-	.051	-	-1.5	-
	2.3	.09	.49	.004	.163	.075	.064	.051	18.9	-.1	-8.0
	2.5	.10	.50	.003	.164	.076	.060	.049	20.1	-2.6	-11.2
	3.8	.15	.54	0.000	.149	.075	.064	.051	17.9	.4	-4.5
	5.1	.20	.58	.002	.147	.073	.063	.050	18.5	.3	-5.5
	6.4	.25	.62	-.001	.140	.072	.058	.049	16.6	.4	-4.3
	7.6	.30	.65	.001	.134	.069	.058	.050	16.0	1.2	-3.4
	8.9	.35	.68	0.000	.132	.067	.055	.049	15.0	1.3	-3.3
	10.2	.40	.71	.002	.125	.065	.052	.047	13.5	1.4	-1.7
	11.4	.45	.73	.003	.127	.062	.048	.045	11.7	1.4	-1.7
	12.7	.50	.75	.002	.112	.058	.047	.045	10.4	2.0	-.4
	15.2	.60	.79	.003	.107	.052	.040	.039	7.9	1.2	-.7
	17.8	.70	.83	.005	.110	.045	.033	.034	5.1	1.4	1.3
	20.3	.80	.85	.004	.106	.035	.027	.026	3.2	.9	.3
	22.9	.90	.87	.003	.107	.026	.018	.020	1.2	.5	1.6
	25.4	1.00	.89	.004	.101	.017	.015	.015	.4	.3	.4
	27.9	1.10	.89	.003	.107	.012	.007	.010	.2	.0	-.0
	33.0	1.30	.89	-	.109	.008	-	.005	-	-.0	-

Table 2. - Continued.

z (mm)	y (mm)	y (in.)	$\frac{U_x}{V_\infty}$	$\frac{U_y}{V_\infty}$	$\frac{U_z}{V_\infty}$	$\frac{u'_x}{V_\infty}$	$\frac{u'_y}{V_\infty}$	$\frac{u'_z}{V_\infty}$	$-\frac{\overline{u_x u_y}}{V_\infty^2}\times 10^4$	$-\frac{\overline{u_x u_z}}{V_\infty^2}\times 10^4$	$-\frac{\overline{u_y u_z}}{V_\infty^2}\times 10^4$
0.0	.5	.02	.29	-	.169	.080	-	.051	-	-5.7	-
	.8	.03	.33	-	.169	.081	-	.050	-	-3.1	-
	1.0	.04	.36	-	.163	.080	-	.052	-	-1.5	-
	1.3	.05	.38	-	.163	.081	-	.051	-	-1.6	-
	1.5	.06	.40	-	.157	.081	-	.052	-	-.9	-
	1.8	.07	.41	-	.153	.081	-	.052	-	-.5	-
	2.0	.08	.42	-	.152	.082	-	.050	-	-1.1	-
	2.3	.09	.43	.001	.148	.081	.057	.051	19.3	-2.1	-10.3
	2.5	.10	.44	.005	.145	.082	.057	.050	19.5	-1.7	-9.4
	3.8	.15	.50	.003	.135	.081	.056	.048	19.2	-2.3	-8.4
	5.1	.20	.54	.001	.125	.078	.058	.049	18.0	.2	-7.2
	6.4	.25	.58	.001	.124	.076	.056	.049	16.9	.6	-6.3
	7.6	.30	.61	.001	.123	.073	.055	.050	16.3	1.5	-6.2
	8.9	.35	.64	0.000	.123	.070	.054	.049	14.8	1.1	-3.1
	10.2	.40	.67	.001	.112	.067	.049	.046	13.5	1.7	-2.5
	11.4	.45	.70	-.001	.114	.064	.047	.045	12.0	1.7	-3.2
	12.7	.50	.72	-.001	.108	.060	.046	.044	10.7	2.1	-1.3
	15.2	.60	.76	0.000	.108	.054	.038	.038	7.7	1.3	-1.6
	17.8	.70	.80	-.003	.104	.045	.032	.032	5.4	.8	.4
	20.3	.80	.82	-.003	.094	.036	.024	.026	3.3	.6	-.1
	22.9	.90	.84	-.004	.091	.026	.017	.019	1.4	.4	.2
	25.4	1.00	.85	-.003	.091	.017	.014	.013	.5	.2	-.3
	27.9	1.10	.86	-.006	.089	.011	.010	.010	.1	.0	.2
▼	33.0	1.30	.83	-	.089	.013	-	.006	-	-.2	-

Table 2. - Continued.

z (mm)	y (mm)	y (in.)	$\frac{U_x}{V_\infty}$	$\frac{U_y}{V_\infty}$	$\frac{U_z}{V_\infty}$	$\frac{u'_x}{V_\infty}$	$\frac{u'_y}{V_\infty}$	$\frac{u'_z}{V_\infty}$	$-\frac{\overline{u_x u_y}}{V_\infty^2}\times 10^4$	$-\frac{\overline{u_x u_z}}{V_\infty^2}\times 10^4$	$-\frac{\overline{u_y u_z}}{V_\infty^2}\times 10^4$
-10.2	.5	.02	.25	-	.130	.082	-	.049	-	-3.6	-
	.8	.03	.29	-	.127	.084	-	.048	-	-3.6	-
	1.0	.04	.31	-	.127	.084	-	.049	-	-2.1	-
	1.3	.05	.33	-	.117	.085	-	.049	-	-1.2	-
	1.5	.06	.35	-	.118	.085	-	.049	-	-2.0	-
	1.8	.07	.37	-	.113	.086	-	.049	-	-2.4	-
	2.0	.08	.38	-	.110	.086	-	.049	-	-1.9	-
	2.3	.09	.39	.002	.112	.086	.060	.051	19.7	-.9	-12.0
	2.5	.10	.40	.002	.112	.086	.058	.048	20.4	-2.2	-14.3
	3.8	.15	.45	0.000	.101	.084	.062	.051	20.2	-.8	-13.0
	5.1	.20	.50	0.000	.096	.082	.061	.048	18.0	-.4	-3.4
	6.4	.25	.54	0.000	.087	.079	.056	.049	16.5	.2	-6.1
	7.6	.30	.58	0.000	.087	.076	.056	.048	16.3	1.6	-5.3
	8.9	.35	.61	-.002	.086	.072	.053	.048	14.2	1.4	-3.6
	10.2	.40	.64	0.000	.080	.068	.051	.046	13.6	1.1	-5.0
	11.4	.45	.66	-.002	.079	.066	.047	.044	11.9	1.6	-2.7
	12.7	.50	.69	-.003	.078	.061	.044	.041	10.3	1.2	-2.2
	15.2	.60	.74	-.004	.080	.053	.040	.037	8.1	1.2	-2.2
	17.8	.70	.77	-.005	.078	.045	.032	.033	5.3	1.0	-.9
	20.3	.80	.80	-.005	.068	.036	.024	.026	2.8	.6	.5
	22.9	.90	.82	-.005	.064	.026	.017	.020	1.3	.4	.9
	25.4	1.00	.83	-.008	.074	.016	.014	.013	.6	.1	-.2
	27.9	1.10	.83	-.009	.080	.011	.011	.009	.2	0.0	-.0
	33.0	1.30	.83	-	.071	.009	-	.005	-	-.1	-

Table 2. - Continued.

z (mm)	y (mm)	y (in.)	$\frac{U_x}{V_\infty}$	$\frac{U_y}{V_\infty}$	$\frac{U_z}{V_\infty}$	$\frac{u'_x}{V_\infty}$	$\frac{u'_y}{V_\infty}$	$\frac{u'_z}{V_\infty}$	$-\frac{\overline{u_x u_y}}{V_\infty^2}\times 10^4$	$-\frac{\overline{u_x u_z}}{V_\infty^2}\times 10^4$	$-\frac{\overline{u_y u_z}}{V_\infty^2}\times 10^4$
-22.9	.5	.02	.21	-	.055	.086	-	.037	-	-4.8	-
↓	.8	.03	.25	-	.045	.089	-	.042	-	-4.5	-
	1.0	.04	.28	-	.050	.090	-	.043	-	-3.8	-
	1.3	.05	.30	-	.047	.091	-	.047	-	-1.5	-
	1.5	.06	.32	-	.037	.092	-	.041	-	-1.9	-
	1.8	.07	.33	-	.040	.091	-	.047	-	-1.1	-
	2.0	.08	.35	-	.043	.092	-	.043	-	-2.8	-
	2.3	.09	.36	.003	.039	.092	.046	.045	15.9	-1.5	-14.9
	2.5	.10	.37	.003	.038	.091	.052	.045	15.7	.5	-13.5
	3.8	.15	.43	.003	.035	.089	.057	.047	17.8	-.5	-7.2
	5.1	.20	.47	.004	.035	.086	.060	.049	16.9	.4	-9.8
	6.4	.25	.51	.001	.031	.082	.059	.048	16.6	-.1	-4.9
	7.6	.30	.54	.002	.032	.079	.055	.047	16.0	.6	-7.9
	8.9	.35	.58	.001	.031	.075	.053	.047	14.7	.4	-2.4
	10.2	.40	.61	0.000	.023	.072	.047	.044	13.3	.5	-4.9
	11.4	.45	.64	-.001	.023	.067	.048	.044	12.2	.3	-2.1
	12.7	.50	.66	-.005	.023	.063	.043	.042	10.5	.8	-.2
	15.2	.60	.71	-.004	.025	.055	.039	.038	8.1	.5	-1.7
	17.8	.70	.74	-.005	.027	.047	.034	.032	5.6	.4	-.3
	20.3	.80	.77	-.007	.018	.038	.024	.026	3.2	.2	-.4
	22.9	.90	.79	-.007	.024	.027	.020	.020	1.6	.2	.4
	25.4	1.00	.80	-.008	.028	.018	.014	.013	.6	-.0	-.2
	27.9	1.10	.81	-.009	.018	.011	.011	.010	.1	.1	.8
	33.0	1.30	.81	-	.023	.006	-	.006	-	0.0	-

Table 2. - Concluded.

z (mm)	y (mm)	y (in.)	$\frac{U_x}{V_\infty}$	$\frac{U_y}{V_\infty}$	$\frac{U_z}{V_\infty}$	$\frac{u'_x}{V_\infty}$	$\frac{u'_y}{V_\infty}$	$\frac{u'_z}{V_\infty}$	$-\frac{\overline{u_x u_y}}{V_\infty^2}\times 10^4$	$-\frac{\overline{u_x u_z}}{V_\infty^2}\times 10^4$	$-\frac{\overline{u_y u_z}}{V_\infty^2}\times 10^4$
-29.0	.5	.02	.21	-	-.013	.085	-	.036	-	6.8	-
	.8	.03	.25	-	-.004	.089	-	.041	-	3.2	-
	1.0	.04	.27	-	-.006	.090	-	.042	-	3.0	-
	1.3	.05	.29	-	-.007	.090	-	.042	-	2.7	-
	1.5	.06	.31	-	-.003	.091	-	.042	-	1.9	-
	1.8	.07	.32	-	.009	.092	-	.043	-	-.3	-
	2.0	.08	.33	-	.001	.091	-	.044	-	.3	-
	2.3	.09	.35	.001	-.002	.091	.049	.043	13.8	1.8	-14.9
	2.5	.10	.36	.001	-.001	.092	.053	.043	15.6	1.3	-15.2
	3.8	.15	.41	.001	.009	.090	.058	.046	16.7	.6	-10.8
	5.1	.20	.46	.004	.007	.087	.058	.045	16.6	-.5	-9.4
	6.4	.25	.50	.004	.002	.084	.054	.043	16.0	1.0	-5.7
	7.6	.30	.53	.001	.006	.079	.056	.048	15.7	.3	-5.8
	8.9	.35	.57	-.002	.003	.076	.053	.048	14.3	1.2	1.9
	10.2	.40	.60	-.001	0.000	.072	.050	.044	13.7	.4	-3.1
	11.4	.45	.62	0.000	-.003	.068	.047	.044	12.2	1.0	-1.1
	12.7	.50	.65	-.004	-.003	.064	.045	.042	10.5	.4	-2.7
	15.2	.60	.69	-.005	.012	.055	.040	.040	8.3	.4	-2.2
	17.8	.70	.73	-.004	.005	.048	.033	.033	5.4	.3	-.2
	20.3	.80	.76	-.008	.009	.039	.027	.025	3.5	.4	1.4
	22.9	.90	.78	-.008	.001	.029	.017	.020	1.7	-.0	-1.0
	25.4	1.00	.79	-.008	.017	.019	.014	.014	.7	-.0	.1
	27.9	1.10	.80	-.008	.006	.012	.010	.009	.2	.1	.4
	33.0	1.30	.80	-	-.004	.007	-	.005	-	.0	-

Table 3

Mean velocities and turbulence stresses upstream of the juncture (x = - 11 mm).

z (mm.)	y (mm)	y (in.)	$\frac{U_x}{V_\infty}$	$\frac{U_y}{V_\infty}$	$\frac{U_z}{V_\infty}$	$\frac{u'_x}{V_\infty}$	$\frac{u'_y}{V_\infty}$	$\frac{u'_z}{V_\infty}$	$-\frac{\overline{u_x u_y}}{V_\infty^2}\times 10^4$	$-\frac{\overline{u_x u_z}}{V_\infty^2}\times 10^4$	$-\frac{\overline{u_y u_z}}{V_\infty^2}\times 10^4$
146.7	.5	.02	.52	-	.061	.086	-	.055	-	-4.8	-
	.8	.03	.56	-	.068	.082	-	.054	-	-3.4	-
	1.0	.04	.59	-	.074	.077	-	.052	-	-2.9	-
	1.3	.05	.61	-	.075	.075	-	.051	-	-1.9	-
	1.5	.06	.63	-	.077	.073	-	.048	-	-2.5	-
	1.8	.07	.63	-	.080	.072	-	.051	-	-1.4	-
	2.0	.08	.65	.006	.076	.070	.040	.049	14.9	-1.3	10.6
	2.3	.09	.65	.006	.080	.070	.036	.046	14.8	-1.2	9.4
	2.5	.10	.66	.009	.083	.068	.041	.050	15.0	-1.1	8.3
	3.8	.15	.70	.003	.078	.068	.039	.044	13.7	-1.2	10.4
	5.1	.20	.74	.004	.080	.065	.043	.044	13.2	-1.3	8.9
	6.4	.25	.77	.002	.073	.063	.045	.045	12.6	-.8	9.3
	7.6	.30	.79	.005	.083	.062	.040	.042	12.0	-.5	11.5
	8.9	.35	.82	.006	.077	.058	.043	.043	10.6	-.5	11.1
	10.2	.40	.84	.002	.076	.056	.041	.044	10.5	-.2	8.9
	11.4	.45	.86	.004	.076	.054	.044	.046	9.5	-.0	9.5
	12.7	.50	.88	.005	.076	.051	.042	.043	8.4	.1	7.6
	15.2	.60	.91	.007	.083	.047	.042	.041	5.9	-.1	6.1
	17.8	.70	.95	.005	.077	.040	.034	.032	4.2	-.2	5.5
	20.3	.80	.97	-	.074	.035	-	.025	-	.1	-
	22.9	.90	.99	.007	.070	.026	.017	.018	1.7	.8	4.4
	25.4	1.00	1.00	-	.071	.020	-	.012	-	.3	-
	27.9	1.10	1.00	.008	.072	.014	.010	.010	-.2	.0	.1
	33.0	1.30	1.00	-	.073	.007	-	.008	-	-.3	-

Table 3. - Continued.

z (mm)	y (mm)	y (in.)	$\frac{U_x}{V_\infty}$	$\frac{U_y}{V_\infty}$	$\frac{U_z}{V_\infty}$	$\frac{u'_x}{V_\infty}$	$\frac{u'_y}{V_\infty}$	$\frac{u'_z}{V_\infty}$	$-\frac{\overline{u_x u_y}}{V_\infty^2}\times 10^4$	$-\frac{\overline{u_x u_z}}{V_\infty^2}\times 10^4$	$-\frac{\overline{u_y u_z}}{V_\infty^2}\times 10^4$
50.8	.5	.02	.50	-	.194	.076	-	.053	-	-9.5	-
	.8	.03	.54	-	.212	.072	-	.055	-	-3.9	-
	1.0	.04	.57	-	.220	.069	-	.053	-	-1.3	-
	1.3	.05	.59	-	.218	.068	-	.053	-	.3	-
	1.5	.06	.61	-	.211	.066	-	.052	-	.9	-
	1.8	.07	.62	-	.211	.067	-	.051	-	.7	-
	2.0	.08	.63	.006	.208	.067	.042	.050	13.4	.2	9.1
	2.3	.09	.64	.005	.217	.066	.045	.050	12.9	.6	10.7
	2.5	.10	.65	.004	.209	.066	.045	.051	13.2	.9	11.0
	3.8	.15	.70	.004	.195	.066	.046	.048	13.5	-.4	10.2
	5.1	.20	.72	.002	.199	.066	.046	.047	12.5	-.1	9.7
	6.4	.25	.75	.004	.191	.065	.044	.047	11.2	.7	12.4
	7.6	.30	.77	.005	.182	.064	.043	.045	11.5	.5	12.2
	8.9	.35	.80	.002	.186	.062	.044	.047	11.0	1.4	11.8
	10.2	.40	.82	.005	.183	.060	.042	.046	10.1	1.0	9.9
	11.4	.45	.84	.004	.184	.057	.042	.044	9.2	1.7	9.5
	12.7	.50	.85	.004	.165	.054	.042	.044	7.5	1.8	10.5
	15.2	.60	.88	.003	.174	.048	.037	.040	5.1	1.7	7.5
	17.8	.70	.91	.005	.161	.042	.030	.031	3.9	1.4	5.9
	20.3	.80	.93	.003	.157	.035	.023	.023	1.7	1.2	4.8
	22.9	.90	.95	-	.157	.028	-	.017	-	1.1	-
	25.4	1.00	.96	.004	.161	.023	.010	.012	-.0	.5	2.5
	27.9	1.10	.98	-	.167	.016	-	.011	-	.2	-
	33.0	1.30	.98	-	.176	.009	-	.009	-	-.3	-

Table 3. - Continued.

z (mm)	y (mm)	y (in.)	$\frac{U_x}{V_\infty}$	$\frac{U_y}{V_\infty}$	$\frac{U_z}{V_\infty}$	$\frac{u'_x}{V_\infty}$	$\frac{u'_y}{V_\infty}$	$\frac{u'_z}{V_\infty}$	$-\frac{\overline{u_x u_y}}{V_\infty^2}\times 10^4$	$-\frac{\overline{u_x u_z}}{V_\infty^2}\times 10^4$	$-\frac{\overline{u_y u_z}}{V_\infty^2}\times 10^4$
25.4	.5	.02	.46	-	.272	.071	-	.059	-	-5.8	-
	.8	.03	.49	-	.284	.071	-	.058	-	-.2	-
	1.0	.04	.51	-	.286	.069	-	.057	-	2.7	-
	1.3	.05	.53	-	.284	.070	-	.056	-	5.0	-
	1.5	.06	.54	-	.282	.070	-	.056	-	5.5	-
	1.8	.07	.56	-	.277	.070	-	.055	-	5.2	-
	2.0	.08	.57	.007	.270	.070	.045	.055	13.6	3.4	7.1
	2.3	.09	.58	.004	.261	.070	.045	.054	13.5	3.0	8.3
	2.5	.10	.59	.006	.264	.069	.048	.055	14.6	2.5	5.2
	3.8	.15	.63	.004	.249	.068	.049	.053	13.7	1.0	9.7
	5.1	.20	.66	.006	.238	.068	.050	.049	13.5	.2	8.9
	6.4	.25	.69	.004	.228	.067	.047	.049	12.8	.0	10.9
	7.6	.30	.72	.003	.223	.066	.046	.049	13.1	1.4	8.0
	8.9	.35	.74	.002	.213	.064	.046	.050	11.6	1.8	7.9
	10.2	.40	.77	.005	.207	.061	.046	.046	11.0	.9	6.9
	11.4	.45	.78	.003	.209	.059	.044	.045	10.0	1.0	7.0
	12.7	.50	.80	.001	.210	.056	.043	.044	8.1	1.6	7.4
	15.2	.60	.83	0.000	.206	.050	.043	.041	5.5	2.0	6.9
	17.8	.70	.87	0.000	.198	.044	.034	.031	4.1	1.6	5.6
	20.3	.80	.88	-.005	.201	.037	.026	.025	2.3	1.4	3.1
	22.9	.90	.91	-	.180	.030	-	.019	-	1.3	-
	25.4	1.00	.92	-.004	.188	.023	.013	.013	.1	.8	2.2
	27.9	1.10	.94	-	.179	.018	-	.012	-	.3	-
	33.0	1.30	.95	-	.189	.011	-	.010	-	-.3	-

Table 3. - Continued.

z (mm)	y (mm)	y (in.)	$\frac{U_x}{V_\infty}$	$\frac{U_y}{V_\infty}$	$\frac{U_z}{V_\infty}$	$\frac{u'_x}{V_\infty}$	$\frac{u'_y}{V_\infty}$	$\frac{u'_z}{V_\infty}$	$-\frac{\overline{u_x u_y}}{V_\infty^2}\times 10^4$	$-\frac{\overline{u_x u_z}}{V_\infty^2}\times 10^4$	$-\frac{\overline{u_y u_z}}{V_\infty^2}\times 10^4$
15.2	.5	.02	.39	-	.343	.070	-	.064	-	.5	-
	.8	.03	.42	-	.361	.073	-	.062	-	5.2	-
	1.0	.04	.44	-	.362	.076	-	.062	-	10.2	-
	1.3	.05	.46	-	.354	.077	-	.061	-	10.7	-
	1.5	.06	.47	-	.350	.077	-	.061	-	11.4	-
	1.8	.07	.48	-	.350	.078	-	.061	-	11.2	-
	2.0	.08	.50	.007	.333	.078	.053	.061	14.2	10.9	7.8
	2.3	.09	.50	.008	.331	.078	.052	.060	14.2	9.1	6.7
	2.5	.10	.52	.005	.322	.078	.049	.059	14.8	6.4	7.8
	3.8	.15	.57	.006	.301	.076	.051	.056	14.3	2.6	9.6
	5.1	.20	.62	.007	.287	.074	.051	.055	14.9	1.9	8.1
	6.4	.25	.65	.007	.273	.072	.051	.053	13.8	2.1	8.9
	7.6	.30	.68	.004	.269	.070	.048	.051	12.4	2.0	11.1
	8.9	.35	.71	.002	.260	.069	.048	.048	12.0	1.4	8.8
	10.2	.40	.73	0.000	.255	.066	.046	.047	10.5	1.5	9.4
	11.4	.45	.75	-.002	.248	.063	.046	.047	9.0	2.3	9.5
	12.7	.50	.77	-.005	.239	.060	.045	.045	6.5	3.5	11.1
	15.2	.60	.81	-.009	.234	.055	.043	.040	4.8	2.5	8.1
	17.8	.70	.84	-.013	.231	.048	.035	.033	3.3	1.8	6.9
	20.3	.80	.86	-.012	.220	.043	.028	.027	1.8	2.3	6.5
	22.9	.90	.88	-	.220	.036	-	.018	-	1.2	-
	25.4	1.00	.89	-.018	.225	.027	.018	.013	-.4	.5	3.2
	27.9	1.10	.91	-	.219	.023	-	.012	-	.5	-
	33.0	1.30	.91	-	.228	.013	-	.009	-	-.5	-

Table 3. - Continued.

z (mm)	y (mm)	y (in.)	$\frac{U_x}{V_\infty}$	$\frac{U_y}{V_\infty}$	$\frac{U_z}{V_\infty}$	$\frac{u'_x}{V_\infty}$	$\frac{u'_y}{V_\infty}$	$\frac{u'_z}{V_\infty}$	$-\frac{\overline{u_x u_y}}{V_\infty^2}\times 10^4$	$-\frac{\overline{u_x u_z}}{V_\infty^2}\times 10^4$	$-\frac{\overline{u_y u_z}}{V_\infty^2}\times 10^4$
0.0	.5	.02	.24	-	.412	.085	-	.078	-	20.2	-
	.8	.03	.25	-	.424	.088	-	.075	-	22.6	-
	1.0	.04	.27	-	.421	.091	-	.075	-	25.3	-
	1.3	.05	.29	-	.422	.095	-	.075	-	26.4	-
	1.5	.06	.31	-	.410	.096	-	.075	-	26.4	-
	1.8	.07	.33	-	.405	.095	-	.074	-	23.7	-
	2.0	.08	.35	0.000	.393	.096	.073	.074	12.0	24.0	2.5
	2.3	.09	.35	-.003	.385	.095	.073	.074	13.4	22.1	-.6
	2.5	.10	.38	.001	.371	.094	.069	.073	12.1	17.8	5.0
	3.8	.15	.44	-.001	.356	.093	.067	.070	11.9	14.0	7.4
	5.1	.20	.50	-.001	.320	.088	.058	.063	12.1	8.2	8.8
	6.4	.25	.55	-.001	.310	.083	.054	.056	11.6	4.6	10.8
	7.6	.30	.59	-.008	.292	.078	.050	.054	10.4	4.0	12.2
	8.9	.35	.63	-.010	.282	.075	.049	.050	10.0	4.1	11.0
	10.2	.40	.65	-.014	.278	.070	.050	.048	8.1	4.5	12.5
	11.4	.45	.67	-.020	.276	.067	.044	.044	7.4	2.6	8.2
	12.7	.50	.70	-.025	.269	.064	.046	.044	6.0	4.4	7.3
	15.2	.60	.73	-.030	.260	.059	.040	.040	4.1	3.6	6.8
	17.8	.70	.75	-.039	.266	.052	.041	.036	2.7	3.8	5.3
	20.3	.80	.77	-.041	.265	.046	.035	.031	1.3	3.1	6.5
	22.9	.90	.79	-	.264	.040	-	.024	-	2.0	-
	25.4	1.00	.81	-.044	.264	.031	.031	.019	-.2	.6	2.0
	27.9	1.10	.81	-	.274	.025	-	.016	-	.6	-
	33.0	1.30	.82	-	.272	.015	-	.009	-	-.1	-

Table 3. - Continued.

z (mm)	y (mm)	y (in.)	$\frac{U_x}{V_\infty}$	$\frac{U_y}{V_\infty}$	$\frac{U_z}{V_\infty}$	$\frac{u'_x}{V_\infty}$	$\frac{u'_y}{V_\infty}$	$\frac{u'_z}{V_\infty}$	$-\frac{\overline{u_x u_y}}{V_\infty^2}\times 10^4$	$-\frac{\overline{u_x u_z}}{V_\infty^2}\times 10^4$	$-\frac{\overline{u_y u_z}}{V_\infty^2}\times 10^4$
-5.1	.5	.02	.18	-	.404	.097	-	.085	-	30.4	-
	.8	.03	.19	-	.411	.097	-	.082	-	29.9	-
	1.0	.04	.20	-	.408	.098	-	.082	-	30.1	-
	1.3	.05	.22	-	.401	.098	-	.084	-	28.9	-
	1.5	.06	.24	-	.398	.099	-	.086	-	31.1	-
	1.8	.07	.25	-	.390	.101	-	.089	-	33.7	-
	2.0	.08	.26	-.018	.374	.101	.106	.090	17.0	34.2	-15.5
	2.3	.09	.28	-.015	.366	.099	.097	.088	11.9	23.2	-9.8
	2.5	.10	.30	-.013	.359	.101	.100	.091	20.1	31.9	-16.4
	3.8	.15	.36	-.006	.345	.100	.089	.083	22.4	22.5	-8.1
	5.1	.20	.43	-.001	.321	.093	.075	.070	15.6	13.1	4.0
	6.4	.25	.49	-.004	.299	.086	.062	.060	11.9	5.4	8.0
	7.6	.30	.53	-.012	.286	.080	.055	.053	9.3	3.8	10.1
	8.9	.35	.57	-.019	.270	.075	.051	.049	7.6	4.2	10.1
	10.2	.40	.60	-.029	.267	.072	.047	.047	5.9	4.3	11.7
	11.4	.45	.62	-.035	.264	.068	.043	.044	5.9	3.6	8.7
	12.7	.50	.64	-.040	.265	.065	.042	.042	3.6	3.9	11.3
	15.2	.60	.67	-.047	.264	.059	.037	.037	2.0	3.1	9.1
	17.8	.70	.70	-.052	.255	.053	.038	.037	1.6	5.2	7.8
	20.3	.80	.72	-.054	.252	.048	.032	.029	1.4	2.8	5.7
	22.9	.90	.73	-	.258	.041	-	.022	-	1.8	-
	25.4	1.00	.75	-.057	.265	.032	.030	.019	-.1	.7	1.4
	27.9	1.10	.75	-	.269	.024	-	.017	-	.8	-
	33.0	1.30	.75	-	.276	.015	-	.010	-	.0	-

Table 3. - Continued.

z (mm)	y (mm)	y (in.)	$\frac{U_x}{V_\infty}$	$\frac{U_y}{V_\infty}$	$\frac{U_z}{V_\infty}$	$\frac{u'_x}{V_\infty}$	$\frac{u'_y}{V_\infty}$	$\frac{u'_z}{V_\infty}$	$-\frac{\overline{u_x u_y}}{V_\infty^2} \times 10^4$	$-\frac{\overline{u_x u_z}}{V_\infty^2} \times 10^4$	$-\frac{\overline{u_y u_z}}{V_\infty^2} \times 10^4$
-12.7	.5	.02	.07	-	.355	.135	-	.091	-	63.0	-
	.8	.03	.07	-	.367	.133	-	.087	-	72.8	-
	1.0	.04	.07	-	.373	.137	-	.089	-	81.6	-
	1.3	.05	.08	-	.370	.137	-	.092	-	83.7	-
	1.5	.06	.09	-	.373	.136	-	.095	-	84.3	-
	1.8	.07	.11	-	.366	.131	-	.096	-	76.6	-
	2.0	.08	.13	.019	.339	.126	.145	.100	86.0	72.1	-71.1
	2.3	.09	.14	.013	.323	.119	.143	.103	90.6	62.5	-74.2
	2.4	.09	.15	.019	.318	.115	.141	.104	81.8	58.3	-71.6
	2.5	.10	.16	.020	.322	.113	.136	.102	80.6	48.5	-66.7
	2.7	.11	.18	.024	.313	.110	.135	.104	77.6	47.3	-68.0
	2.8	.11	.19	.019	.308	.110	.127	.104	65.0	32.5	-62.1
	2.9	.11	.20	.023	.306	.104	.130	.104	69.6	36.4	-62.1
	3.0	.12	.22	.023	.301	.101	.126	.101	55.8	28.6	-53.6
	3.3	.13	.24	.022	.303	.105	.114	.106	52.2	24.3	-47.9
	3.6	.14	.27	.022	.292	.099	.104	.102	37.9	11.3	-36.1
	3.8	.15	.29	.022	.285	.098	.101	.100	27.7	9.9	-22.9
	5.1	.20	.37	.007	.264	.092	.082	.084	14.1	6.1	-2.1
	7.6	.30	.47	-.029	.247	.082	.059	.057	12.4	6.0	-.3
	10.2	.40	.53	-.052	.235	.074	.043	.046	2.5	4.7	14.4
	15.2	.60	.60	-	.231	.062	-	.036	-	3.4	-
	20.3	.80	.63	-.082	.235	.049	.030	.028	.2	3.3	7.3
	25.4	1.00	.66	-	.240	.035	-	.018	-	1.4	-
	33.0	1.30	.65	-	.247	.014	-	.009	-	.2	-

Table 3. - Continued.

z (mm)	y (mm)	y (in.)	$\frac{U_x}{V_\infty}$	$\frac{U_y}{V_\infty}$	$\frac{U_z}{V_\infty}$	$\frac{u'_x}{V_\infty}$	$\frac{u'_y}{V_\infty}$	$\frac{u'_z}{V_\infty}$	$-\frac{\overline{u_x u_y}}{V_\infty^2}\times 10^4$	$-\frac{\overline{u_x u_z}}{V_\infty^2}\times 10^4$	$-\frac{\overline{u_y u_z}}{V_\infty^2}\times 10^4$
-15.2	.5	.02	-.00	-	.343	.151	-	.098	-	71.4	-
	.8	.03	-.01	-	.360	.155	-	.092	-	81.7	-
	1.0	.04	-.01	-	.371	.156	-	.092	-	80.8	-
	1.3	.05	-.00	-	.373	.156	-	.091	-	76.8	-
	1.5	.06	.02	-	.378	.155	-	.089	-	73.7	-
	1.8	.07	.04	-	.368	.149	-	.093	-	73.6	-
	2.0	.08	.06	.039	.325	.142	.144	.096	124.0	72.2	-56.8
	2.3	.09	.08	.038	.301	.116	.138	.097	85.1	38.5	-54.6
	2.5	.10	.13	.022	.271	.097	.122	.103	43.5	.7	-56.7
	3.8	.15	.26	.024	.254	.098	.100	.099	18.3	-1.1	-19.5
	5.1	.20	.36	.004	.245	.091	.081	.087	16.1	1.6	-8.3
	6.4	.25	.41	-.021	.230	.087	.060	.066	9.6	.7	1.8
	7.6	.30	.45	-.038	.227	.082	.058	.054	6.3	1.3	9.1
	8.9	.35	.49	-.051	.218	.079	.049	.049	3.6	4.7	14.4
	10.2	.40	.51	-.062	.220	.075	.043	.046	2.6	3.9	12.9
	11.4	.45	.52	-.070	.220	.071	.041	.042	1.6	3.1	14.6
	12.7	.50	.54	-.076	.220	.068	.037	.040	3.4	2.7	8.5
	15.2	.60	.57	-.081	.214	.063	.033	.036	1.2	3.5	11.4
	17.8	.70	.59	-.085	.216	.055	.032	.033	1.3	3.3	6.9
	20.3	.80	.61	-.088	.220	.049	.027	.026	.3	1.5	7.3
	22.9	.90	.62	-	.226	.042	-	.023	-	1.7	-
	25.4	1.00	.63	-.081	.226	.034	.026	.020	-.0	1.4	3.0
	27.9	1.10	.63	-	.228	.025	-	.015	-	.8	-
	33.0	1.30	.59	-	.215	.015	-	.010	-	-.4	-

Table 3. - Continued.

z (mm)	y (mm)	y (in.)	$\frac{U_x}{V_\infty}$	$\frac{U_y}{V_\infty}$	$\frac{U_z}{V_\infty}$	$\frac{u'_x}{V_\infty}$	$\frac{u'_y}{V_\infty}$	$\frac{u'_z}{V_\infty}$	$-\frac{\overline{u_x u_y}}{V_\infty^2}\times 10^4$	$-\frac{\overline{u_x u_z}}{V_\infty^2}\times 10^4$	$-\frac{\overline{u_y u_z}}{V_\infty^2}\times 10^4$
-20.3	.5	.02	-.18	-	.260	.143	-	.089	-	138.6	-
	.8	.03	-.21	-	.273	.132	-	.087	-	128.1	-
	1.0	.04	-.21	-	.275	.123	-	.085	-	108.7	-
	1.3	.05	-.21	-	.273	.114	-	.088	-	90.9	-
	1.5	.06	-.21	-	.269	.116	-	.088	-	59.6	-
	1.8	.07	-.15	-	.280	.113	-	.097	-	41.8	-
	2.0	.08	-.10	.049	.258	.113	.108	.099	42.0	27.7	-26.1
	2.3	.09	.01	.032	.240	.125	.131	.092	44.7	29.5	-42.8
	2.4	.09	.04	-	.271	.119	-	.094	-	30.2	-
	2.5	.10	.06	.024	.229	.113	.121	.097	28.5	24.8	-39.2
	2.7	.11	.11	-	.254	.110	-	.105	-	19.9	-
	2.8	.11	.13	-	.245	.109	-	.104	-	18.3	-
	2.9	.11	.16	-	.227	.105	-	.104	-	7.7	-
	3.0	.12	.18	-	.220	.104	-	.102	-	3.6	-
	3.3	.13	.21	-	.206	.103	-	.100	-	1.1	-
	3.6	.14	.25	-	.191	.102	-	.098	-	-3.0	-
	3.8	.15	.25	-.004	.175	.102	.090	.096	2.3	-4.0	-17.8
	5.1	.20	.33	-.025	.178	.098	.077	.083	1.1	-.6	-10.9
	7.6	.30	.41	-.066	.165	.085	.055	.054	4.6	3.1	4.9
	10.2	.40	.46	-.084	.160	.076	.042	.044	2.2	2.2	14.0
	15.2	.60	.51	-.098	.155	.063	.032	.035	1.6	2.5	11.5
	20.3	.80	.54	-.097	.161	.050	.028	.028	1.4	1.8	5.2
	25.4	1.00	.56	-.088	.164	.036	.019	.016	-.2	.3	3.6
▼	33.0	1.30	.55	-	.168	.015	-	.009	-	0.0	-

Table 3. - Concluded.

z (mm)	y (mm)	y (in.)	$\frac{U_x}{V_\infty}$	$\frac{U_y}{V_\infty}$	$\frac{U_z}{V_\infty}$	$\frac{u'_x}{V_\infty}$	$\frac{u'_y}{V_\infty}$	$\frac{u'_z}{V_\infty}$	$-\frac{\overline{u_x u_y}}{V_\infty^2} \times 10^4$	$-\frac{\overline{u_x u_z}}{V_\infty^2} \times 10^4$	$-\frac{\overline{u_y u_z}}{V_\infty^2} \times 10^4$
-29.0	.5	.02	-.35	-	-.022	.166	-	.016	-	-29.7	-
	.8	.03	-.35	-	-.022	.142	-	.015	-	-24.7	-
	1.0	.04	-.33	-	-.021	.126	-	.030	-	-17.4	-
	1.3	.05	-.31	-	-.018	.117	-	.049	-	-11.5	-
	1.5	.06	-.28	-	-.023	.108	-	.063	-	-10.9	-
	1.8	.07	-.26	-	-.009	.103	-	.069	-	-3.5	-
	2.0	.08	-.22	.027	-.009	.102	.087	.087	23.5	-1.4	-60.6
	2.3	.09	-.21	.018	-.001	.098	.088	.093	14.2	1.3	-42.3
	2.5	.10	-.20	.014	.011	.095	.089	.097	9.2	1.4	-22.6
	3.8	.15	.25	-.055	.001	.104	.090	.071	9.0	-.9	10.4
	5.1	.20	.31	-.077	.001	.100	.057	.058	10.1	-2.7	8.3
	6.4	.25	.37	-	0.000	.092	-	.055	-	-2.2	-
	7.6	.30	.39	-.093	-.003	.085	.050	.049	10.5	-1.6	-10.0
	8.9	.35	.43	-	0.000	.079	-	.046	-	-1.8	-
	10.2	.40	.44	-	-.012	.075	-	.042	-	-.1	-
	11.4	.45	.46	-	0.000	.071	-	.040	-	-1.9	-
	12.7	.50	.45	-.111	0.000	.068	.039	.036	6.5	-1.2	7.6
	15.2	.60	.49	-	.005	.062	-	.034	-	-1.9	-
	17.8	.70	.50	-	0.000	.057	-	.028	-	-1.5	-
	20.3	.80	.51	-	-.011	.051	-	.023	-	-.3	-
	22.9	.90	.51	-.104	0.000	.043	.029	.021	1.7	-.9	2.2
	25.4	1.00	.53	-	.006	.033	-	.018	-	-.5	-
	27.9	1.10	.53	-	0.000	.026	-	.012	-	-.2	-
	33.0	1.30	.51	-	-.006	.016	-	.008	-	-.0	-

Table 4

Mean velocities and turbulence stresses in the juncture (x = 76 mm).

z (mm)	y (mm)	y (in.)	$\frac{U_x}{V_\infty}$	$\frac{U_y}{V_\infty}$	$\frac{U_z}{V_\infty}$	$\frac{u'_x}{V_\infty}$	$\frac{u'_y}{V_\infty}$	$\frac{u'_z}{V_\infty}$	$-\frac{\overline{u_x u_y}}{V_\infty^2}\times 10^4$	$-\frac{\overline{u_x u_z}}{V_\infty^2}\times 10^4$	$-\frac{\overline{u_y u_z}}{V_\infty^2}\times 10^4$
152.4	.5	.02	.50	-	-.003	.090	-	.046	-	-1.8	-
	.8	.03	.55	-	.002	.084	-	.045	-	-.7	-
	1.0	.04	.57	-	-.004	.080	-	.045	-	-1.3	-
	1.3	.05	.60	-	.008	.076	-	.047	-	-.5	-
	1.5	.06	.61	-	0.000	.074	-	.047	-	-.3	-
	1.8	.07	.63	-	.002	.073	-	.047	-	.4	-
	2.0	.08	.64	-	.002	.071	-	.047	-	.2	-
	2.3	.09	.65	.007	.002	.070	.042	.046	12.4	.4	4.9
	2.5	.10	.66	.007	.001	.069	.041	.046	12.1	.8	6.4
	3.8	.15	.70	.004	.001	.065	.043	.044	11.5	-.0	3.2
	5.1	.20	.74	.002	.001	.063	.044	.043	11.1	.9	4.9
	6.4	.25	.76	.001	.004	.060	.044	.044	10.4	.4	2.3
	7.6	.30	.79	.001	.006	.059	.044	.044	10.4	.7	4.1
	8.9	.35	.81	.004	-.016	.057	.044	.045	9.7	.8	4.3
	10.2	.40	.83	.004	.007	.056	.042	.044	9.3	.4	3.6
	11.4	.45	.85	.003	-.010	.054	.041	.043	8.3	.8	3.7
	12.7	.50	.87	.001	.005	.052	.040	.041	7.6	.4	2.1
	15.2	.60	.90	.004	-.011	.047	.036	.039	5.8	.8	3.8
	17.8	.70	.93	.001	-.007	.041	.033	.035	4.0	.8	2.7
	20.3	.80	.96	.005	-.003	.036	.026	.028	2.6	.6	2.4
	22.9	.90	.98	.001	-.010	.027	.022	.022	.5	.5	.2
	25.4	1.00	.99	.002	-.017	.018	.022	.017	-.3	.2	.3
	27.9	1.10	1.00	.003	-.007	.010	.020	.015	-.7	.2	.4
↓	33.0	1.30	1.00	-	-.026	.005	-	.012	-	.1	-

Table 4. - Continued.

z (mm)	y (mm)	y (in.)	$\frac{U_x}{V_\infty}$	$\frac{U_y}{V_\infty}$	$\frac{U_z}{V_\infty}$	$\frac{u'_x}{V_\infty}$	$\frac{u'_y}{V_\infty}$	$\frac{u'_z}{V_\infty}$	$-\frac{\overline{u_x u_y}}{V_\infty^2}\times 10^4$	$-\frac{\overline{u_x u_z}}{V_\infty^2}\times 10^4$	$-\frac{\overline{u_y u_z}}{V_\infty^2}\times 10^4$
101.6	.5	.02	.53	-	-.003	.086	-	.055	-	-2.5	-
	.8	.03	.58	-	.006	.078	-	.054	-	-.7	-
	1.0	.04	.61	-	.011	.074	-	.052	-	-.6	-
	1.3	.05	.63	-	.018	.069	-	.052	-	.2	-
	1.5	.06	.65	-	.023	.067	-	.051	-	.3	-
	1.8	.07	.66	-	.025	.064	-	.050	-	.9	-
	2.0	.08	.67	-	.026	.062	-	.051	-	1.2	-
	2.3	.09	.68	.010	.023	.061	.056	.049	12.2	1.1	9.4
	2.5	.10	.70	.010	.022	.060	.055	.048	11.9	1.0	6.0
	3.8	.15	.74	.011	.022	.055	.056	.046	11.0	1.0	6.1
	5.1	.20	.77	.009	.021	.053	.056	.046	10.3	1.8	6.1
	6.4	.25	.79	.006	.023	.052	.058	.046	10.7	1.4	3.5
	7.6	.30	.81	.008	.017	.052	.057	.045	10.6	1.3	3.1
	8.9	.35	.83	.008	.015	.051	.056	.045	10.2	1.5	5.4
	10.2	.40	.85	.007	.015	.050	.056	.046	9.8	1.1	3.5
	11.4	.45	.87	.010	.006	.049	.054	.044	9.4	1.0	3.6
	12.7	.50	.89	.006	.012	.047	.053	.043	8.5	1.2	5.0
	15.2	.60	.92	.009	.006	.043	.050	.040	7.0	1.2	3.1
	17.8	.70	.95	.008	.007	.037	.043	.035	4.8	1.0	1.6
	20.3	.80	.97	.008	-.005	.030	.036	.027	2.9	.7	2.2
	22.9	.90	.99	.009	.002	.024	.028	.020	.9	.5	.7
	25.4	1.00	1.00	.009	-.005	.016	.024	.017	-.3	.2	.3
	27.9	1.10	1.00	.009	.005	.009	.021	.013	-.6	.2	.6
	33.0	1.30	1.01	-	-.012	.005	-	.009	-	.0	-

Table 4. - Continued.

z (mm)	y (mm)	y (in.)	$\frac{U_x}{V_\infty}$	$\frac{U_y}{V_\infty}$	$\frac{U_z}{V_\infty}$	$\frac{u'_x}{V_\infty}$	$\frac{u'_y}{V_\infty}$	$\frac{u'_z}{V_\infty}$	$-\frac{\overline{u_x u_y}}{V_\infty^2}\times 10^4$	$-\frac{\overline{u_x u_z}}{V_\infty^2}\times 10^4$	$-\frac{\overline{u_y u_z}}{V_\infty^2}\times 10^4$
50.8	.5	.02	.59	-	.011	.094	-	.062	-	-11.6	-
	.8	.03	.64	-	.031	.085	-	.062	-	-7.5	-
	1.0	.04	.67	-	.035	.079	-	.060	-	-5.5	-
	1.3	.05	.69	-	.051	.074	-	.060	-	-2.8	-
	1.5	.06	.71	-	.057	.071	-	.059	-	-1.3	-
	1.8	.07	.73	-	.059	.068	-	.058	-	-.4	-
	2.0	.08	.75	-	.066	.066	-	.059	-	1.0	-
	2.3	.09	.75	.023	.073	.063	.053	.058	10.2	1.8	9.2
	2.5	.10	.76	.023	.066	.061	.053	.058	9.8	2.0	9.6
	3.8	.15	.80	.026	.059	.056	.054	.055	8.5	3.3	4.9
	5.1	.20	.82	.027	.049	.054	.057	.054	8.9	3.2	3.5
	6.4	.25	.84	.028	.038	.055	.058	.053	10.0	2.1	2.2
	7.6	.30	.86	.029	.028	.056	.059	.052	10.7	1.1	3.7
	8.9	.35	.88	.031	.020	.056	.058	.051	10.8	.4	1.8
	10.2	.40	.90	.030	.017	.055	.057	.050	10.8	.3	3.5
	11.4	.45	.91	.032	-.006	.053	.056	.049	10.0	.6	3.6
	12.7	.50	.93	.034	.008	.052	.054	.047	9.4	.6	3.3
	15.2	.60	.95	.030	-.007	.048	.050	.042	8.0	.5	3.0
	17.8	.70	.98	.032	.003	.042	.044	.036	5.8	.7	2.2
	20.3	.80	1.00	.029	-.011	.037	.037	.029	3.6	.5	2.4
	22.9	.90	1.02	.025	-.004	.029	.029	.022	2.2	.3	1.1
	25.4	1.00	1.04	.026	-.013	.023	.018	.014	.4	.2	-.0
	27.9	1.10	1.04	.027	-.004	.016	.015	.011	-.4	.1	.8
	33.0	1.30	1.05	-	-.009	.014	-	.003	-	.1	-

Table 4. - Continued.

z (mm)	y (mm)	y (in.)	$\frac{U_x}{V_\infty}$	$\frac{U_y}{V_\infty}$	$\frac{U_z}{V_\infty}$	$\frac{u'_x}{V_\infty}$	$\frac{u'_y}{V_\infty}$	$\frac{u'_z}{V_\infty}$	$-\frac{\overline{u_x u_y}}{V_\infty^2}\times 10^4$	$-\frac{\overline{u_x u_z}}{V_\infty^2}\times 10^4$	$-\frac{\overline{u_y u_z}}{V_\infty^2}\times 10^4$
35.6	.5	.02	.64	-	.037	.107	-	.082	-	-11.1	-
	.8	.03	.68	-	.054	.102	-	.083	-	-7.1	-
	1.0	.04	.71	-	.061	.096	-	.082	-	-4.2	-
	1.3	.05	.73	-	.072	.092	-	.081	-	-1.8	-
	1.5	.06	.75	-	.076	.088	-	.083	-	.8	-
	1.8	.07	.76	-	.075	.084	-	.083	-	4.0	-
	2.0	.08	.77	-	.079	.082	-	.081	-	5.5	-
	2.3	.09	.77	.024	.081	.080	.082	.082	18.3	7.4	7.5
	2.5	.10	.77	.028	.094	.077	.085	.081	18.1	8.2	7.1
	3.8	.15	.79	.035	.092	.073	.094	.078	20.4	8.9	-15.0
	5.1	.20	.81	.043	.075	.074	.099	.076	23.2	8.2	-23.0
	6.4	.25	.82	.048	.072	.075	.100	.074	25.0	5.2	-18.3
	7.6	.30	.84	.051	.046	.075	.097	.071	25.4	1.9	-16.1
	8.9	.35	.86	.051	.016	.073	.093	.067	22.5	-.7	-8.3
	10.2	.40	.89	.050	.022	.072	.083	.060	18.5	-1.4	-7.6
	11.4	.45	.90	.045	-.003	.067	.077	.056	15.9	-2.0	-1.1
	12.7	.50	.92	.041	.002	.060	.070	.052	12.9	-1.1	-1.2
	15.2	.60	.96	.033	-.015	.050	.057	.044	8.7	-.8	2.1
	17.8	.70	.99	.031	-.017	.042	.046	.036	5.9	-.5	2.3
	20.3	.80	1.01	.026	-.016	.036	.036	.027	3.0	.0	2.7
	22.9	.90	1.03	.023	-.027	.028	.026	.021	.9	.1	2.2
	25.4	1.00	1.04	.022	-.024	.021	.019	.014	-.1	.2	2.3
	27.9	1.10	1.05	.021	-.020	.016	.017	.010	-.5	.1	3.6
	33.0	1.30	1.05	-	-.017	.016	-	.005	-	.1	-

Table 4. - Continued.

z (mm)	y (mm)	y (in.)	$\frac{U_x}{V_\infty}$	$\frac{U_y}{V_\infty}$	$\frac{U_z}{V_\infty}$	$\frac{u'_x}{V_\infty}$	$\frac{u'_y}{V_\infty}$	$\frac{u'_z}{V_\infty}$	$-\frac{\overline{u_x u_y}}{V_\infty^2} \times 10^4$	$-\frac{\overline{u_x u_z}}{V_\infty^2} \times 10^4$	$-\frac{\overline{u_y u_z}}{V_\infty^2} \times 10^4$
30.5	.5	.02	.60	-	.062	.107	-	.088	-	-8.2	-
	.8	.03	.66	-	.081	.104	-	.094	-	-11.0	-
	1.0	.04	.69	-	.098	.099	-	.098	-	-11.6	-
	1.3	.05	.72	-	.100	.095	-	.098	-	-12.2	-
	1.5	.06	.73	-	.110	.090	-	.100	-	-10.9	-
	1.8	.07	.75	-	.117	.086	-	.101	-	-8.6	-
	2.0	.08	.76	-	.131	.083	-	.098	-	-7.4	-
	2.3	.09	.76	.047	.122	.080	.099	.095	14.2	-4.9	5.0
	2.5	.10	.76	.049	.129	.084	.092	.098	13.3	-5.1	-1.2
	3.8	.15	.78	.058	.116	.078	.103	.089	11.4	1.4	-18.0
	5.1	.20	.79	.067	.108	.080	.111	.082	11.9	2.3	-23.0
	6.4	.25	.80	.065	.068	.085	.114	.080	16.9	1.4	-26.5
	7.6	.30	.81	.061	.028	.089	.111	.074	20.9	-3.2	-22.0
	8.9	.35	.83	.054	.003	.090	.105	.068	22.7	-6.4	-14.2
	10.2	.40	.86	.046	-.006	.085	.096	.062	22.2	-6.8	-1.9
	11.4	.45	.89	.033	-.011	.077	.087	.058	19.2	-6.1	2.6
	12.7	.50	.92	.028	-.022	.068	.076	.054	14.4	-4.0	2.7
	15.2	.60	.97	.017	-.029	.053	.059	.044	9.1	-1.5	1.7
	17.8	.70	1.01	.009	-.033	.042	.048	.037	5.4	-1.0	2.1
	20.3	.80	1.03	.004	-.034	.034	.039	.030	2.5	-.3	2.1
	22.9	.90	1.05	.001	-.022	.024	.031	.021	.4	-.1	1.1
	25.4	1.00	1.06	-.001	-.026	.015	.026	.017	-.5	.1	2.9
	27.9	1.10	1.06	0.000	-.032	.010	.024	.013	-.6	.1	4.7
↓	33.0	1.30	1.07	-	-.020	.011	-	.008	-	.1	-

Table 4. - Continued.

z (mm)	y (mm)	y (in.)	$\frac{U_x}{V_\infty}$	$\frac{U_y}{V_\infty}$	$\frac{U_z}{V_\infty}$	$\frac{u'_x}{V_\infty}$	$\frac{u'_y}{V_\infty}$	$\frac{u'_z}{V_\infty}$	$-\frac{\overline{u_x u_y}}{V_\infty^2}\times 10^4$	$-\frac{\overline{u_x u_z}}{V_\infty^2}\times 10^4$	$-\frac{\overline{u_y u_z}}{V_\infty^2}\times 10^4$
27.9	.5	.02	.62	-	.095	.116	-	.098	-	-34.4	-
	.8	.03	.68	-	.116	.109	-	.106	-	-40.2	-
	1.0	.04	.72	-	.135	.113	-	.103	-	-41.0	-
	1.3	.05	.75	-	.135	.105	-	.104	-	-35.2	-
	1.5	.06	.77	-	.142	.099	-	.110	-	-36.7	-
	1.8	.07	.78	-	.150	.093	-	.108	-	-29.5	-
	2.0	.08	.79	-	.143	.088	-	.103	-	-24.3	-
	2.3	.09	.79	.049	.146	.084	.089	.098	7.3	-20.4	10.8
	2.5	.10	.79	.052	.150	.081	.092	.096	4.9	-15.9	8.6
	3.8	.15	.80	.051	.131	.076	.107	.084	-1.5	-4.3	-3.8
	5.1	.20	.80	.050	.094	.081	.121	.083	-2.5	.4	-13.0
	6.4	.25	.80	.051	.048	.087	.130	.085	4.3	1.3	-15.8
	7.6	.30	.81	.042	.013	.092	.124	.078	12.5	-1.3	-13.0
	8.9	.35	.84	.037	-.026	.092	.112	.072	18.7	-4.9	-6.4
	10.2	.40	.86	.033	-.044	.086	.100	.064	18.6	-7.6	.2
	11.4	.45	.90	.025	-.046	.076	.089	.059	18.0	-6.5	7.7
	12.7	.50	.93	.024	-.044	.067	.076	.055	12.7	-4.7	3.2
	15.2	.60	.96	.020	-.056	.052	.058	.044	8.2	-2.4	3.4
	17.8	.70	1.01	.017	-.039	.042	.044	.035	4.8	-1.0	3.7
	20.3	.80	1.03	.015	-.041	.033	.033	.027	2.7	-.1	2.4
	22.9	.90	1.05	.014	-.042	.023	.027	.020	.4	.0	2.0
	25.4	1.00	1.05	.014	-.046	.015	.024	.015	-.3	-.1	3.8
	27.9	1.10	1.06	.012	-.052	.010	.022	.012	-.1	.1	6.4
	33.0	1.30	1.06	-	-.058	.012	-	.007	-	.1	-

Table 4. - Continued.

z (mm)	y (mm)	y (in.)	$\frac{U_x}{V_\infty}$	$\frac{U_y}{V_\infty}$	$\frac{U_z}{V_\infty}$	$\frac{u'_x}{V_\infty}$	$\frac{u'_y}{V_\infty}$	$\frac{u'_z}{V_\infty}$	$-\frac{\overline{u_x u_y}}{V_\infty^2}\times 10^4$	$-\frac{\overline{u_x u_z}}{V_\infty^2}\times 10^4$	$-\frac{\overline{u_y u_z}}{V_\infty^2}\times 10^4$
25.4	.5	.02	.69	-	.125	.114	-	.100	-	-41.8	-
	.8	.03	.75	-	.138	.112	-	.101	-	-43.2	-
	1.0	.04	.79	-	.148	.104	-	.094	-	-45.4	-
	1.3	.05	.81	-	.166	.101	-	.097	-	-42.4	-
	1.5	.06	.82	-	.161	.094	-	.095	-	-36.9	-
	1.8	.07	.83	-	.167	.088	-	.090	-	-29.6	-
	2.0	.08	.83	-	.168	.081	-	.087	-	-23.2	-
	2.3	.09	.83	.030	.170	.078	.086	.084	5.6	-18.5	4.1
	2.5	.10	.83	.029	.161	.075	.090	.081	2.2	-14.5	3.6
	3.8	.15	.83	.018	.140	.075	.106	.076	-.9	-5.4	-6.7
	5.1	.20	.82	.012	.113	.082	.118	.082	2.4	1.0	-12.0
	6.4	.25	.82	.007	.070	.089	.123	.085	10.0	2.6	-13.4
	7.6	.30	.84	.003	.029	.094	.117	.079	17.3	1.0	-4.5
	8.9	.35	.86	0.000	-.010	.091	.107	.072	20.2	-3.7	4.8
	10.2	.40	.89	.001	-.037	.084	.093	.064	18.3	-6.4	10.3
	11.4	.45	.92	.001	-.056	.075	.082	.058	15.6	-6.7	5.6
	12.7	.50	.94	0.000	-.051	.065	.073	.051	12.5	-4.8	4.0
	15.2	.60	.99	0.000	-.060	.051	.055	.042	7.7	-2.0	2.8
	17.8	.70	1.02	-.005	-.053	.041	.043	.034	4.4	-1.0	1.7
	20.3	.80	1.05	-.004	-.049	.031	.034	.026	2.3	-.3	3.5
	22.9	.90	1.06	-.006	-.048	.022	.027	.019	.2	-.0	2.7
	25.4	1.00	1.07	-.007	-.045	.014	.024	.014	-.3	-.0	4.2
	27.9	1.10	1.07	-.005	-.048	.010	.024	.012	-.2	.0	6.6
	33.0	1.30	1.07	-	-.056	.012	-	.006	-	.2	-

Table 4. - Continued.

z (mm)	y (mm)	y (in.)	$\frac{U_x}{V_\infty}$	$\frac{U_y}{V_\infty}$	$\frac{U_z}{V_\infty}$	$\frac{u'_x}{V_\infty}$	$\frac{u'_y}{V_\infty}$	$\frac{u'_z}{V_\infty}$	$-\frac{\overline{u_x u_y}}{V_\infty^2}\times 10^4$	$-\frac{\overline{u_x u_z}}{V_\infty^2}\times 10^4$	$-\frac{\overline{u_y u_z}}{V_\infty^2}\times 10^4$
22.9	.5	.02	.73	-	.146	.115	-	.084	-	-37.8	-
	.8	.03	.79	-	.166	.108	-	.081	-	-35.3	-
	1.0	.04	.83	-	.173	.096	-	.081	-	-30.5	-
	1.3	.05	.85	-	.165	.087	-	.077	-	-24.0	-
	1.5	.06	.86	-	.171	.080	-	.076	-	-19.4	-
	1.8	.07	.86	-	.166	.074	-	.073	-	-15.9	-
	2.0	.08	.87	-	.152	.070	-	.071	-	-12.4	-
	2.3	.09	.86	.006	.158	.068	.074	.068	-.7	-10.2	-7.9
	2.5	.10	.86	.003	.153	.068	.077	.067	-.1	-8.7	-8.6
	3.8	.15	.85	-.013	.111	.071	.092	.068	.8	-3.6	-10.7
	5.1	.20	.84	-.026	.077	.079	.101	.073	6.5	.1	-11.6
	6.4	.25	.84	-.029	.037	.086	.101	.078	11.9	2.0	-7.2
	7.6	.30	.86	-.027	.006	.088	.094	.073	14.5	-1.8	2.6
	8.9	.35	.88	-.025	-.023	.083	.083	.069	14.9	-6.3	12.5
	10.2	.40	.91	-.018	-.038	.076	.074	.060	13.8	-7.1	7.4
	11.4	.45	.93	-.013	-.042	.068	.065	.055	11.2	-5.5	5.9
	12.7	.50	.96	-.010	-.055	.059	.062	.050	9.2	-4.2	4.4
	15.2	.60	.99	-.004	-.050	.047	.048	.041	6.3	-2.0	3.7
	17.8	.70	1.02	-.001	-.060	.038	.039	.032	3.7	-.6	3.2
	20.3	.80	1.04	-.001	-.056	.028	.032	.023	1.6	-.3	2.3
	22.9	.90	1.06	-.001	-.052	.020	.026	.017	-.0	.1	3.8
	25.4	1.00	1.07	.002	-.052	.014	.023	.012	.1	.0	7.8
	27.9	1.10	1.07	.003	-.037	.009	.025	.011	.6	.0	11.5
	33.0	1.30	1.07	-	-.060	.010	-	.008	-	.1	-

Table 4. - Continued.

z (mm)	y (mm)	y (in.)	$\frac{U_x}{V_\infty}$	$\frac{U_y}{V_\infty}$	$\frac{U_z}{V_\infty}$	$\frac{u'_x}{V_\infty}$	$\frac{u'_y}{V_\infty}$	$\frac{u'_z}{V_\infty}$	$-\frac{\overline{u_x u_y}}{V_\infty^2}\times 10^4$	$-\frac{\overline{u_x u_z}}{V_\infty^2}\times 10^4$	$-\frac{\overline{u_y u_z}}{V_\infty^2}\times 10^4$
21.6	.5	.02	.77	-	.161	.104	-	.076	-	-21.7	-
	.8	.03	.82	-	.170	.094	-	.073	-	-18.5	-
	1.0	.04	.85	-	.178	.085	-	.068	-	-16.3	-
	1.3	.05	.87	-	.181	.075	-	.067	-	-13.5	-
	1.5	.06	.87	-	.173	.067	-	.065	-	-10.6	-
	1.8	.07	.87	-	.167	.063	-	.063	-	-8.3	-
	2.0	.08	.88	-	.164	.061	-	.062	-	-7.5	-
	2.3	.09	.87	.008	.154	.059	.075	.062	-2.6	-6.0	-3.6
	2.5	.10	.88	.002	.153	.060	.077	.060	-2.7	-5.0	-3.1
	3.8	.15	.87	-.013	.115	.064	.088	.061	-.6	-2.1	-6.2
	5.1	.20	.87	-.029	.071	.070	.095	.066	4.1	.3	-3.0
	6.4	.25	.88	-.037	.040	.075	.097	.067	8.9	-.6	-.2
	7.6	.30	.89	-.035	.006	.076	.091	.067	11.1	-2.8	5.3
	8.9	.35	.91	-.029	-.016	.072	.084	.064	11.0	-6.8	3.6
	10.2	.40	.93	-.022	-.028	.065	.077	.058	10.8	-6.1	9.9
	11.4	.45	.95	-.015	-.042	.058	.071	.054	9.7	-5.0	6.4
	12.7	.50	.97	-.013	-.047	.052	.064	.048	8.7	-3.3	7.7
	15.2	.60	1.00	-.005	-.039	.041	.053	.040	6.1	-1.7	4.9
	17.8	.70	1.03	.002	-.043	.031	.045	.031	3.7	-.8	3.2
	20.3	.80	1.05	0.000	-.051	.023	.035	.025	2.2	-.3	5.4
	22.9	.90	1.06	.005	-.041	.015	.028	.019	.6	-.0	6.6
	25.4	1.00	1.06	.007	-.035	.010	.027	.014	.9	.0	10.0
	27.9	1.10	1.07	.007	-.032	.007	.027	.012	1.3	.0	14.3
↓	33.0	1.30	1.06	-	-.030	.004	-	.011	-	.0	-

Table 4. - Continued.

z (mm)	y (mm)	y (in.)	$\frac{U_x}{V_\infty}$	$\frac{U_y}{V_\infty}$	$\frac{U_z}{V_\infty}$	$\frac{u'_x}{V_\infty}$	$\frac{u'_y}{V_\infty}$	$\frac{u'_z}{V_\infty}$	$-\frac{\overline{u_x u_y}}{V_\infty^2}\times 10^4$	$-\frac{\overline{u_x u_z}}{V_\infty^2}\times 10^4$	$-\frac{\overline{u_y u_z}}{V_\infty^2}\times 10^4$
20.3	.5	.02	.76	-	.152	.105	-	.076	-	-20.6	-
	.8	.03	.83	-	.170	.096	-	.073	-	-17.8	-
	1.0	.04	.86	-	.166	.085	-	.071	-	-15.2	-
	1.3	.05	.87	-	.175	.075	-	.067	-	-11.6	-
	1.5	.06	.88	-	.158	.069	-	.065	-	-10.4	-
	1.8	.07	.88	-	.162	.065	-	.063	-	-8.4	-
	2.0	.08	.88	-	.157	.061	-	.061	-	-7.4	-
	2.3	.09	.88	-.004	.142	.060	.063	.060	-1.7	-6.3	-6.2
	2.5	.10	.88	-.007	.137	.060	.065	.058	-1.5	-5.6	-6.3
	3.8	.15	.87	-.022	.108	.064	.073	.061	.6	-3.1	-5.6
	5.1	.20	.87	-.036	.061	.071	.077	.063	3.5	-1.1	-2.9
	6.4	.25	.88	-.043	.023	.075	.074	.066	6.1	-.4	-.8
	7.6	.30	.89	-.043	.011	.076	.067	.063	8.0	-3.7	.4
	8.9	.35	.91	-.037	-.014	.072	.064	.063	8.8	-6.3	3.0
	10.2	.40	.93	-.033	-.031	.065	.058	.057	8.6	-5.4	5.2
	11.4	.45	.95	-.028	-.033	.059	.057	.052	8.2	-4.4	4.6
	12.7	.50	.98	-.022	-.044	.052	.054	.049	7.6	-3.9	2.2
	15.2	.60	1.00	-.015	-.049	.043	.046	.039	4.9	-1.7	4.0
	17.8	.70	1.03	-.014	-.052	.035	.037	.030	2.9	-.9	3.1
	20.3	.80	1.05	-.009	-.040	.025	.032	.022	1.3	-.2	5.1
	22.9	.90	1.06	-.006	-.048	.017	.027	.017	.1	-.1	4.7
	25.4	1.00	1.07	-.005	-.041	.012	.025	.013	.0	.1	9.3
	27.9	1.10	1.07	-.005	-.035	.009	.025	.010	.5	.1	12.6
	33.0	1.30	1.07	-	-.034	.009	-	.009	-	-.0	-

Table 4. - Continued.

z (mm)	y (mm)	y (in.)	$\frac{U_x}{V_\infty}$	$\frac{U_y}{V_\infty}$	$\frac{U_z}{V_\infty}$	$\frac{u'_x}{V_\infty}$	$\frac{u'_y}{V_\infty}$	$\frac{u'_z}{V_\infty}$	$-\frac{\overline{u_x u_y}}{V_\infty^2}\times 10^4$	$-\frac{\overline{u_x u_z}}{V_\infty^2}\times 10^4$	$-\frac{\overline{u_y u_z}}{V_\infty^2}\times 10^4$
17.8	.5	.02	.80	-	.135	.099	-	.071	-	-10.0	-
	.8	.03	.86	-	.150	.088	-	.069	-	-8.3	-
	1.0	.04	.89	-	.147	.077	-	.065	-	-7.1	-
	1.3	.05	.90	-	.141	.067	-	.062	-	-5.6	-
	1.5	.06	.91	-	.139	.061	-	.059	-	-5.5	-
	1.8	.07	.91	-	.131	.056	-	.057	-	-5.2	-
	2.0	.08	.91	-	.128	.054	-	.056	-	-4.4	-
	2.3	.09	.91	-.003	.117	.052	.064	.054	-2.0	-4.3	-.1
	2.5	.10	.91	-.005	.113	.051	.066	.053	-1.1	-4.1	-2.7
	3.8	.15	.91	-.021	.075	.052	.072	.051	1.8	-3.6	-4.2
	5.1	.20	.92	-.030	.042	.057	.075	.052	4.1	-2.8	-3.2
	6.4	.25	.93	-.035	.026	.058	.074	.053	5.2	-3.3	-1.8
	7.6	.30	.94	-.036	-.005	.057	.070	.052	7.0	-4.1	.1
	8.9	.35	.96	-.034	-.022	.055	.066	.052	7.6	-4.6	.8
	10.2	.40	.97	-.032	-.034	.052	.062	.049	7.9	-4.0	1.2
	11.4	.45	.98	-.027	-.033	.048	.057	.046	7.6	-3.2	4.6
	12.7	.50	1.00	-.023	-.043	.045	.054	.042	6.5	-2.5	2.7
	15.2	.60	1.02	-.018	-.052	.037	.046	.034	4.3	-1.3	3.8
	17.8	.70	1.04	-.017	-.051	.028	.038	.026	2.5	-.5	2.3
	20.3	.80	1.05	-.011	-.044	.022	.028	.018	.4	-.0	3.6
	22.9	.90	1.06	-.011	-.043	.014	.027	.015	.6	.0	5.7
	25.4	1.00	1.06	-.005	-.045	.010	.027	.011	1.0	-.0	11.5
	27.9	1.10	1.06	-.004	-.048	.008	.028	.011	1.8	.1	13.4
	33.0	1.30	1.07	-	-.054	.007	-	.009	-	.1	-

Table 4. - Continued.

z (mm)	y (mm)	y (in.)	$\frac{U_x}{V_\infty}$	$\frac{U_y}{V_\infty}$	$\frac{U_z}{V_\infty}$	$\frac{u'_x}{V_\infty}$	$\frac{u'_y}{V_\infty}$	$\frac{u'_z}{V_\infty}$	$-\frac{\overline{u_x u_y}}{V_\infty^2}\times 10^4$	$-\frac{\overline{u_x u_z}}{V_\infty^2}\times 10^4$	$-\frac{\overline{u_y u_z}}{V_\infty^2}\times 10^4$
15.2	.5	.02	.79	-	.109	.106	-	.064	-	-12.4	-
	.8	.03	.86	-	.122	.096	-	.063	-	-10.9	-
	1.0	.04	.89	-	.129	.084	-	.060	-	-10.1	-
	1.3	.05	.91	-	.119	.072	-	.059	-	-6.8	-
	1.5	.06	.92	-	.115	.064	-	.057	-	-5.8	-
	1.8	.07	.92	-	.115	.058	-	.054	-	-5.6	-
	2.0	.08	.92	-	.108	.055	-	.052	-	-4.6	-
	2.3	.09	.92	-.002	.094	.053	.054	.051	-.1	-4.5	-1.8
	2.5	.10	.92	-.003	.087	.052	.056	.050	-.0	-4.6	-2.2
	3.8	.15	.92	-.017	.045	.053	.062	.045	2.2	-4.3	-2.6
	5.1	.20	.93	-.024	.026	.054	.062	.045	3.8	-4.3	-1.8
	6.4	.25	.94	-.030	.016	.054	.062	.047	5.5	-4.0	-.5
	7.6	.30	.96	-.032	-.002	.055	.058	.045	6.0	-3.9	-.3
	8.9	.35	.97	-.032	-.015	.052	.055	.046	6.6	-3.4	1.6
	10.2	.40	.99	-.030	-.031	.051	.051	.042	6.4	-2.9	2.6
	11.4	.45	.99	-.029	-.035	.047	.049	.040	6.0	-2.3	3.3
	12.7	.50	1.01	-.029	-.032	.044	.046	.039	5.4	-2.3	2.0
	15.2	.60	1.03	-.026	-.058	.036	.041	.033	3.6	-1.5	2.3
	17.8	.70	1.05	-.020	-.055	.027	.036	.024	1.9	-.2	2.8
	20.3	.80	1.07	-.017	-.054	.019	.028	.018	.3	-.1	3.1
	22.9	.90	1.07	-.015	-.052	.013	.025	.015	-.0	-.0	5.2
	25.4	1.00	1.08	-.013	-.051	.009	.024	.012	.3	.0	8.8
	27.9	1.10	1.08	-.009	-.053	.007	.024	.012	.9	.1	15.0
	33.0	1.30	1.08	-	-.058	.005	-	.010	-	.0	-

Table 4. - Concluded.

z (mm)	y (mm)	y (in.)	$\frac{U_x}{V_\infty}$	$\frac{U_y}{V_\infty}$	$\frac{U_z}{V_\infty}$	$\frac{u'_x}{V_\infty}$	$\frac{u'_y}{V_\infty}$	$\frac{u'_z}{V_\infty}$	$-\frac{\overline{u_x u_y}}{V_\infty^2}\times 10^4$	$-\frac{\overline{u_x u_z}}{V_\infty^2}\times 10^4$	$-\frac{\overline{u_y u_z}}{V_\infty^2}\times 10^4$
10.2	.5	.02	.87	-	.082	.113	-	.068	-	-15.5	-
	.8	.03	.92	-	.091	.092	-	.064	-	-11.7	-
	1.0	.04	.94	-	.094	.076	-	.057	-	-7.7	-
	1.3	.05	.95	-	.079	.063	-	.058	-	-5.2	-
	1.5	.06	.95	-	.073	.056	-	.053	-	-4.1	-
	1.8	.07	.95	-	.073	.052	-	.050	-	-3.0	-
	2.0	.08	.95	-	.065	.049	-	.048	-	-2.8	-
	2.3	.09	.95	-.013	.063	.047	.050	.047	1.4	-2.6	-.6
	2.5	.10	.95	-.014	.052	.047	.050	.044	1.5	-2.9	.5
	3.8	.15	.96	-.029	.020	.045	.054	.041	2.8	-4.0	.4
	5.1	.20	.97	-.036	.015	.045	.053	.041	3.7	-3.9	.8
	6.4	.25	.98	-.042	-.002	.044	.052	.041	4.3	-3.4	.7
	7.6	.30	.99	-.045	-.016	.043	.048	.041	4.6	-3.4	.0
	8.9	.35	1.00	-.042	-.021	.042	.046	.040	4.2	-2.9	2.4
	10.2	.40	1.02	-.044	-.034	.039	.045	.040	4.1	-2.4	1.7
	11.4	.45	1.03	-.044	-.032	.037	.042	.037	3.5	-1.5	2.0
	12.7	.50	1.03	-.044	-.047	.034	.040	.035	3.1	-1.5	2.0
	15.2	.60	1.05	-.043	-.040	.027	.035	.027	2.1	-.6	2.6
	17.8	.70	1.06	-.036	-.042	.020	.029	.022	.9	-.3	3.3
	20.3	.80	1.06	-.035	-.060	.014	.030	.017	1.2	-.0	6.1
	22.9	.90	1.07	-.032	-.056	.010	.028	.013	.4	.0	6.5
	25.4	1.00	1.07	-.027	-.058	.007	.030	.011	2.1	-.0	11.0
	27.9	1.10	1.07	-.022	-.041	.006	.031	.011	2.4	.1	13.3
	33.0	1.30	1.07	-	-.045	.005	-	.010	-	-.1	-

Table 5
Variation of local mean flow direction upstream of the body leading edge.

x (mm)	y (mm)	z (mm)	θ (degrees)
-38	.5	0.0	28.
-38	.5	-2.5	28.
-38	.5	-5.1	27.
-38	.5	-7.6	28.
-38	.5	-10.2	24.
-38	.5	-12.7	24.
-38	.5	-15.2	21.
-38	.5	-17.8	19.
-38	.5	-20.3	15.
-38	.5	-22.9	12.
-38	.5	-25.4	5.
-38	.5	-26.2	3.
-38	.5	-26.9	0.
-38	.5	-27.9	0.
-38	.5	-29.0	-2.
-38	.5	-29.7	-3.
-38	.5	-30.5	-5.
-38	.5	-31.2	-7.
-38	.5	-32.0	-7.
-38	.5	-33.0	-9.
-38	.5	-34.3	-12.
-38	.5	-35.6	-14.

Table 5. - Continued.

x (mm)	y (mm)	z (mm)	θ (degrees)
-38	1.0	0.0	24.
-38	1.0	-2.5	25.
-38	1.0	-5.1	23.
-38	1.0	-7.6	23.
-38	1.0	-10.2	21.
-38	1.0	-12.7	20.
-38	1.0	-15.2	18.
-38	1.0	-17.8	15.
-38	1.0	-20.3	13.
-38	1.0	-22.9	8.
-38	1.0	-25.4	4.
-38	1.0	-26.2	3.
-38	1.0	-26.9	2.
-38	1.0	-27.9	2.
-38	1.0	-29.0	-0.
-38	1.0	-29.7	-2.
-38	1.0	-30.5	-3.
-38	1.0	-31.2	-5.
-38	1.0	-32.0	-5.
-38	1.0	-33.0	-7.
-38	1.0	-34.3	-9.
-38	1.0	-35.6	-11.

Table 5. - Continued.

x (mm)	y (mm)	z (mm)	θ (degrees)
-38	2.3	0.0	19.
-38	2.3	-2.5	18.
-38	2.3	-5.1	18.
-38	2.3	-7.6	17.
-38	2.3	-10.2	16.
-38	2.3	-12.7	14.
-38	2.3	-15.2	13.
-38	2.3	-17.8	11.
-38	2.3	-20.3	9.
-38	2.3	-22.9	5.
-38	2.3	-25.4	2.
-38	2.3	-26.2	3.
-38	2.3	-26.9	1.
-38	2.3	-27.9	-0.
-38	2.3	-29.0	-0.
-38	2.3	-29.7	-1.
-38	2.3	-30.5	-2.
-38	2.3	-31.2	-3.
-38	2.3	-32.0	-3.
-38	2.3	-33.0	-4.
-38	2.3	-34.3	-6.
-38	2.3	-35.6	-7.

Table 5. - Continued.

x (mm)	y (mm)	z (mm)	θ (degrees)
-38	5.1	0.0	14.
-38	5.1	-2.5	13.
-38	5.1	-5.1	13.
-38	5.1	-7.6	11.
-38	5.1	-10.2	11.
-38	5.1	-12.7	10.
-38	5.1	-15.2	9.
-38	5.1	-17.8	7.
-38	5.1	-20.3	6.
-38	5.1	-22.9	4.
-38	5.1	-25.4	2.
-38	5.1	-26.2	2.
-38	5.1	-26.9	1.
-38	5.1	-27.9	1.
-38	5.1	-29.0	-2.
-38	5.1	-29.7	0.
-38	5.1	-30.5	0.
-38	5.1	-31.2	-1.
-38	5.1	-32.0	-2.
-38	5.1	-33.0	-2.
-38	5.1	-34.3	-3.
-38	5.1	-35.6	-4.

Table 5. - Continued.

x (mm)	y (mm)	z (mm)	θ (degrees)
-38	27.9	0.0	6.
-38	27.9	-2.5	6.
-38	27.9	-5.1	6.
-38	27.9	-7.6	6.
-38	27.9	-10.2	5.
-38	27.9	-12.7	4.
-38	27.9	-15.2	4.
-38	27.9	-17.8	3.
-38	27.9	-20.3	2.
-38	27.9	-22.9	2.
-38	27.9	-25.4	1.
-38	27.9	-26.2	2.
-38	27.9	-26.9	0.
-38	27.9	-27.9	2.
-38	27.9	-29.0	-0.
-38	27.9	-29.7	0.
-38	27.9	-30.5	0.
-38	27.9	-31.2	0.
-38	27.9	-32.0	0.
-38	27.9	-33.0	-0.
-38	27.9	-34.3	-1.
-38	27.9	-35.6	-1.

Table 5. - Continued.

x (mm)	y (mm)	z (mm)	θ (degrees)
-11	.5	25.4	32.
-11	.5	22.9	33.
-11	.5	20.3	36.
-11	.5	17.8	38.
-11	.5	15.2	40.
-11	.5	12.7	42.
-11	.5	10.2	46.
-11	.5	7.6	49.
-11	.5	5.1	52.
-11	.5	2.5	56.
-11	.5	0.0	59.
-11	.5	-1.3	61.
-11	.5	-2.5	63.
-11	.5	-3.8	64.
-11	.5	-5.1	66.
-11	.5	-6.4	67.
-11	.5	-7.6	68.
-11	.5	-8.9	69.
-11	.5	-10.2	71.
-11	.5	-11.4	74.
-11	.5	-12.7	77.
-11	.5	-14.0	80.
-11	.5	-15.2	87.
-11	.5	-16.5	103.
-11	.5	-17.8	107.
-11	.5	-19.1	120.
-11	.5	-20.3	132.
-11	.5	-21.6	139.
-11	.5	-22.9	150.
-11	.5	-24.1	155.
-11	.5	-25.4	168.
-11	.5	-26.2	171.
-11	.5	-26.9	176.
-11	.5	-27.9	179.
-11	.5	-29.0	184.
-11	.5	-29.7	187.
-11	.5	-30.5	191.
-11	.5	-31.2	194.
-11	.5	-32.0	198.
-11	.5	-33.0	203.
-11	.5	-34.3	209.
-11	.5	-35.6	216.

Table 5. - Continued.

x (mm)	y (mm)	z (mm)	θ (degrees)
-11	1.3	25.4	29.
-11	1.3	20.3	33.
-11	1.3	15.2	35.
-11	1.3	10.2	42.
-11	1.3	5.1	48.
-11	1.3	2.5	51.
-11	1.3	0.0	55.
-11	1.3	-1.3	56.
-11	1.3	-2.5	57.
-11	1.3	-3.8	59.
-11	1.3	-5.1	61.
-11	1.3	-6.4	63.
-11	1.3	-7.6	65.
-11	1.3	-8.9	67.
-11	1.3	-10.2	70.
-11	1.3	-11.4	73.
-11	1.3	-12.7	77.
-11	1.3	-14.0	83.
-11	1.3	-15.2	92.
-11	1.3	-16.5	98.
-11	1.3	-17.8	108.
-11	1.3	-19.1	122.
-11	1.3	-20.3	133.
-11	1.3	-21.6	142.
-11	1.3	-22.9	149.
-11	1.3	-24.1	158.
-11	1.3	-25.4	164.
-11	1.3	-26.2	169.
-11	1.3	-26.9	173.
-11	1.3	-27.9	178.
-11	1.3	-29.0	183.
-11	1.3	-29.7	190.
-11	1.3	-30.5	191.
-11	1.3	-31.2	197.
-11	1.3	-32.0	204.
-11	1.3	-33.0	207.
-11	1.3	-34.3	214.
-11	1.3	-35.6	226.

Table 5. - Continued.

x (mm)	y (mm)	z (mm)	θ (degrees)
-11	2.0	25.4	27.
-11	2.0	20.3	29.
-11	2.0	15.2	34.
-11	2.0	10.2	38.
-11	2.0	5.1	43.
-11	2.0	2.5	45.
-11	2.0	0.0	47.
-11	2.0	-1.3	49.
-11	2.0	-2.5	51.
-11	2.0	-3.8	52.
-11	2.0	-5.1	53.
-11	2.0	-6.4	55.
-11	2.0	-7.6	57.
-11	2.0	-8.9	59.
-11	2.0	-10.2	62.
-11	2.0	-11.4	64.
-11	2.0	-12.7	68.
-11	2.0	-14.0	72.
-11	2.0	-15.2	76.
-11	2.0	-16.5	84.
-11	2.0	-17.8	93.
-11	2.0	-19.1	101.
-11	2.0	-20.3	111.
-11	2.0	-21.6	125.
-11	2.0	-22.9	132.
-11	2.0	-24.1	140.
-11	2.0	-25.4	153.
-11	2.0	-26.2	159.
-11	2.0	-26.9	164.
-11	2.0	-27.9	171.
-11	2.0	-29.0	179.
-11	2.0	-29.7	190.
-11	2.0	-30.5	192.
-11	2.0	-31.2	195.
-11	2.0	-32.0	198.
-11	2.0	-33.0	209.
-11	2.0	-34.3	215.
-11	2.0	-35.6	221.

Table 5. - Continued.

x (mm)	y (mm)	z (mm)	θ (degrees)
-11	3.1	25.4	24.
-11	3.1	20.3	26.
-11	3.1	15.2	30.
-11	3.1	10.2	33.
-11	3.1	5.1	37.
-11	3.1	2.5	39.
-11	3.1	0.0	41.
-11	3.1	-1.3	42.
-11	3.1	-2.5	44.
-11	3.1	-3.8	45.
-11	3.1	-5.1	47.
-11	3.1	-6.4	48.
-11	3.1	-7.6	49.
-11	3.1	-8.9	51.
-11	3.1	-10.2	53.
-11	3.1	-11.4	55.
-11	3.1	-12.7	56.
-11	3.1	-14.0	56.
-11	3.1	-15.2	58.
-11	3.1	-16.5	57.
-11	3.1	-17.8	58.
-11	3.1	-19.1	57.
-11	3.1	-20.3	56.
-11	3.1	-21.6	53.
-11	3.1	-22.9	49.
-11	3.1	-24.1	40.
-11	3.1	-25.4	20.
-11	3.1	-26.2	13.
-11	3.1	-26.9	9.
-11	3.1	-27.9	4.
-11	3.1	-29.0	1.
-11	3.1	-29.7	-6.
-11	3.1	-30.5	-3.
-11	3.1	-31.2	-7.
-11	3.1	-32.0	-12.
-11	3.1	-33.0	-20.
-11	3.1	-34.3	-36.
-11	3.1	-35.6	-39.

Table 5. - Continued.

x (mm)	y (mm)	z (mm)	θ (degrees)
-11	3.6	25.4	23.
-11	3.6	20.3	26.
-11	3.6	15.2	28.
-11	3.6	10.2	30.
-11	3.6	5.1	35.
-11	3.6	2.5	37.
-11	3.6	0.0	38.
-11	3.6	-1.3	40.
-11	3.6	-2.5	40.
-11	3.6	-3.8	41.
-11	3.6	-5.1	43.
-11	3.6	-6.4	45.
-11	3.6	-7.6	46.
-11	3.6	-8.9	47.
-11	3.6	-10.2	49.
-11	3.6	-11.4	49.
-11	3.6	-12.7	49.
-11	3.6	-14.0	50.
-11	3.6	-15.2	50.
-11	3.6	-16.5	49.
-11	3.6	-17.8	47.
-11	3.6	-19.1	45.
-11	3.6	-20.3	42.
-11	3.6	-21.6	38.
-11	3.6	-22.9	34.
-11	3.6	-24.1	25.
-11	3.6	-25.4	11.
-11	3.6	-26.2	11.
-11	3.6	-26.9	9.
-11	3.6	-27.9	4.
-11	3.6	-29.0	0.
-11	3.6	-29.7	-3.
-11	3.6	-30.5	-4.
-11	3.6	-31.2	-7.
-11	3.6	-32.0	-9.
-11	3.6	-33.0	-14.
-11	3.6	-34.3	-20.
-11	3.6	-35.6	-28.

Table 5. - Concluded.

x (mm)	y (mm)	z (mm)	θ (degrees)
-11	25.4	0.0	18.
-11	25.4	-5.1	19.
-11	25.4	-10.2	20.
-11	25.4	-12.7	20.
-11	25.4	-15.2	19.
-11	25.4	-17.8	18.
-11	25.4	-20.3	17.
-11	25.4	-21.6	16.
-11	25.4	-22.9	14.
-11	25.4	-24.1	11.
-11	25.4	-25.4	11.
-11	25.4	-26.2	8.
-11	25.4	-26.9	6.
-11	25.4	-27.9	4.
-11	25.4	-29.0	2.
-11	25.4	-29.7	-0.
-11	25.4	-30.5	-1.
-11	25.4	-31.2	-2.
-11	25.4	-32.0	-5.
-11	25.4	-33.0	-6.
-11	25.4	-34.3	-8.
-11	25.4	-35.6	-11.

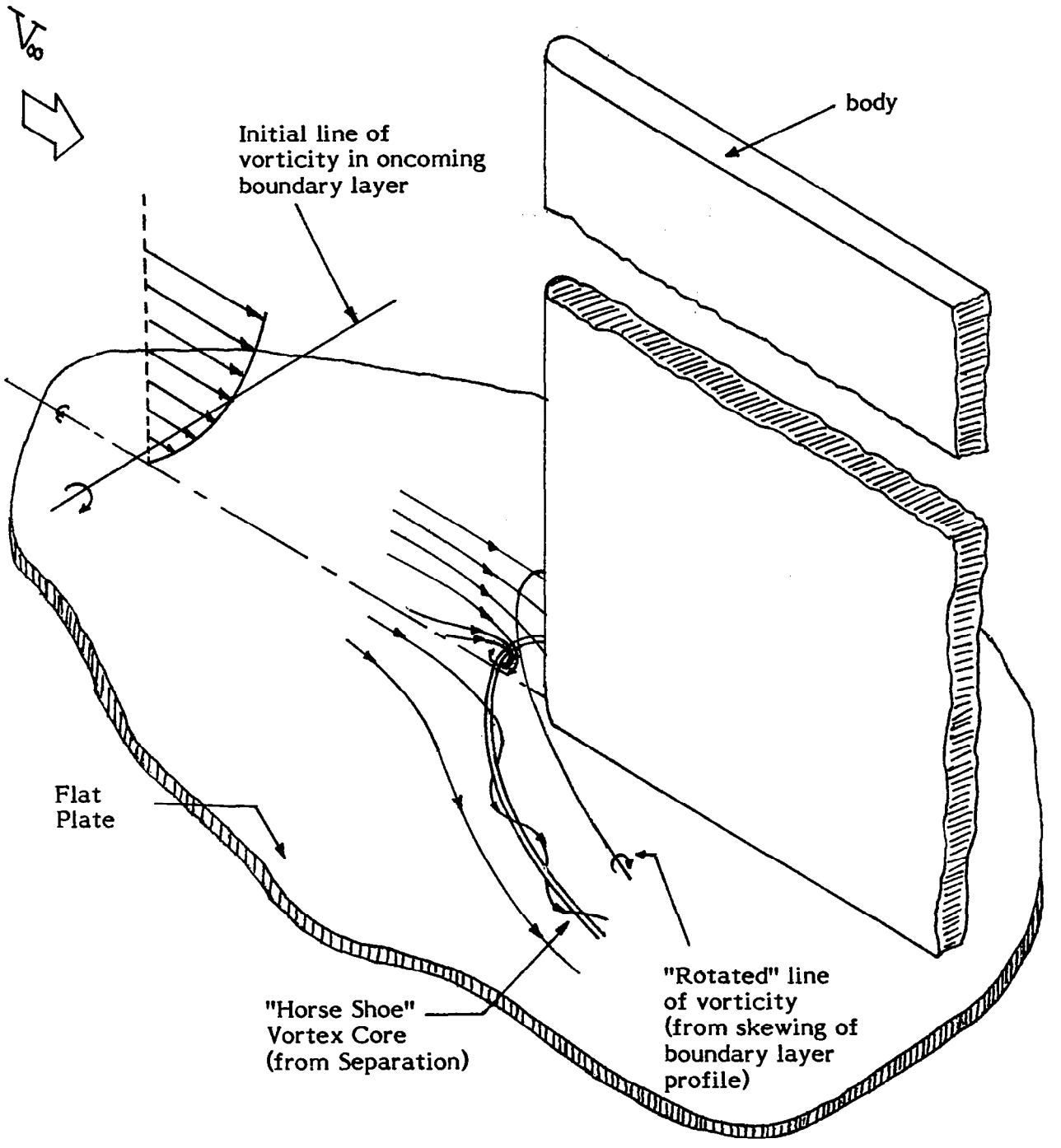

Figure 1. - Schematic of the flow in a juncture.

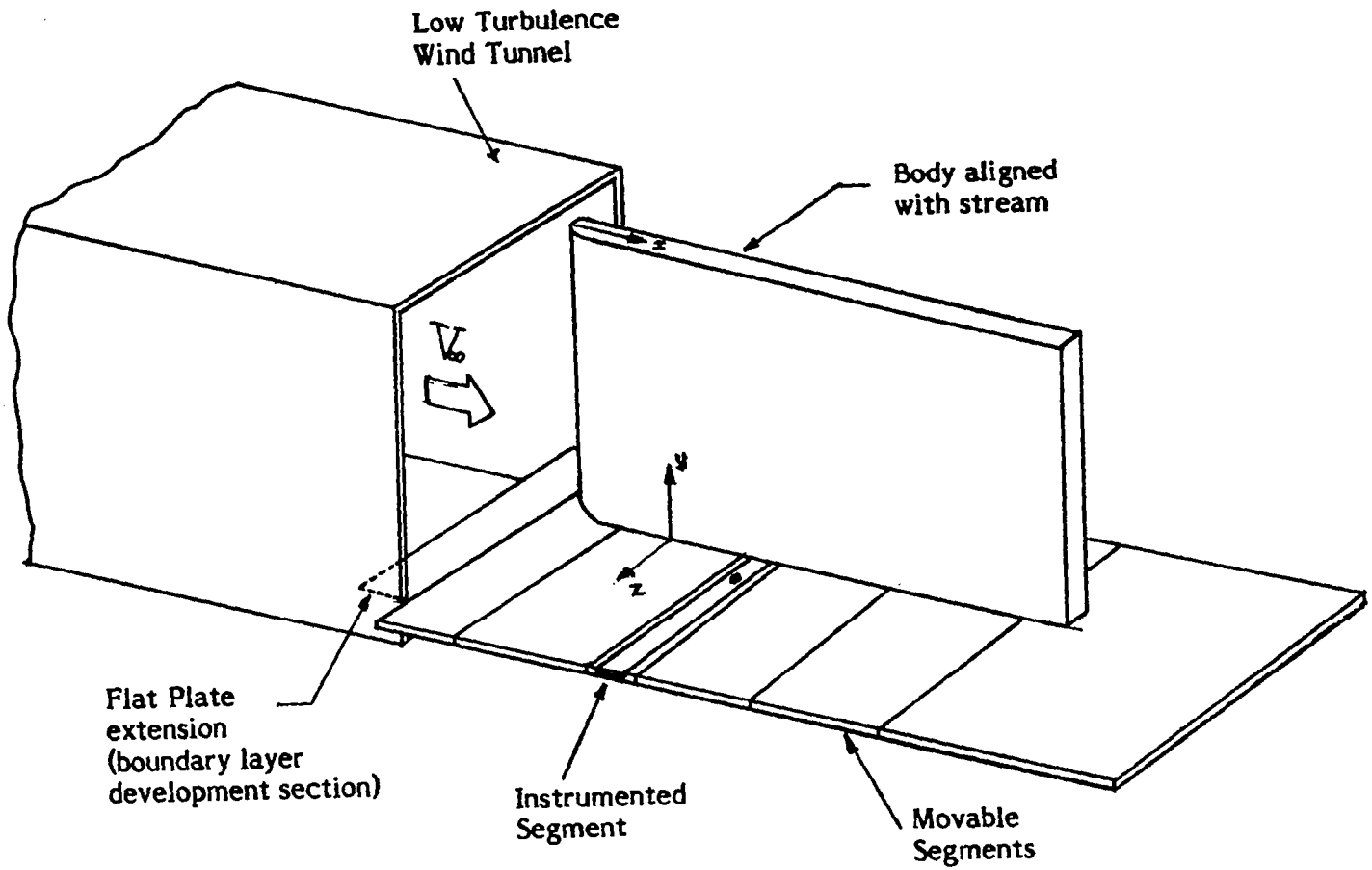

Figure 2. - Flat plate and body at the exit of the wind tunnel.

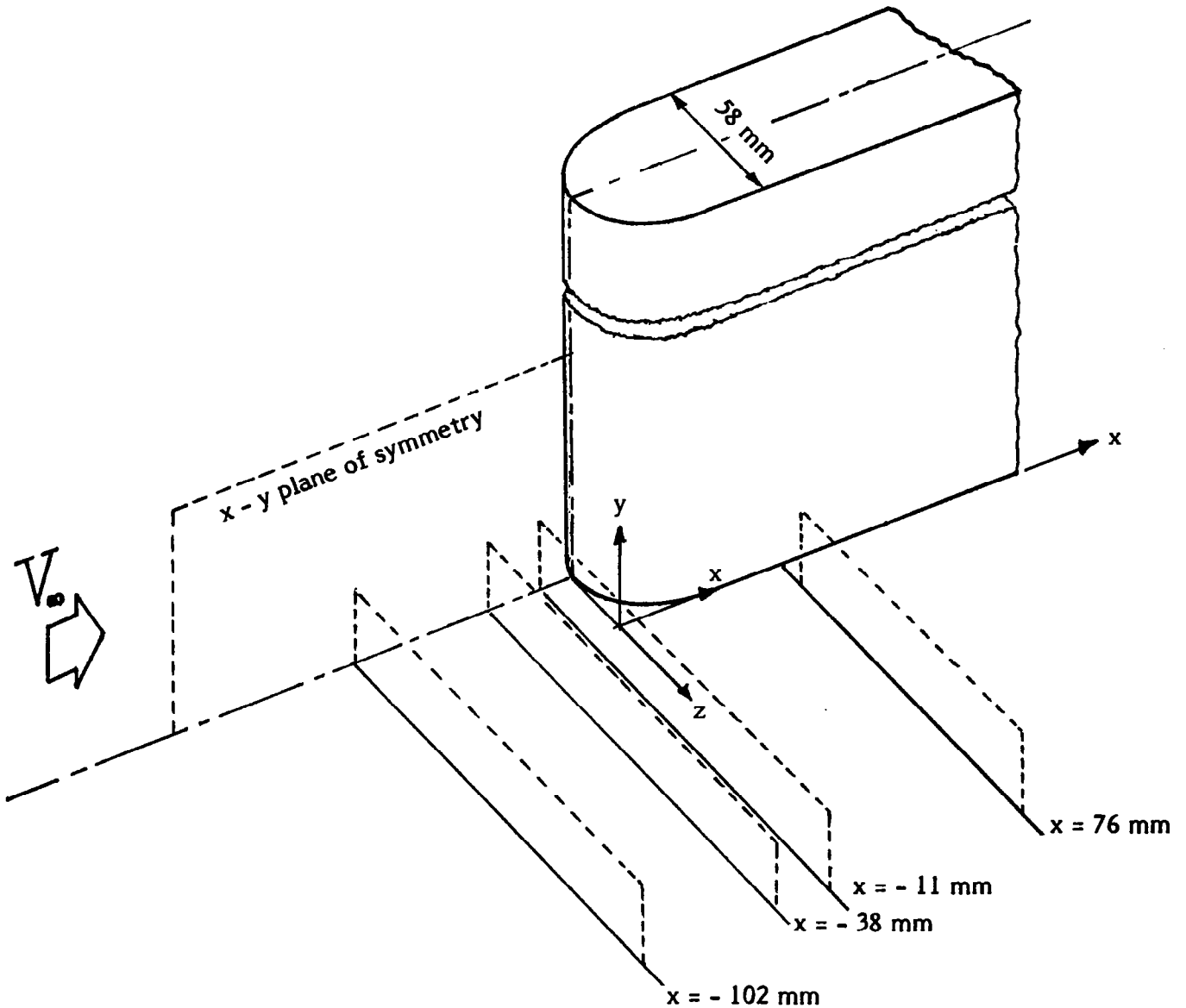

Figure 3. - Location of streamwise measuring stations.

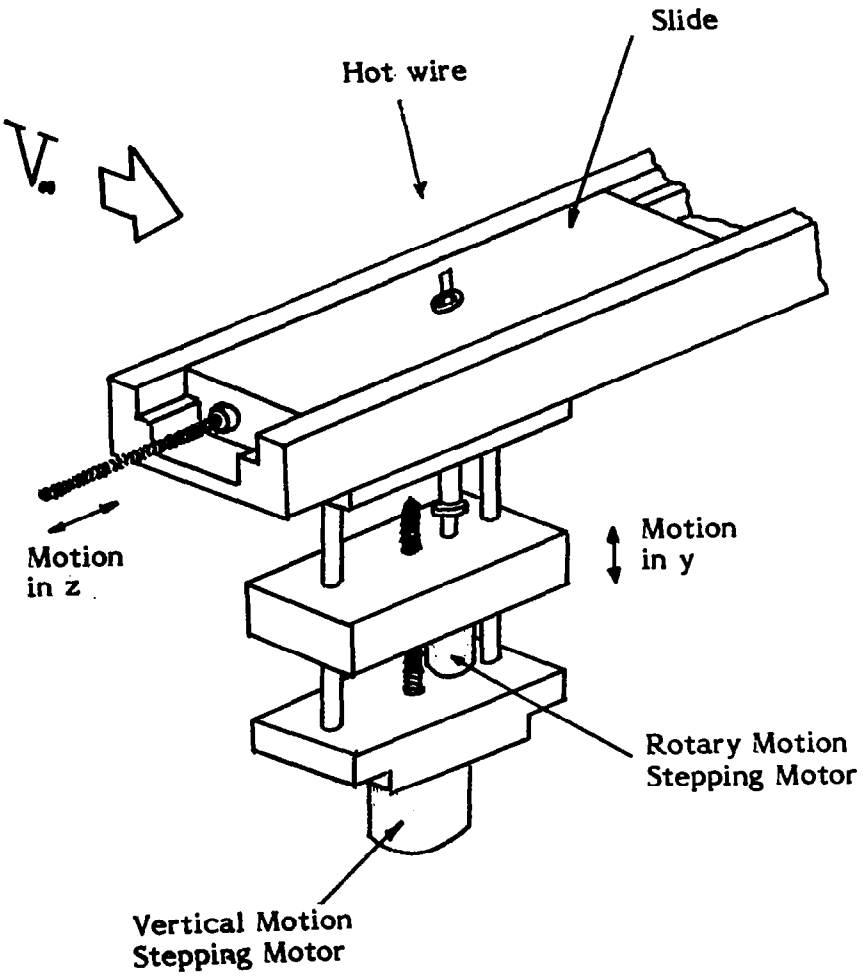

Figure 4. - Details of instrumented segment.

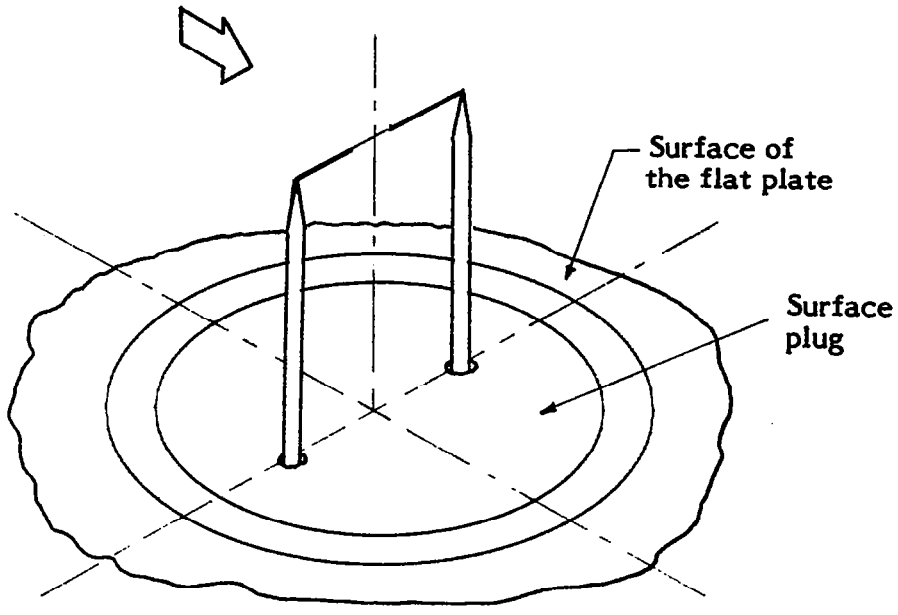

(a) Horizontal wire.

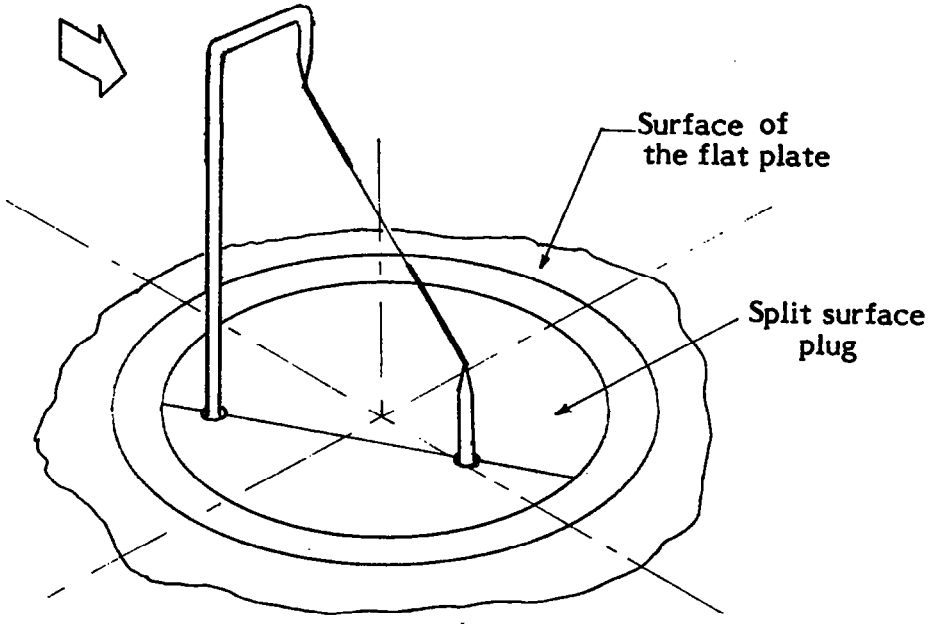

(b) Slant wire.

Figure 5. - Details of hot wires.

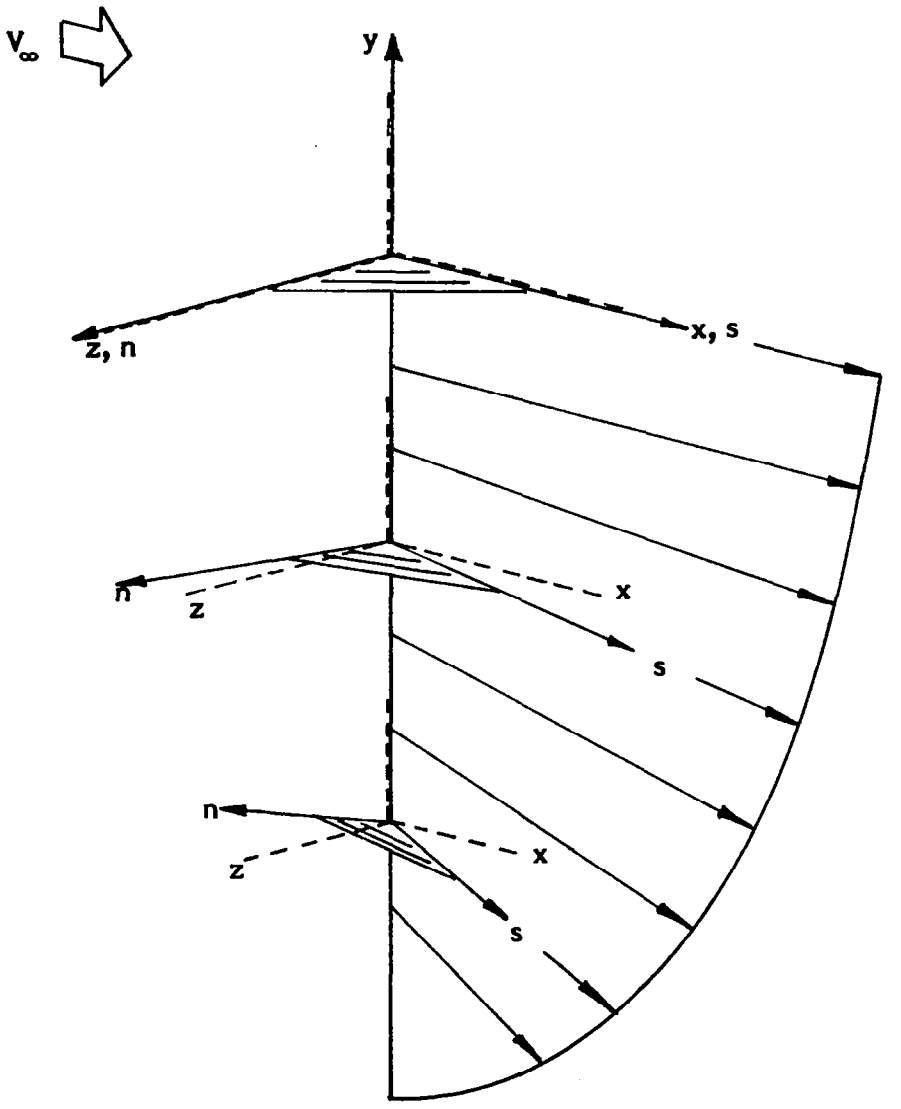

Hot-wire coordinates (for taking data)

Laboratory coordinates (for data presentation)

Figure 6. - Coordinate axes.

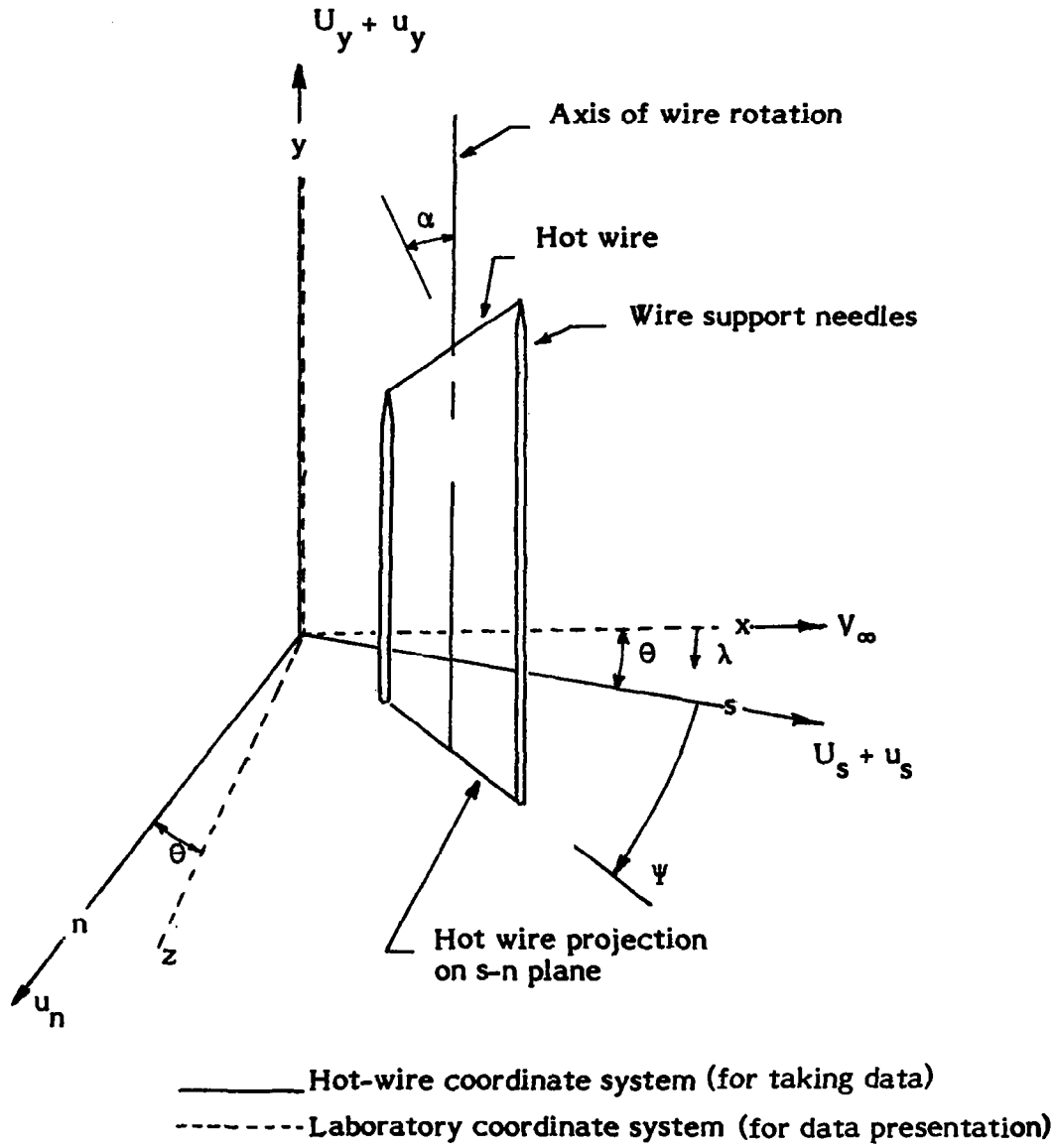

Figure 7. - Schematic of hot wire in the Cartesian coordinate system.

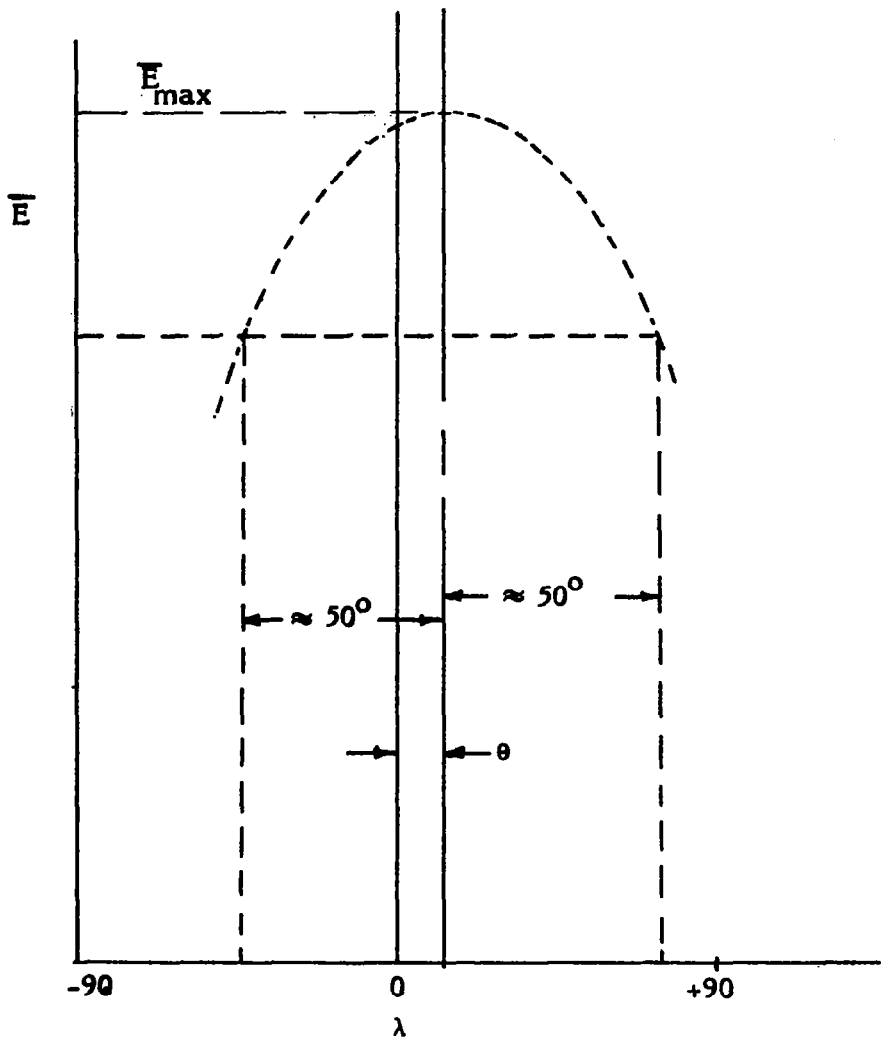

Figure 8. - Typical variation in mean voltage output with angle of rotation.Horizontal wire (α = 0).

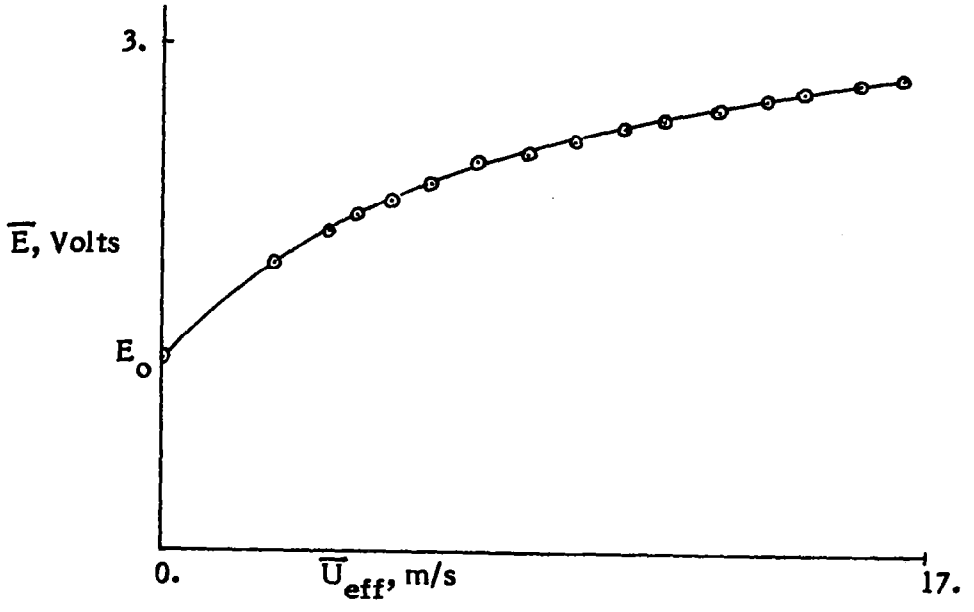

(a) Nonlinear results.

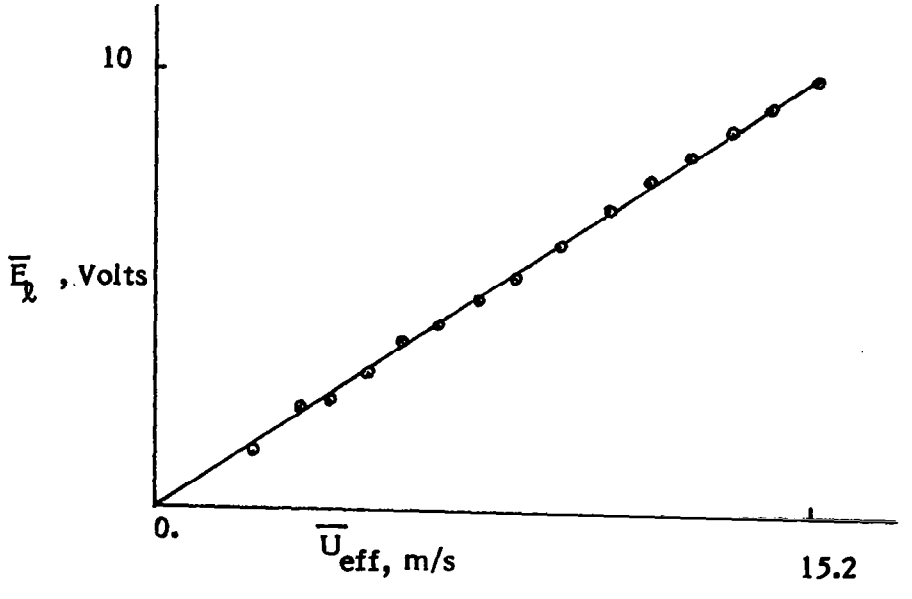

(b) Linearized results.

Figure 9. - Typical hot wire calibration results.
Straight wire ($\alpha = 0$).

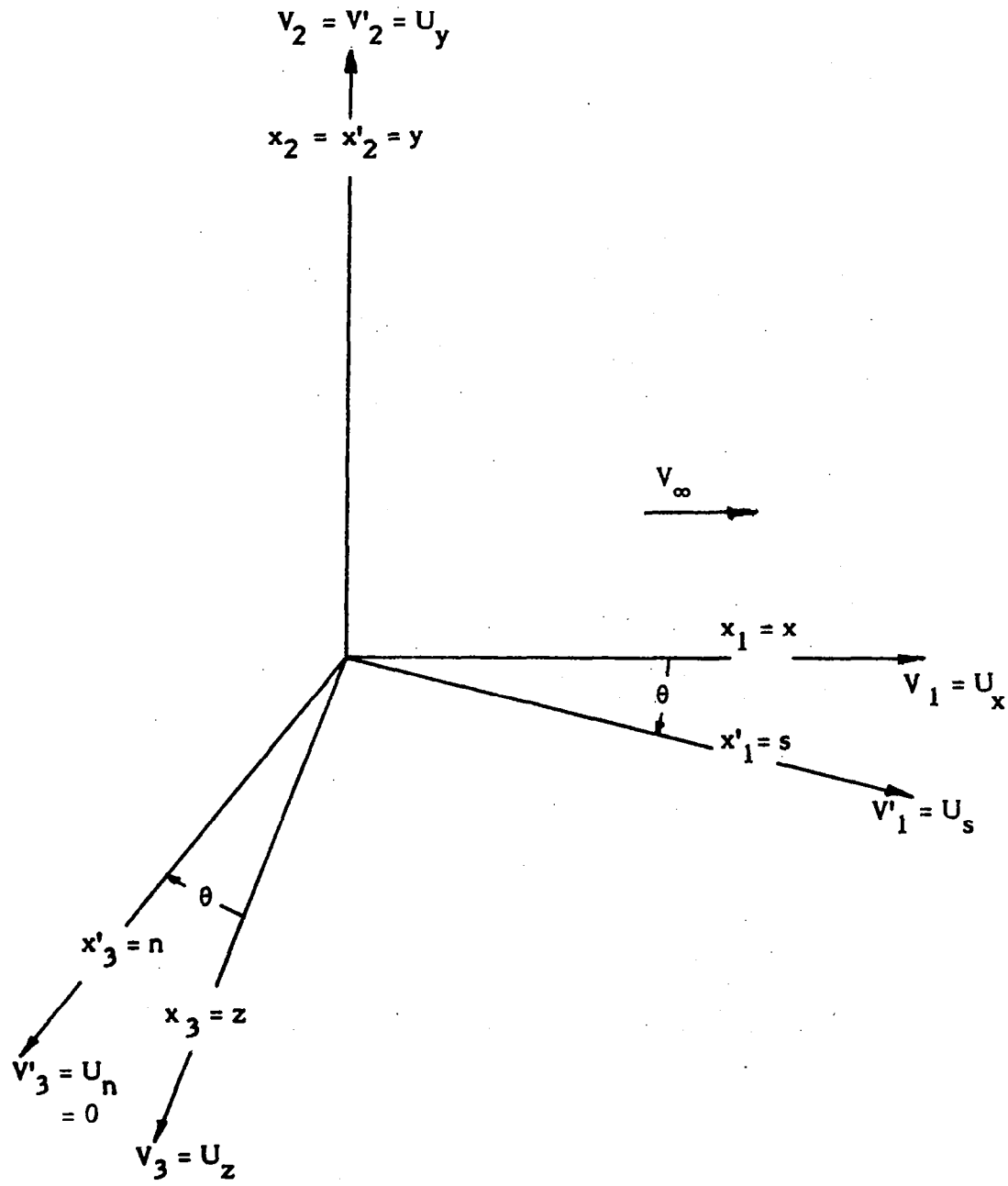

Figure 10. - The two Cartesian co-ordinate systems.

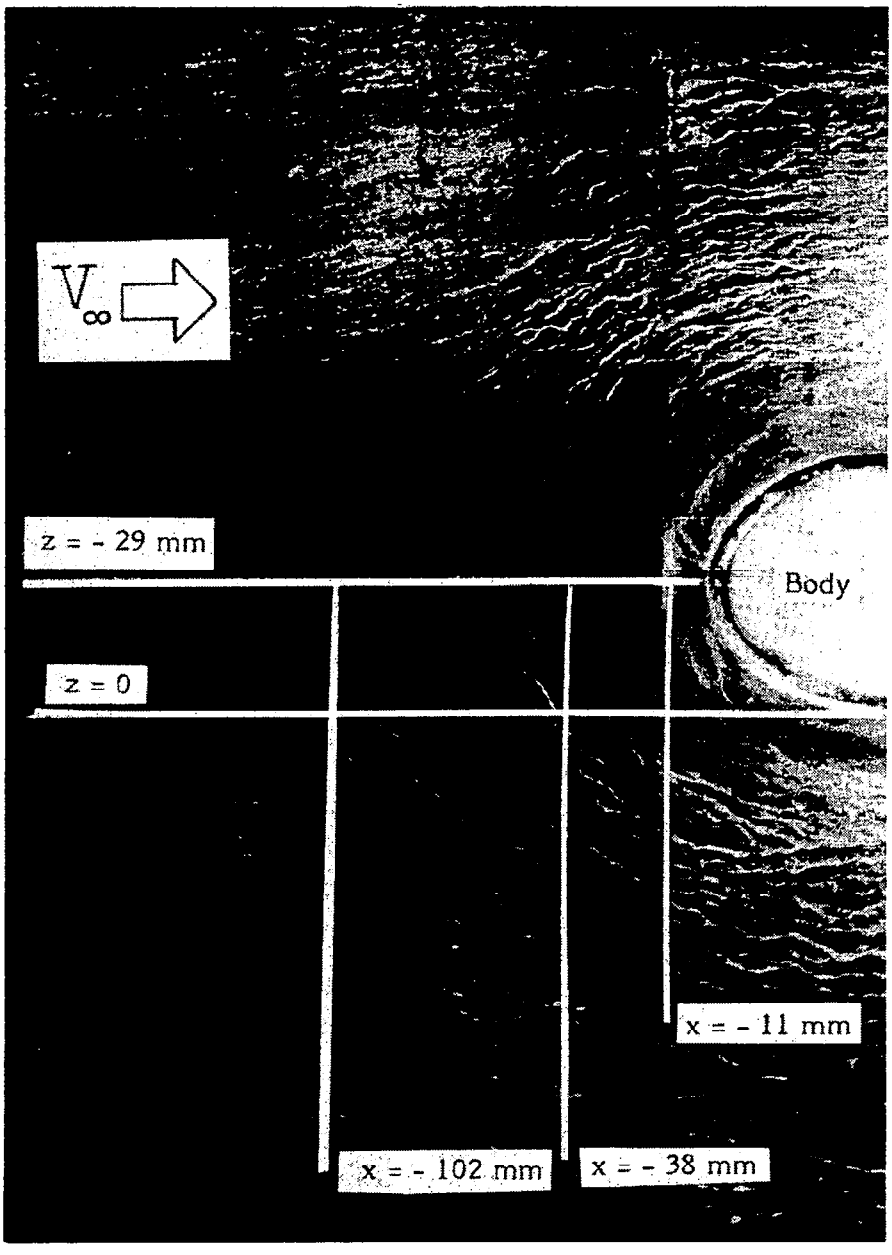

Figure 11. - Surface oil-flow visualization near the body leading edge.

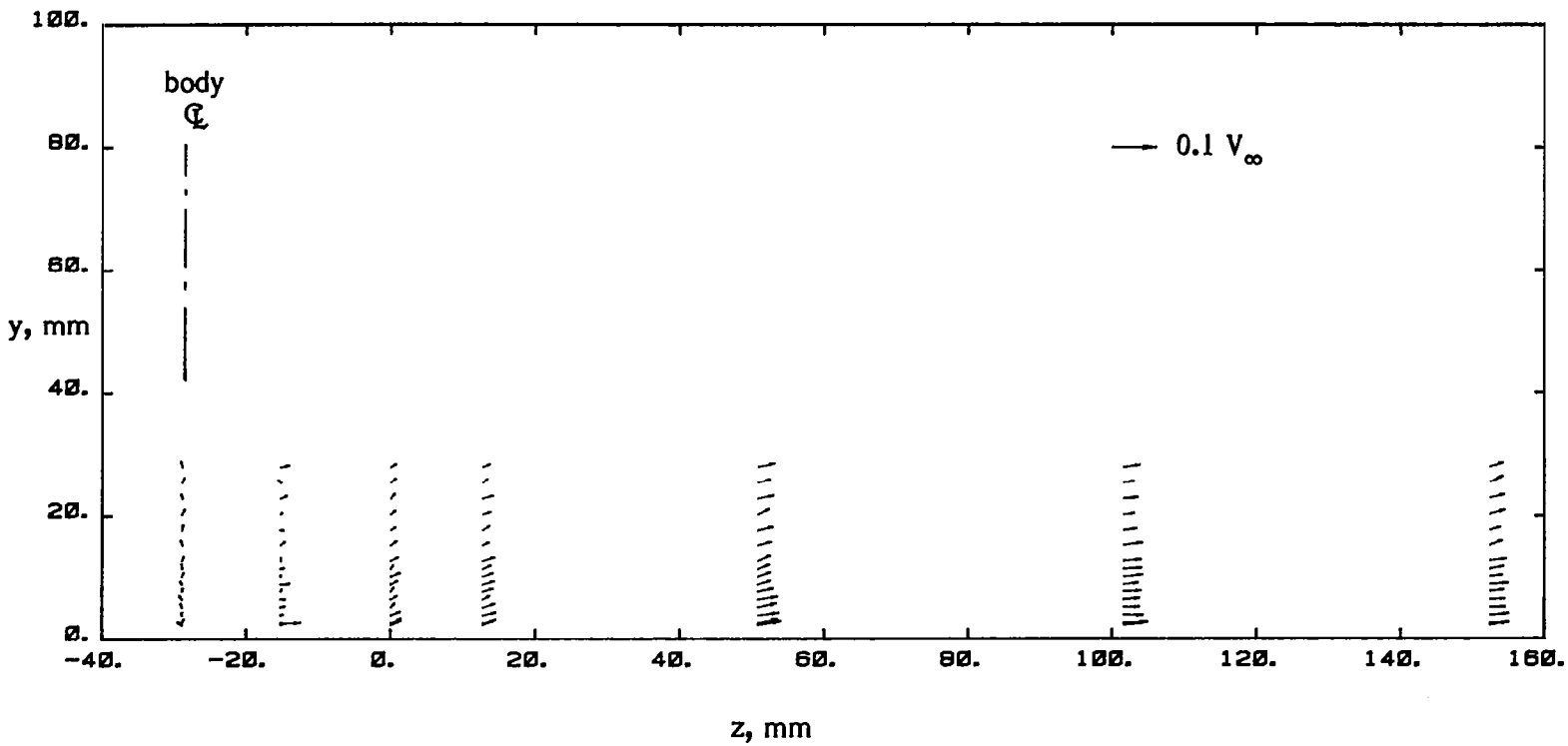

(a) x = -102 mm.

Figure 12. - Vector component plots in y - z planes.

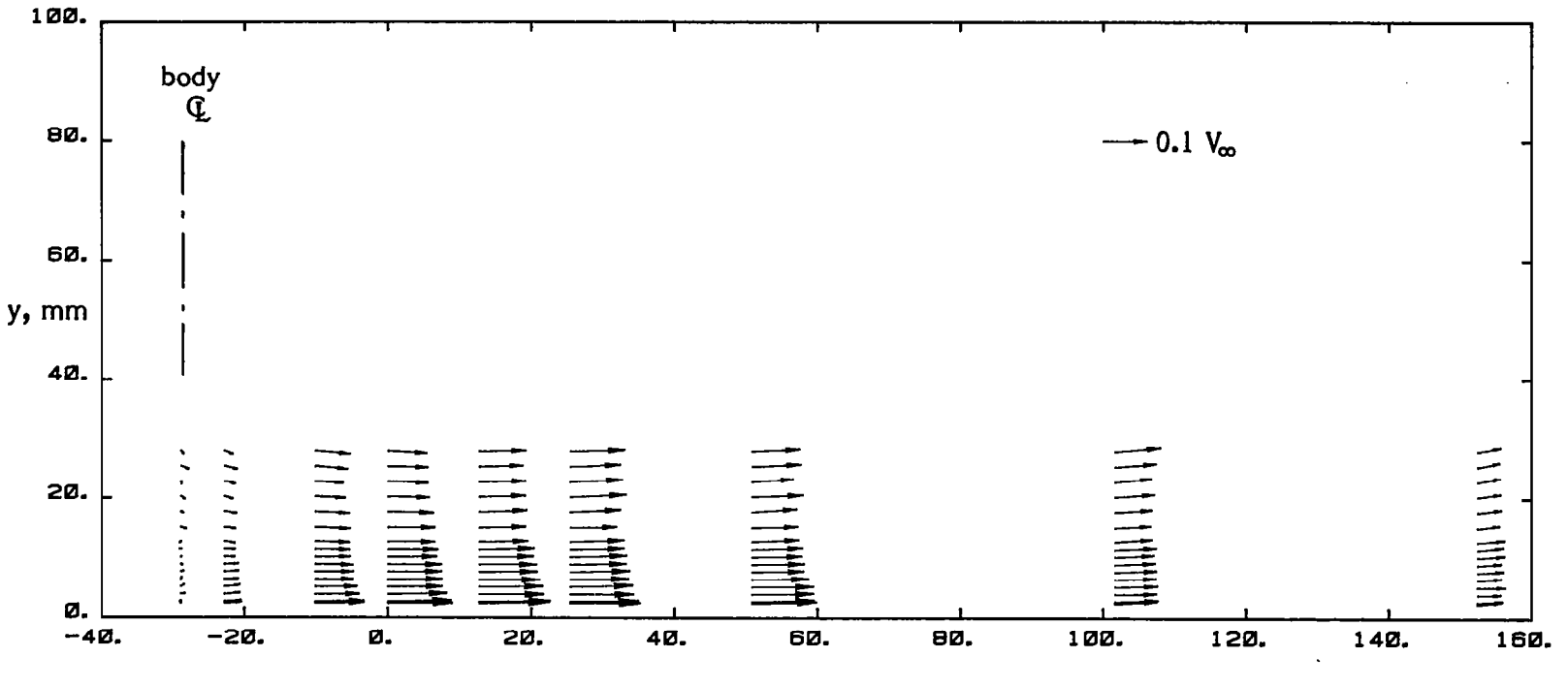

(b) x =-38 mm.

Figure 12. - Continued.

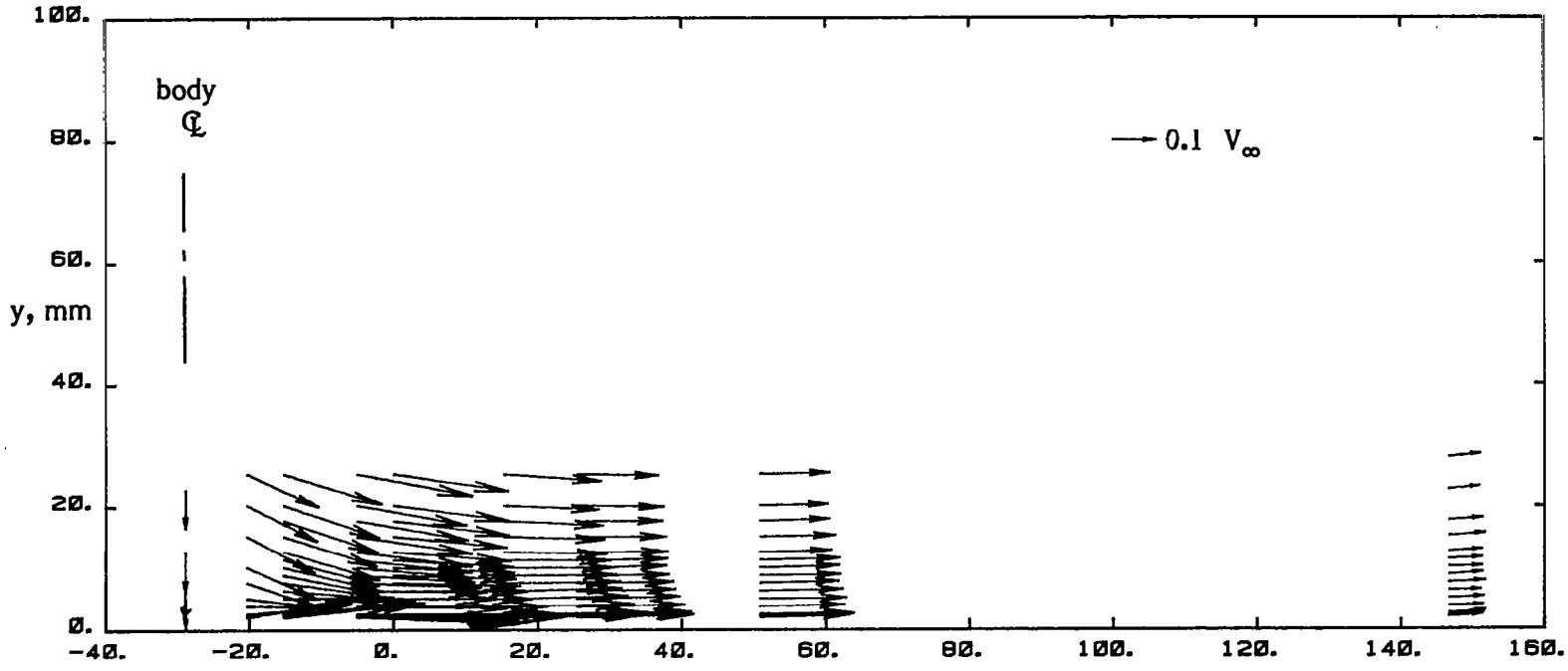

(c) x = - 11 mm.

Figure 12. - Continued.

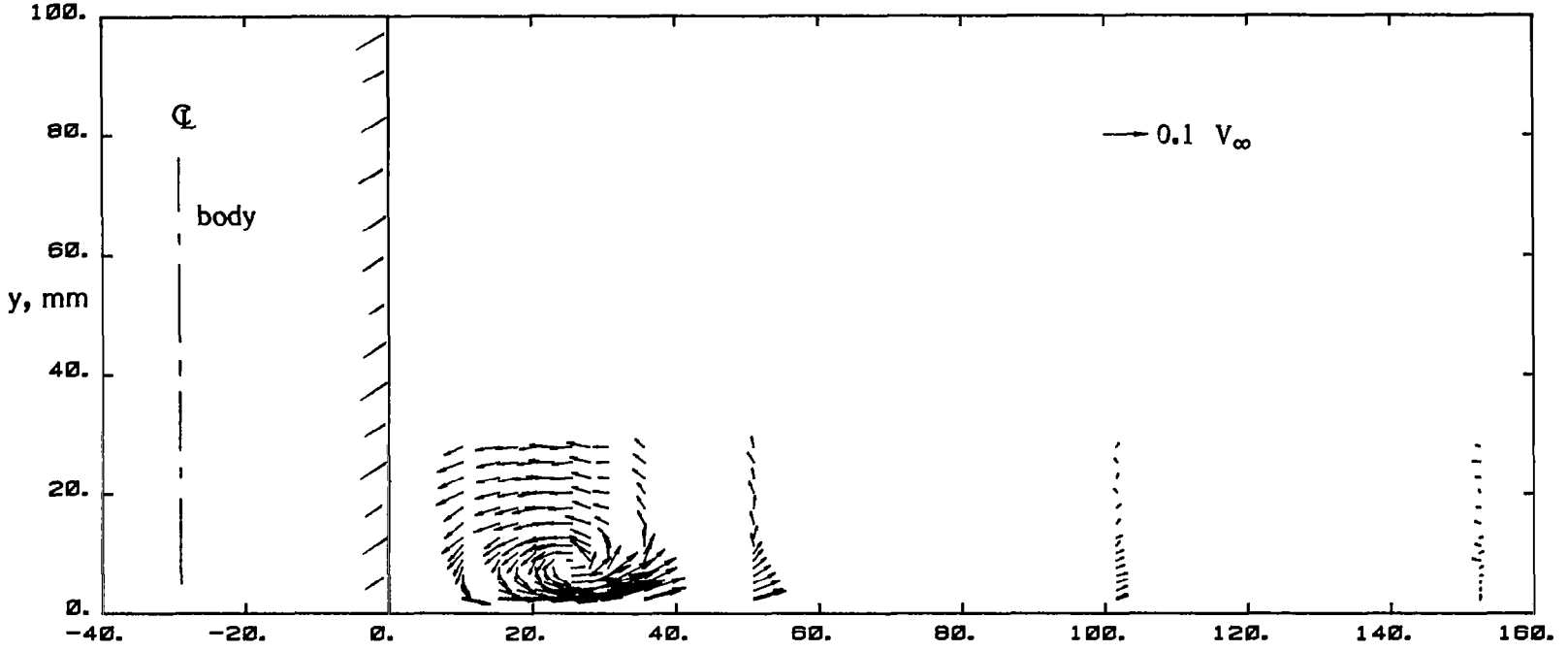

(d) x = 76 mm.

Figure 12. - Continued.

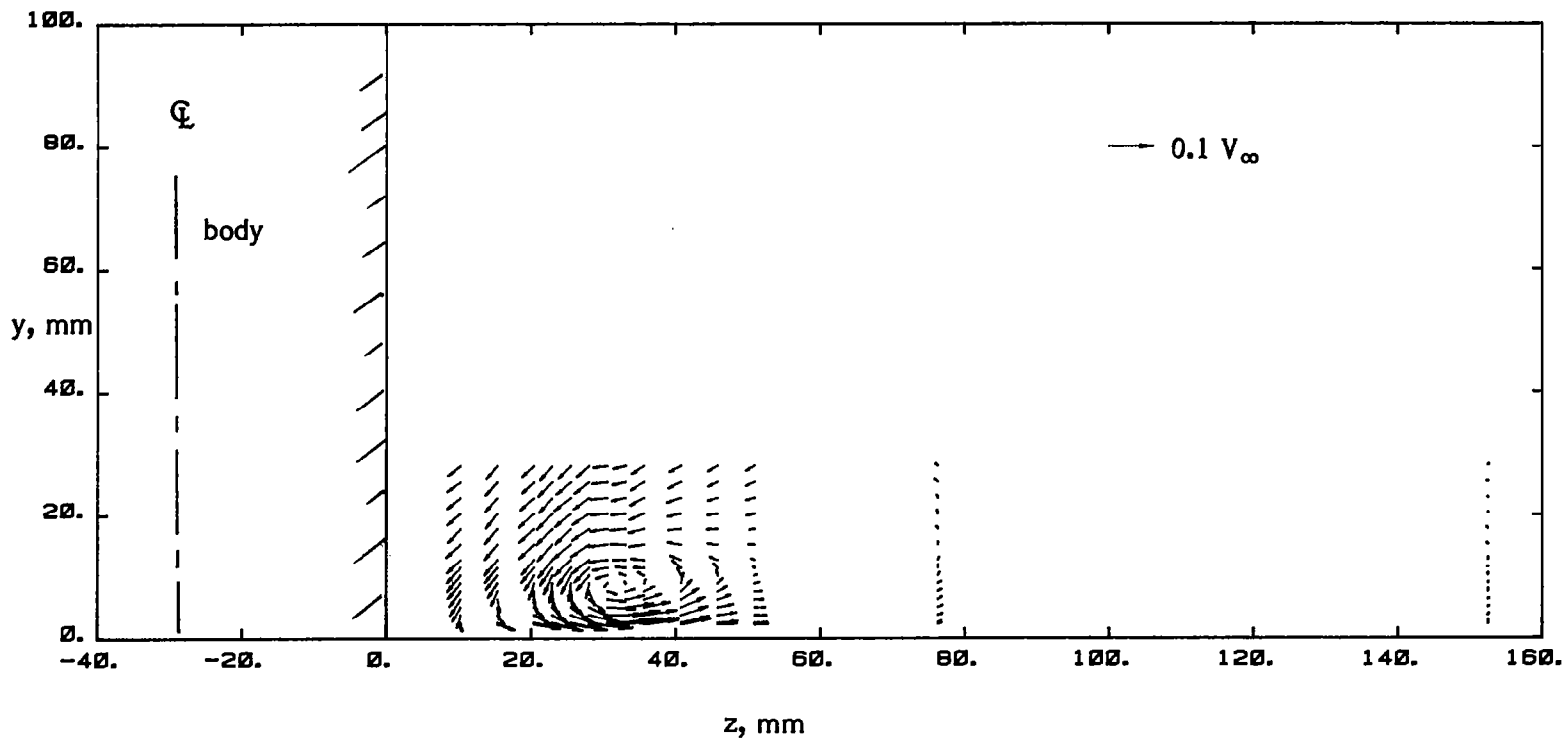

(e) x = 165 mm (reference 5).

Figure 12. - Continued.

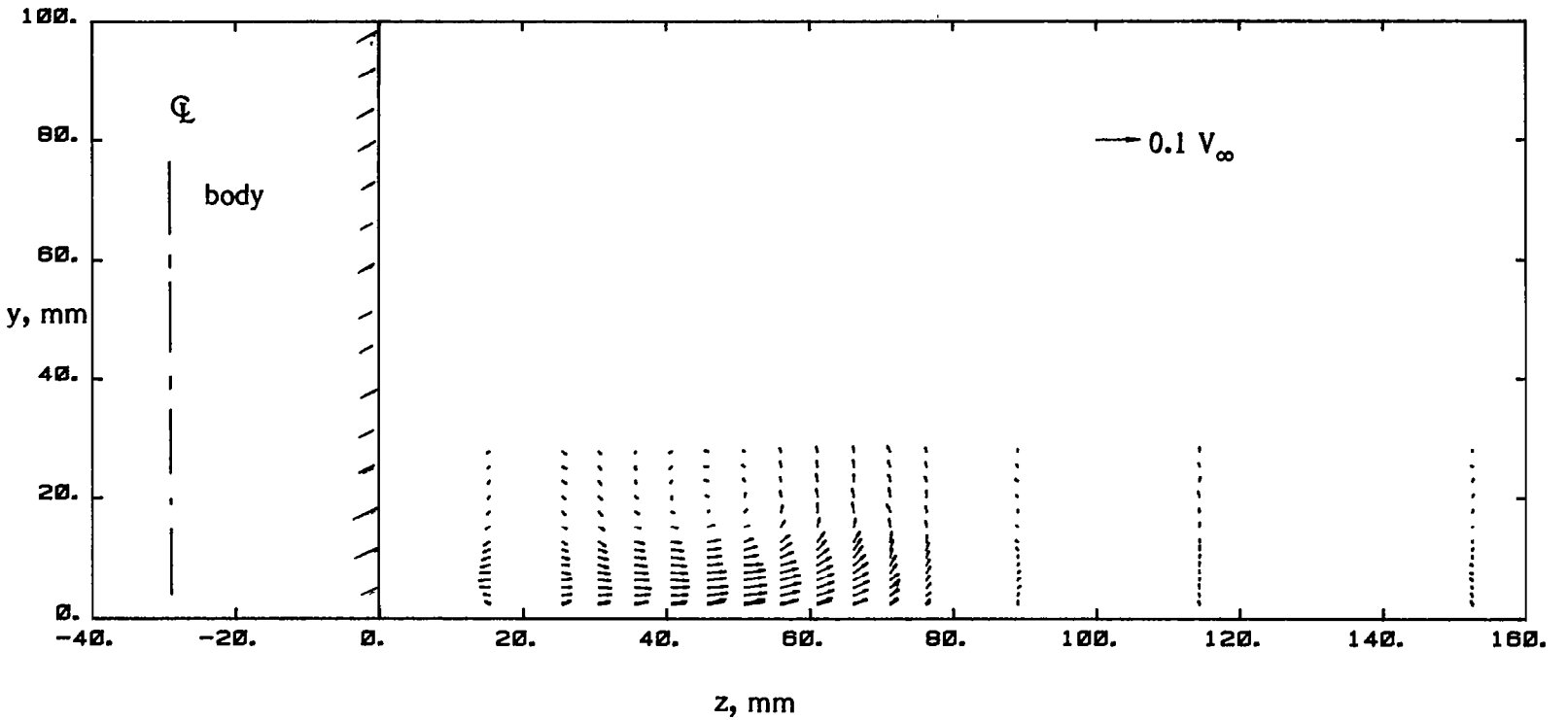

(f) x = 902 mm (reference 5).

Figure 12. - Concluded.

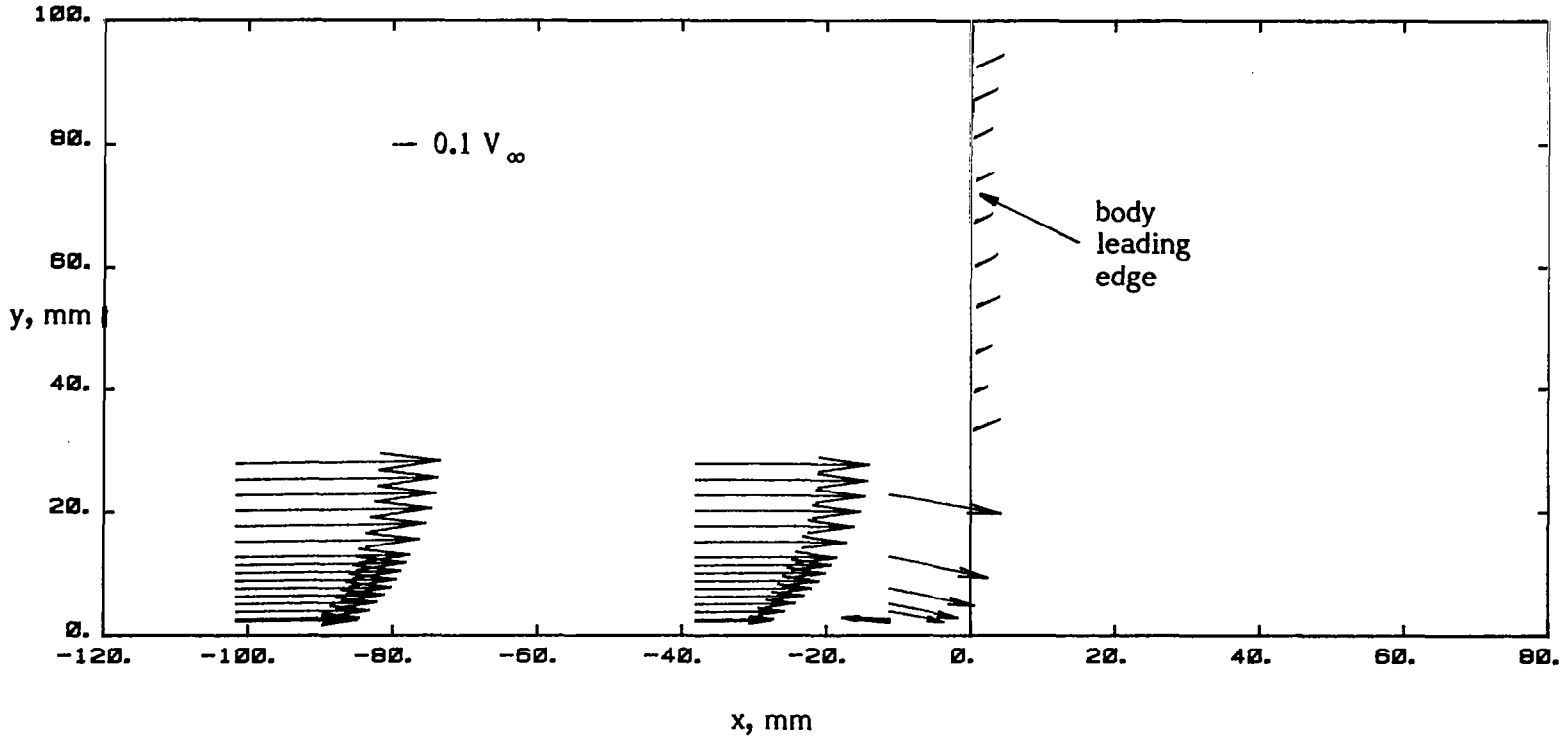

Figure 13. - Vector component plot in x - y plane of symmetry.

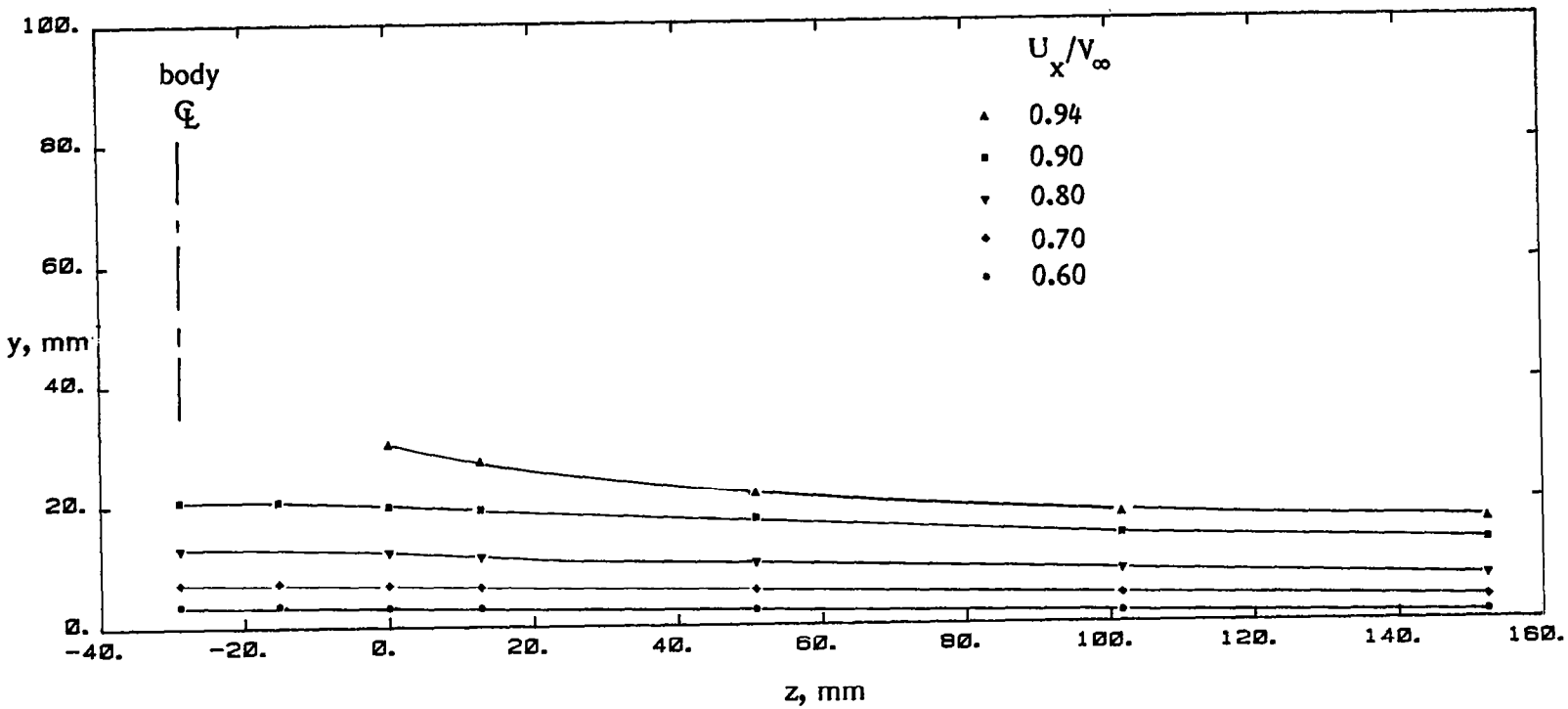

(a) x = - 102 mm.

Figure 14. - Contour plot of mean velocity U_x.

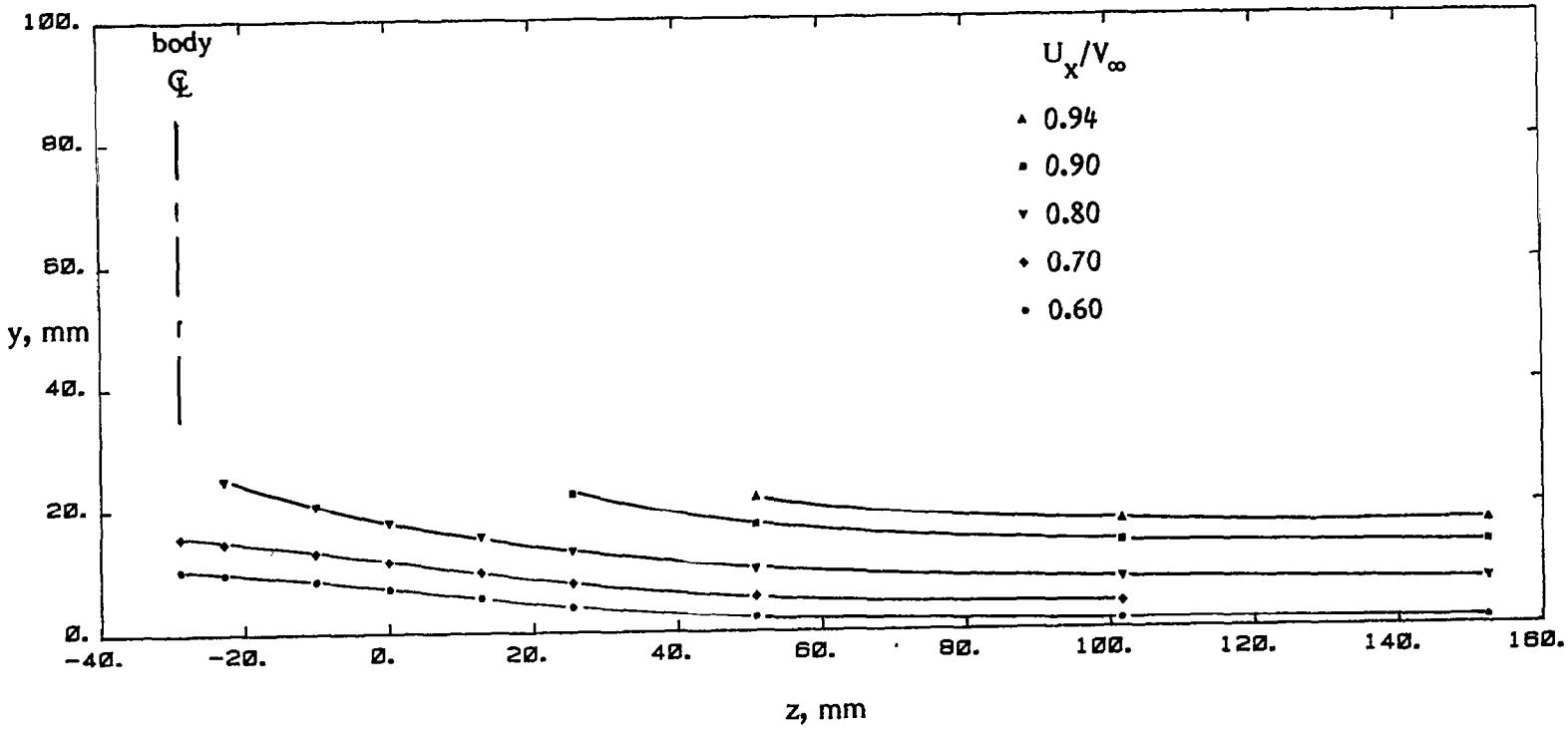

(b) x = - 38 mm.

Figure 14. - Continued.

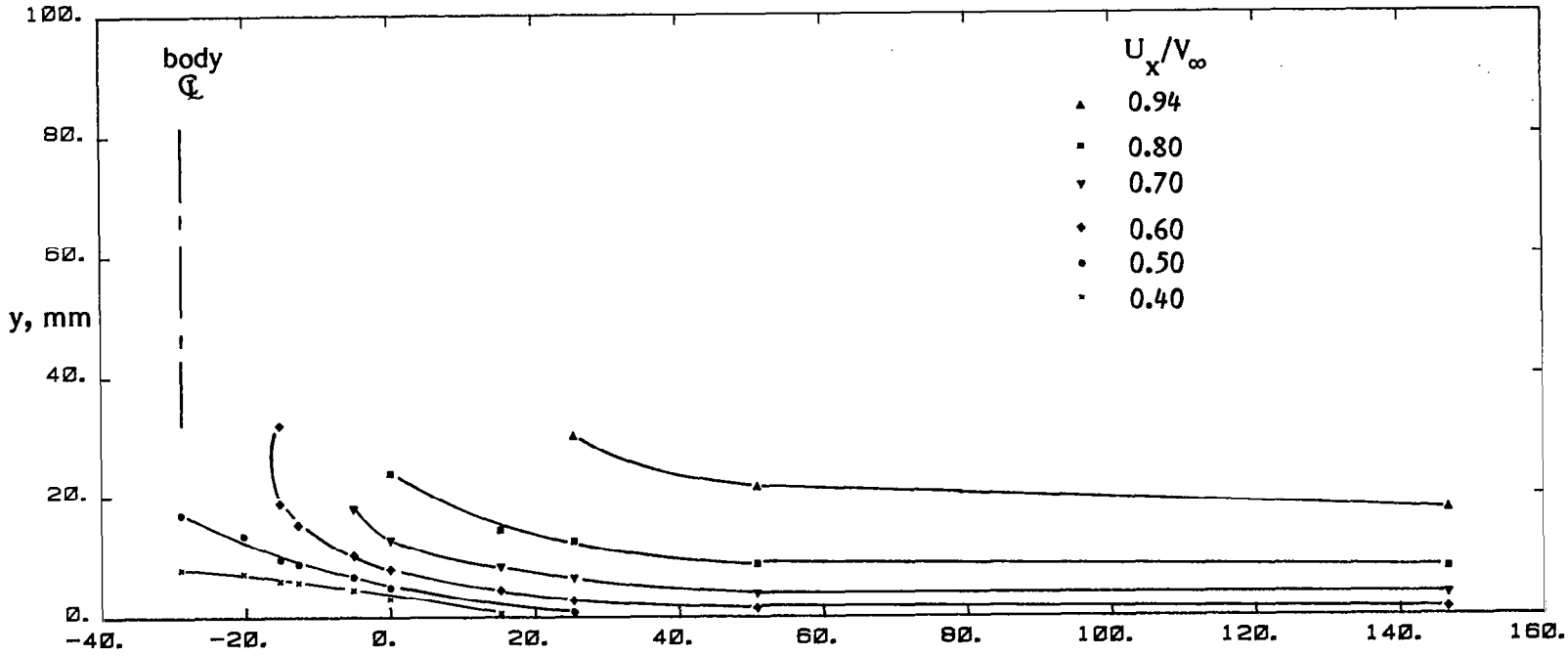

(c) x = - 11 mm.

Figure 14. - Continued.

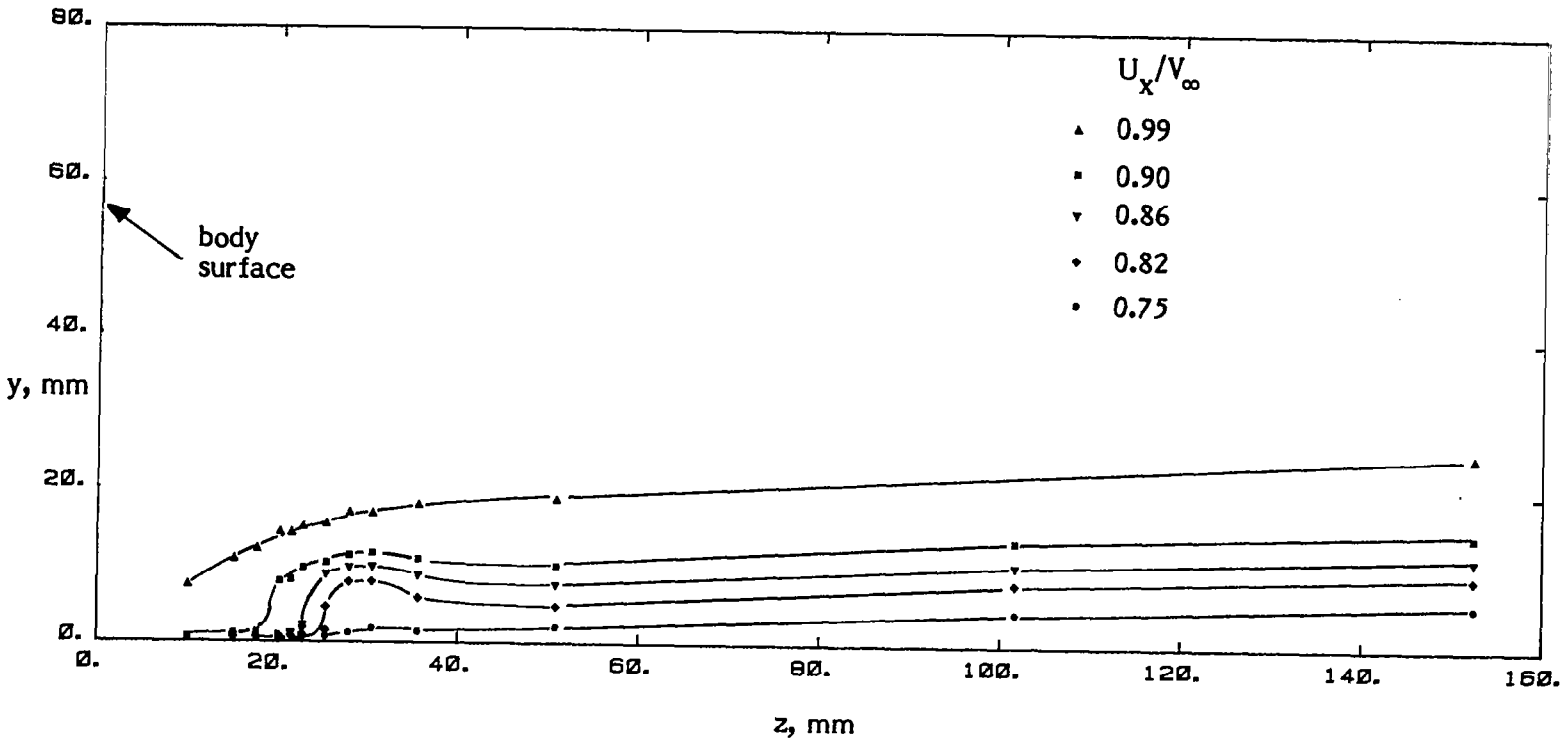

(d) x = 76 mm.

Figure 14. - Continued.

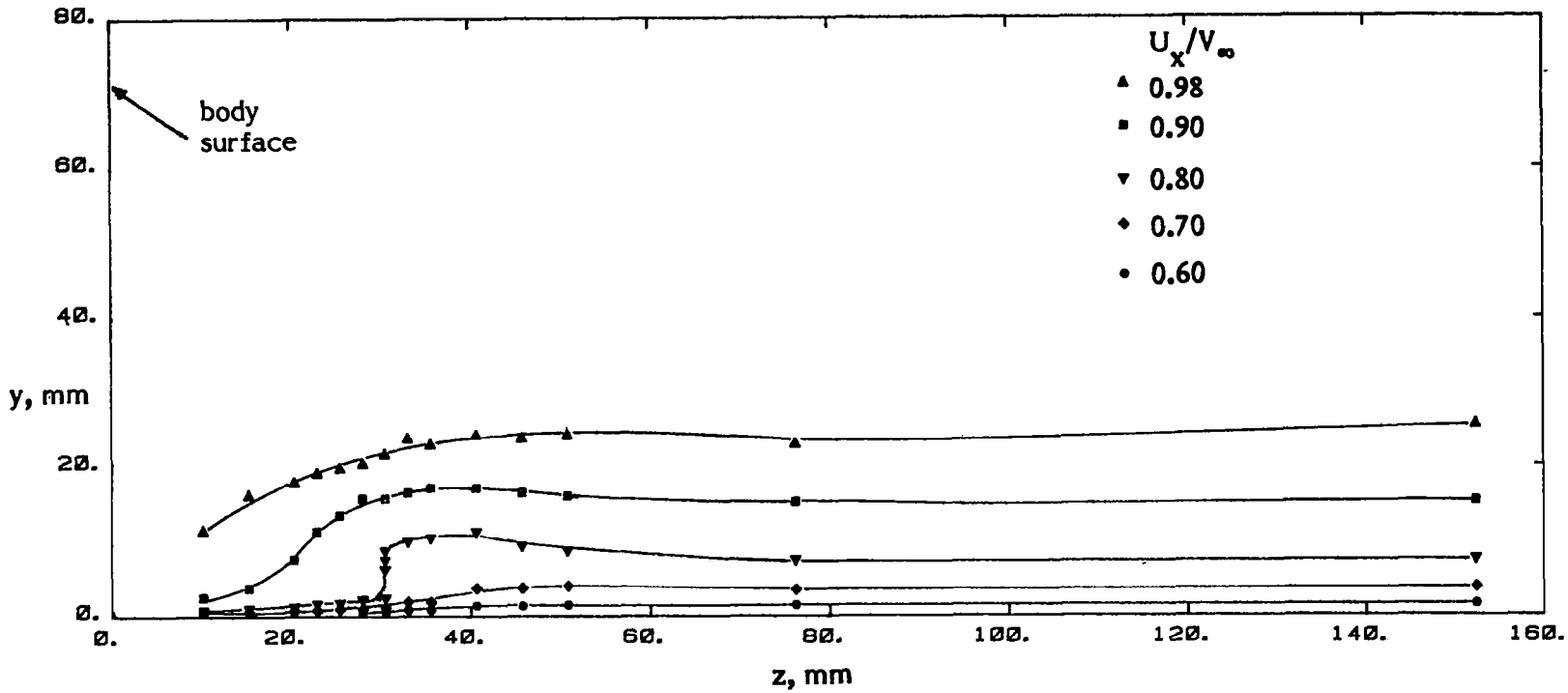

(e) x = 165 mm (reference 5).

Figure 14. - Continued.

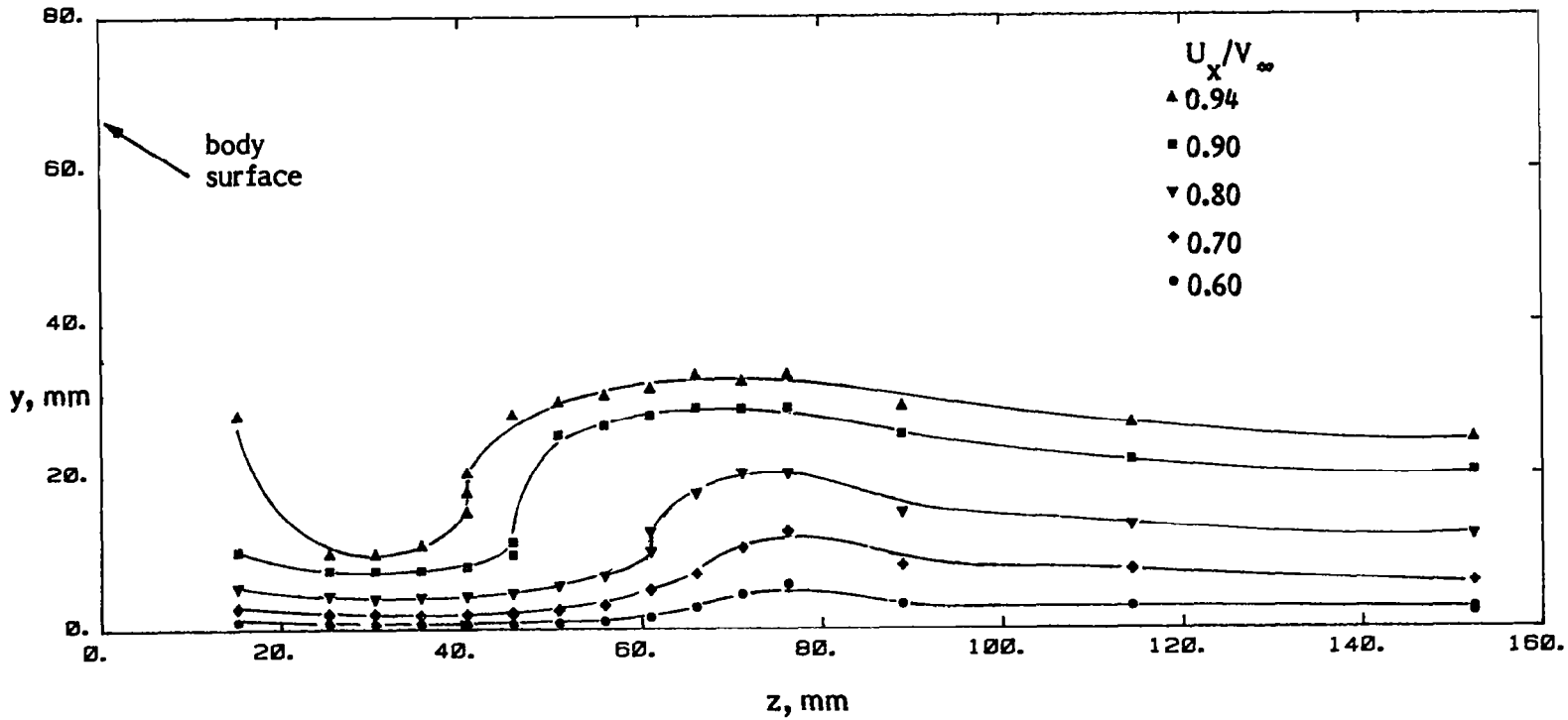

(f) x = 902 mm (reference 5).

Figure 14. - Concluded.

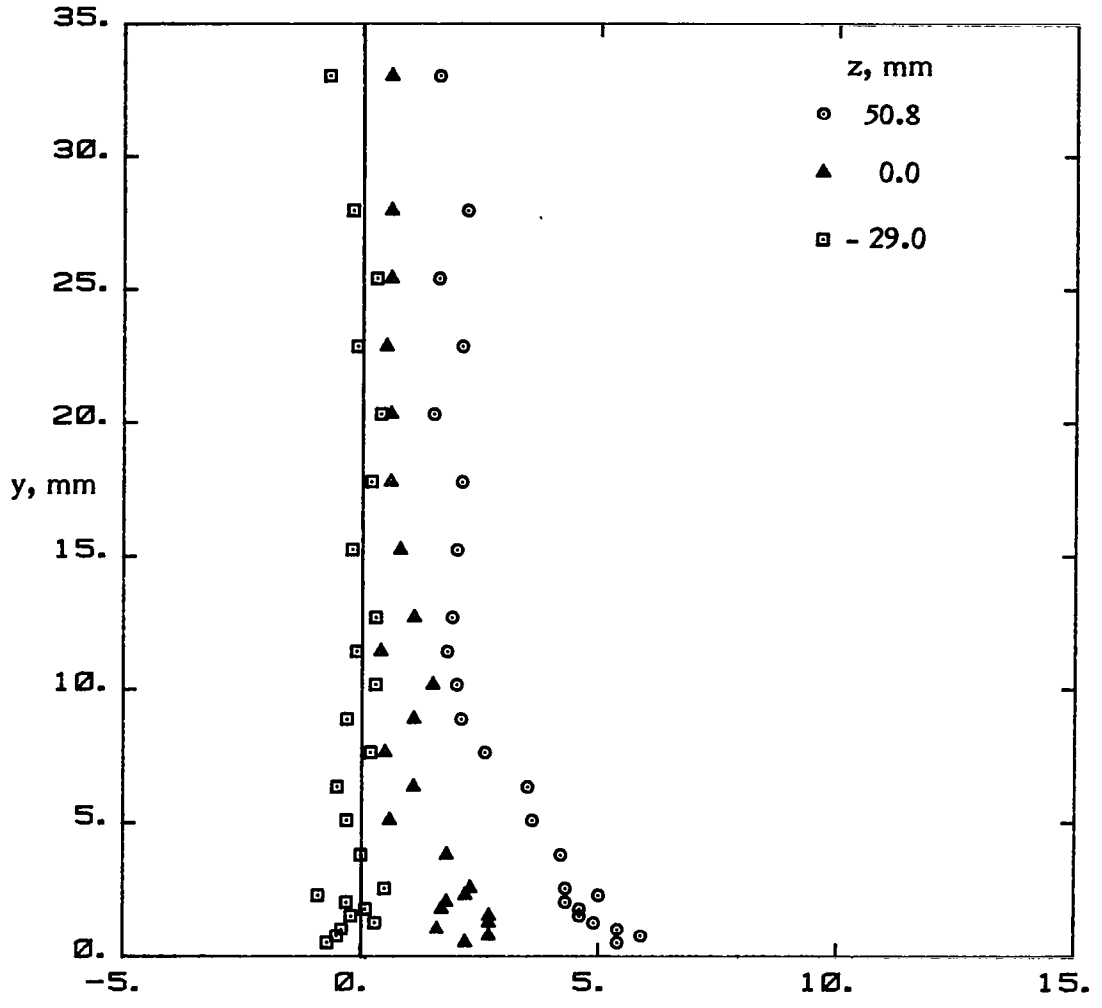

(a) x = - 102 mm.

Figure 15. - Variation of local mean flow direction.

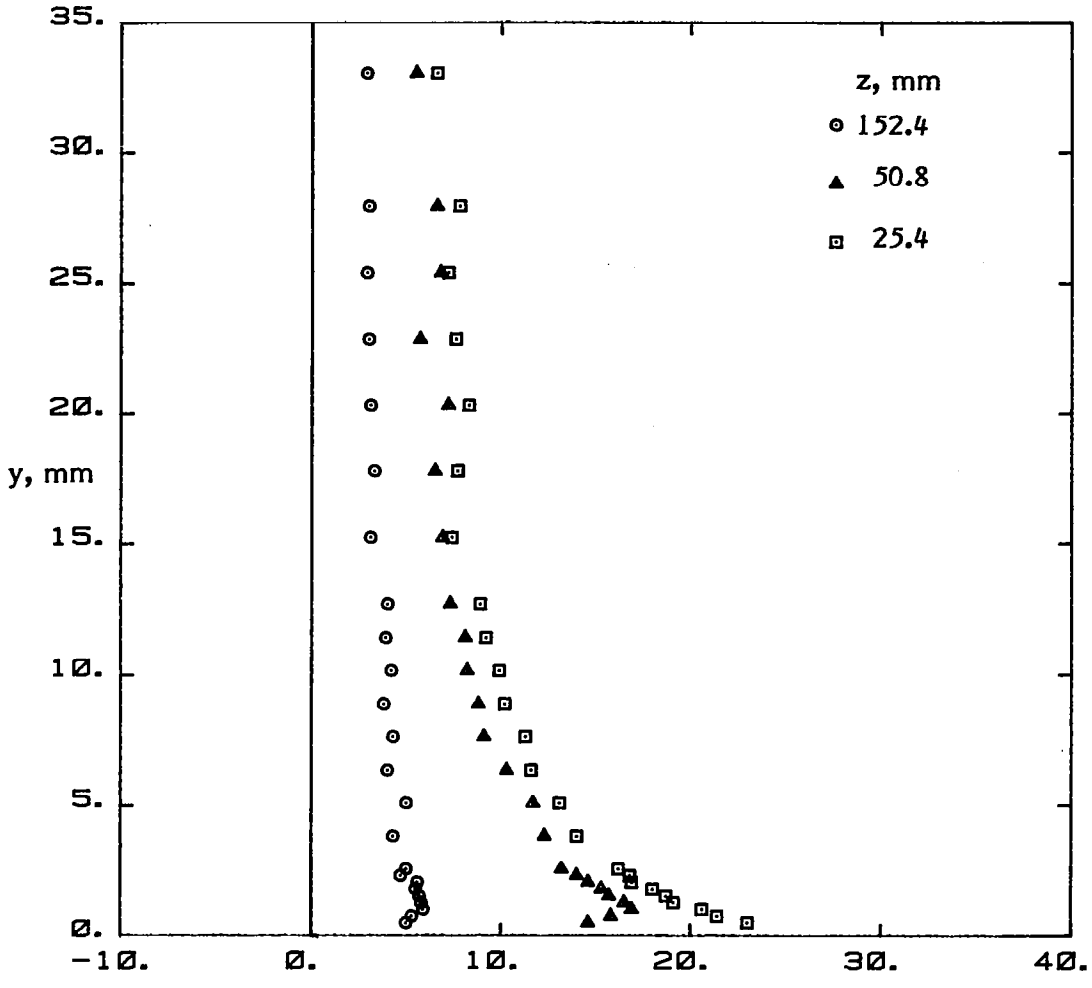

(b) x = - 38 mm.

Figure 15. - Continued.

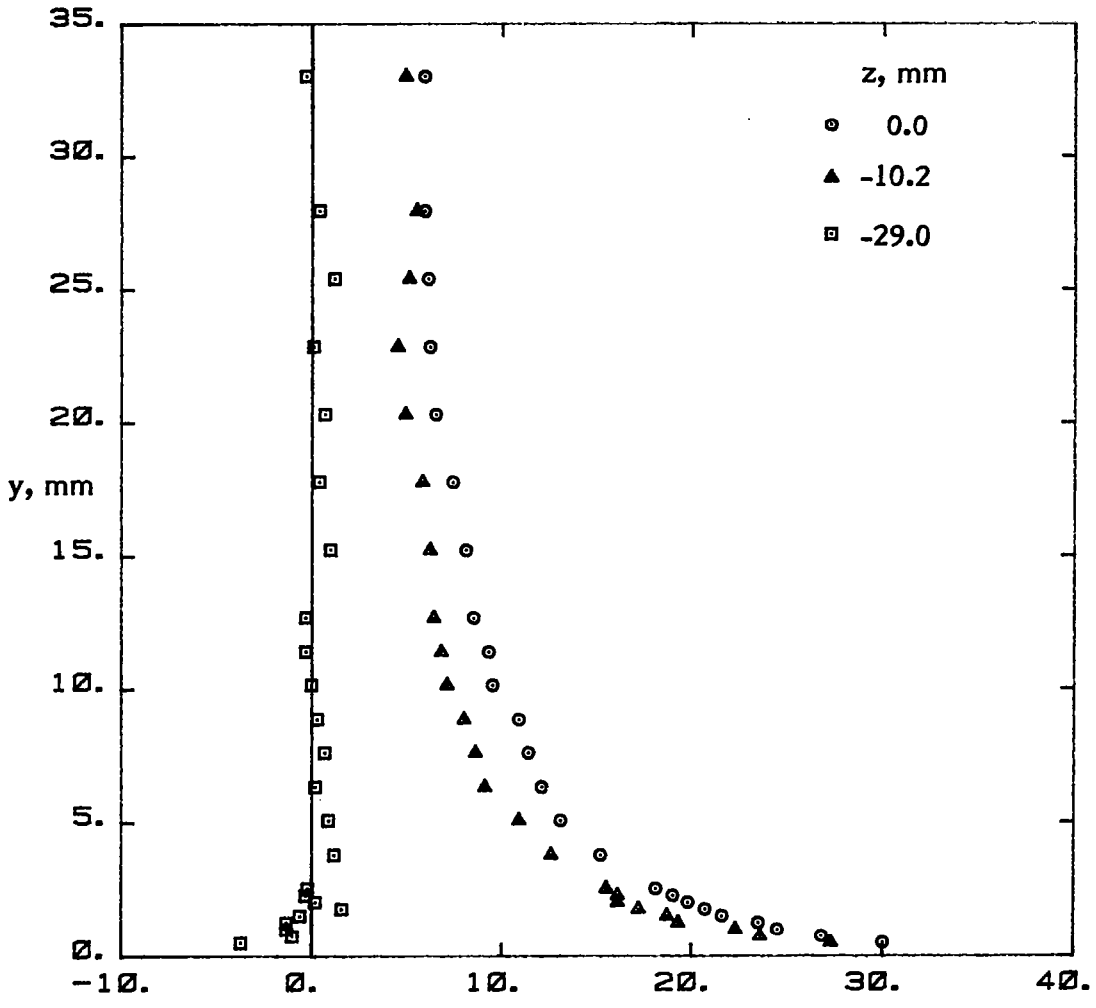

(c) x = - 38 mm.

Figure 15. - Continued.

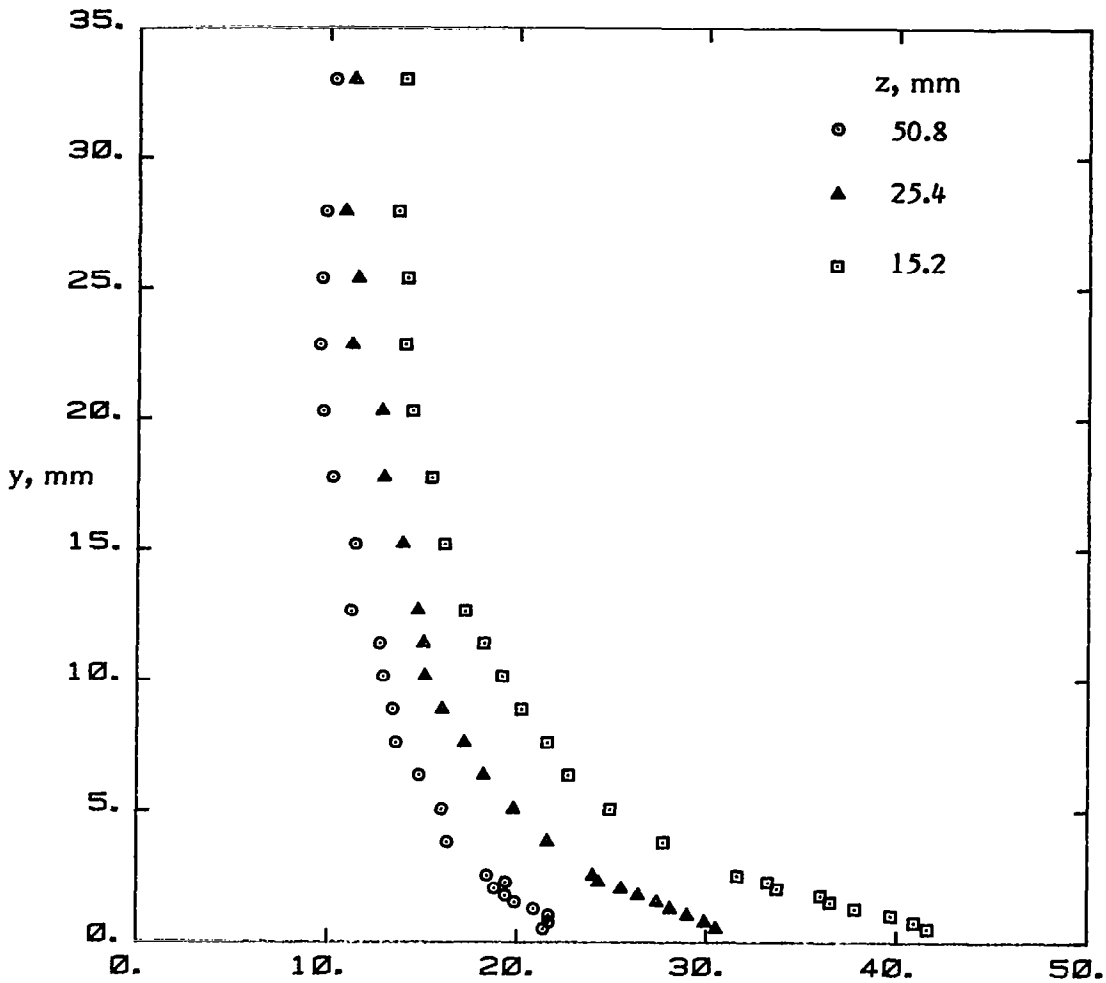

(d) x = - 11 mm.

Figure 15. - Continued.

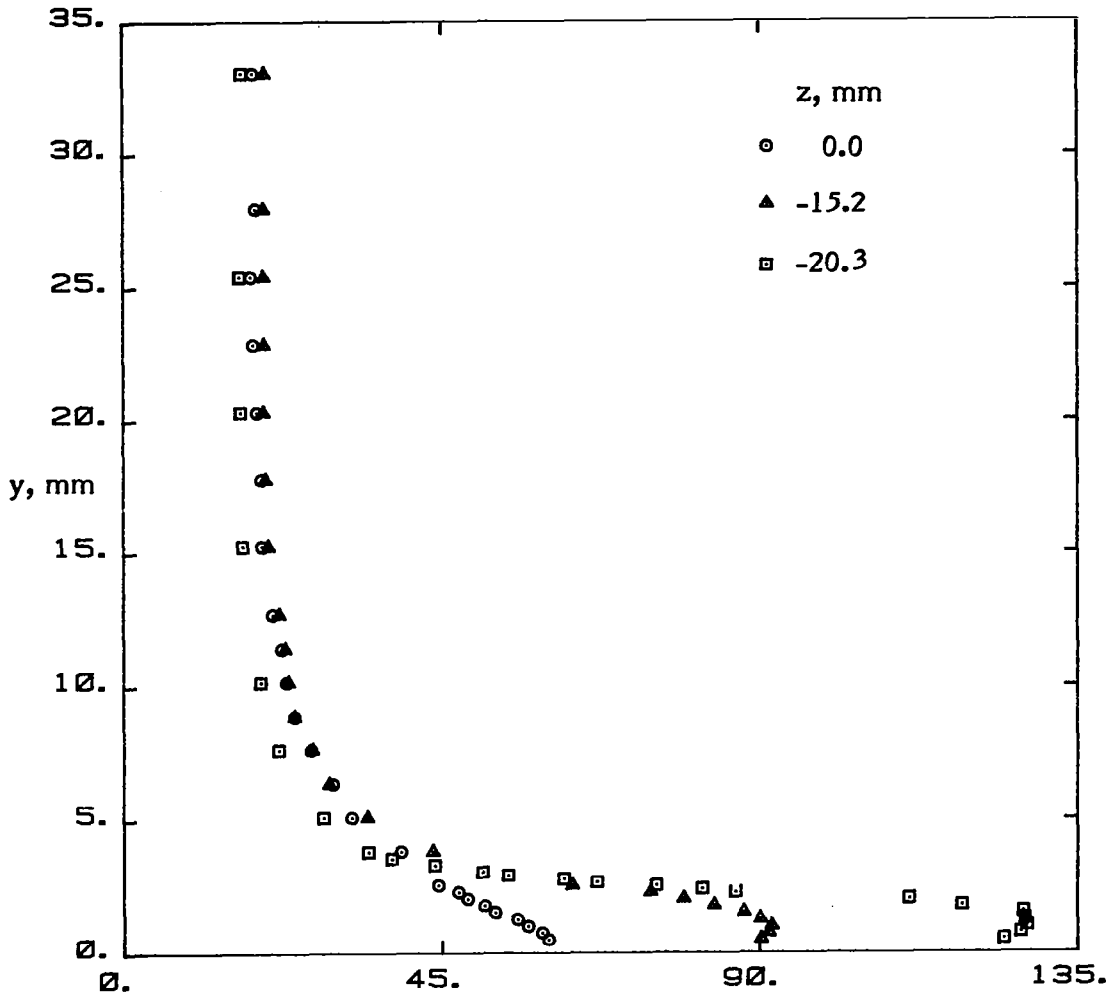

(e) x = - 11 mm.

Figure 15. - Continued.

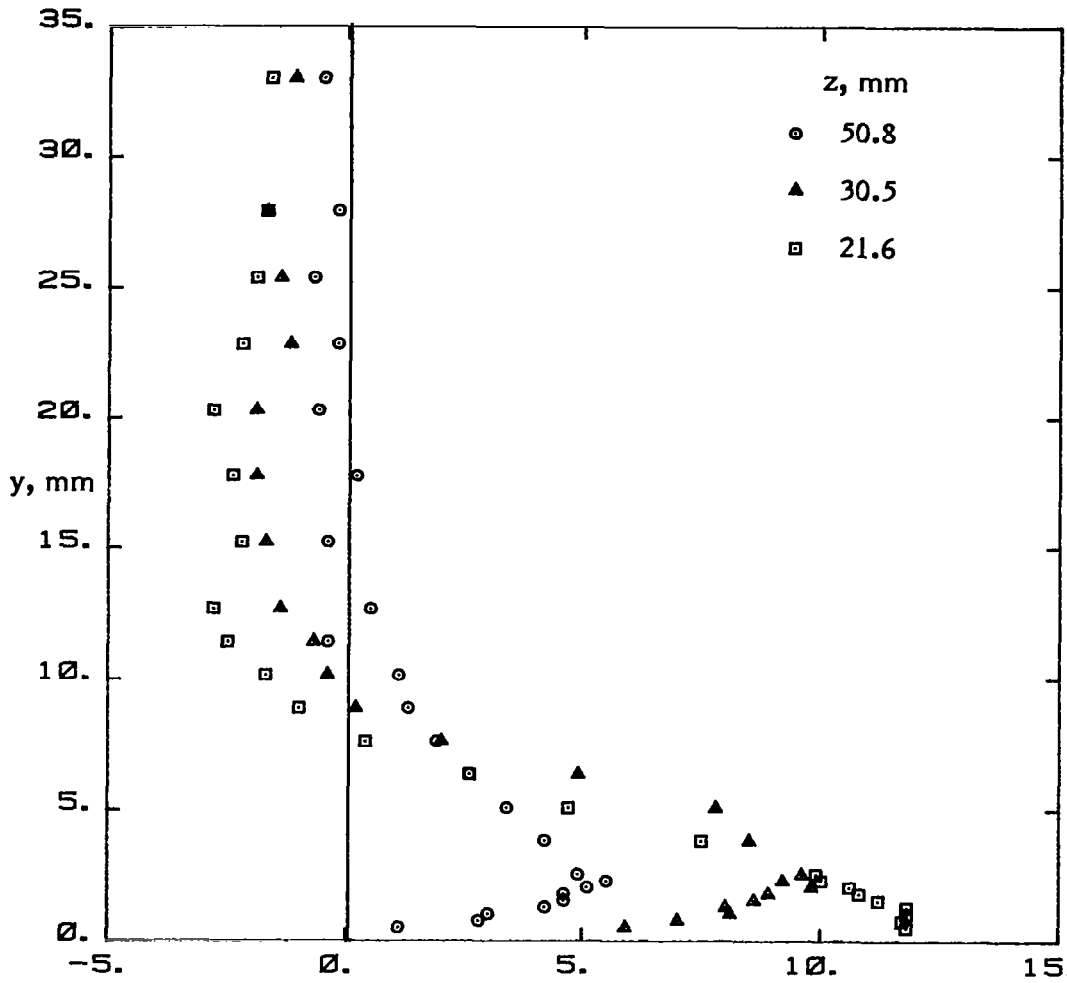

(f) x = 76 mm.

Figure 15. - Concluded.

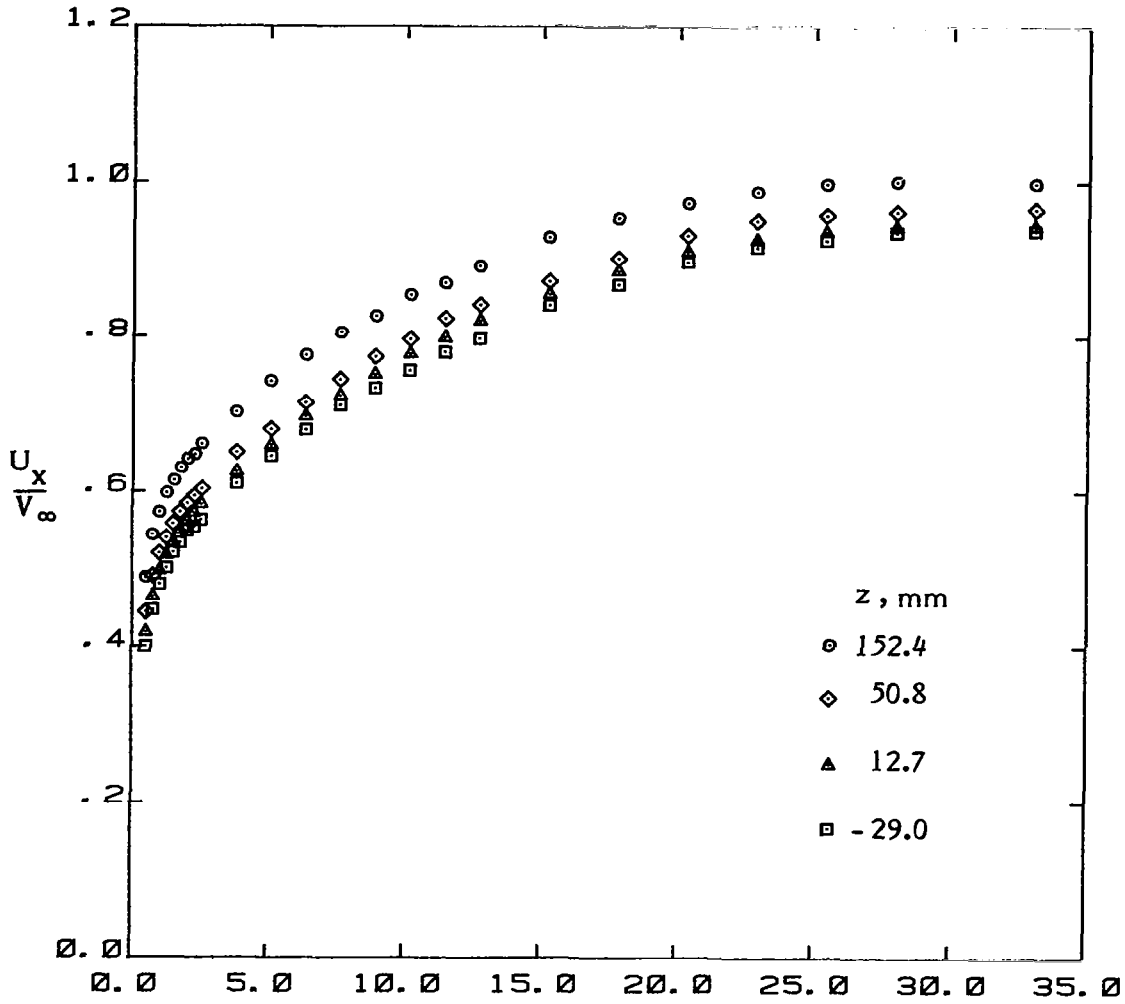

(a) Mean velocity U_x.

Figure 16. - Mean velocities and turbulence stresses upstream of the juncture (x = - 102 mm).

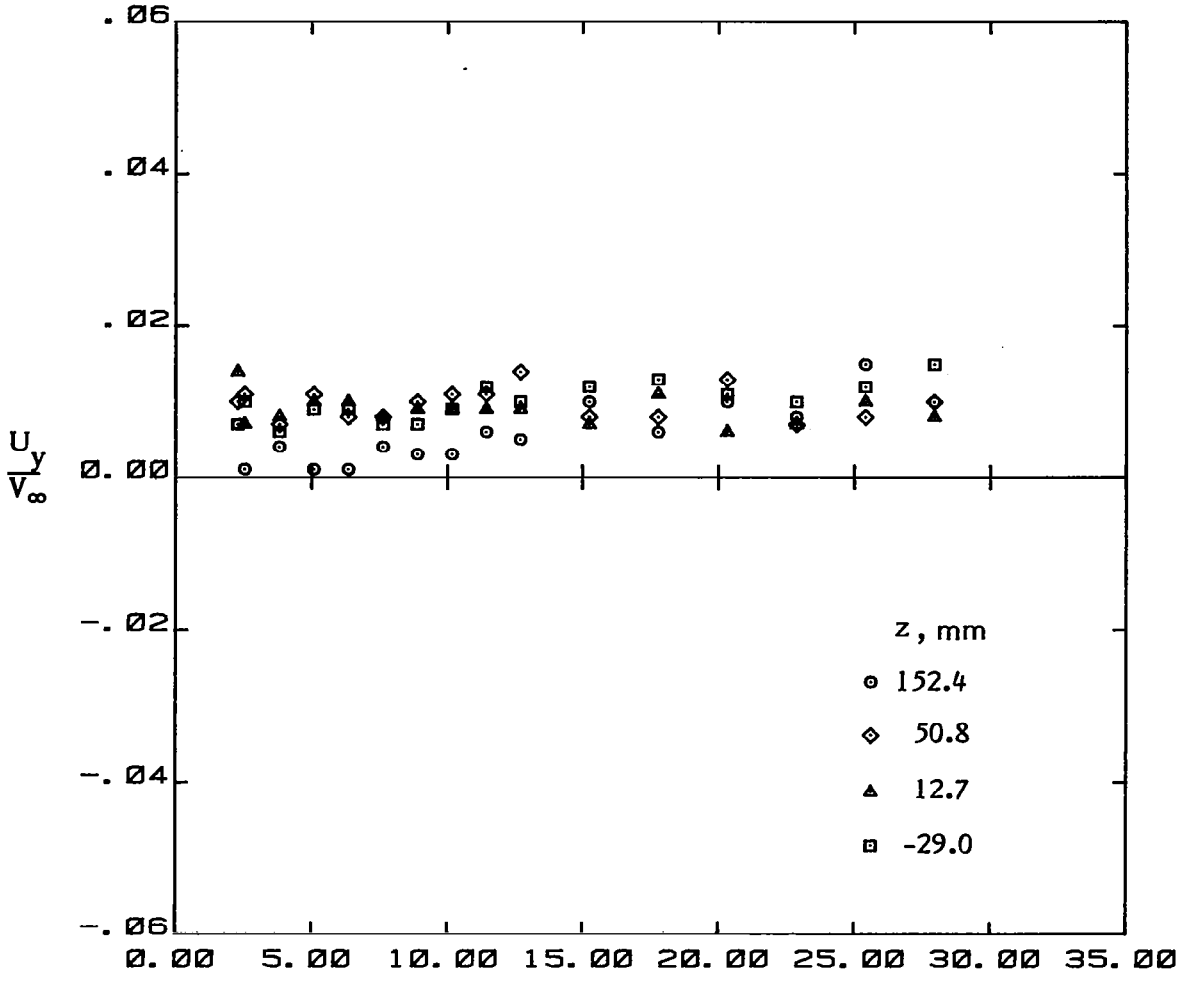

(b) Mean Velocity U_y.

Figure 16. - Continued.

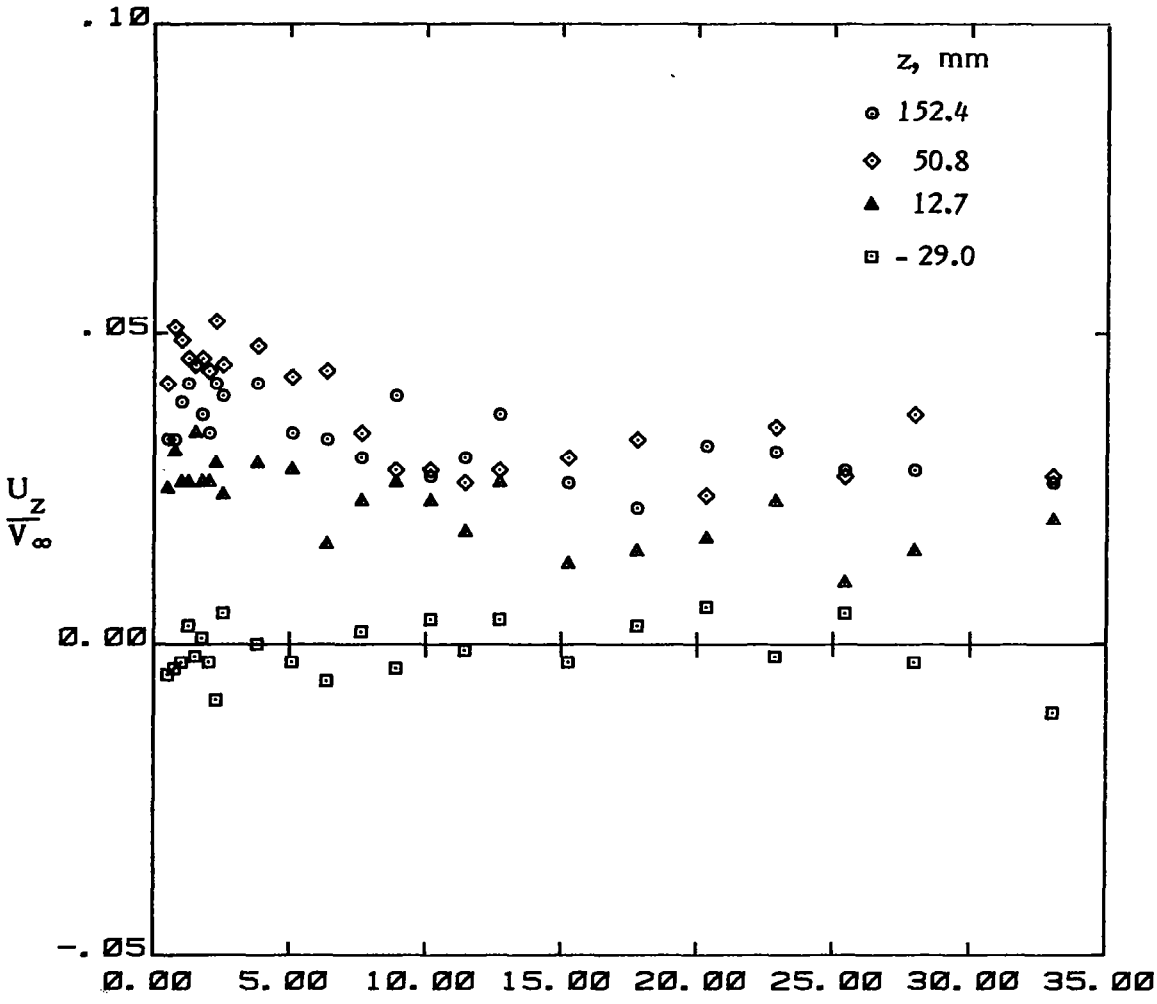

(c) Mean Velocity U_z.

Figure 16. - Continued.

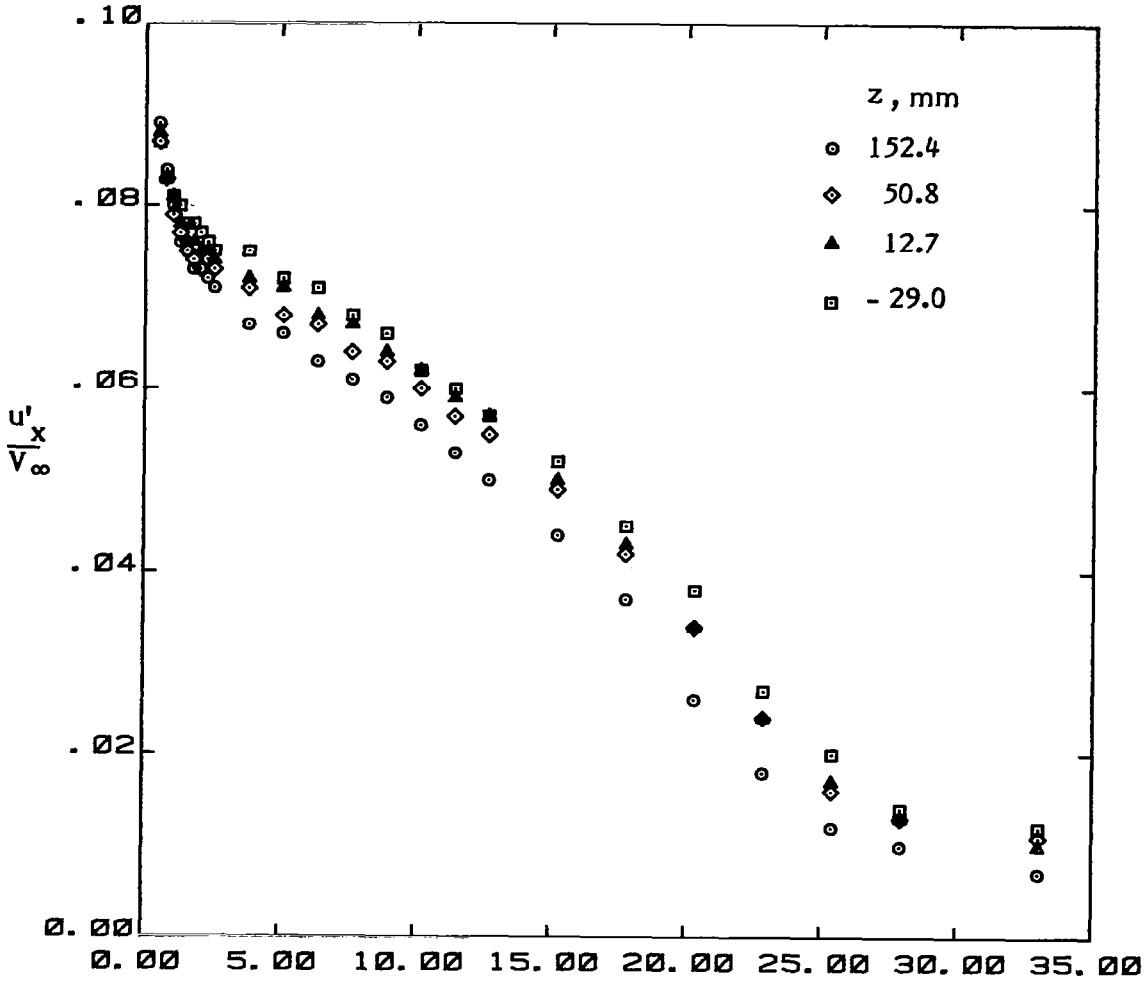

(d) Turbulent normal stress u'_x.

Figure 16. - Continued.

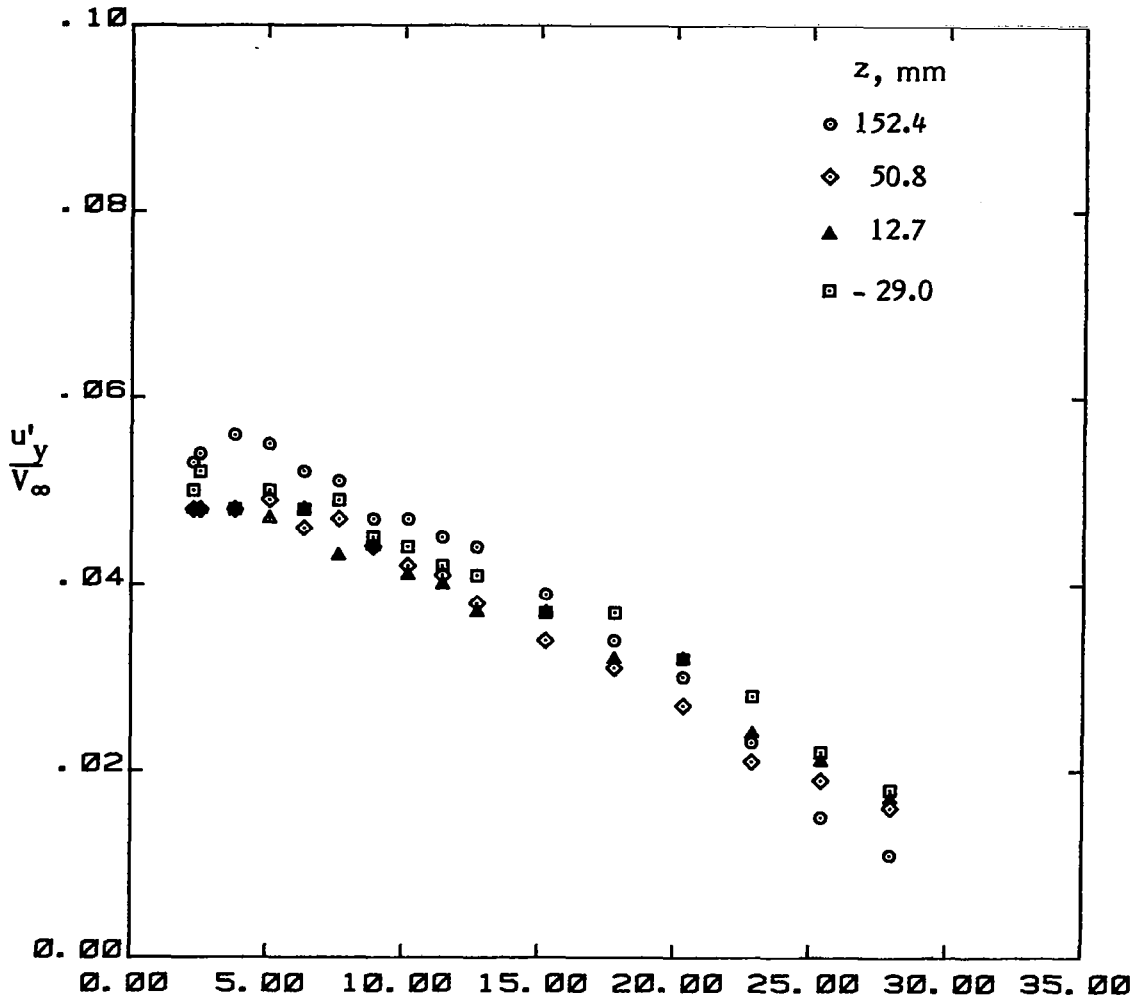

(e) Turbulent normal stress u'_y.

Figure 16. - Continued.

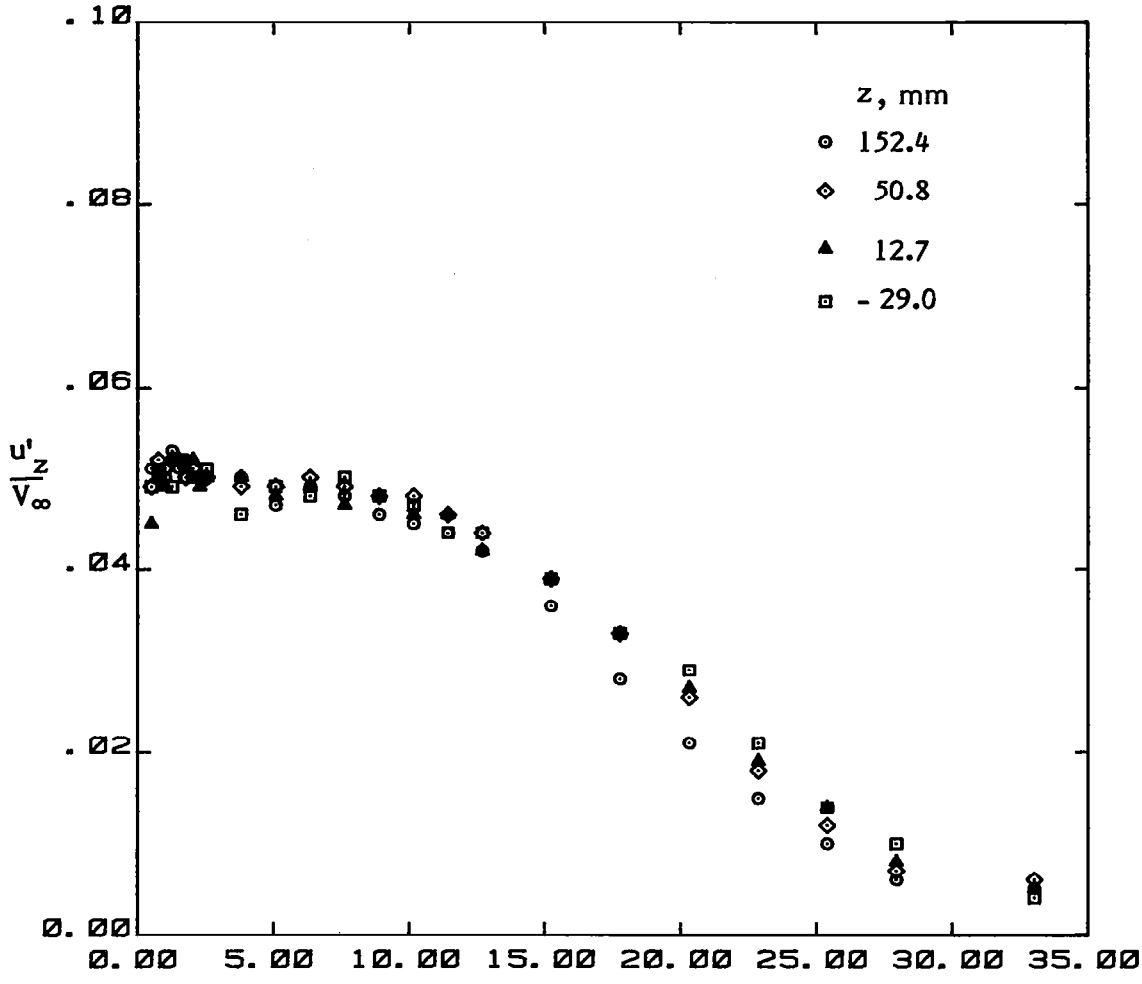

(f) Turbulent normal stress u'_z.

Figure 16. - Continued.

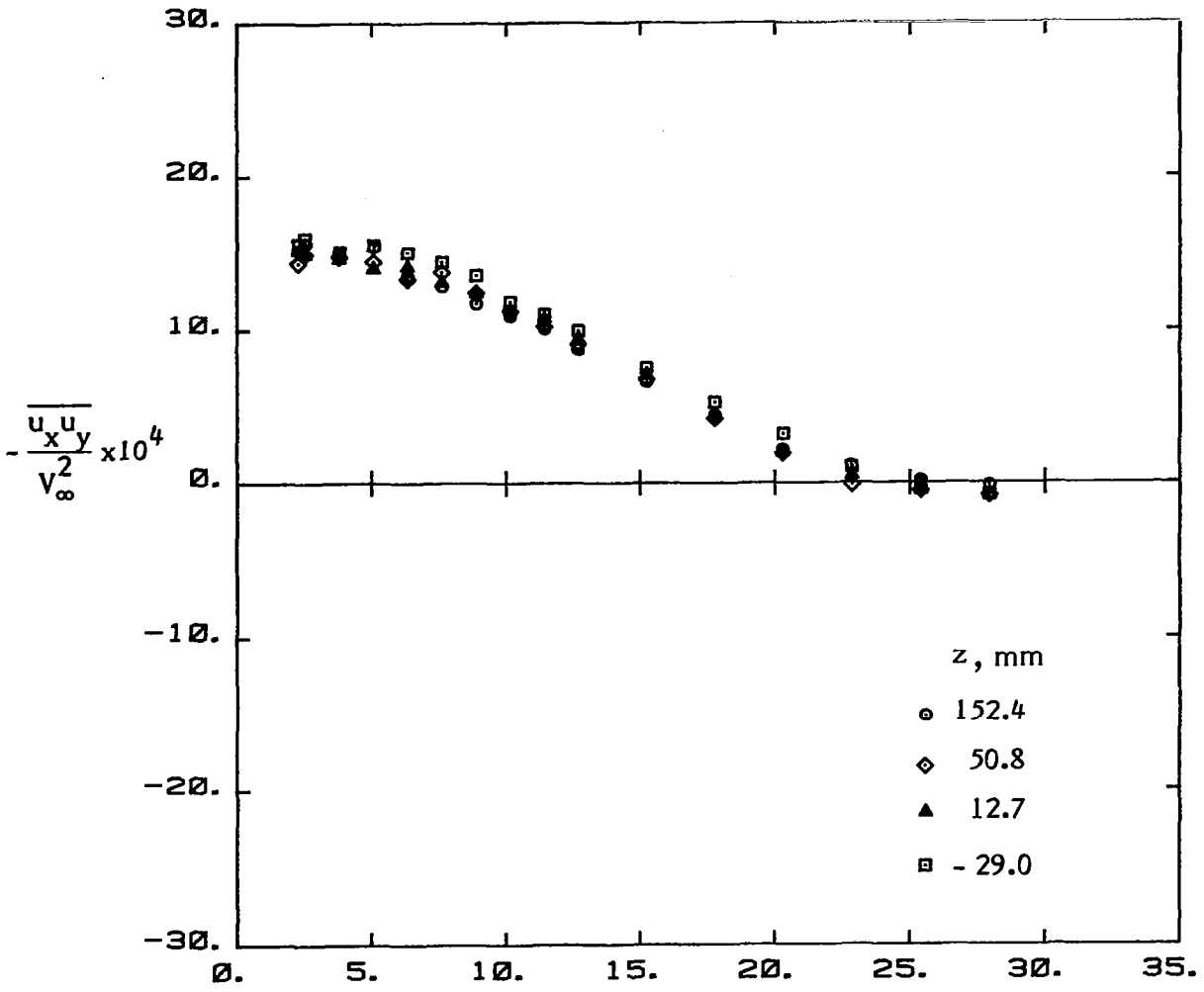

(g) Turbulent shear stress $\overline{u_x u_y}$.

Figure 16. - Continued.

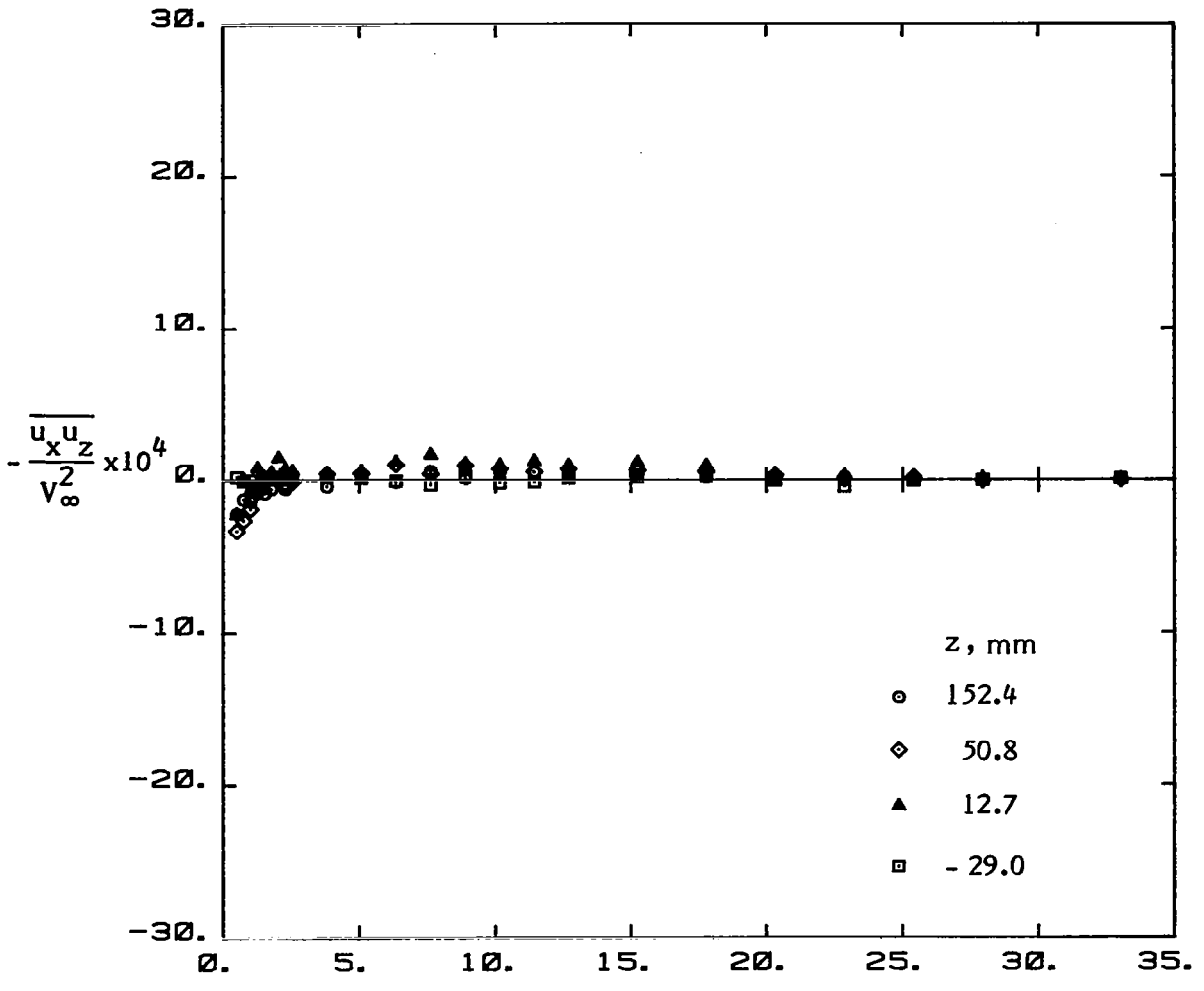

(h) Turbulent shear stress $\overline{u_x u_z}$.

Figure 16. - Continued.

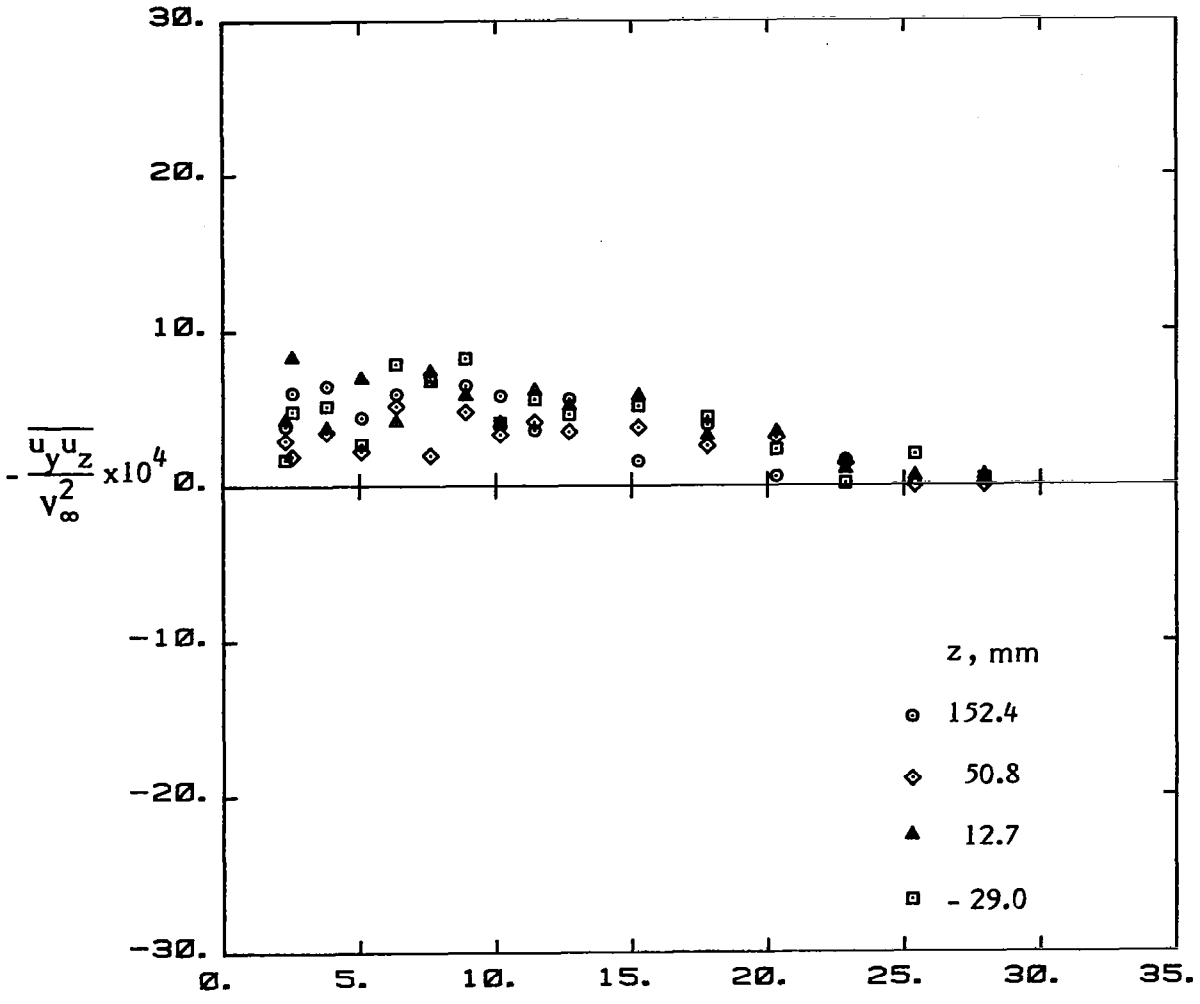

(i) Turbulent shear stress $\overline{u_y u_z}$.

Figure 16. - Concluded.

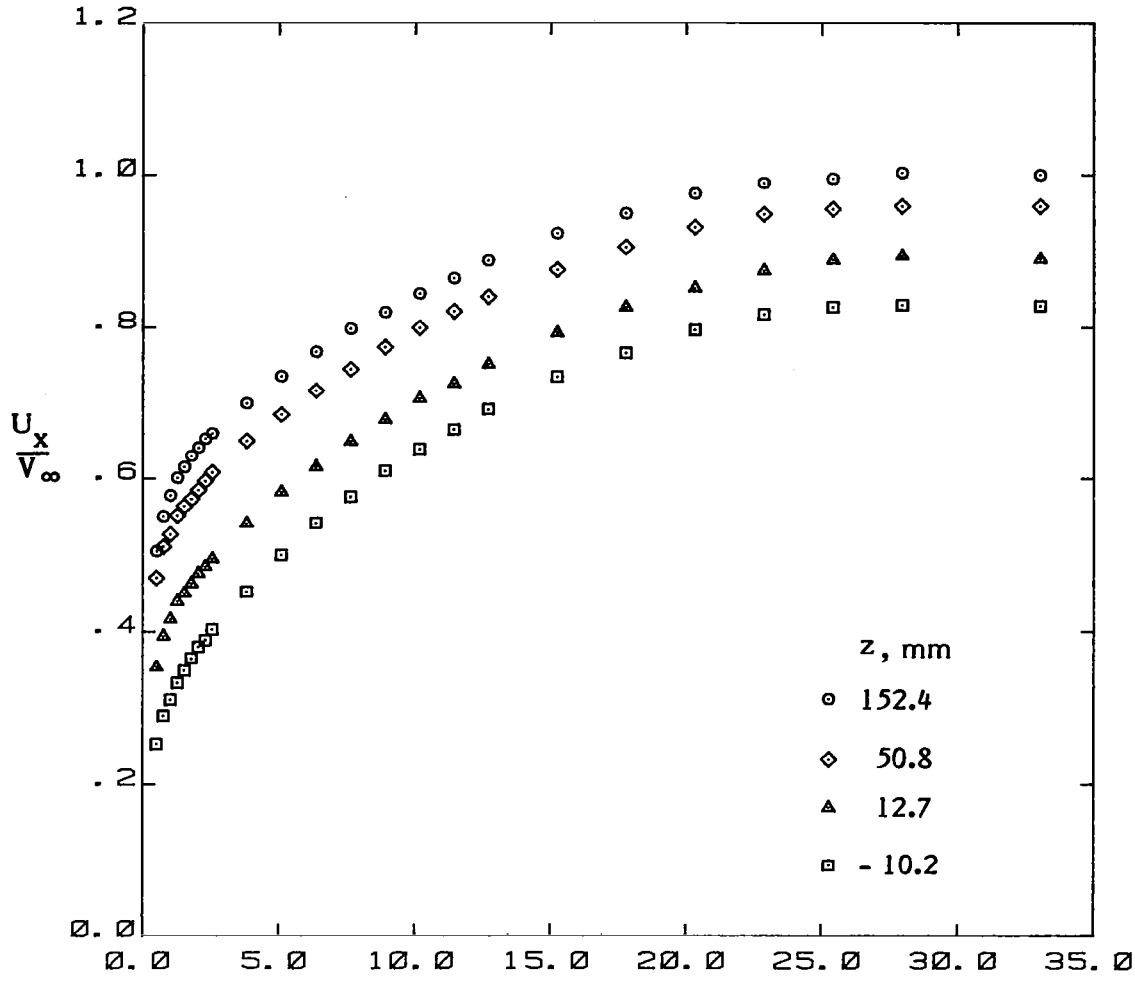

(a) Mean velocity U_x.

Figure 17. - Mean velocities and turbulence stresses upstream of the juncture (x = - 38 mm).

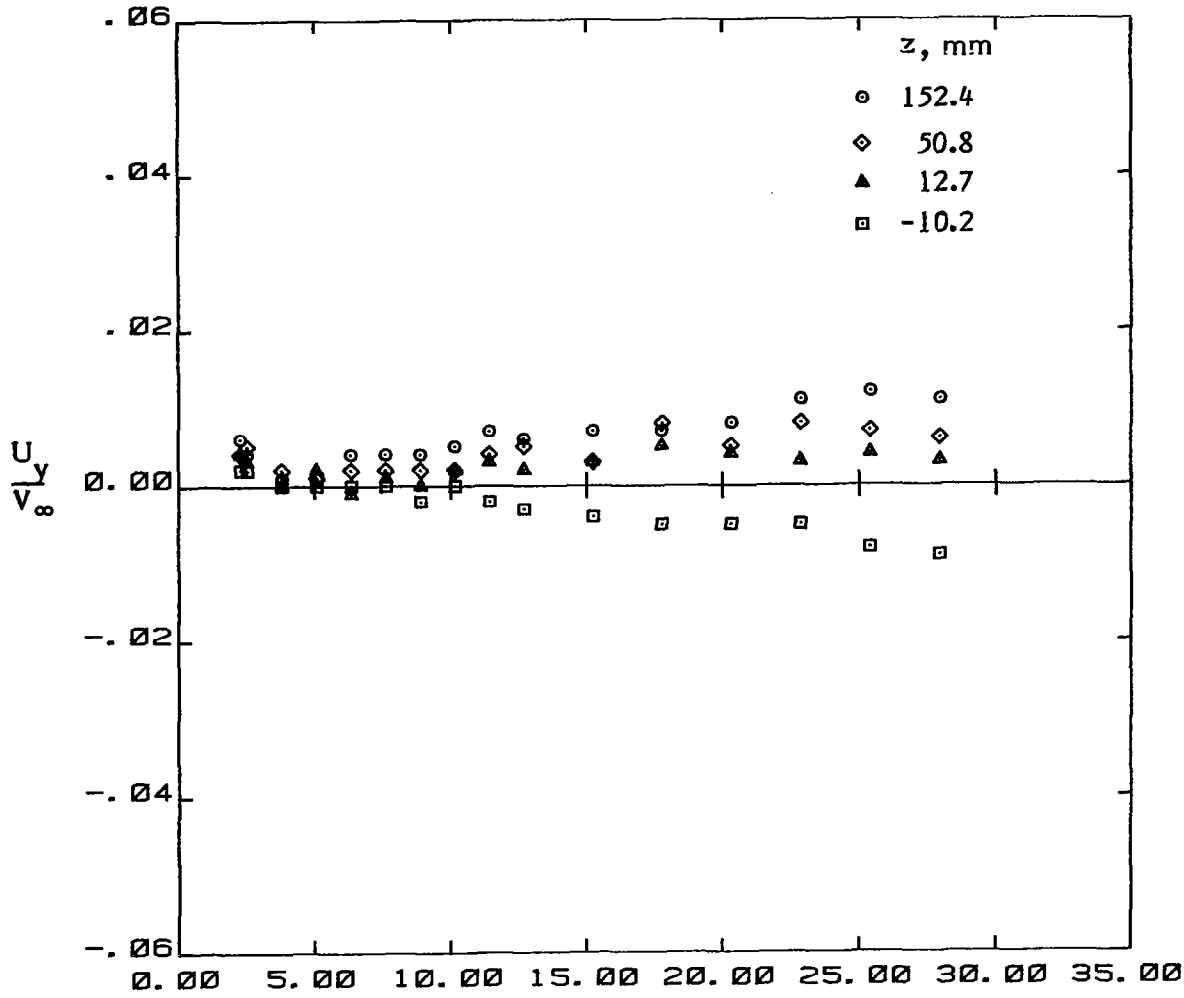

(b) Mean velocity U_y.

Figure 17. - Continued.

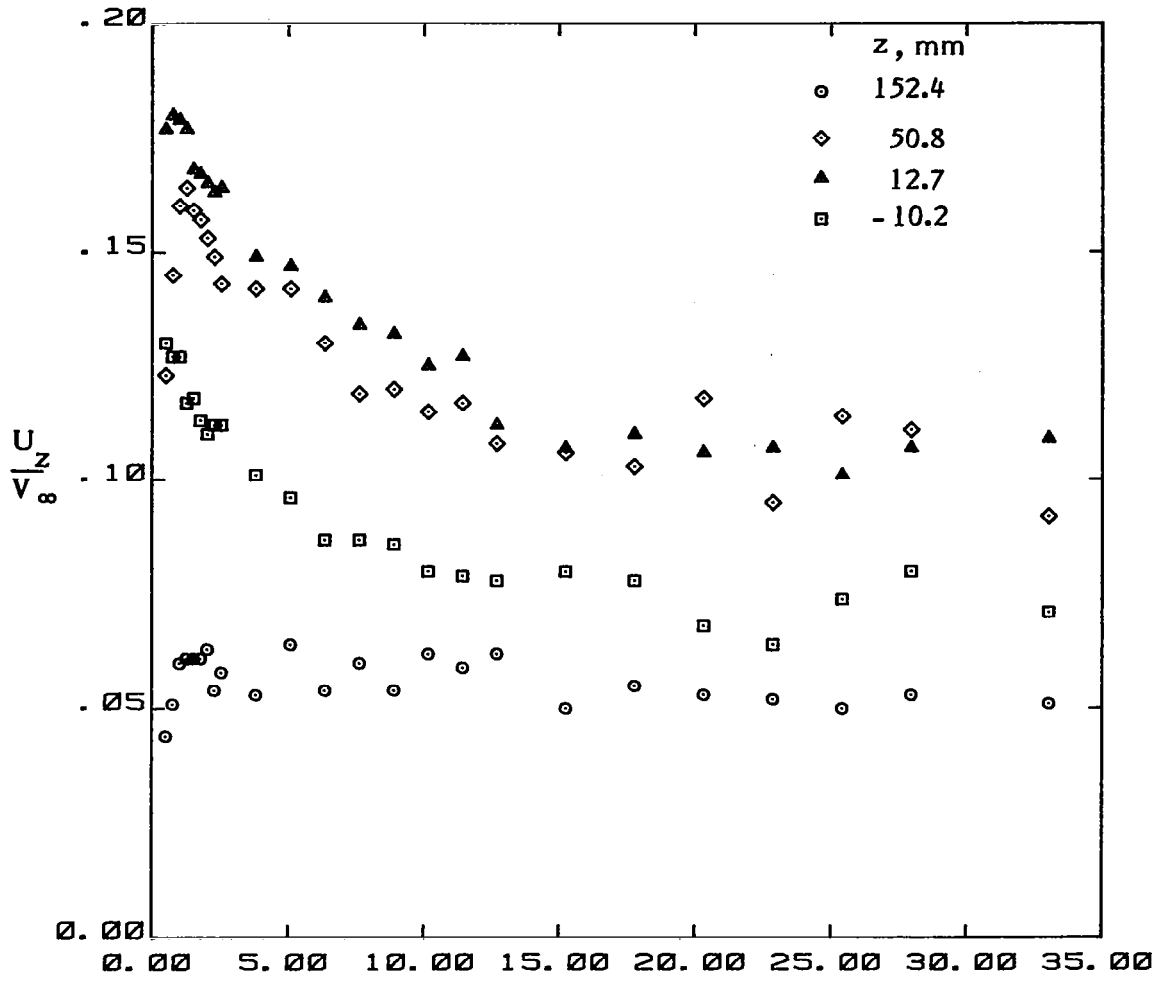

(c) Mean velocity U_z.

Figure 17. - Continued.

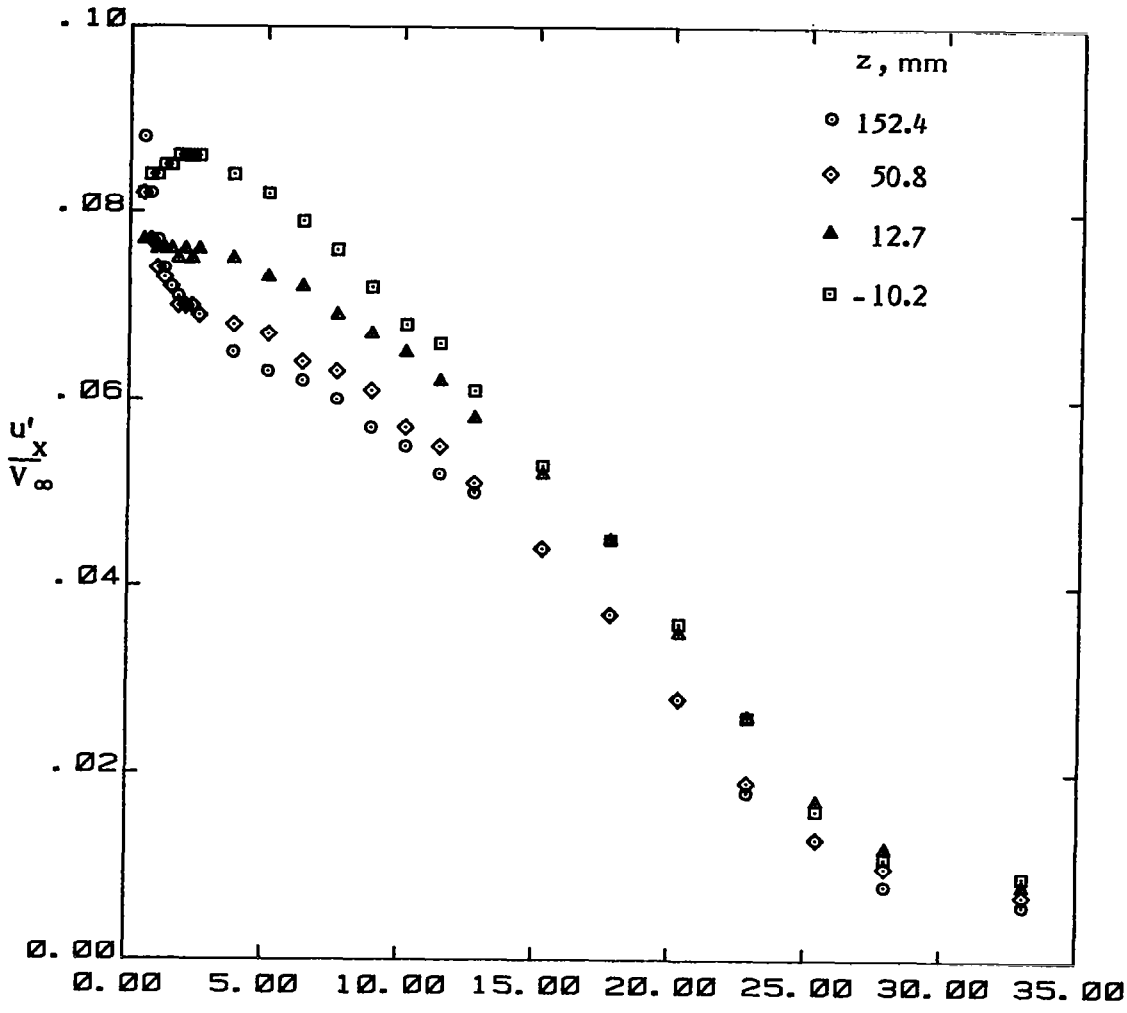

(d) Turbulent normal stress u'_x.

Figure 17. - Continued.

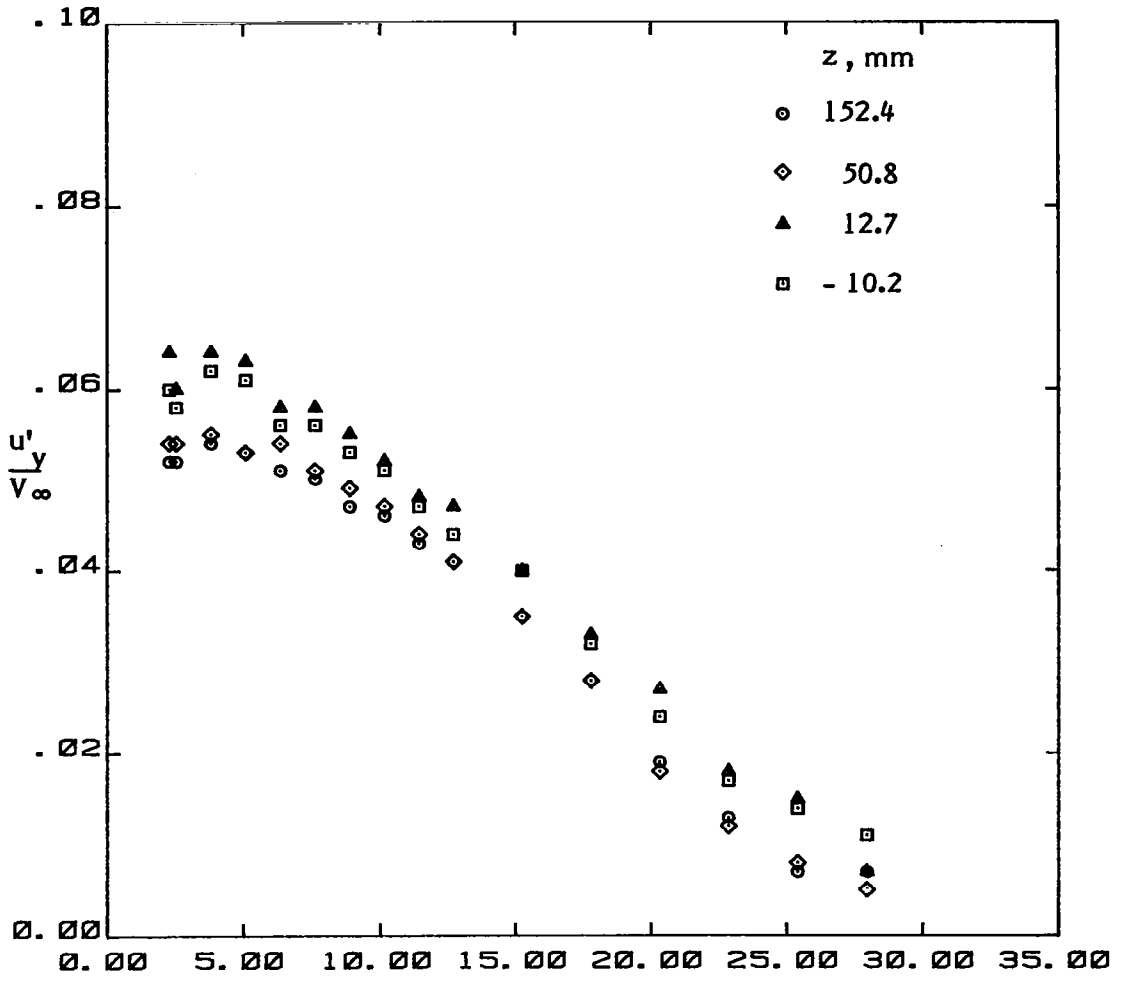

(e) Turbulent normal stress u'_y.

Figure 17. - Continued.

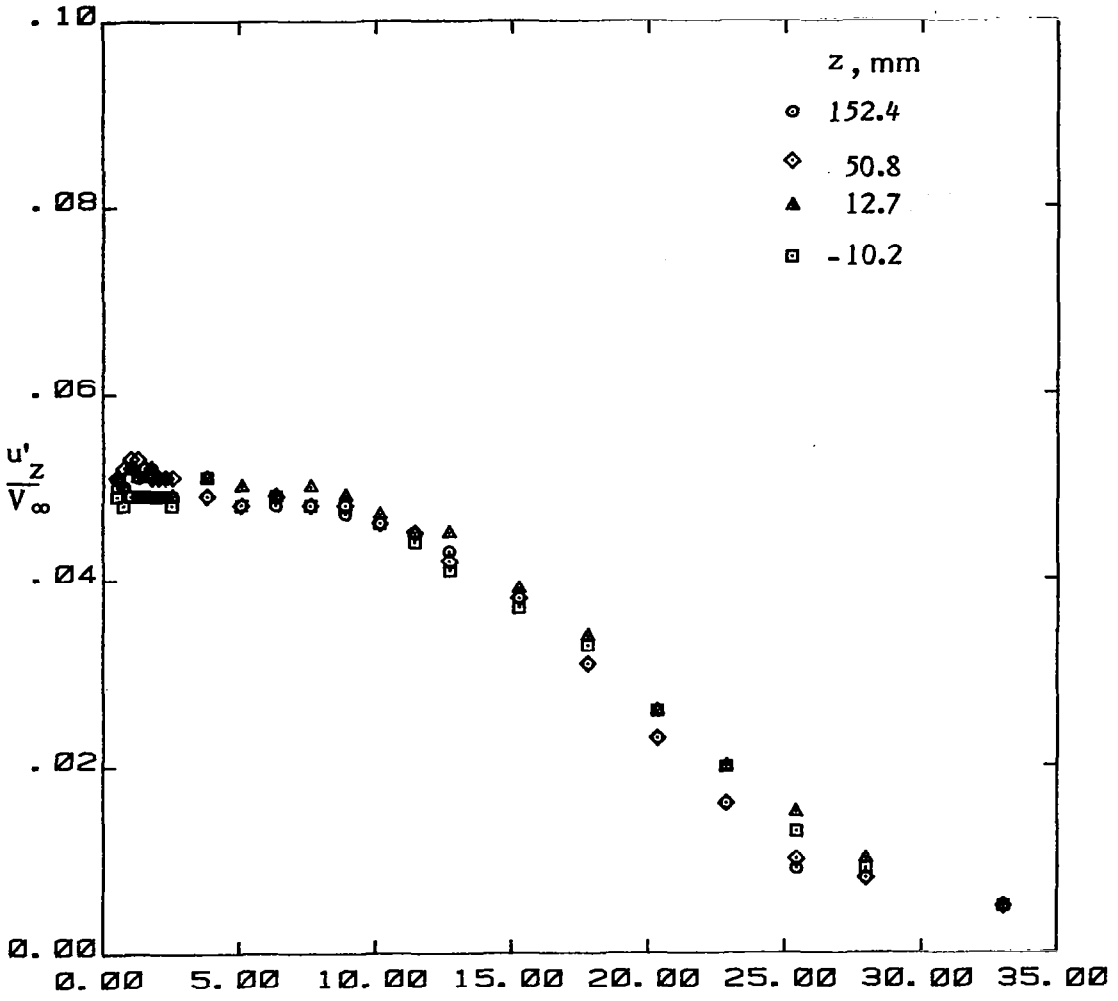

(f) Turbulent normal stress u'_z.

Figure 17. - Continued.

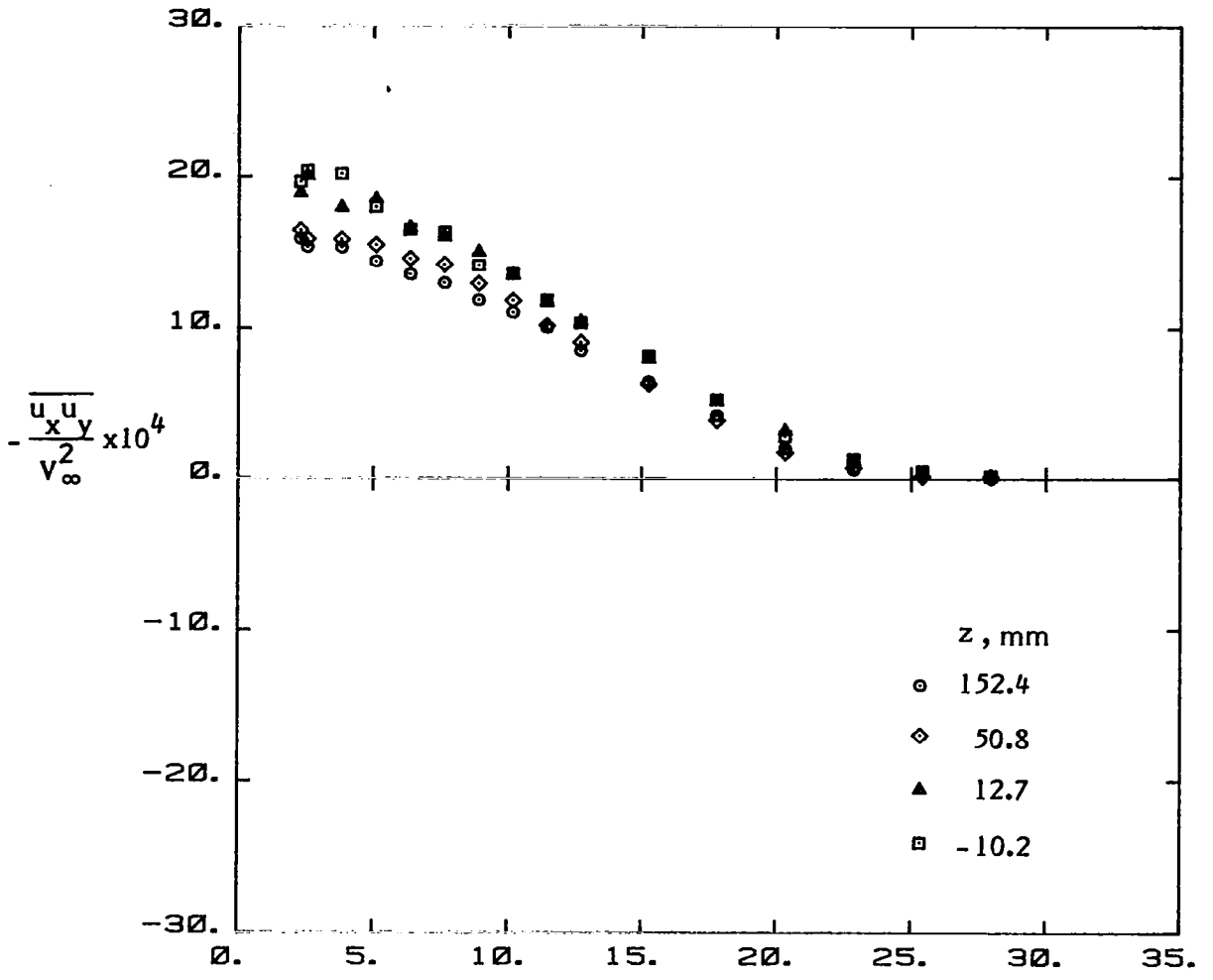

(g) Turbulent shear stress $\overline{u_x u_y}$.

Figure 17. - Continued.

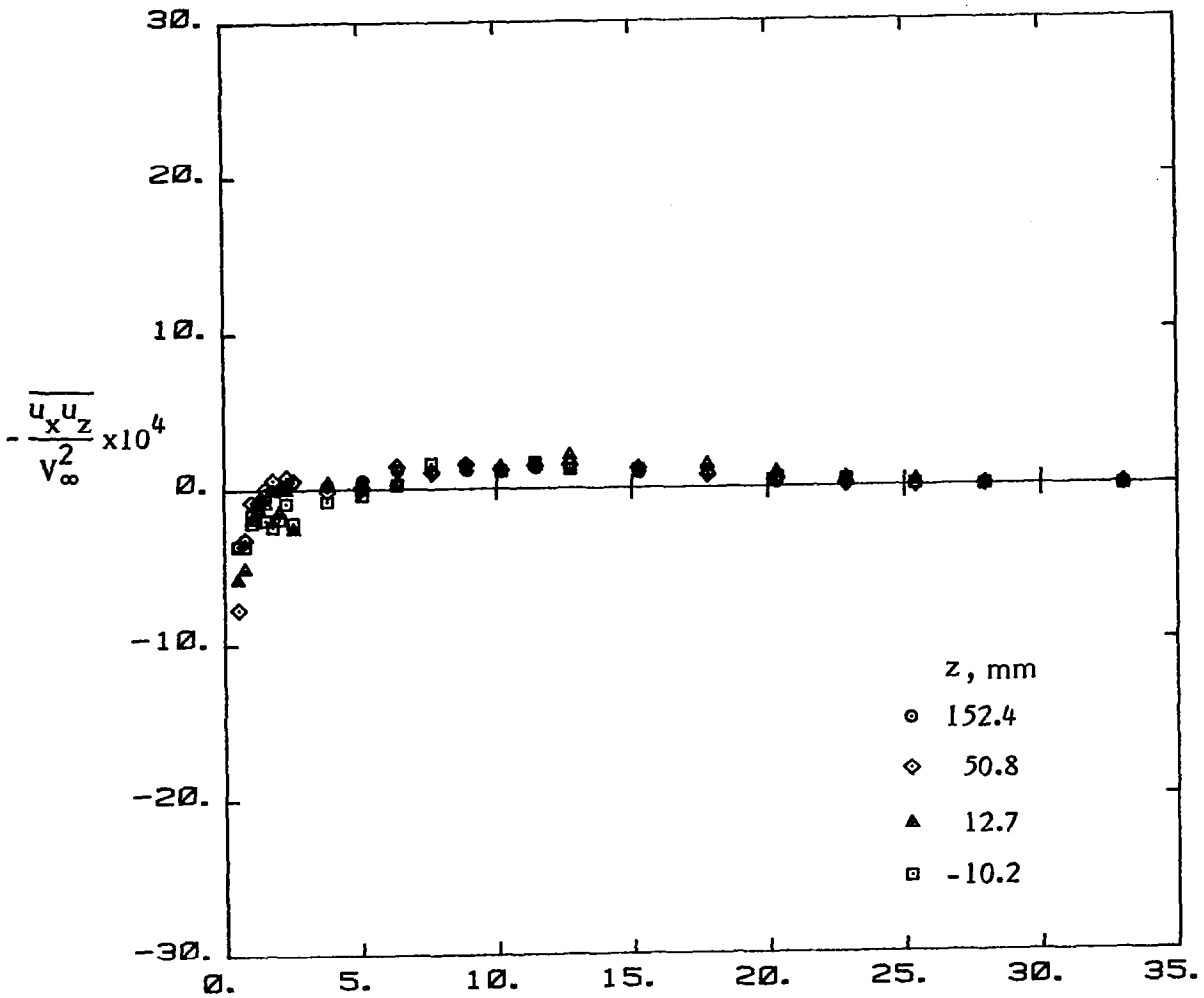

(h) Turbulent shear stress $\overline{u_x u_z}$.

Figure 17. - Continued.

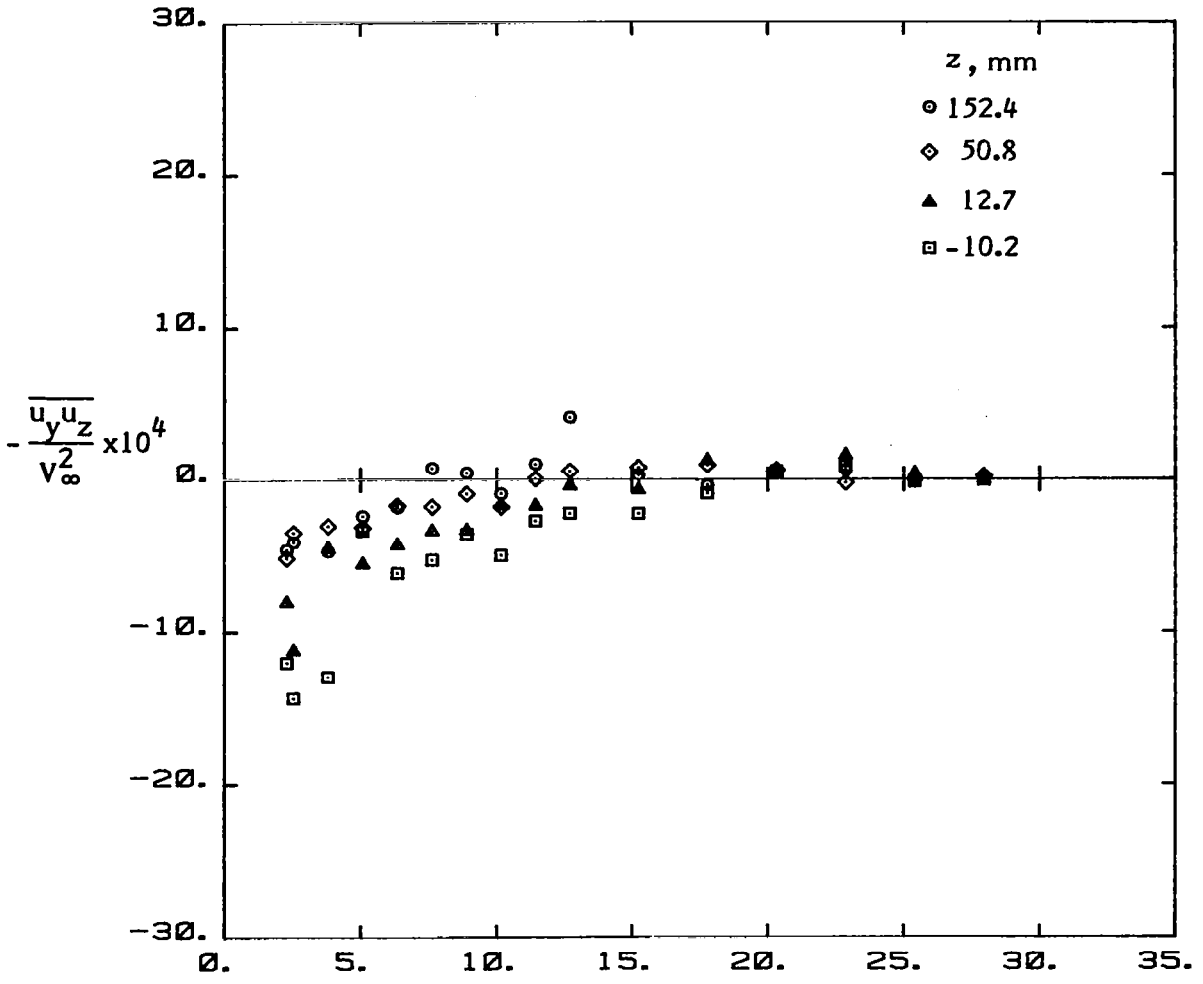

(i) Turbulent shear stress $\overline{u_y u_z}$.

Figure 17. - Concluded.

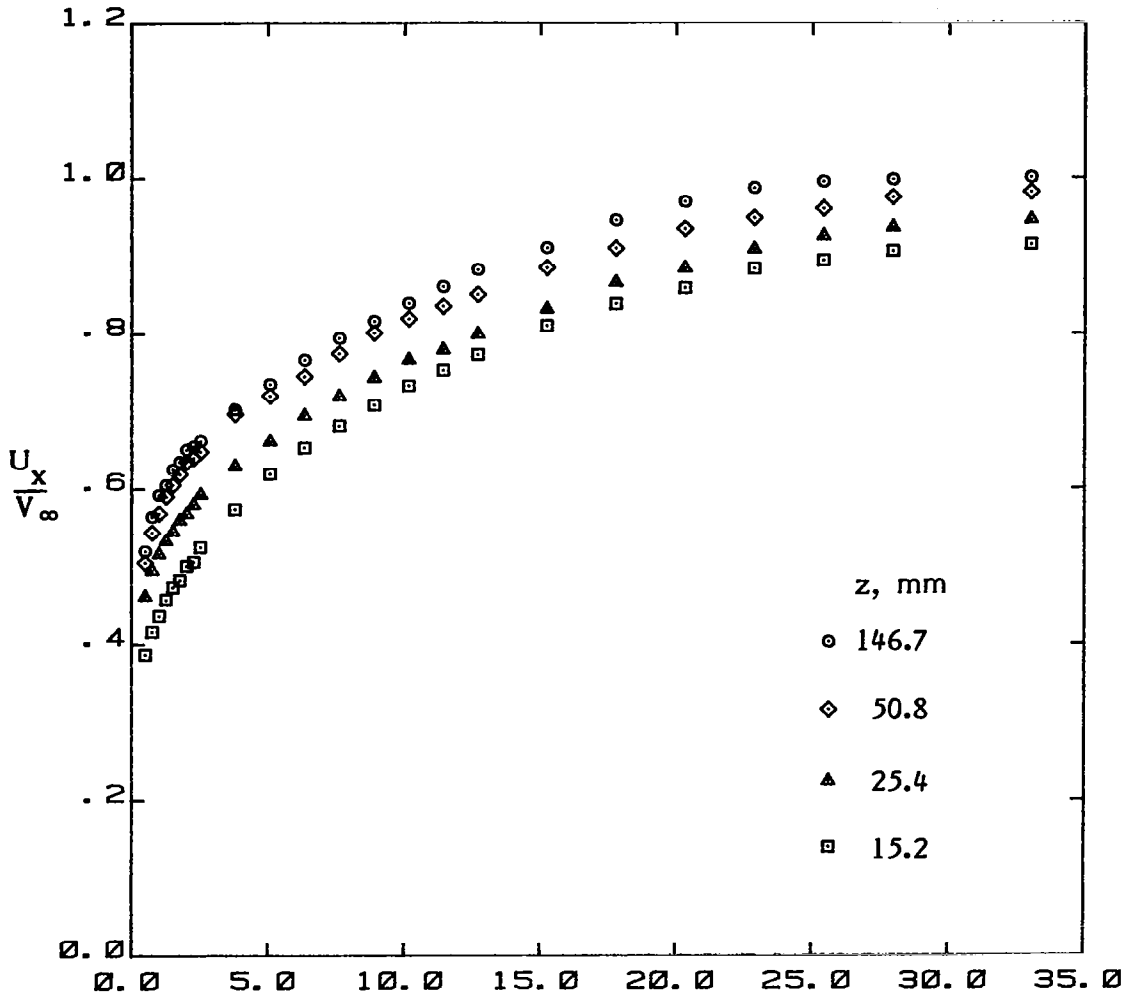

(a) Mean velocity U_x.

Figure 18. - Mean velocities and turbulence stresses upstream of the juncture (x = - 11 mm).

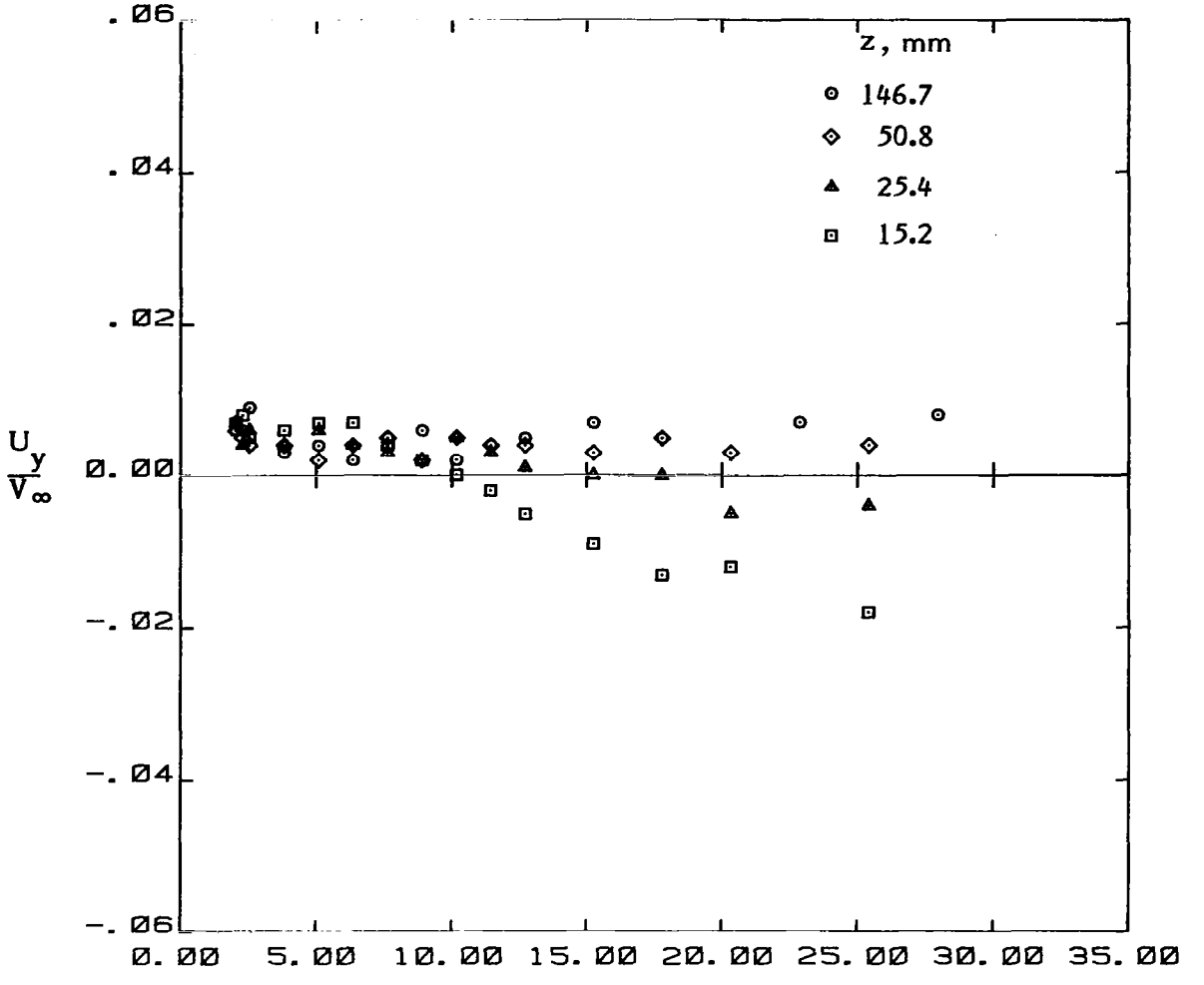

(b) Mean velocity U_y.

Figure 18. - Continued.

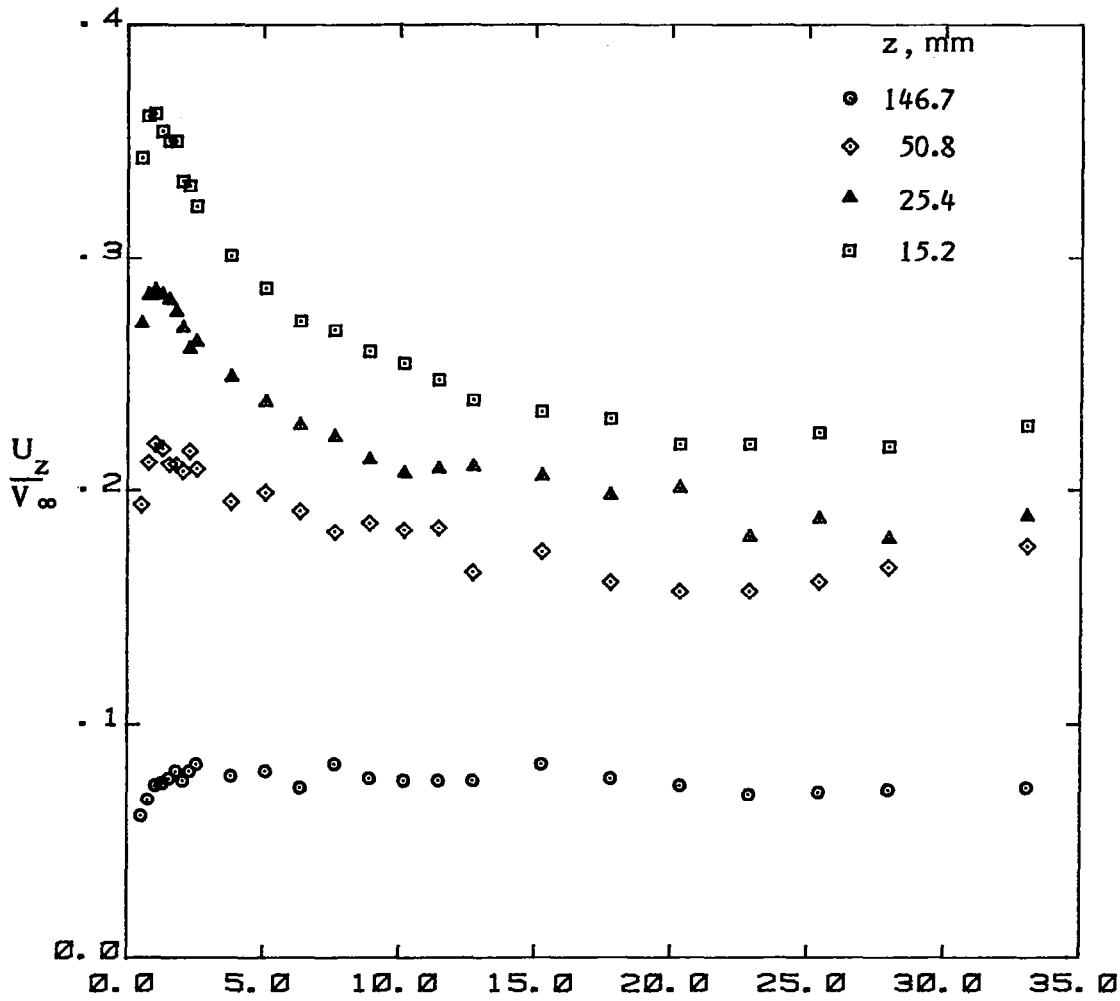

(c) Mean velocity U_z.

Figure 18. - Continued.

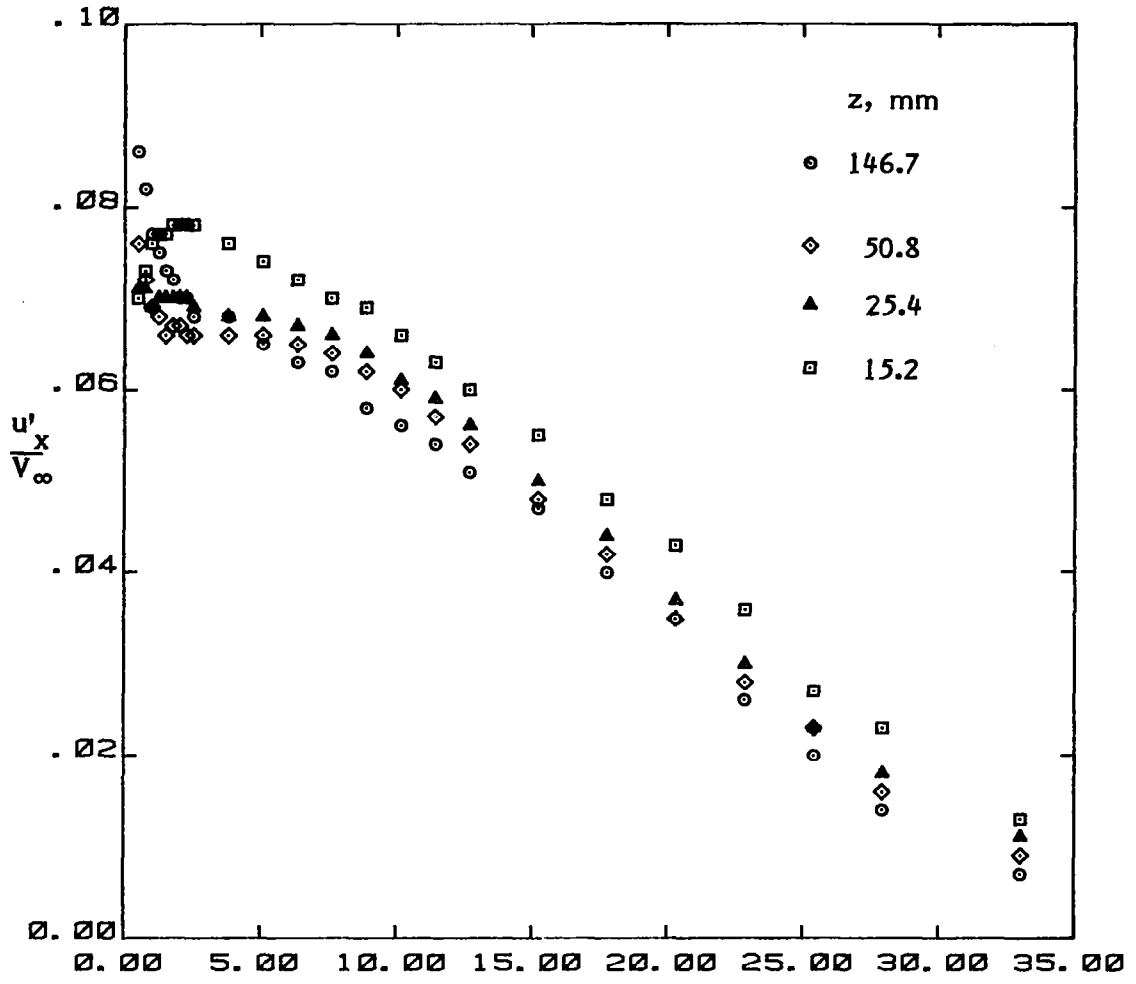

(d) Turbulent normal stress u'_x.

Figure 18. - Continued.

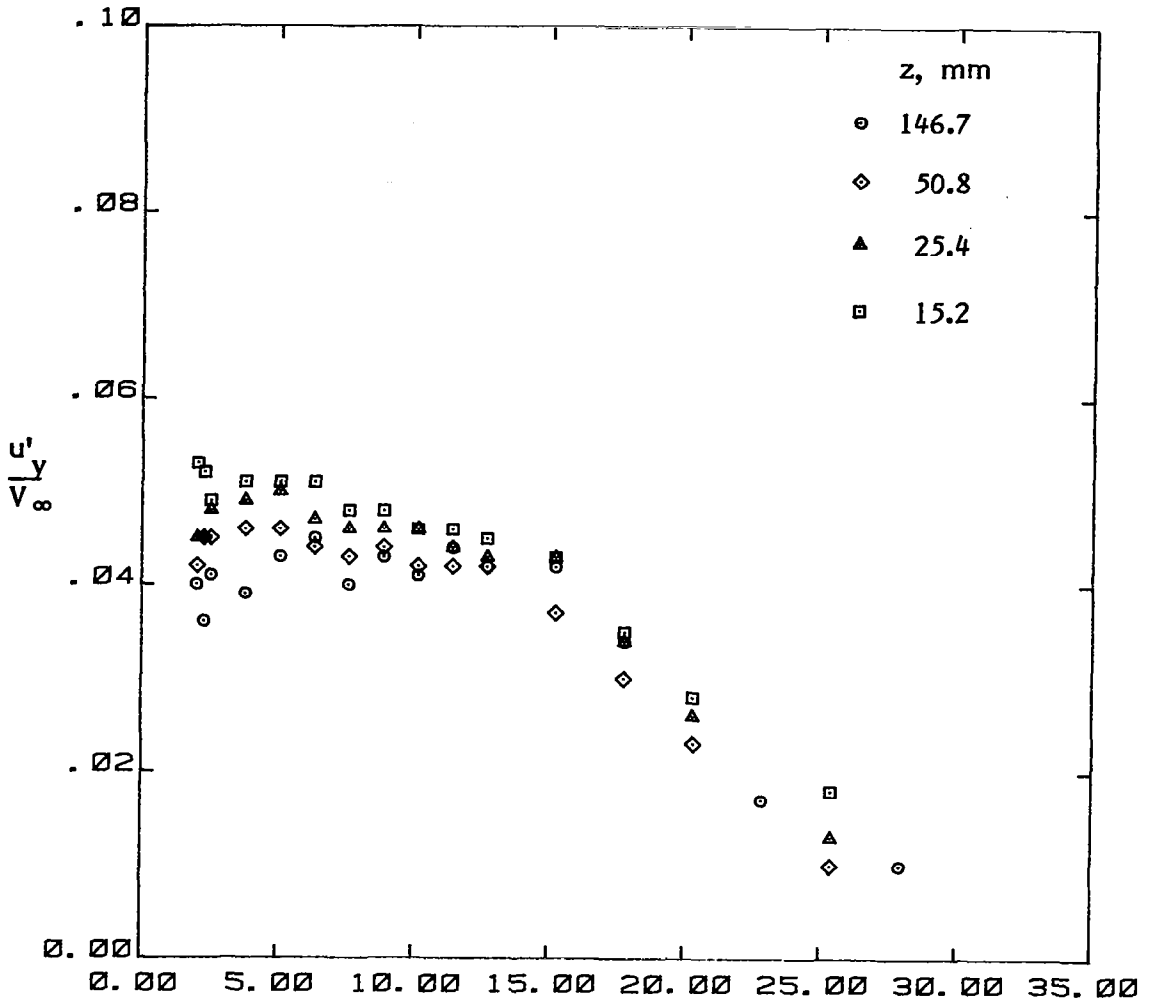

(e) Turbulent normal stress u'_y.

Figure 18. - Continued.

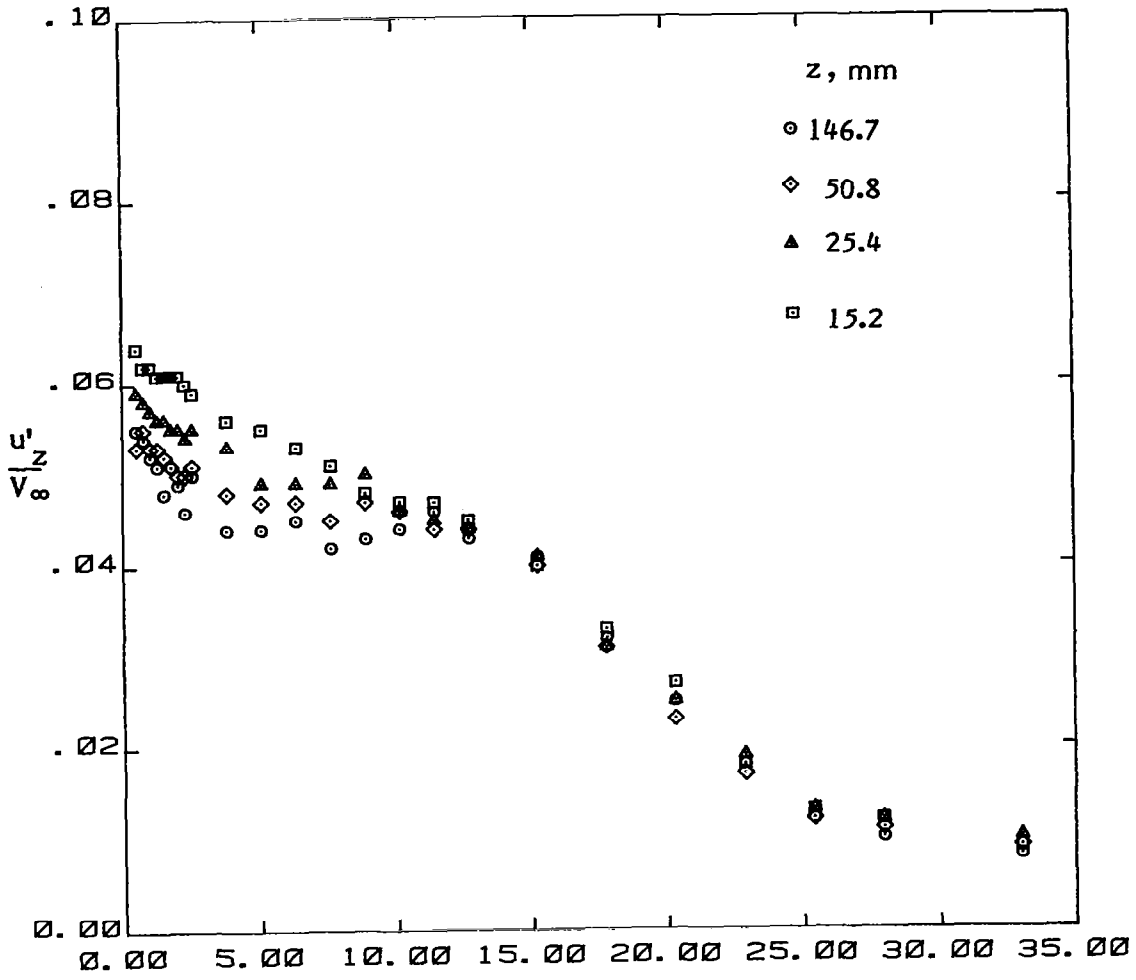

(f) Turbulent normal stress u'_z.

Figure 18. - Continued.

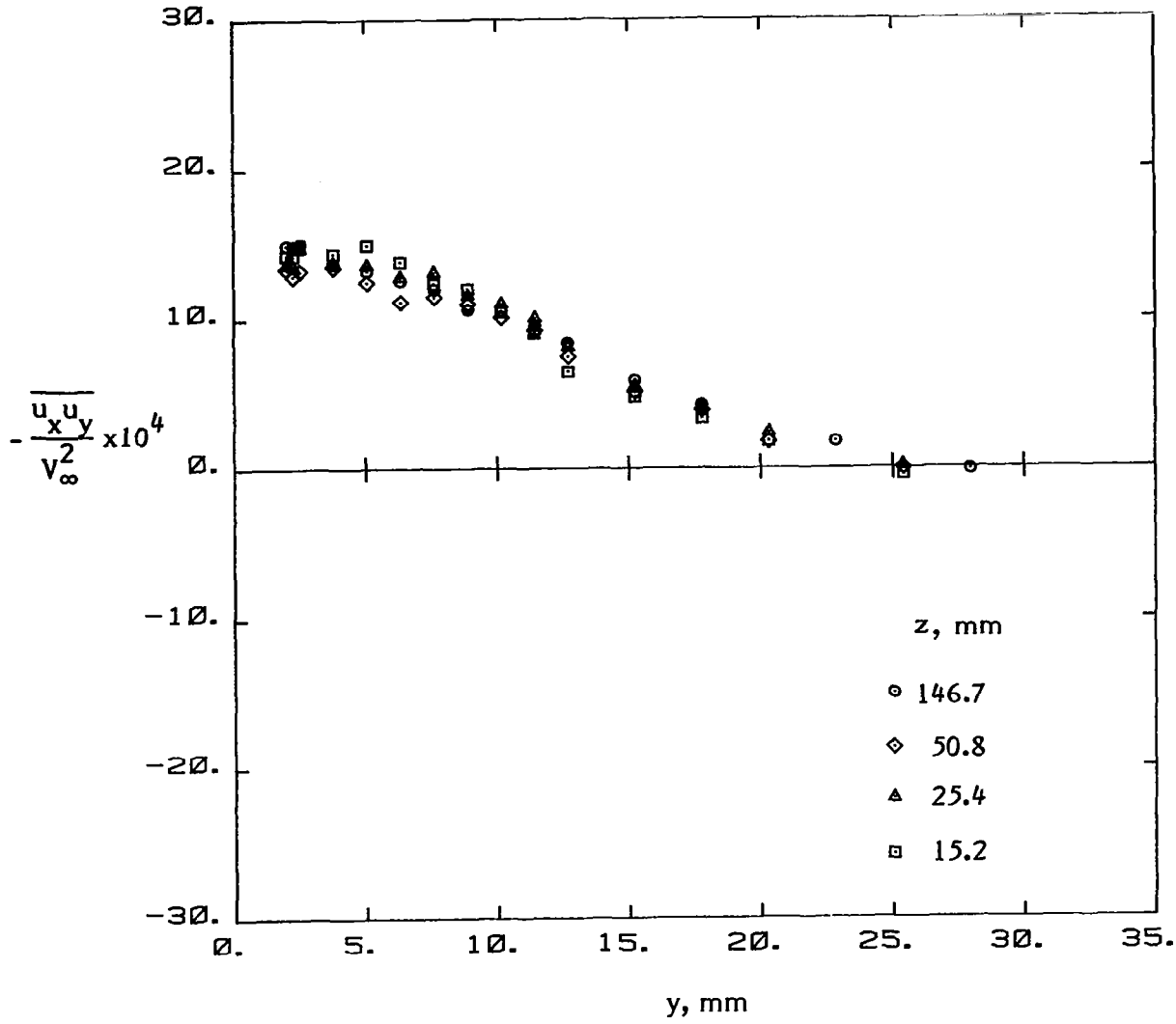

(g) Turbulent shear stress $\overline{u_x u_y}$.

Figure 18. - Continued.

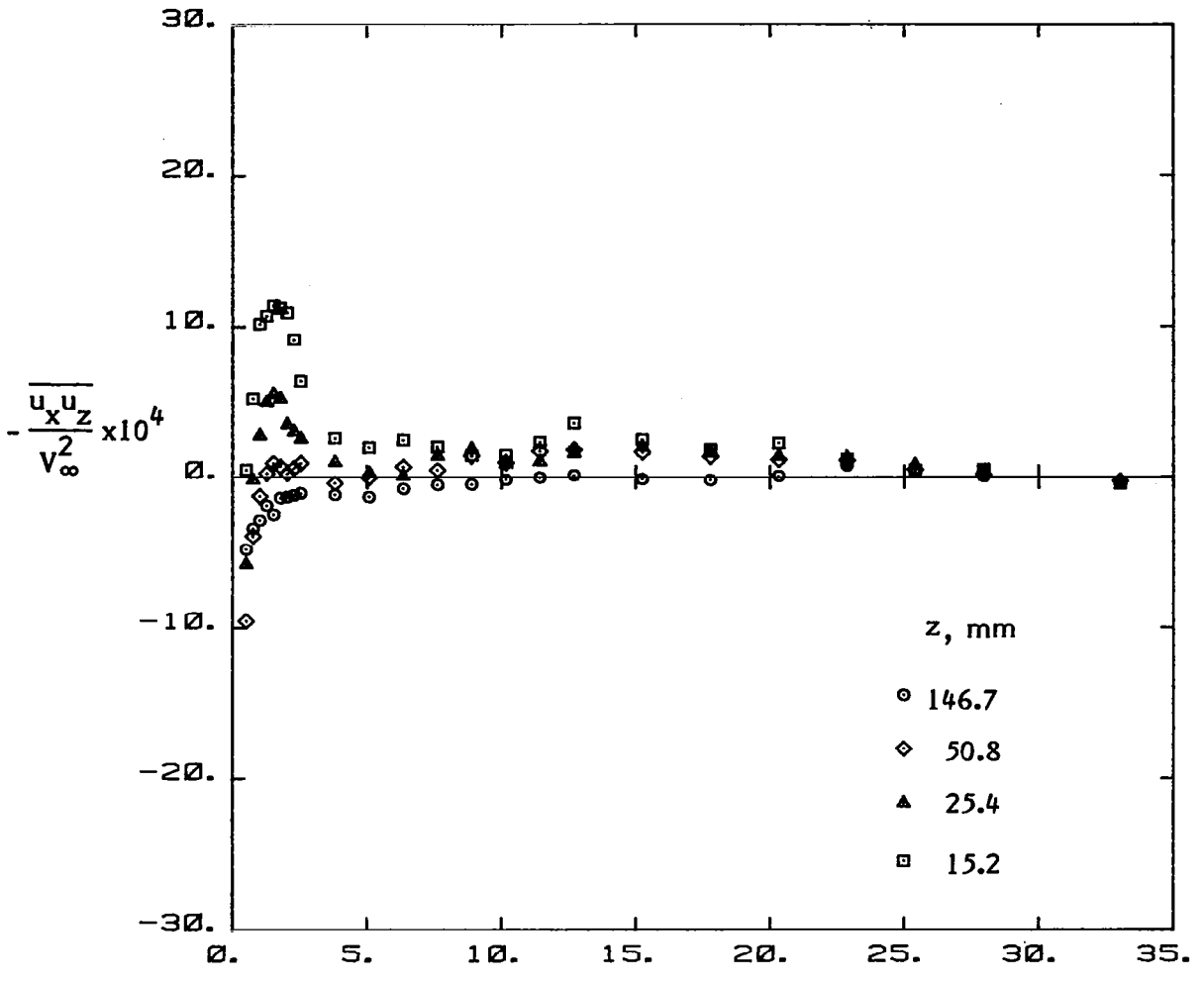

(h) Turbulent shear stress $\overline{u_x u_z}$.

Figure 18. - Continued.

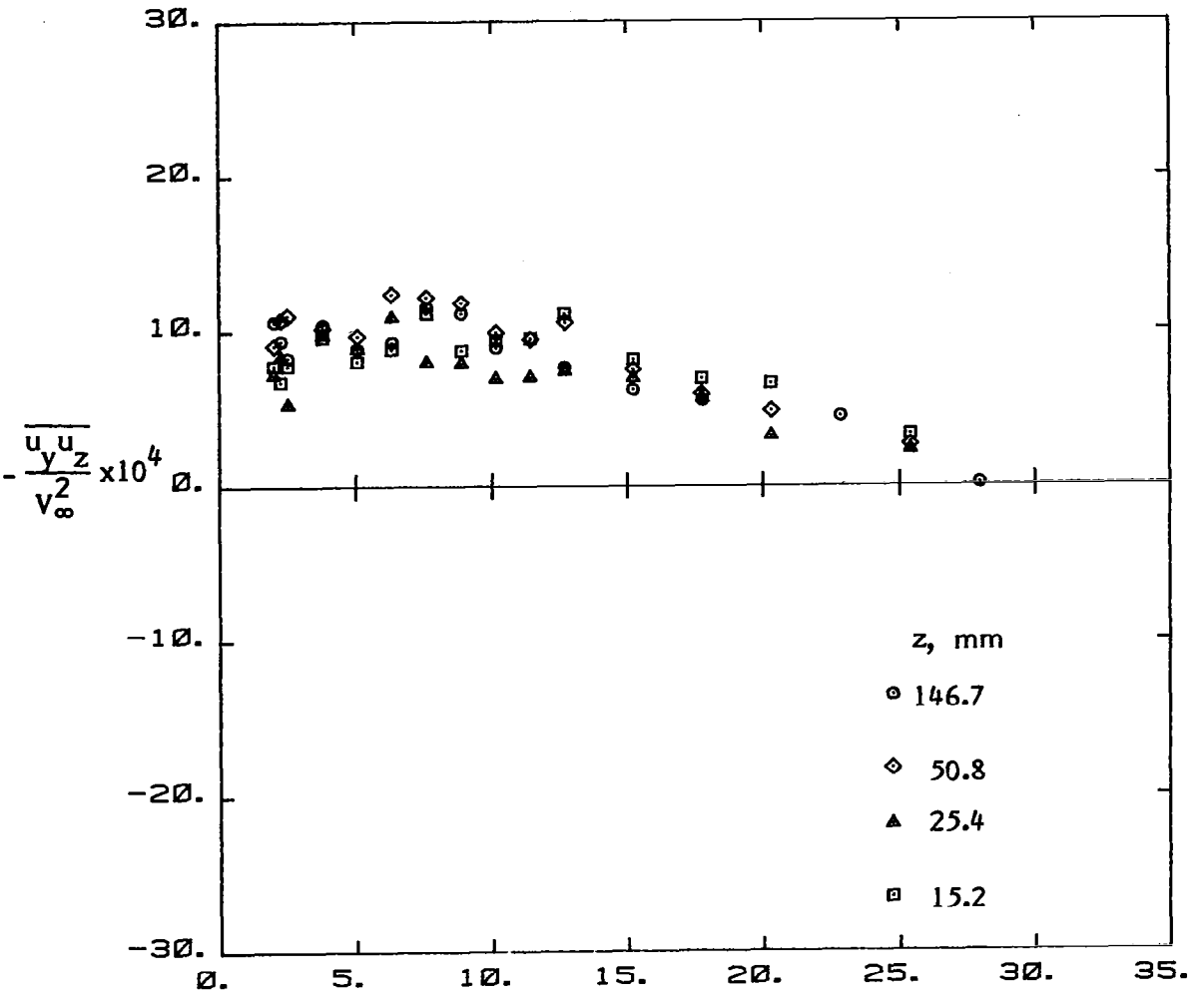

(i) Turbulent shear stress $\overline{u_y u_z}$.

Figure 18. - Concluded.

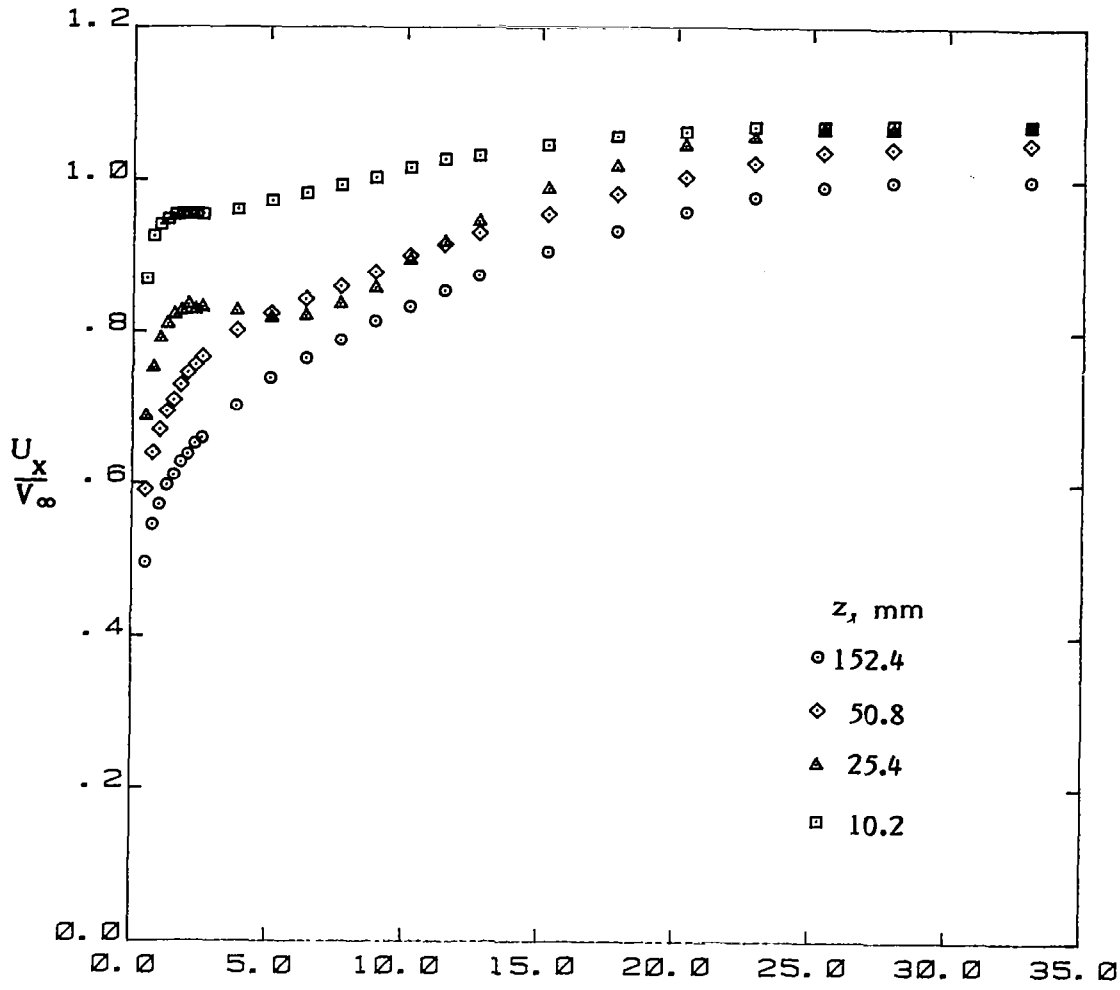

(a) Mean velocity U_x.

Figure 19. - Mean velocities and turbulence stresses in the juncture (x = 76 mm).

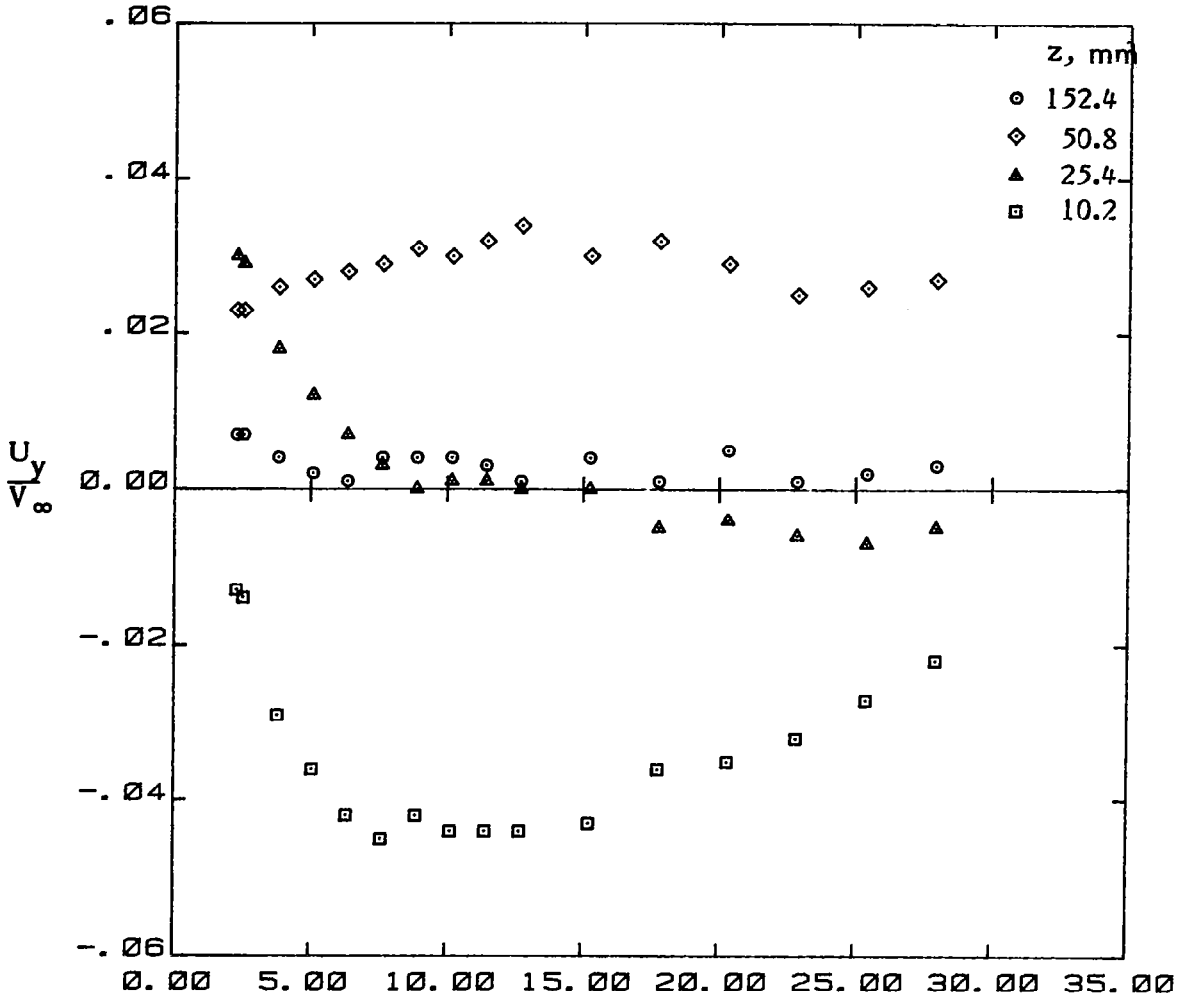

(b) Mean velocity U_y.

Figure 19. - Continued.

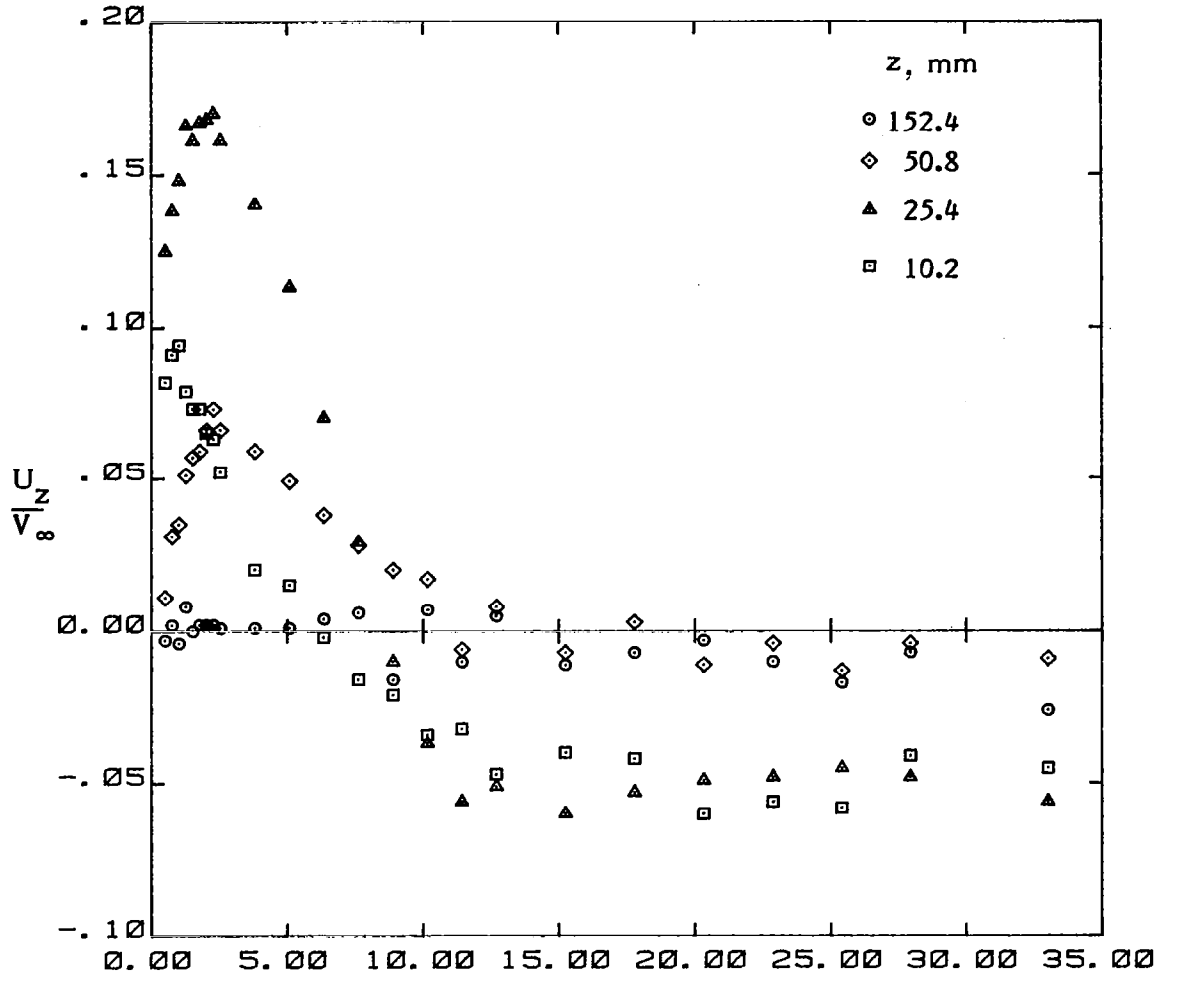

(c) Mean velocity U_z.

Figure 19. - Continued.

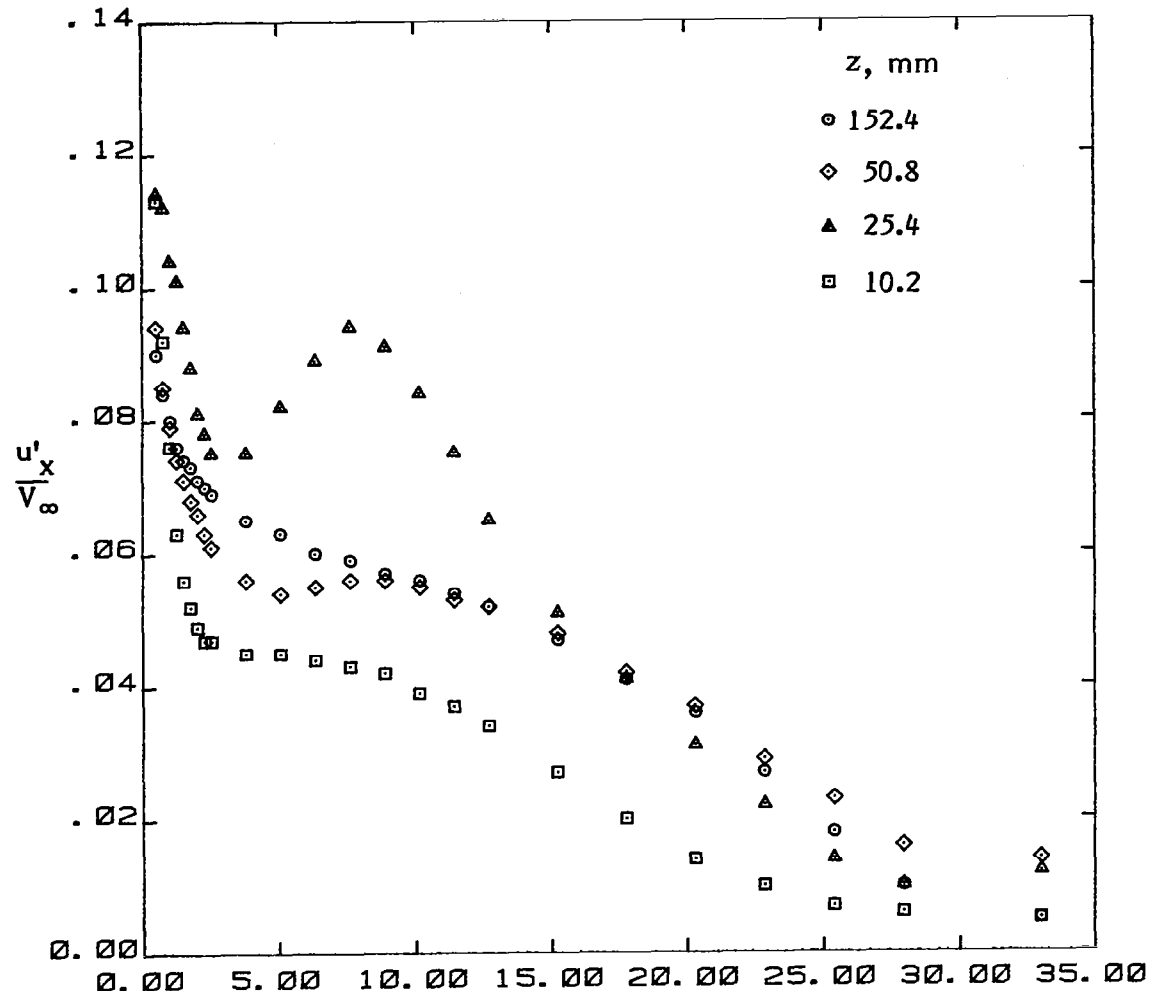

(d) Turbulent normal stress u'_x.

Figure 19. - Continued.

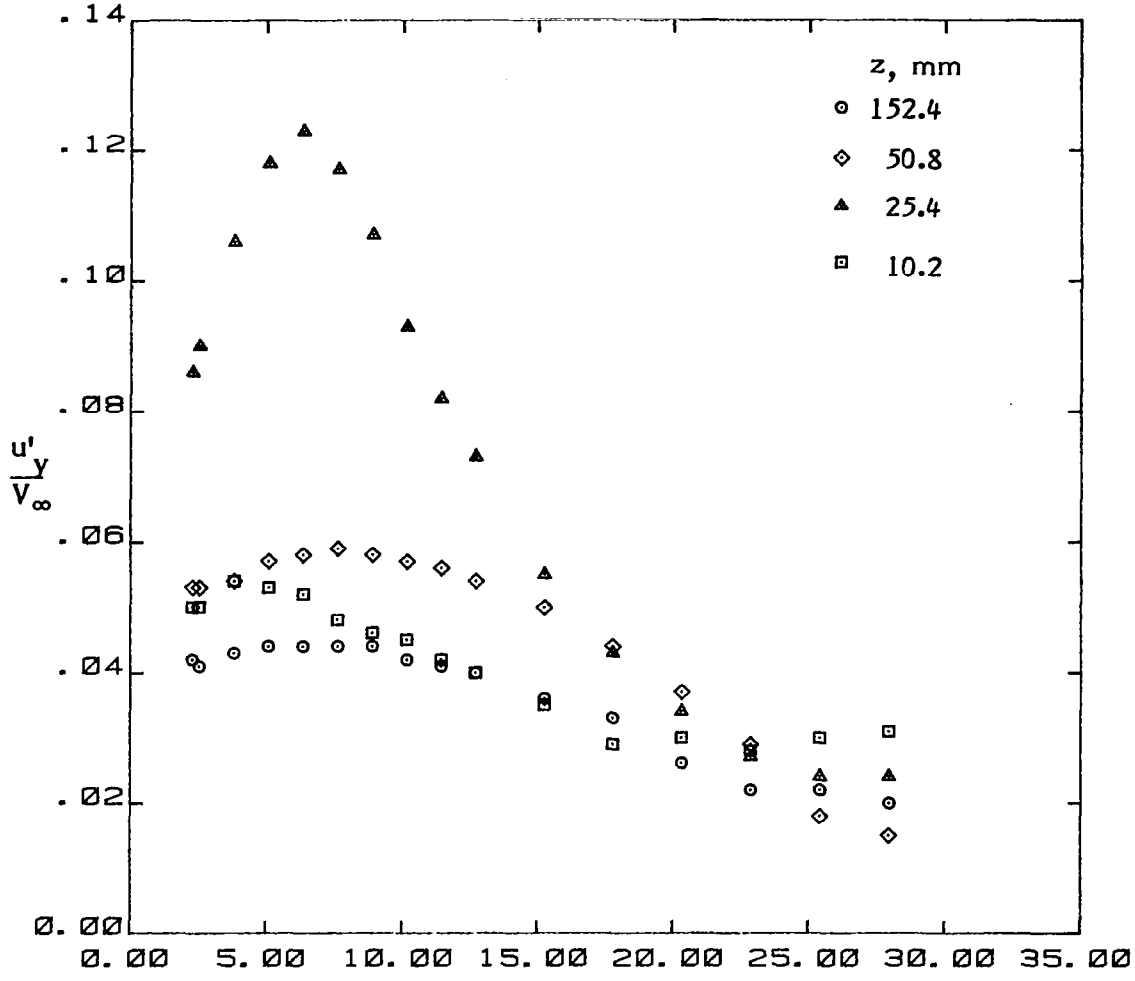

(e) Turbulent normal stress u'_y.

Figure 19. - Continued.

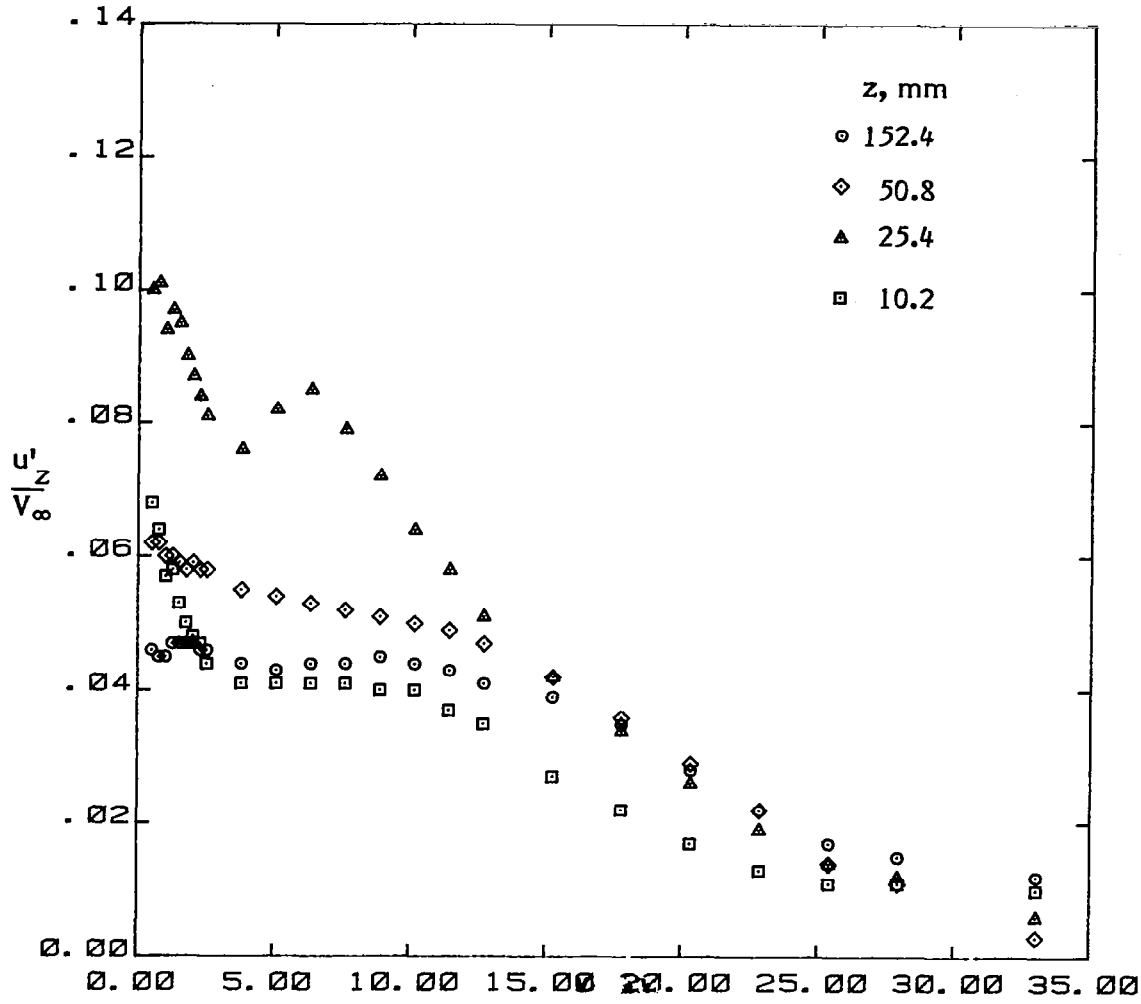

(f) Turbulent normal stress u'_z.

Figure 19. - Continued.

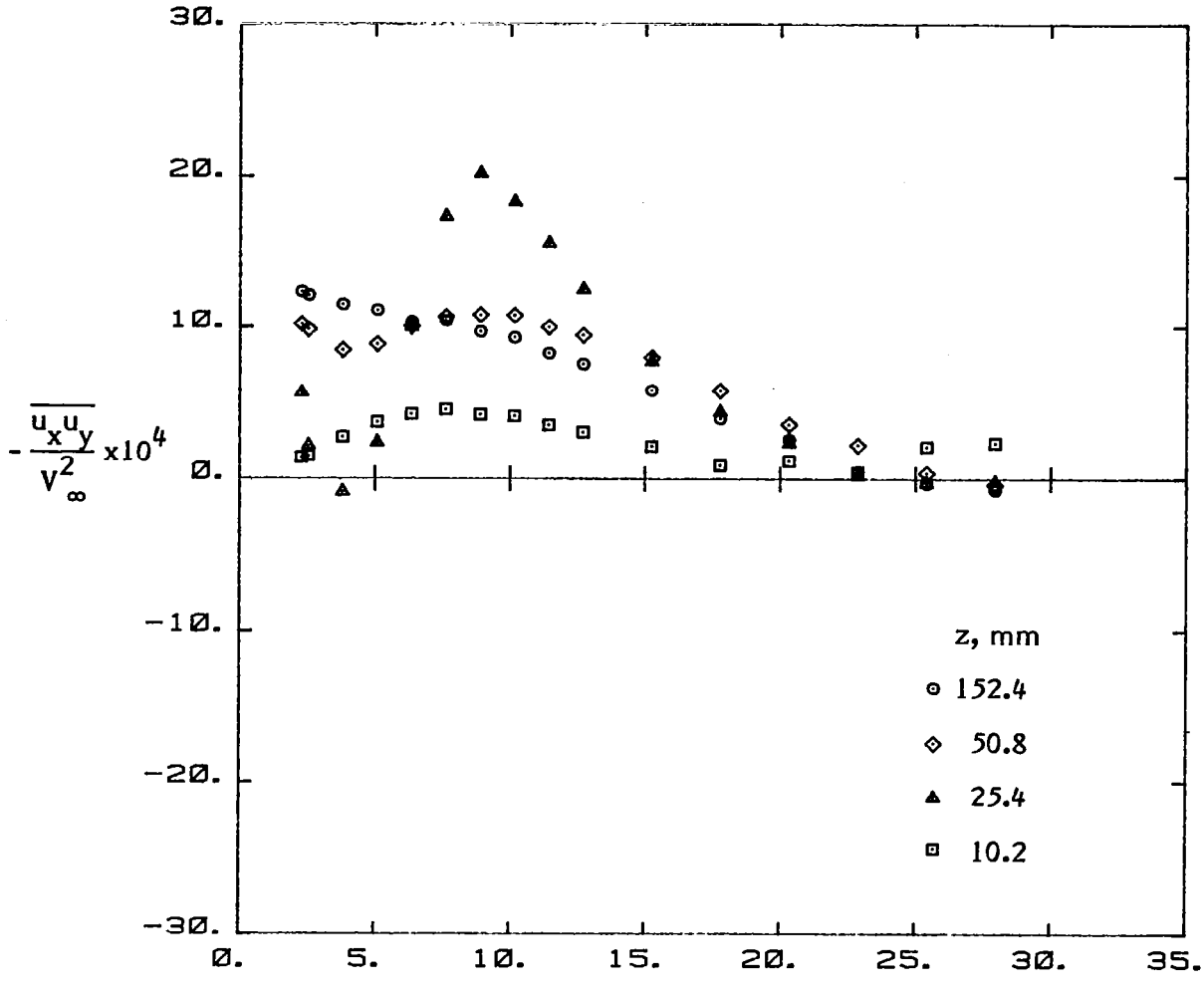

(g) Turbulent shear stress $\overline{u_x u_y}$.

Figure 19. - Continued.

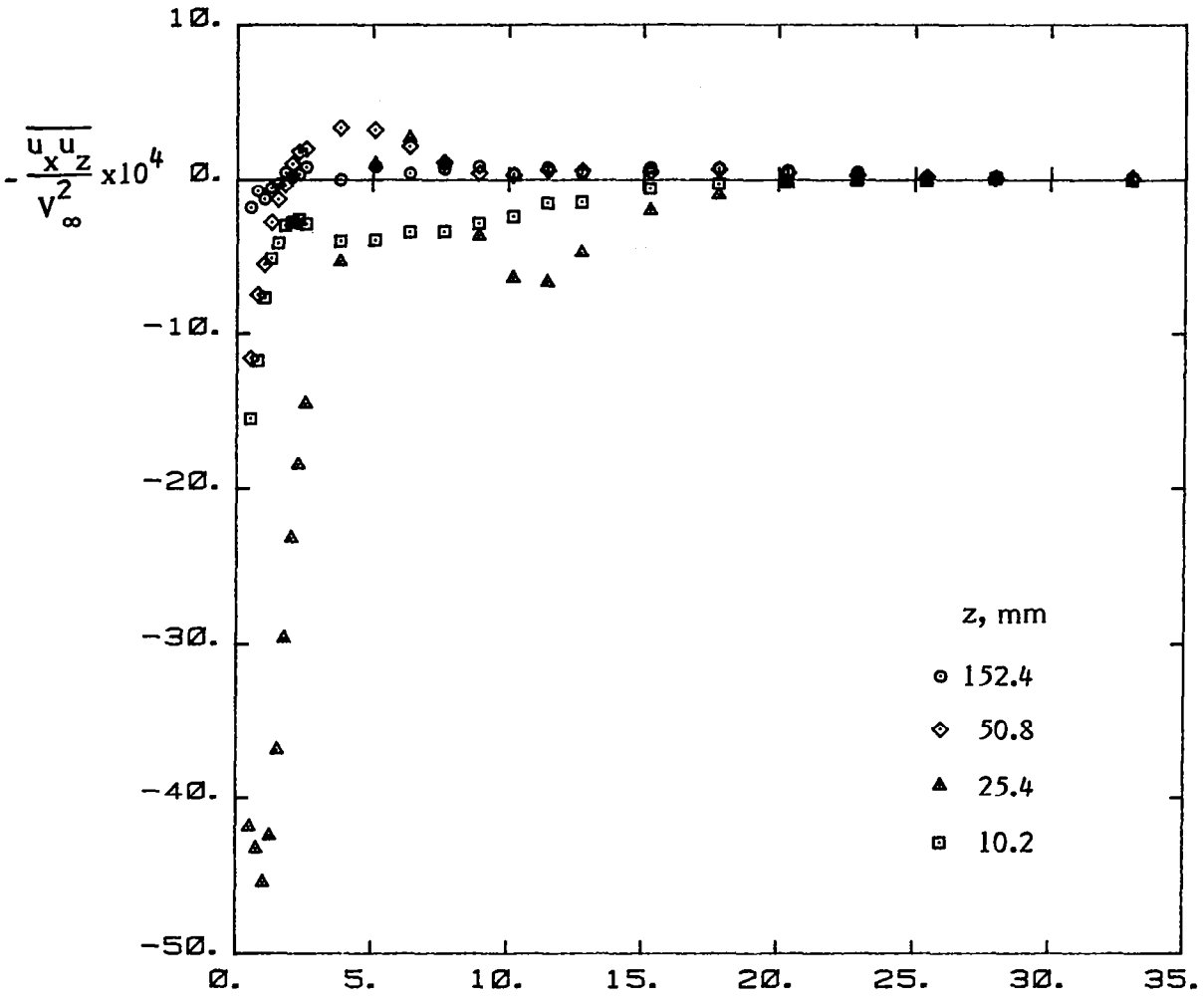

(h) Turbulent shear stress $\overline{u_x u_z}$.

Figure 19. - Continued.

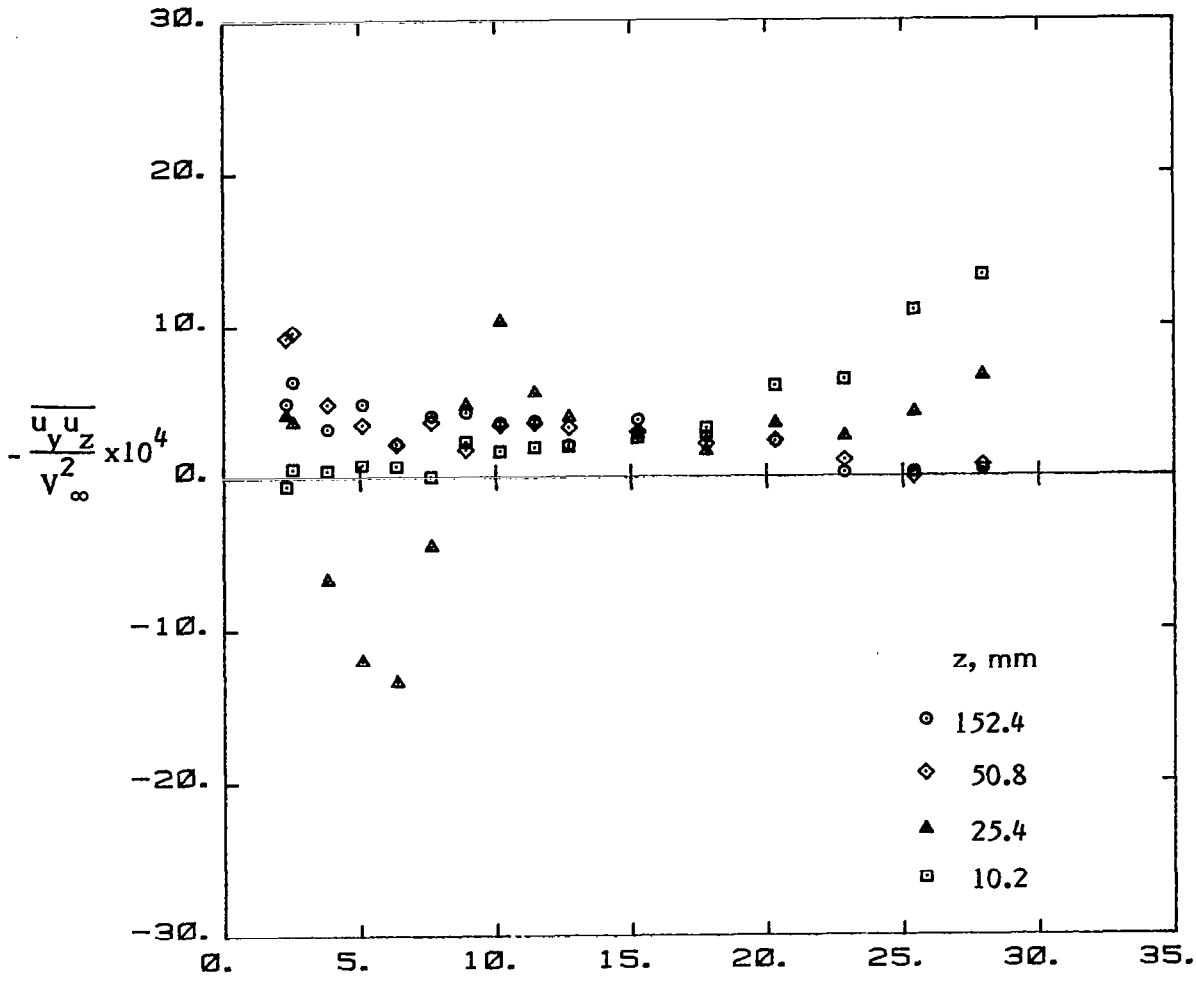

(i) Turbulent shear stress $\overline{u_y u_z}$.

Figure 19. - Concluded.

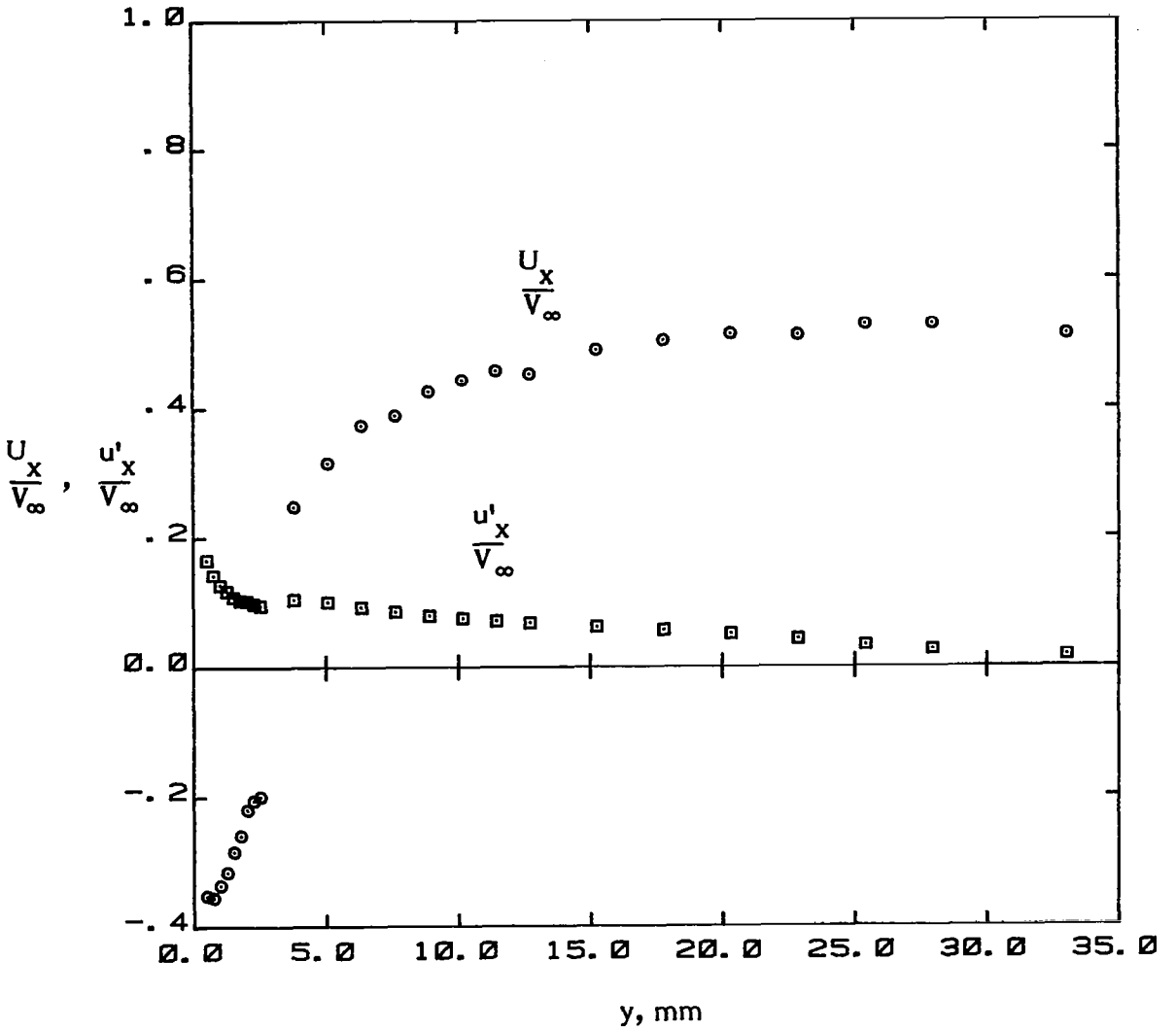

Figure 20. - Mean velocity U_x and turbulent normal stress u'_x in the plane of symmetry near the body leading edge (x = - 11 mm, z = - 29.0 mm).

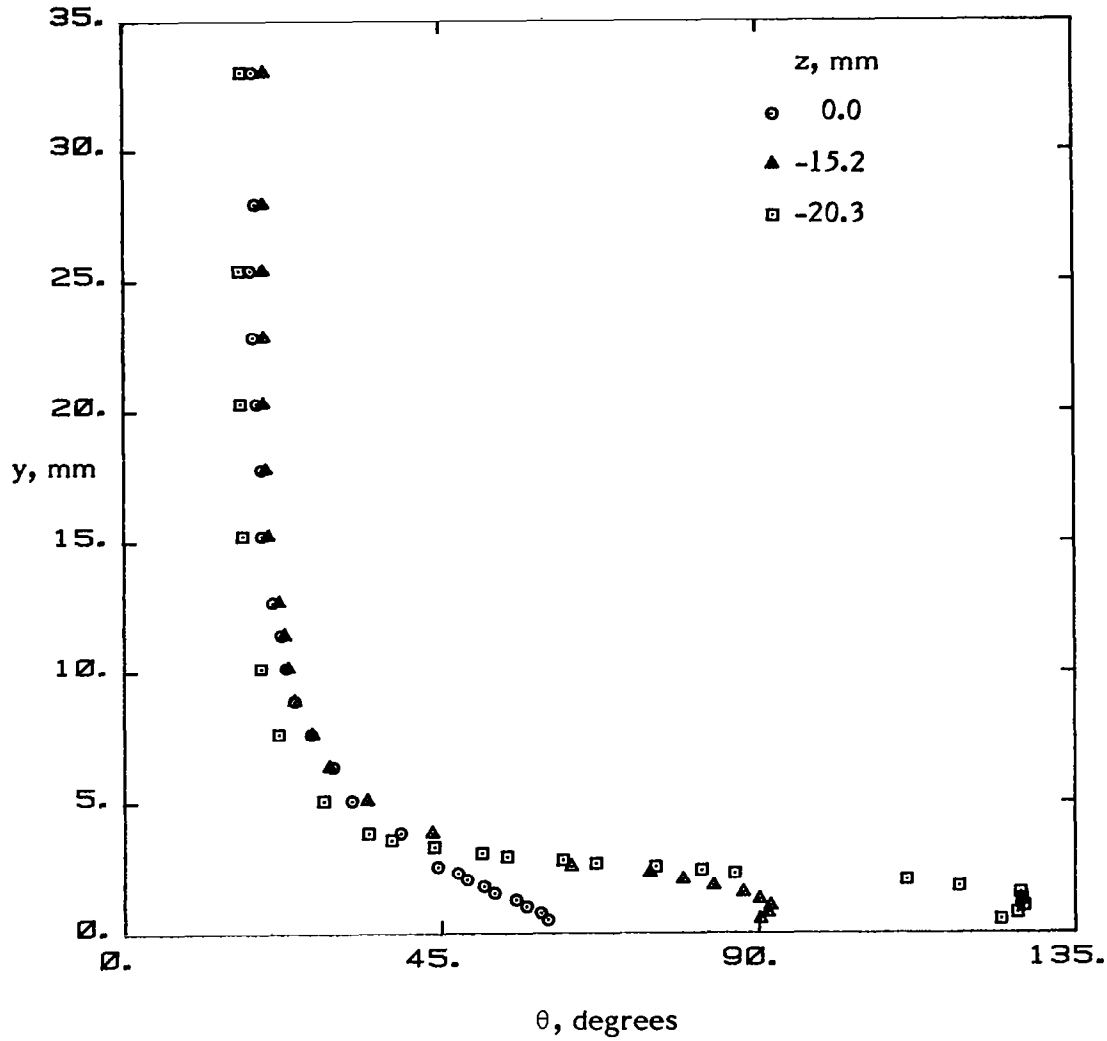

Figure 21. - Variation of local mean flow direction in the vicinity of the body leading edge (x = - 11 mm).

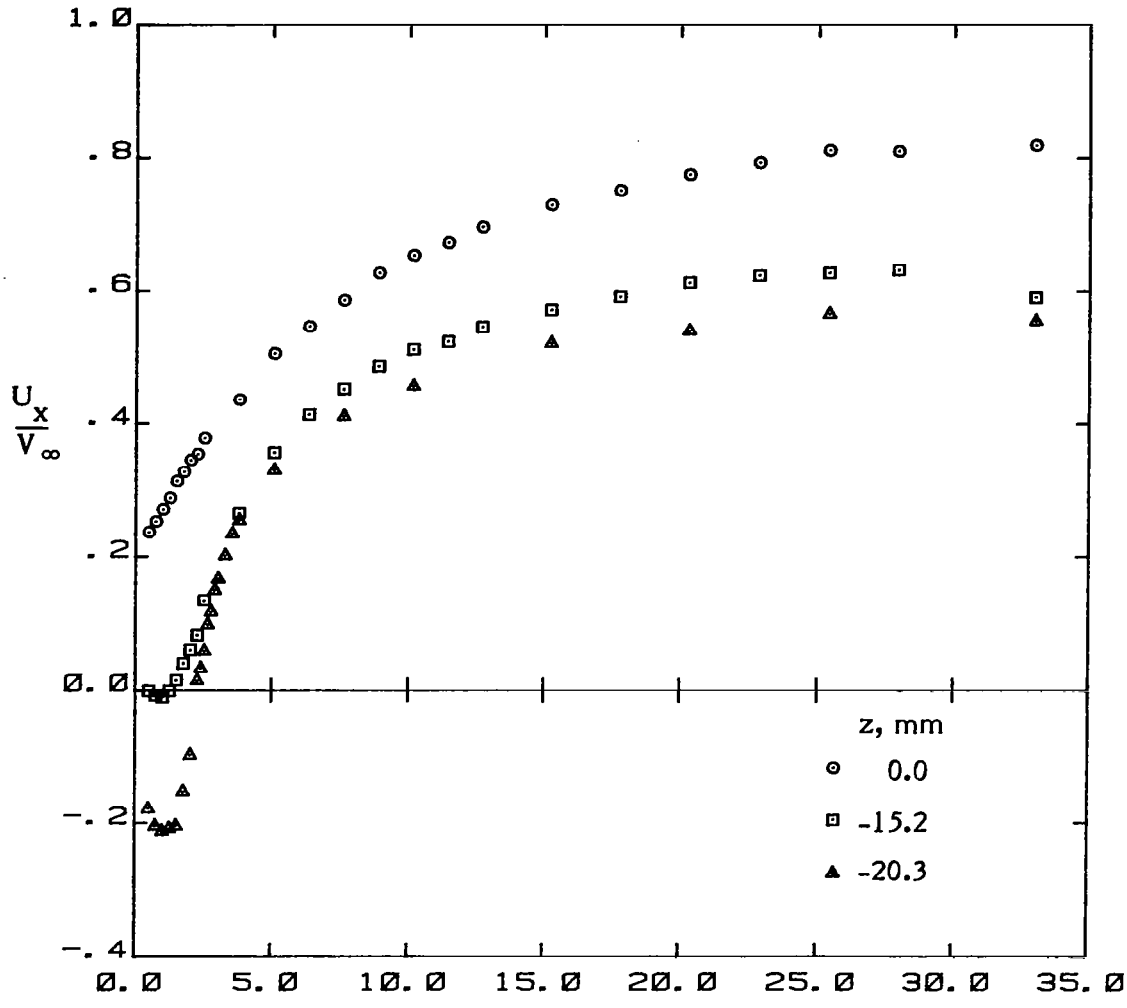

(a) Mean velocity U_x.

Figure 22. - Mean velocities and turbulence stresses in the vicinity of the body leading edge (x = - 11 mm).

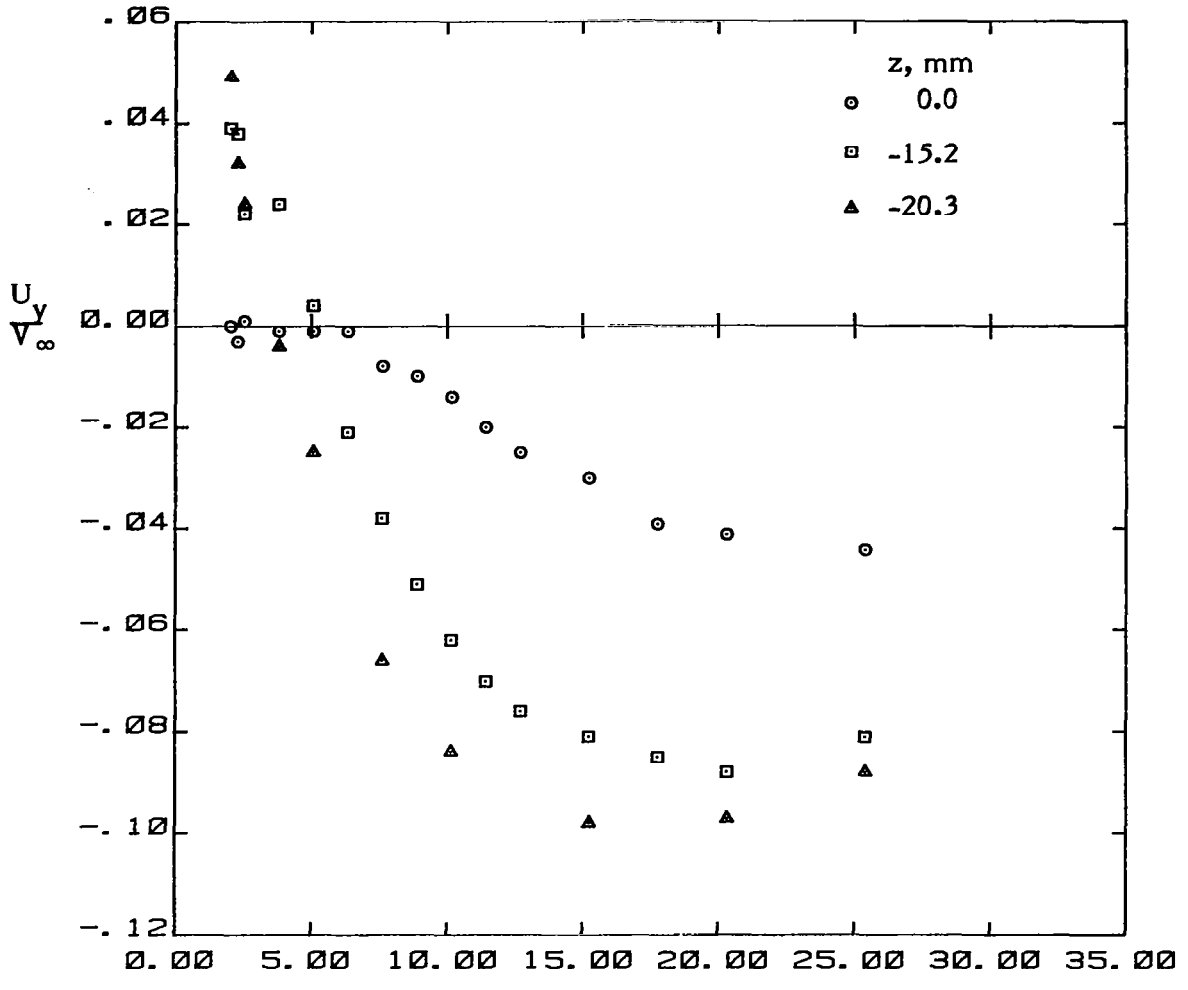

(b) Mean velocity U_y.

Figure 22. - Continued.

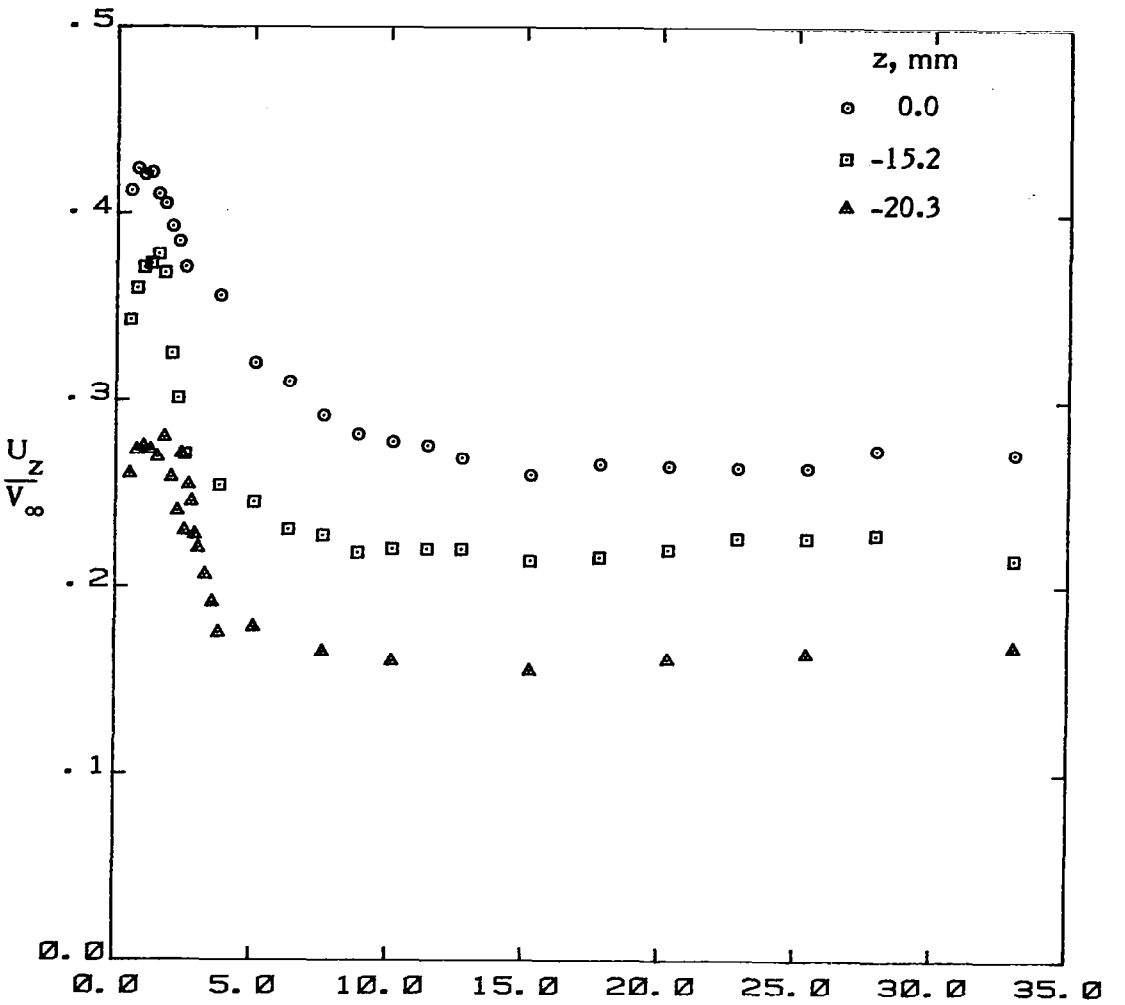

(c) Mean velocity U_z.

Figure 22. - Continued.

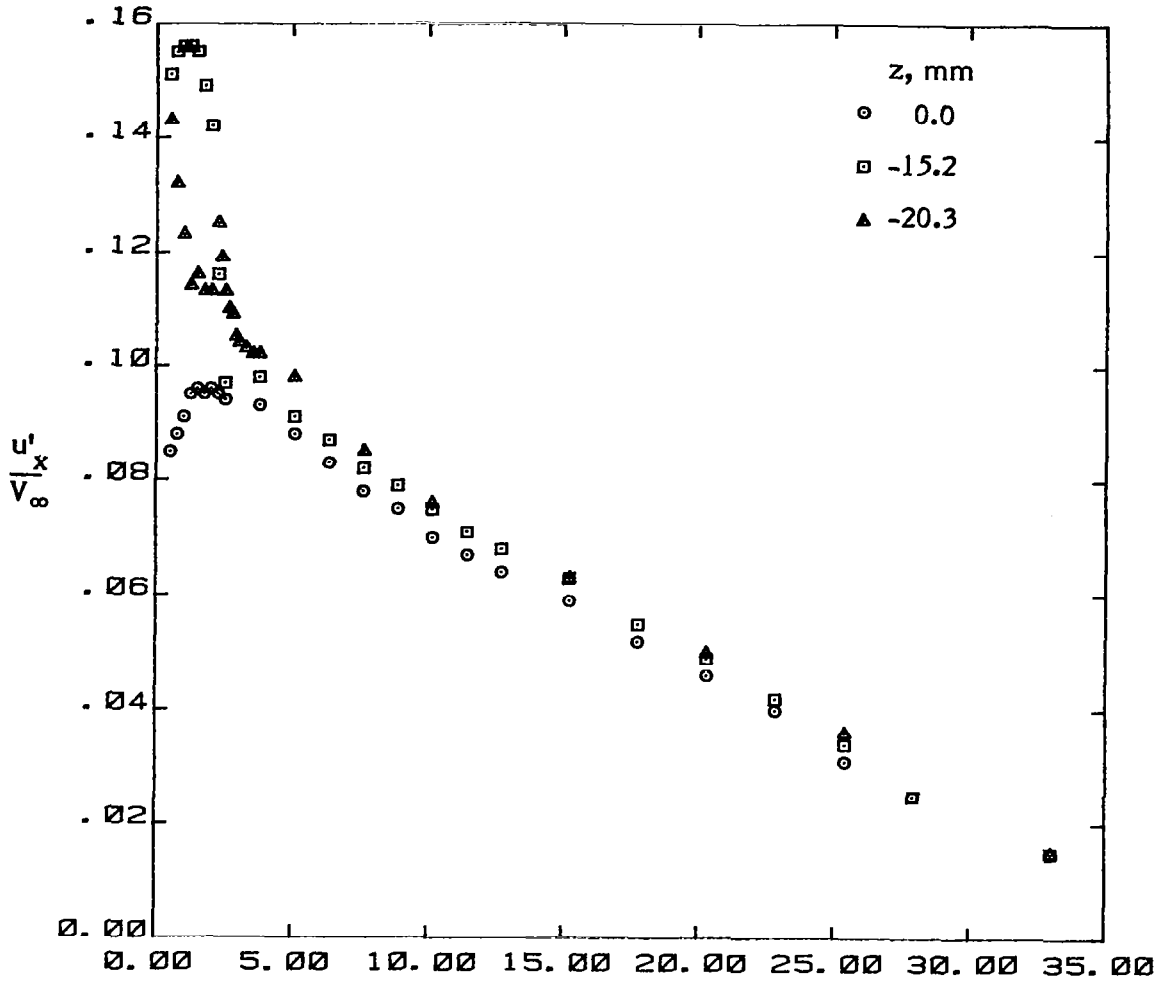

(d) Turbulent normal stress u'_x.

Figure 22. - Continued.

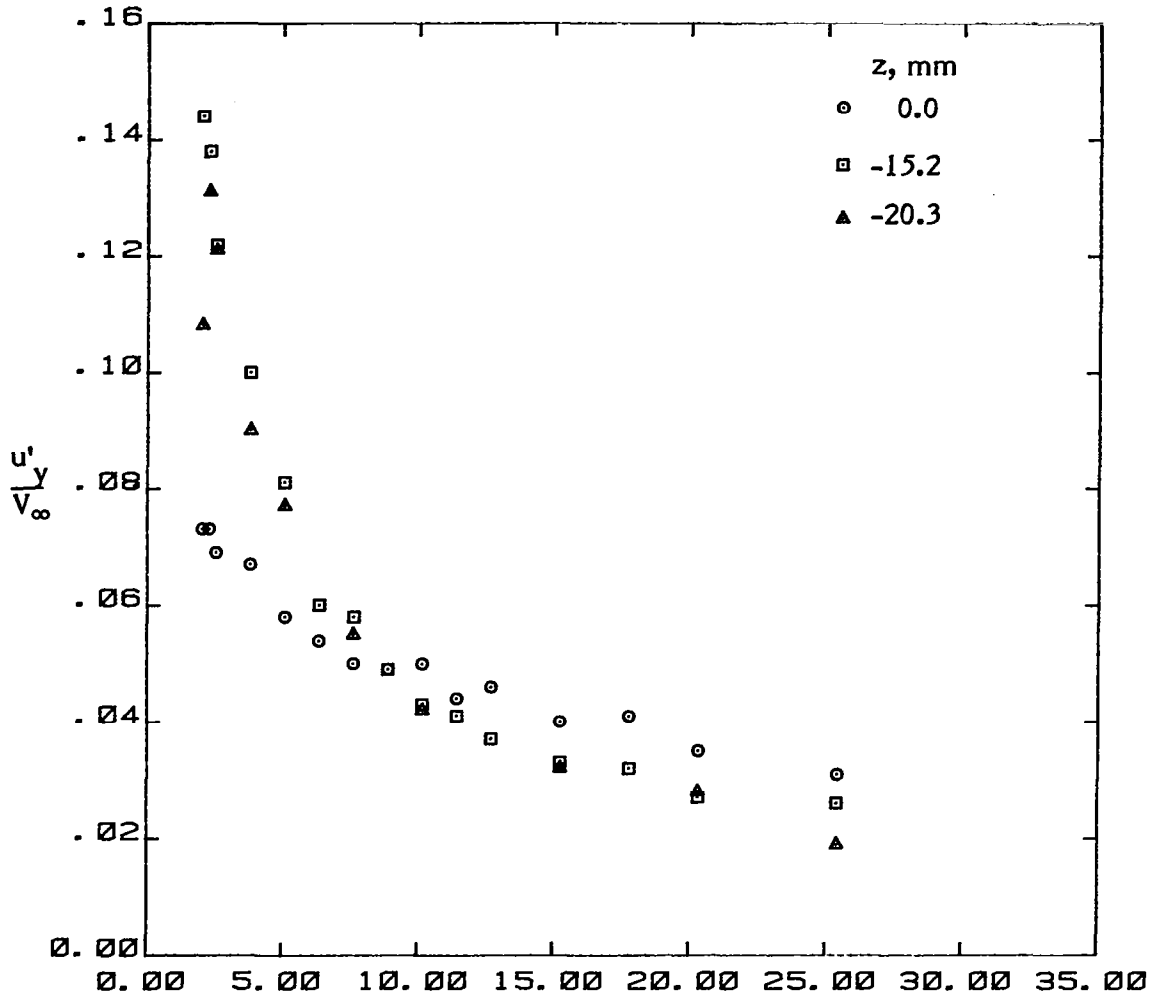

(e) Turbulent normal stress u'_y.

Figure 22. - Continued.

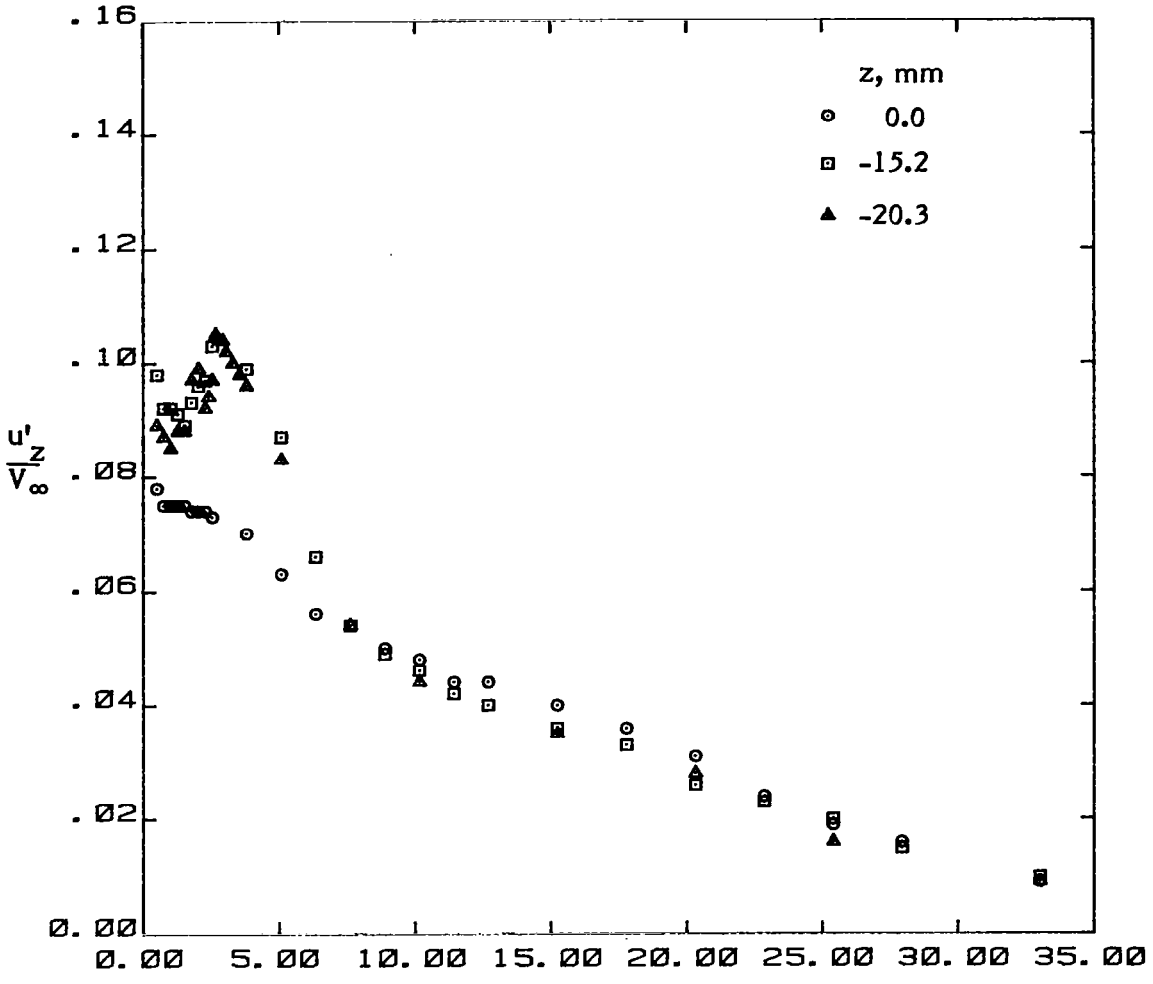

(f) Turbulent normal stress u'_z.

Figure 22. - Continued.

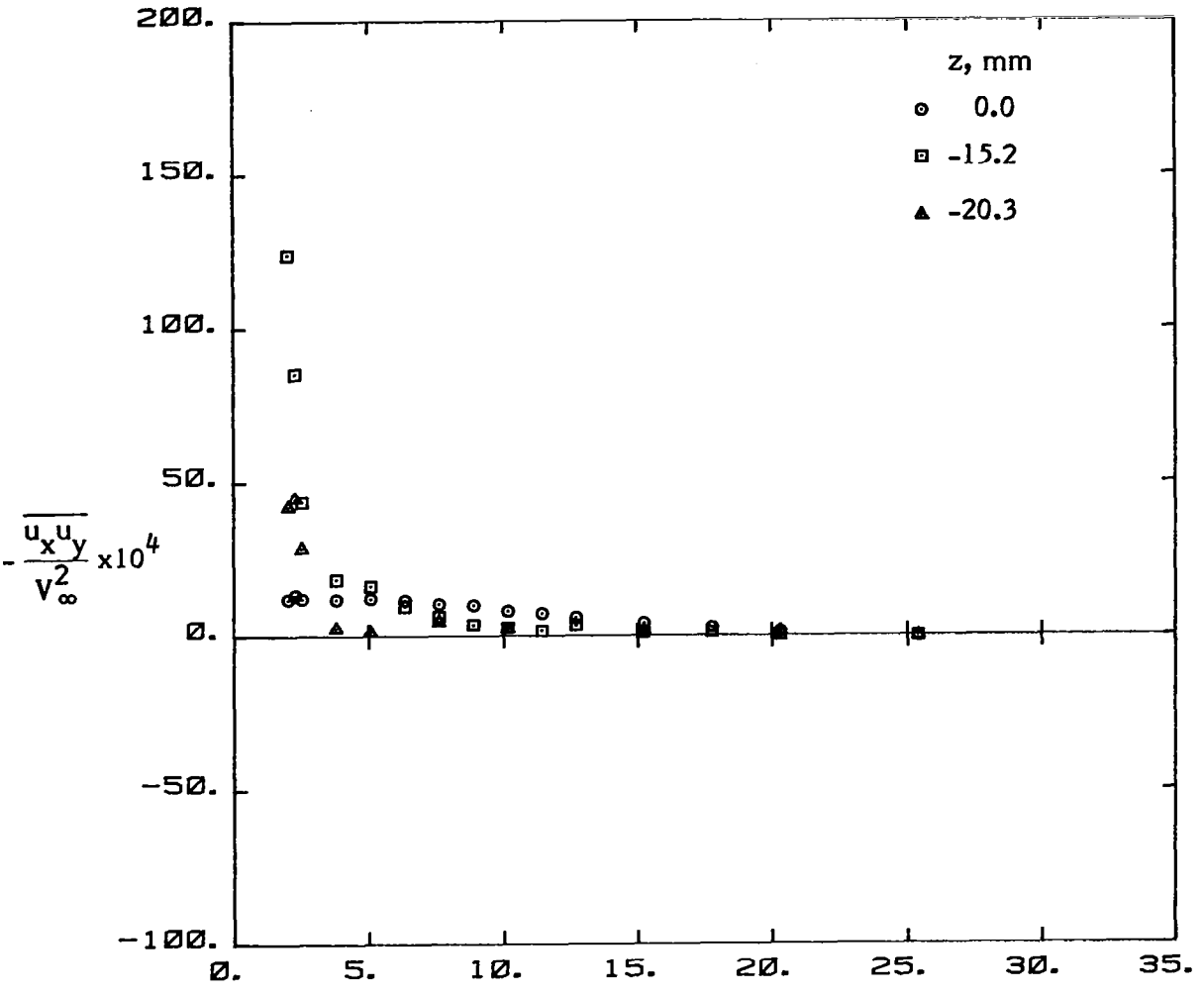

(g) Turbulent shear stress $\overline{u_x u_y}$.

Figure 22. - Continued.

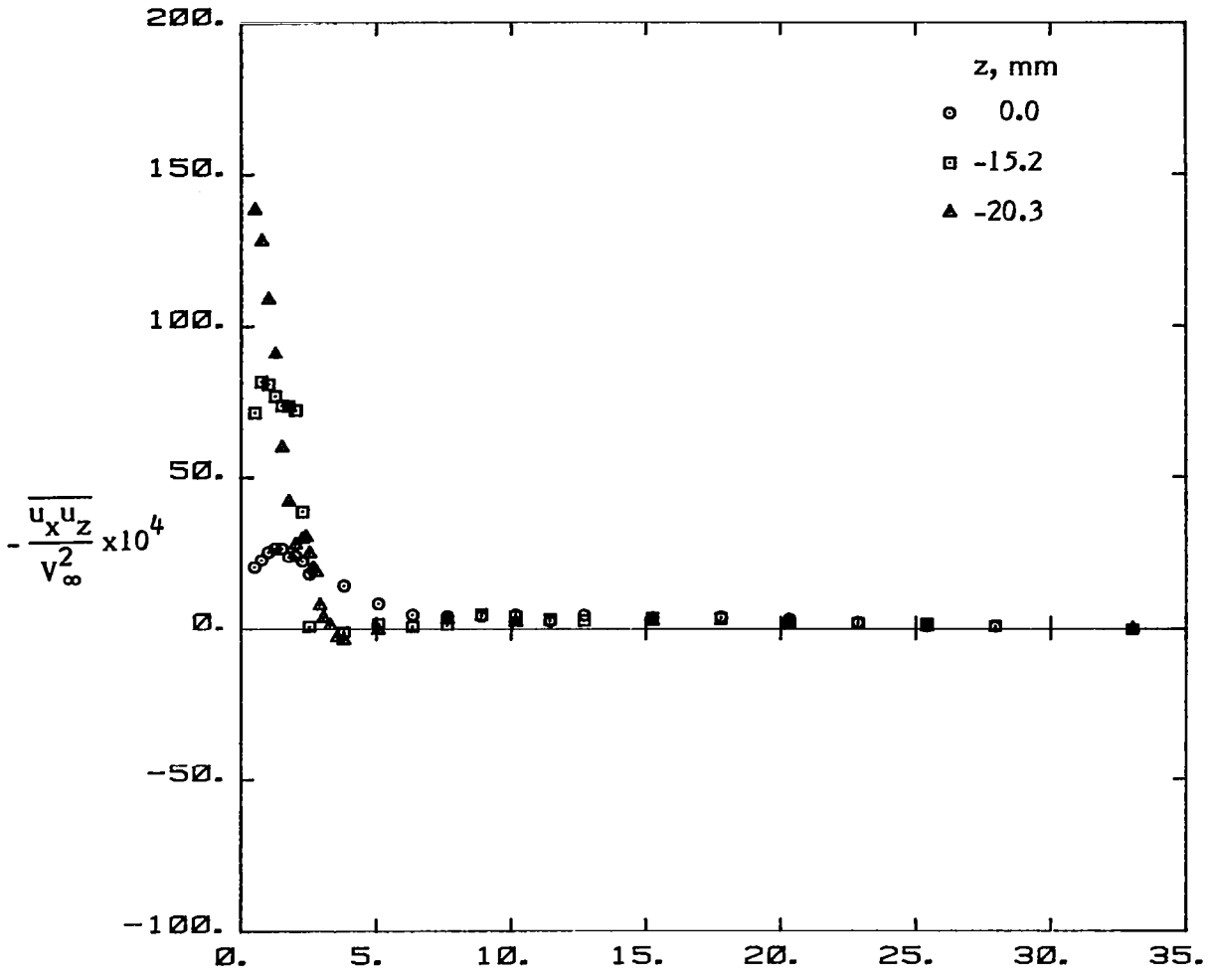

(h) Turbulent shear stress $\overline{u_x u_z}$.

Figure 22. - Continued.

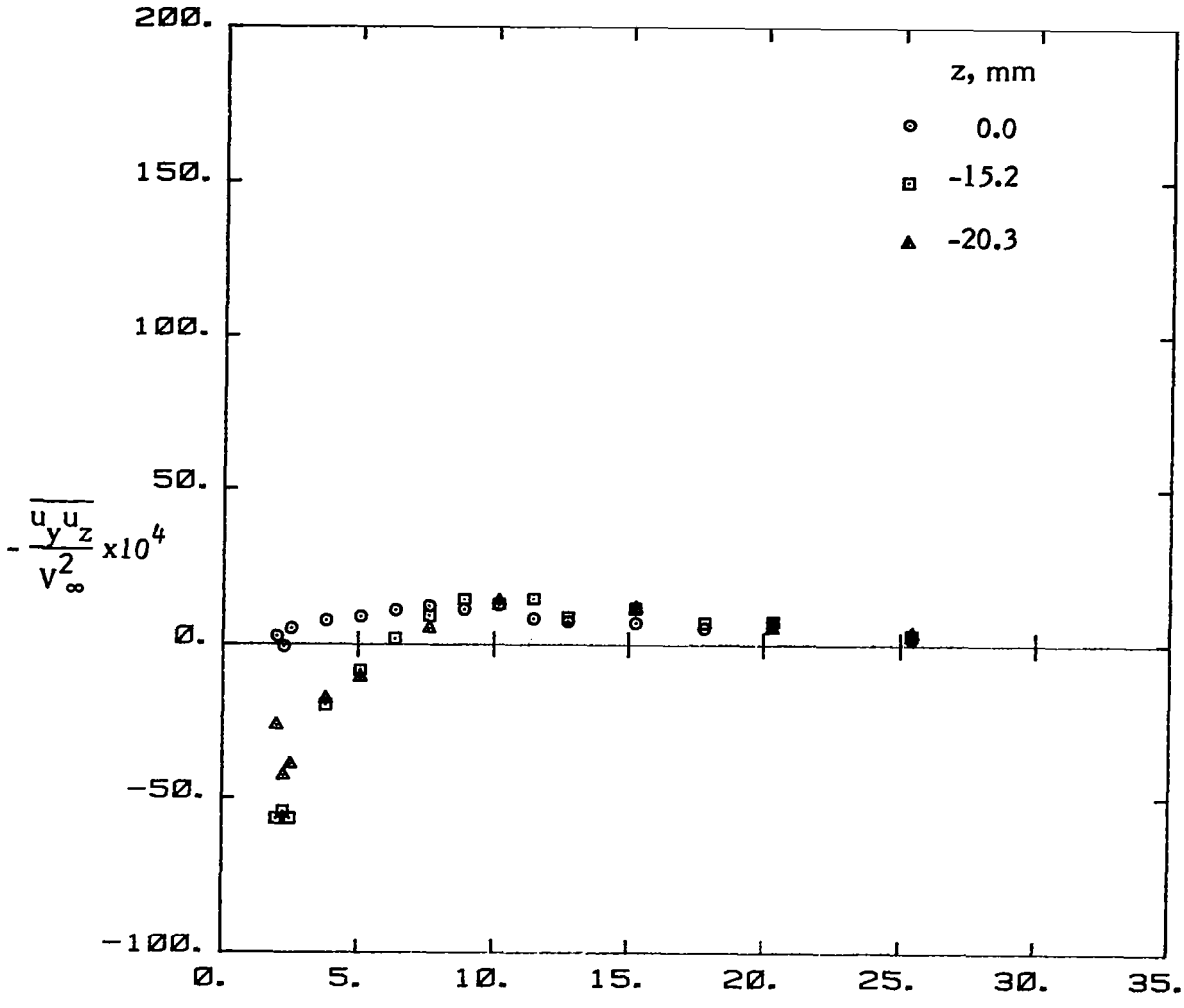

(i) Turbulent shear stress $\overline{u_y u_z}$.

Figure 22. - Concluded.

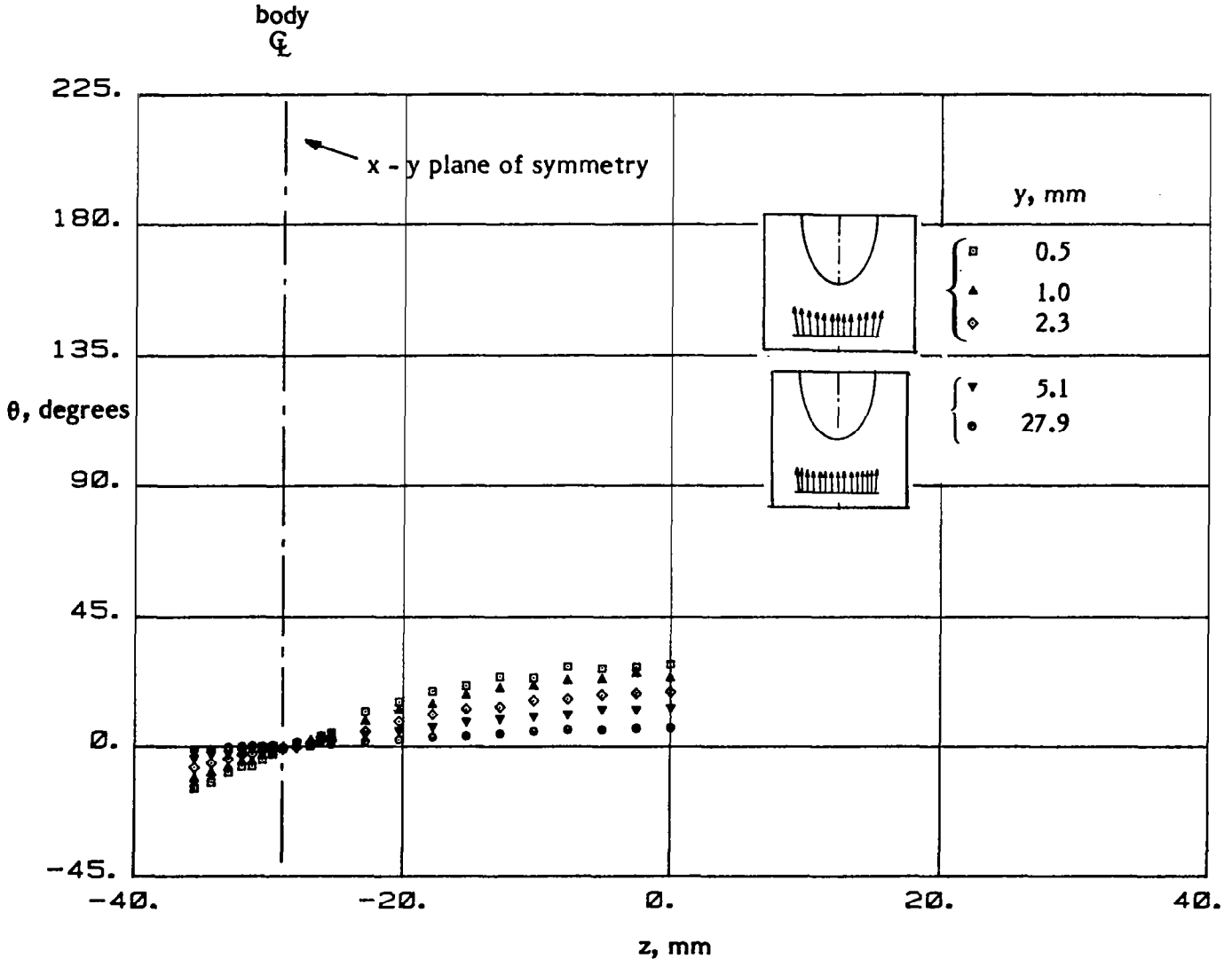

(a) x = - 38 mm.

Figure 23. - Variation of local mean flow direction upstream of the body leading edge.

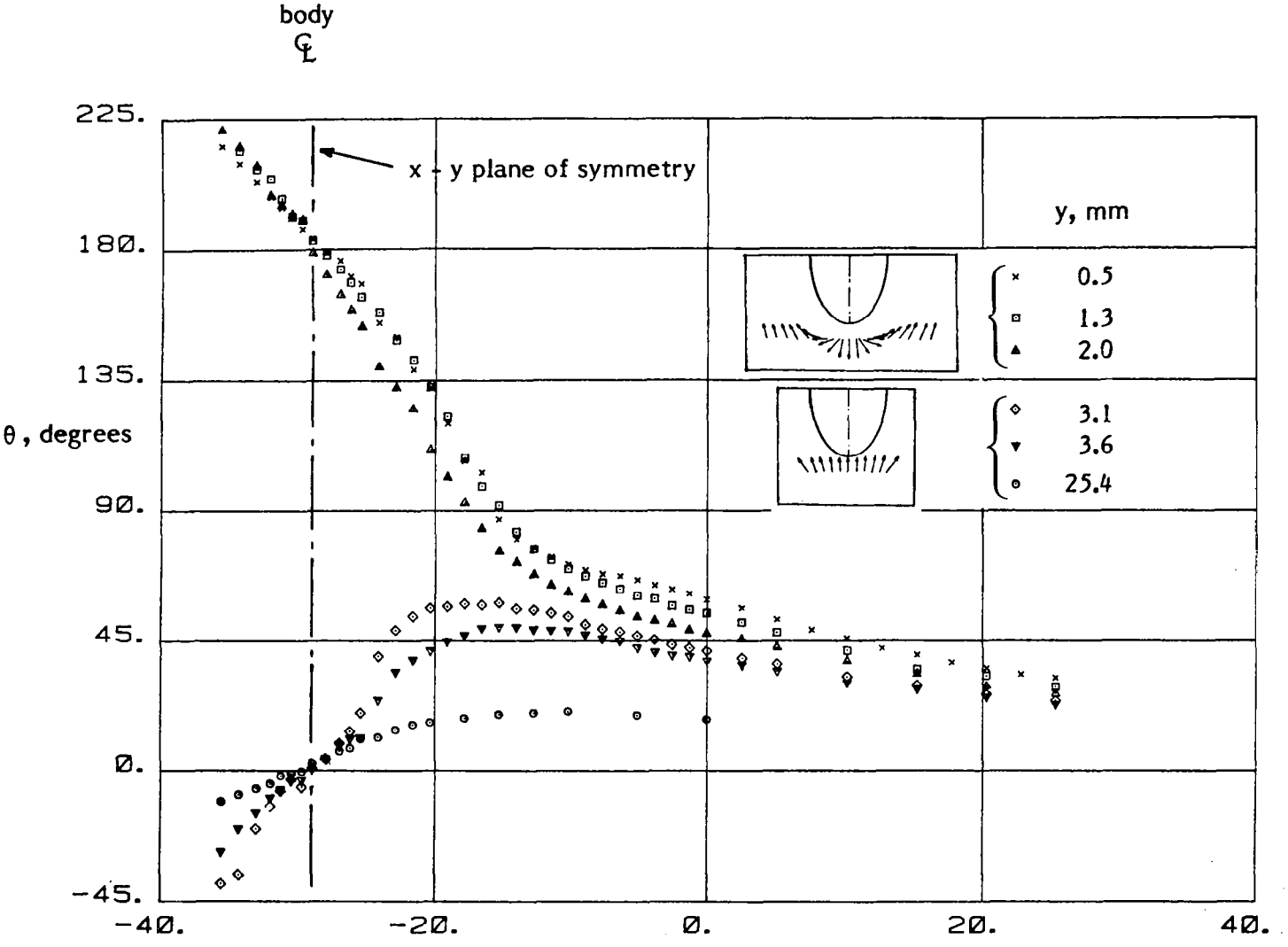

(b) x = - 11 mm.

Figure 23. - Concluded.

This page is intentially left blank.

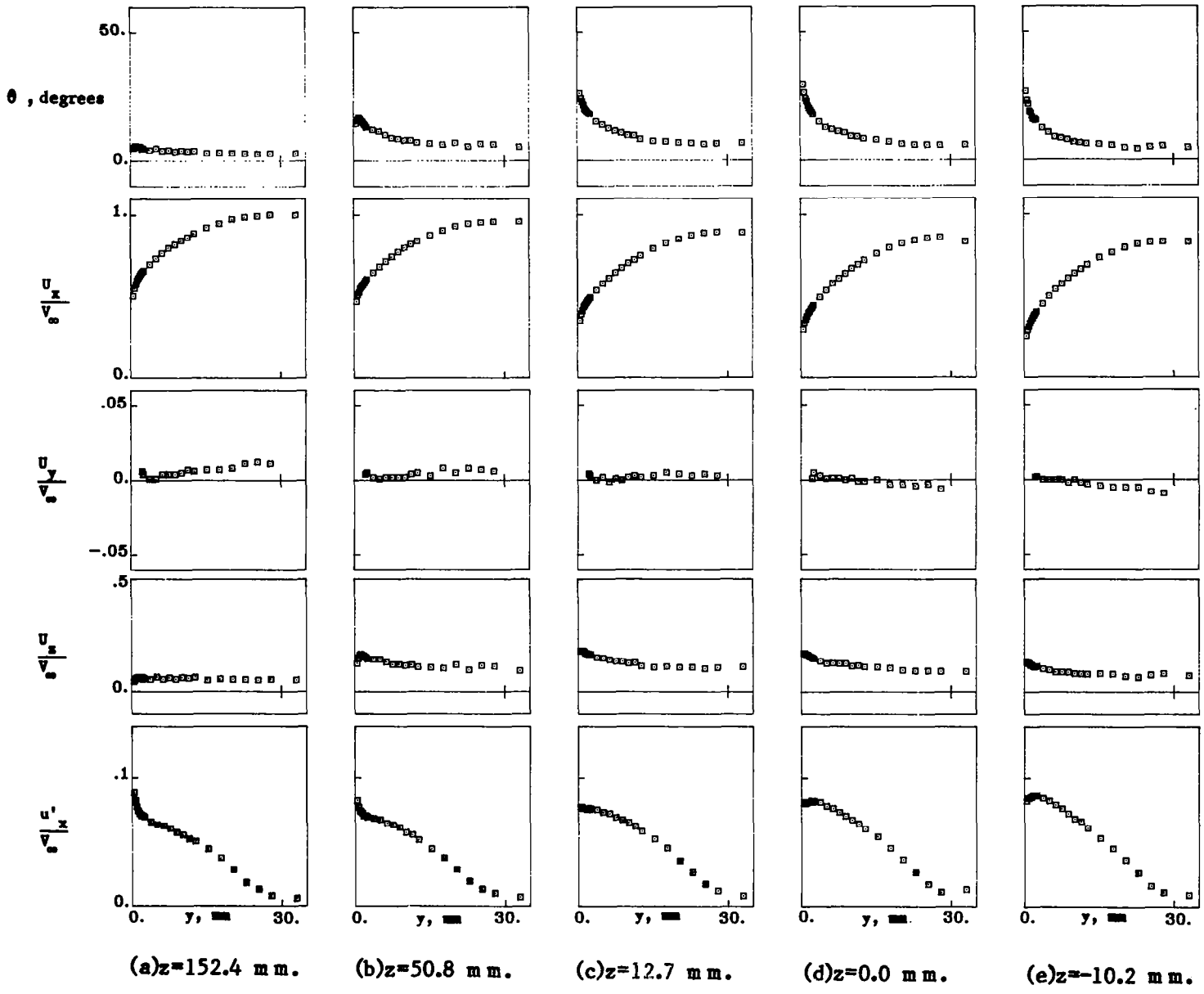

Figure 24. - Mean velocities and turbulence stresses upstream of the juncture (x = −38 mm).

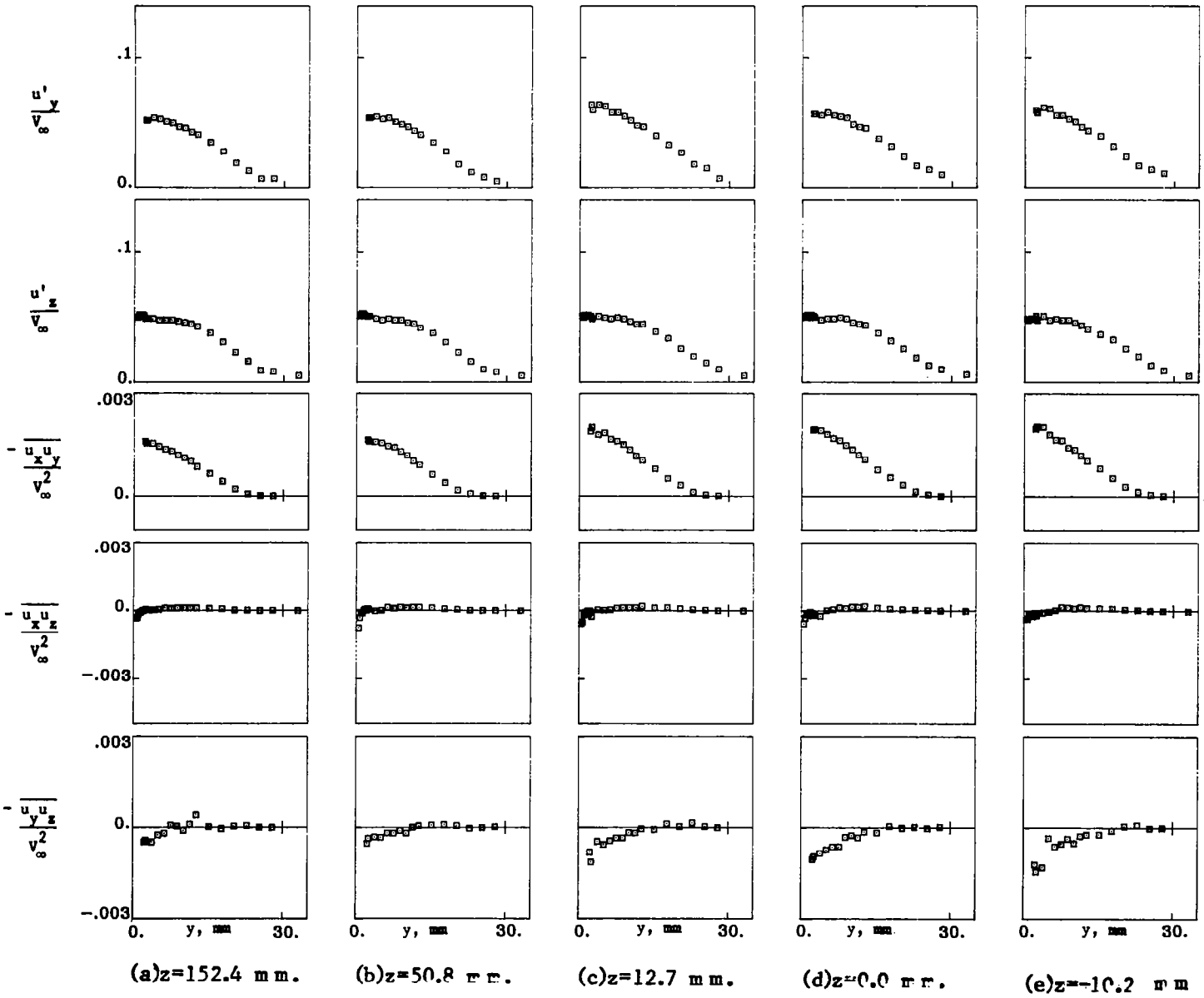

Figure 24. - Concluded.

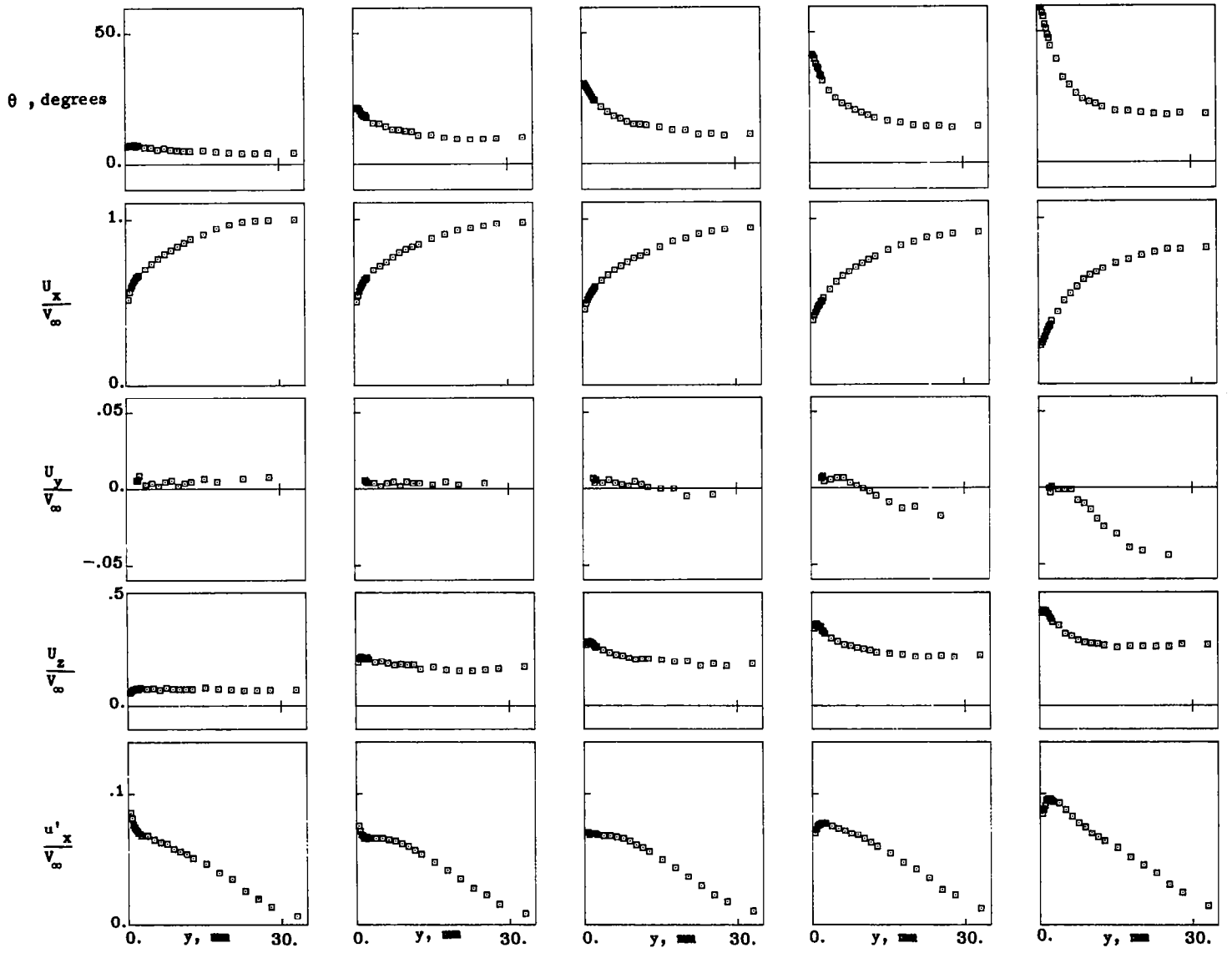

Figure 25. - Mean velocities and turbulence stresses upstream of the juncture (x = − 11 mm).

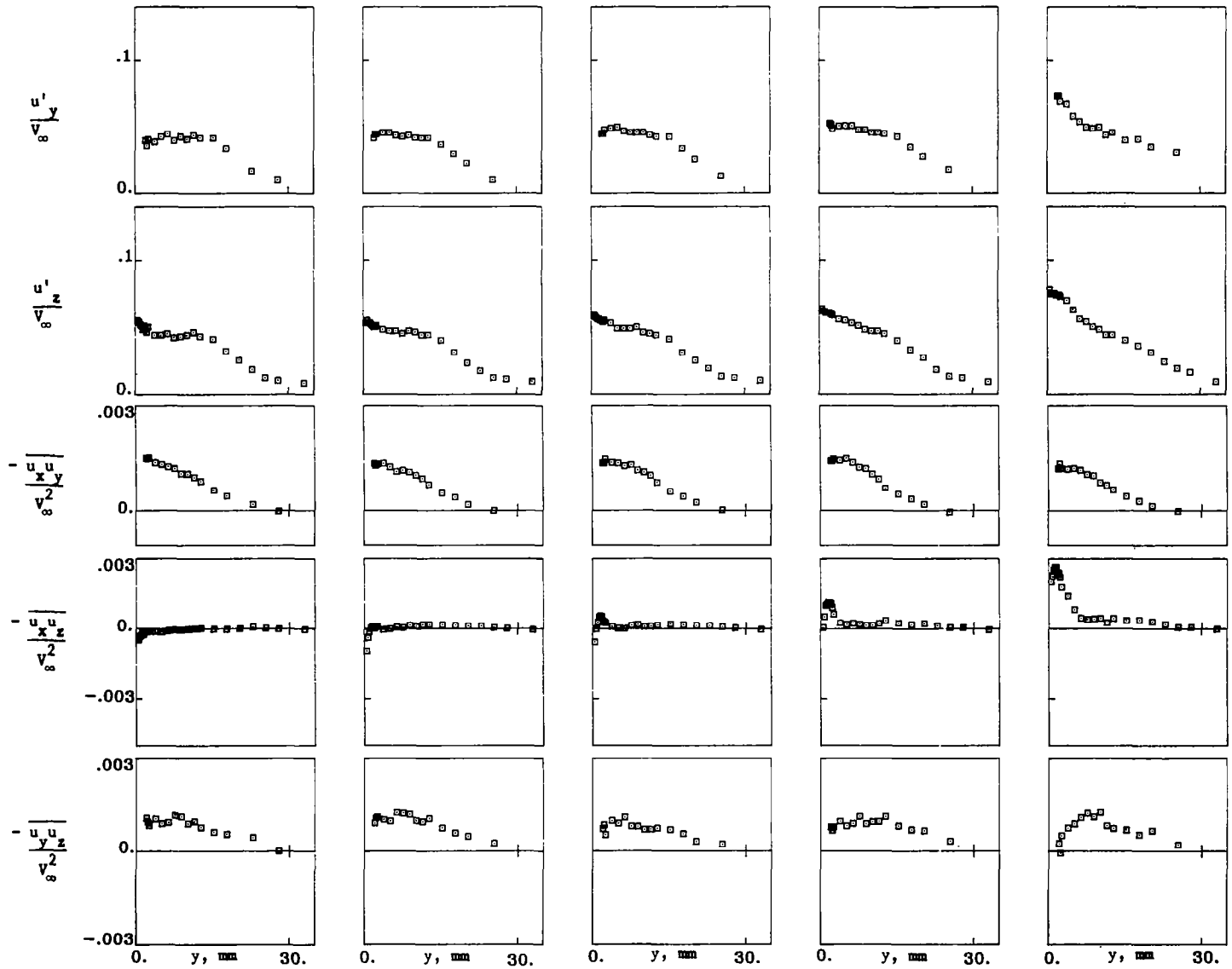

Figure 25. - Concluded.

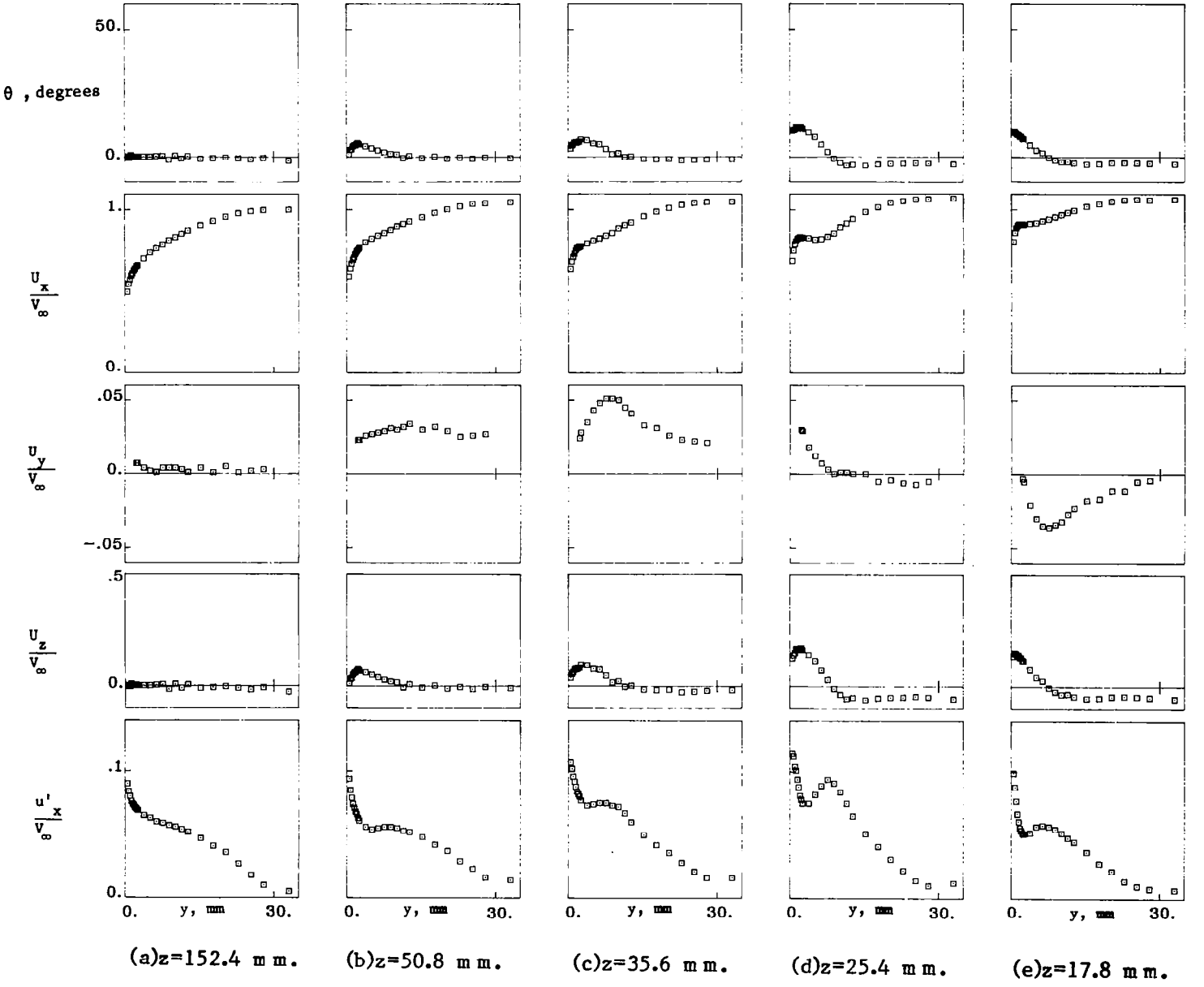

Figure 26. – Mean velocities and Turbulence stresses in the juncture (x = 76 mm).

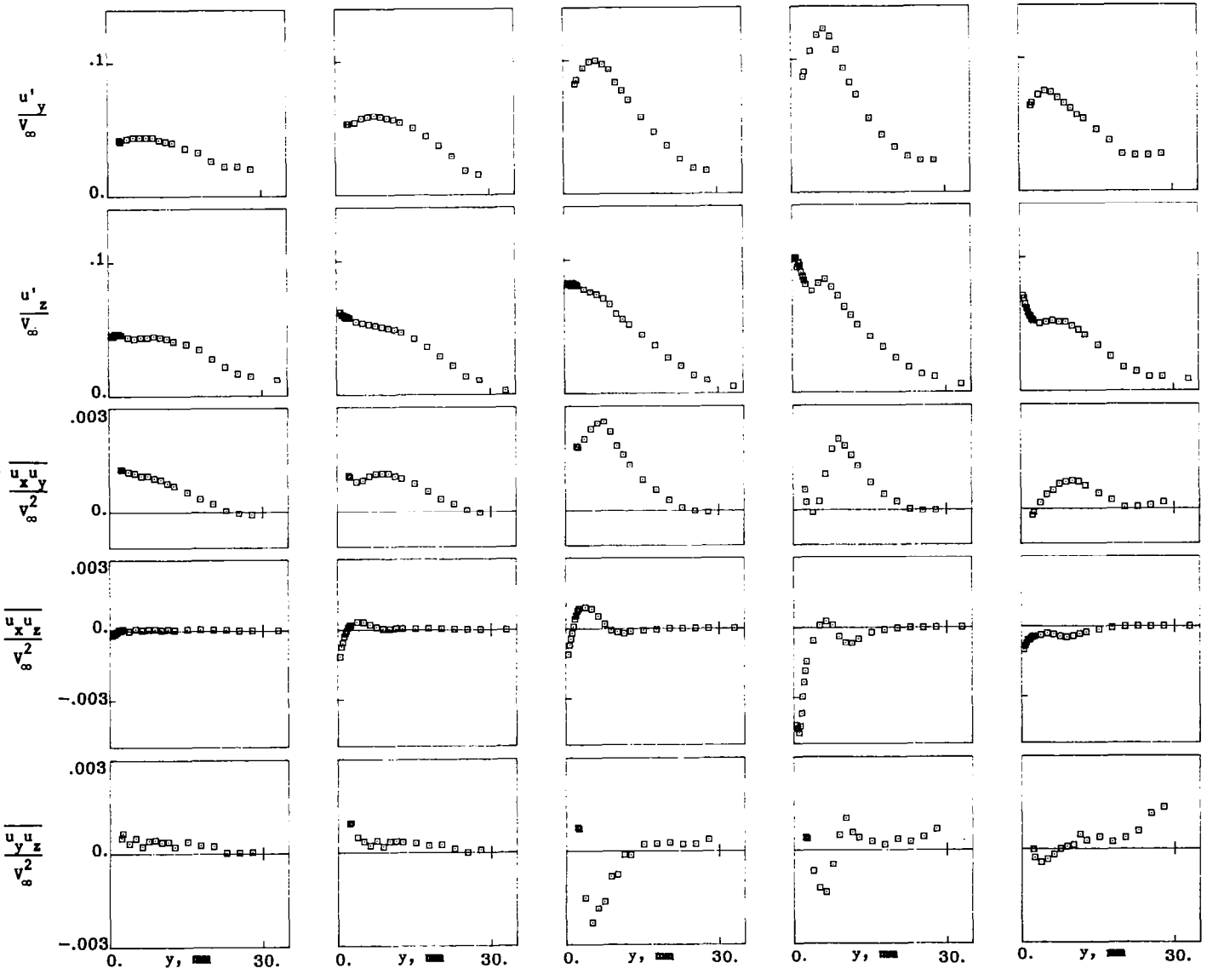

(a)z=152.4 mm. (b)z=50.8 mm. (c)z=35.6 mm. (d)z=25.4 mm. (e)z=17.8 mm.

Figure 26. - Concluded

1. Report No.	2. Government Accession No.	3. Recipient's Catalog No.
NASA CR-3695		

4. Title and Subtitle	5. Report Date
MEAN VELOCITIES AND REYNOLDS STRESSES UPSTREAM OF A SIMULATED WING-FUSELAGE JUNCTURE	June 1983
	6. Performing Organization Code
7. Author(s)	8. Performing Organization Report No.
H. McMahon, J. Hubbartt, and L. R. Kubendran	
	10. Work Unit No.
9. Performing Organization Name and Address	
Georgia Institute of Technology 225 North Avenue, N.W. Atlanta, GA 30332	11. Contract or Grant No. NAG1-40
	13. Type of Report and Period Covered Contractor report
12. Sponsoring Agency Name and Address	
National Aeronautics and Space Administration Washington, DC 20546	14. Sponsoring Agency Code

15. Supplementary Notes

Langley Technical Monitor: James Scheiman

Final Report

16. Abstract

Values of three mean velocity components and six turbulence stresses measured in a turbulent shear layer upstream of a simulated wing-fuselage juncture and immediately downstream of the start of the juncture are presented and discussed. Two single-sensor hot-wire probes were used in the measurements.

The separated region just upstream of the wing contains an area of reversed flow near the fuselage surface where the turbulence level is high. Outside of this area the flow skews as it passes around the body, and in this skewed region the magnitude and distribution of the turbulent normal and shear stresses within the shear layer are modified slightly by the skewing and deceleration of the flow. A short distance downstream of the wing leading edge the secondary flow vortex is tightly rolled up and redistributes both mean flow and turbulence in the juncture.

The data acquisition technique employed here allows a hot wire to be used in a reversed flow region to indicate flow direction.

17. Key Words (Suggested by Author(s))	18. Distribution Statement
Secondary Flow Turbulent Boundary Layer Reynolds Stress Separated Flow	Unclassified - Unlimited Subject Category 02

19. Security Classif. (of this report)	20. Security Classif. (of this page)	21. No. of Pages	22. Price
Unclassified	Unclassified	170	A08

For sale by the National Technical Information Service, Springfield, Virginia 22161

NASA-Langley, 1983